JOHANN WOLFGANG GOETHE
UNIVERSITÄT
FRANKFURT AM MAIN

The influence of the microtubule-targeting agent pretubulysin on inflammatory processes of the vascular endothelium

Dissertation

zur Erlangung des Doktorgrades

der Naturwissenschaften

vorgelegt am Fachbereich 14

der Johann Wolfgang Goethe-Universität

in Frankfurt am Main

von

Tobias Primke

aus Offenbach am Main

Frankfurt (2024)

Vom Fachbereich Biochemie, Chemie und Pharmazie (FB14) der
Johann Wolfgang Goethe Universität angenommen.

Dekan: Prof. Dr. Clemens Glaubitz

1. Gutachter: Prof. Dr. Robert Fürst

2. Gutachter: Prof. Dr. Rolf Marschalek

Datum der Disputation: 11.06.2024

Table of Contents

Abbreviations

Table I. List of abbreviations.

Abbreviation	Full name
ActD	Actinomycin D
ADP	Adenosin diphosphate
AE	Adverse effects
AICAR	5-aminoimidazole-4-carboxamide ribonucleotide
AKT	Ak strain transforming
ALL	Acute lymphatic leukemia
AML	Acute monocytic leukemia
AMP	Adenosin monophosphate
AP-1	Activator protein-1
APC	Antigen-presenting cell
APS	Ammonium persulfate
ARE	Antioxidant-response element
ASC	Apoptosis-associated speck-like protein containing a caspase
ASK	Apoptosis-signal related kinase
ATCC	American type culture collection
ATF	Activating-transcription factor
ATP	Adenosin triphosphate
BAX	Bcl-2-associated X protein
BCA	Bicinchoninic acid
Bcl-2	B-cell Leukemia 2
BD	Bromodomain
bDMARD	Biological disease-modifying anti-rheumatic drug
BET	Bromodomain and extra terminal domain
BID	BH3 interacting-domain death agonist
Brd4	Bromodomain-containing protein 4
BSA	Bovine serum albumin
bZIP	Basic region leucine zipper
$CaCl_2$	Calcium chloride dihydrate
CAM	Cell adhesion molecule
cAMP	Cyclic adenoseine monophosphate
CHAM	Chorioallantoic membrane
CAS	Chemicals abstracts service
CBP	CREB-binding protein
CD	Cluster of differentiation
CDC	Center for disease control and prevention
CDK	Cyclin-dependent kinase
cDNA	Complementary DNA
C/EBP	CCAAT/Enhancer-binding-protein
ChIP	Chromatin immunoprecipitation
CHX	Cycloheximide
cIAP	Cellular inhibitor of apoptosis protein
CLR	C-type lectin-like receptor
COL	Colchicine
COX	Cyclooxygenase
CREB	cAMP response element-binding
csDMARD	Conventional and synthetic disease-modifying anti-rheumatic drug

Table I. Continuation of the list of abbreviations.

Abbreviation	Full name
CTG	Cell tracker green
DAMP	Damage-associated molecular pattern
DD	Death domain
DHF	Dihydrofolate
DHFR	Dihydrofolate reductase
DMARD	Disease-modifying anti-rheumatic drug
DMSO	Dimethyl sulfoxid
DNA	Desoxyribonucleic acid
DNase	Desoxyribonuclease
dNTP	Desoxynucleotide triphosphate
DRB	5,6-Dichloro-1-β-D-ribofuranosylbenzimidazole
DSG	Disuccinimidyl glutarate
DSIF	DRB sensitivity-inducing factor
DSMZ	German Collection of Microorganisms and Cell Cultures
DTT	1,4-Dithiothreitol
DUSP	Dual-specificity phosphatase
EC	Endothelial cells
EC_{50}	Half-maximal excitatory concentration
ECGM	Endothelial cell growth medium
ECL	Enhanced chemiluminescence
ECM	Extracellular matrix
EDTA	Ethylenediaminetetraacetic acid
EGTA	Ethylene glycol-bis(β-aminoethyl ether)-N,N,N′,N′-tetraacetic acid
EHMT1	Euchromatic histone-lysine N-methyltransferases 1
eIF2α	Elongation initiation factor 2α
Elk	ETS-like protein
ELL	Eleven-nineteen lysine-rich in leukemia
ERK	Extracellular signal-regulated kinase
ESAM	Endothelial selective adhesion molecule
e-sele	E-selektin gene
Ets	Erythroblast transformation specific
FA	Formaldehyde
FCS	Fetal calf serum
FDA	Food and drug agency
FITC	Fluorescein isothiocyanate
FMF	Familial Mediterranean fever
GAPDH	Glyceraldehyde 3-phosphate dehydrogenase
GC	Glucocorticoid
GCN	General control non-depressible
GDP	Guanosin diphosphate
GLP	G9a-like protein
GM-CSF	Granulocyte-macrophage colony-stimulating factor
GPCR	G protein-coupled receptor
GR	Glucocorticoid receptor
GRE	GR element
GSK	Glycogen synthase kinase
GTP	Guanosin triphosphate
H_2O_2	Hydrogen peroxide

Table I. Continuation of the list of abbreviations.

Abbreviation	Full name
H3	Histone 3
H3K14ac	Acetylation of histone 3 lysine 14
H3K4me3	Trimethylation of lysine 4 on histone 3
H3K9ac	Acetylation of histone 3 lysine 9
HAT	Histone-acetyltransferase
HCl	Hydrochloric acid
HDAC	Histone-deacetylase
HEPES	4-(2-hydroxyethyl)-1-piperazineethanesulfonic acid
HFS-PI	Hypochromic fluorochrome solution containin PI
HMEC-1	Human dermal microvascular endothelial cell line-1
HMT	Histone methyltransferase
HRP	Horse raddish peroxidase
HUVEC	Human umbilical vein endothelial cell
IC_{50}	Half-maximal inhibitory concentration
ICAM-1	Intracellular adhesion molecule 1
IgG	Immunoglobulin B
IKK	IκB kinase
IL	Interleukin
IL-1R	Interleukin-1 Receptor
IL-1β	Interleukin-1β
IMD	Imiquimod
IMQPD	Imiquimod-induced psoriasiform dermatitis
INF	Interferon
IRAK	IL-1R-related kinase
IRE	Interferon-response element
IRF	Interferon regulatory factor
IκBα	Nuclear factor of kappa light polypeptide gene enhancer in B-cells inhibitor α
JAK	Janus kinase
JAM	Junction adhesion molecule
JIP	JNK-interacting protein
JNK	c-Jun-N-terminal-kinase
JNKIN8	JNK-inhibitor 8
KCl	Potassium chloride
kDa	Kilodalton
KH_2PO_4	Potassium dihydrogen phosphate
KOH	Potassium hydroxide
LB	Lysogenic broth
LDH	lactate dehydrogenase
LFA-1	Lymphocyte function-associated antigen 1
LiCl	Lithium chloride
M199	Medium 199
MAP	Microtubule-associated protein
MAPK	Mitogen-activated protein kinase
MAPKAPK	MAPK-activated protein kinase
MAPKK	Mitogen-activated protein kinase kinase
MAPKKK	Mitogen-activated protein kinase kinase kinase
MDA	Microtubule-destabilizing agent
$MgCl_2$	Magnesium chloride

Table I. Continuation of the list of abbreviations.

Abbreviation	Full name
MHC	Major histocompability compex
MKK	MAP kinase kinase
MLK	Mixed-lineage kinase
MMP	Matrix metalloprotease
MNK	MAP kinase-interacting serine/threonine-protein kinase
mRNA	Messenger ribonucleic acid
MSA	Microtubule-stabilizing agent
MSU	Monosodium urate
MTA	Microtubule-targeting agent
MTOC	Microtubule-organizing center
MTX	Methotrexate
MyD88	Myeloid differentiation-factor 88
Na_2HPO_4	Disodium hydrogen phophate dihydrate
Na_3VO_4	Sodium orthovanadate
NaCl	Sodium chloride
NAD	Nicotinamide adenine dinucleotide
NaF	Sodium fluoride
$NaHCO_3$	Sodium bicarbonate
NELF	Negative elongation factor
NEMO	NFκB essential modulator
NFAT	Nuclear factors of activated T-cells
NFκB	Nuclear factor κ-light-chain-enhancer of activated B-cells
nGRE	negative GR element
NIK	NFκB-inducible kinase
NK cell	Natural killer cell
NLR	NOD-like receptor
NLR	NOD-like receptor
NLR3	Nucleotide-binding domain, leucine-rich repeat-containing 3
NLRP3	NLR family pyrin domain containing 3
NLS	Nuclear translocation signal
NO	Nitric oxide
NOD	Nucleotide-binding oligomerization domain
NP	Natural products
NP40	Nonidet P40 substitute
NSAID	Nonsteroidal anti-inflammatory drug
OPP	*O*-propargyl-puromycin
$p90^{rsk}$	90 kDa ribosomal S6 kinase
PAC	Paclitaxel
PAMP	Pathogen-associated molecular pattern
PARP	Poly(ADP-ribose)-polymerase 1
PASI	Psoriasis area and severity index
PBS	Phosphate-buffered saline
PBS-T	Phosphate-buffered saline with Tween 20
PCR	Polymerase chain reaction
PDB	Protein database
PDE-4	Phosphodiesterase-4
PE	Phycoerythrin
PECAM-1	Platelet and endothelial cell adhesion molecule 1

Table I. Continuation of the list of abbreviations.

Abbreviation	Full name
PI	Propidium iodide
PI3K	Phosphoinositide 3-kinase
PIC	Pre-initiation complex
PIP2	Phosphatidylinositol-4,5-bisphosphate
PIP3	Phosphatidylinositol-3,4,5-triphosphate
PKA	Protein kinase A
PKB	Protein kinase B
PKCζ	Protein kinase C ζ-type
PLB	Passive lysis buffer
PLC	Phospholipase C
PMSF	Phenylmethylsulfonyl fluoride
Pol II	RNA polymerase II
PP2	Phosphatase 2
PPM1J	Protein phosphatase, Mg^{2+}/Mn^{2+} Dependent 1J
PRR	Pattern recognition receptor
PSGL1	P-selectin glycoprotein ligand 1
PT	Pretubulysin
pTEFb	Positive transcription elongation factor b
PVDF	Polyvinylidene fluoride
qRT-PCR	Quantitative real-time PCR
RA	Rheumatic arthritis
RBP	RNA-binding protein
RHD	Rel homology DNA-binding domain
RIPA	Radioimmunoprecipitation assay buffer
RIPK	Receptor-interacting serine/threonine protein-kinase
RLR	RIG-I-like receptor
RNA	Ribonucleic acid
RNase A	Ribonuclease A
ROS	Reactive oxygen species
RPMI	Roswell Park Memorial Institute
RT	Room temperature
RTK	Receptor tyrosine kinase
s.c.	subcutaneous
SAPK	Stress-activated protein kinase
SCI	Systemic chronic inflammation
SDS	Sodium dodecyl sulfate
SDS-PAGE	Sodium dodecyl sulfate-polyacrylamide gelelectrophoresis
SEM	Standard error of the mean
SETD6	SET-domain containing 6
siRNA	small interfering RNA
STAT	Signal transducer and activator of transcription
Stsp	Staurosporin
TAB	TAK-binding protein
TAD	Transactivation domain
TAK	Tumor growth factor-β activated kinase
TBP	TATA-binding protein
TBS	Tris-buffered saline
TBS-T	Tris-buffered saline with Tween 20

Table I. Continuation of the list of abbreviations.

Abbreviation	Full name
TCR	T-cell receptor
TEMED	Tetramethylethylenediamine
TFII	Transcription factor II
TGF	Tumor growth factor
THF	Tetrahydrofolate
TIR	Toll/Interleukin-1 Receptor
TLR	Toll-like receptor
TNF	Tumor necrosis factor
TNFR	TNF-Receptor
TRADD	TNFR1-associated death domain
TRAF	Tumor necrosis factor-receptor associated factor
TRAM	TRIF-adapter molecule
TRIF	TIR domain-containing adaptor protein-inducing interferon beta
TRIS	Tris(hydroxymethyl)aminomethan
TSS	Transcription start site
UTR	Untranslated region
UV	Ultra-violett
VCAM-1	Vascular cell adhesion molecule 1
VIN	Vincristine
VLA-4	Very late antigen 4
VVO	Vesiculo-vacuolar organelles
γ-TuRC	γ-tubulin ring complex

List of figures

List of tables

1. Introduction

1.1 Inflammation

Inflammation comprises a process inevitable for the defense of multicellular lifeforms from detrimental factor like cellular damage or pathogens. However, if non-resolved, the inflammatory state gives rise to a multitude of chronical-inflammatory diseases and ultimately cancer, reducing a patients quality of life and life span [1–3]. In fact at this day, chronic inflammatory diseases are recognized as the leading cause for disease-related death, with more than 50 % of all deaths being attributable to inflammation-related morbidities like cardiovascular diseases, i.e. stroke and ischemic heart diseases, diabetes, cancer and neurodegenerative as well as autoimmune disorders [4]. Inflammation constitutes an evolutionarily conserved process and involves the activation of immune and non-immune cells that act in concert to protect an organism from noxious factors and also promotes the repair of damaged tissues. A normal and acute inflammatory response is thereby characterized by the temporal upregulation of inflammatory activity, which is resolved when the inflammatory trigger is eliminated [5]. Failure to resolve this state can give rise to systemic chronic inflammation (SCI). Unlike the short-termed and high magnitude acute inflammatory state, SCI constitutes a state of low magnitude inflammation, which is persistent, non-resolving and leads to tissue damage [2, 6–8]. There are several factors that can contribute to the emergence of SCI, like the ability of some pathogens to resist the host's defenses for pro-longed periods of time, extended exposure to low levels of toxic materials, pro-longed expression of inflammatory inducers due to environmental factors leading to oxidative stress, defects in cells of the immune system inducing recurring or non-resolving auto-inflammatory disorders or the erroneous detection of normal components of the body by cells of the immune system as foreign objects in auto-immune disorders [9, 10] .

The inflammatory state is enacted by the immune system of a host, which can be subdivided into the innate and the adaptive immune system. While the innate immune system serves as a fast and non-specific first line of defense against invading pathogens, the adaptive immune system constitutes the immunological 'memory' of an organisms and relies on antigen-specific and -dependent factors, which confer immunity to pathogens that an organism has encountered before, leading to a more robust and efficient immunological response.

1.2 The immune system

The first line of defense constituted by the innate immune system that precede the inflammatory response are the anatomical, physiological and endocytic or phagocytic barriers set up by multicellular organism (Fig. 1). Anatomical barriers comprises the skin, which serves as a mechanical barrier and prevents microbial growth due to its acidic environment, and the mucosal membranes, which trap foreign objects in mucous and propel them out by the action of cilia and also set an environment for cultivation of physiological flora that competes with pathogens for attachment [11]. Physiological

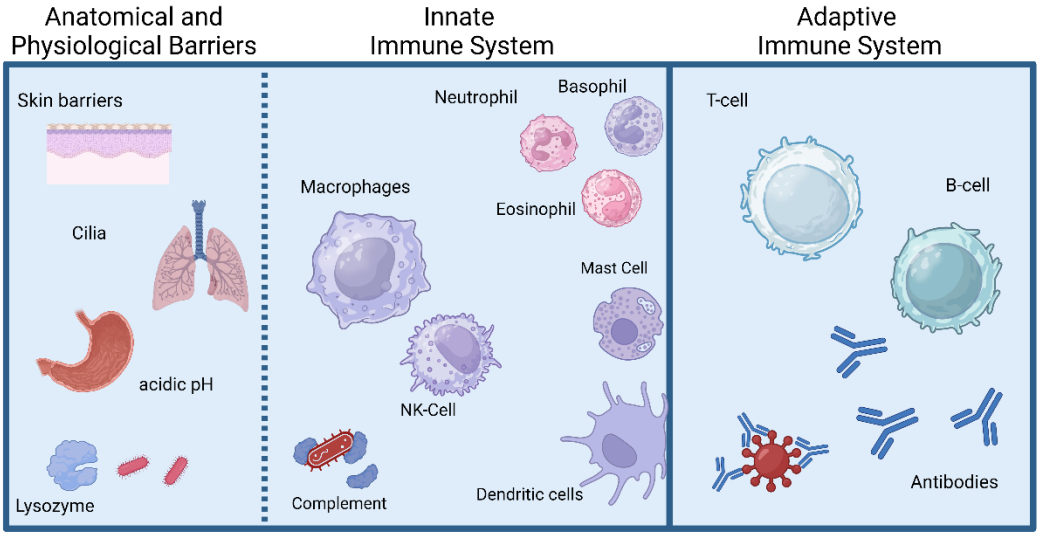

Figure 1. The factors constituting the human immune system in form of the anatomical and physiological barriers, the innate immune system and the adaptive immune system with some cellular and humoral compartments. Adapted from [11].

barriers are comprised of the acidic pH environment of the stomach or the body temperature and fever response of a host that kill and prevent the growth of pathogens. This also includes chemical mediators like lysozyme, which cleaves bacterial cell walls or the complement system, which is constituted by a large number of plasma proteins that bind to or 'opsonize' pathogens to rupture or prime the pathogens for elimination by immune cells and induce an inflammatory response. The endo- and phagocytic barriers are based on the ability of various cells to internalize and break-down foreign molecules or the ability of specialized cells to internalize or 'phagocytose' and digest whole pathogenic organisms. A large number of different cells are involved in the innate immune response. This comprises the before mentioned phagocytes like monocytes or macrophages and neutrophil granulocytes, but also dendritic cells, mast cells, basophil and eosinophil granulocytes, natural killer (NK) cells, as well as innate lymphoid cells [12]. As part of the innate immune system, the ability of these cells to detect pathogens largely relies upon a limited repertoire of cell damage and pathogen-detecting receptors, the so called pattern-recognition receptors (PRRs), which target factors that are conserved over a large number of different pathogenic organisms [13]. Macrophages and neutrophils both share the ability to phagocytose pathogenic organisms like bacteria. However, unlike neutrophils, macrophages are also antigen-presenting cells (APCs) involved in deriving antigens from pathogens and presenting them to T-cells, linking the actions of the innate immune system to the adaptive immunity. Some of the most important

APCs are the dendritic cells, which exclusively phagocytose pathogens for derivation of antigenic peptides from pathogens and presenting them via major histocompatibility complex (MHC) molecules in order to activate the T-cells of the adaptive immune system for recognition of pathogens. Mast cells, basophils and eosinophils share important functions in the acute inflammatory response following exposure to allergic stimuli. While basophils reside in circulation, mast cells have an important function as so-called 'sentinel cells', which reside in the tissues and produce pro-inflammatory cytokines and immune cell recruiting chemokines upon infection or injury, i.e. cytokines like the tumor-necrosis factor (TNF) or proteins of the interleukin family or chemokines like members of the chemokine (C-C motif) ligand (CCL) or (C-X-C motif) ligand (CXCL) family of proteins. NK cells play an important role in detection and destruction of transformed or infected cells, by releasing proteins that induce the lysis of target cells, but also serve as important producers of cytokines in form of interferon-γ, which recruits APCs and is a crucial mediator of the anti-viral response.

The primary function of the adaptive immune system is the recognition of foreign antigens and the activation of pathogen-specific immunological responses leading to destruction of the pathogens and infected cells. In addition, the cells of the adaptive immune system are involved in generation of the immunologic memory in order to enable a quick immunological response in case of a reinfection with the same pathogen [12]. The cells involved in the adaptive immune response are the antigen-specific T-cells and B-cells. Each T-cell expresses a single type of T-cell receptor (TCR) on their cell surface, which is specific for an antigen derived from a pathogen and presented by an APC. The primary function of T-cells is the production of cytokines to regulate the immune response (T-helper-cells) , as well as the destruction of infected or transformed cells (cytotoxic T-cells) [14]. Unlike T-cells, B-cells do not need activation by an APC but can directly interact with antigens via antigen-specific receptors. The primary function of B-cells is the production of antigen-specific antibodies, which assist the cell-mediated immunity by labeling pathogens for detection by the complement system or immune effector cells.

While the innate and adaptive immune system both act in concert to prevent immunological incursions by systemically recruiting and activating the cells of the immune system, commonly termed white-blood cells or leukocytes, the immediate inflammatory response is especially dependent on the leukocytes of the innate immune system that reside in the tissues or continuously circulate in the blood stream in order to react to an inflammatory stimulus.

1.3 The inflammatory response

The inflammatory response represents the coordinated activation of signaling cascades leading to the secretion of inflammatory mediators by sentinel immune cells residing in the tissues and the concomitant recruitment of immune effector cells that circulate in the blood stream to the site of inflammation in order to eliminate the inflammatory trigger. Such triggers can either be pathogen-associated molecular patterns (PAMPs) derived from pathogens or cell-damage-associated molecular patterns (DAMPs) in form of biomolecules that are released upon cell damage [15–17]. DAMPs and PAMPs are detected by the PRRs expressed by immune or non-immune cells, leading to the activation of intracellular pro-inflammatory signaling cascades, like the pro-inflammatory nuclear factor κ-light-chain-enhancer of activated B-cells (NFκB) or activator protein-1 (AP-1) signaling [18]. Several families of PRRs are known to be expressed by mammalian cells including the toll-like receptors (TLRs), RIG-I-like receptors (RLRs), NOD-like receptors (NLRs) and C-type lectin-like receptors (CLRs) [13]. The TLRs constitute the largest family of the PRRs with 10 different members having been identified in humans to this day [19, 20]. TLRs are type-1 transmembrane glycoproteins consisting of an extracellular domain, a transmembrane domain and an intracellular domain. Most TLRs form homo- or heterodimers on the surface of cells or endosomal compartments to detect lipids, lipoproteins and proteins or the nucleic acid of pathogens via their extracellular domain [21]. While the extracellular domain of TLRs contain leucine-rich repeats, which are responsible for pattern recognition, the intracellular domains contain the Toll/Interleukin-1 Receptor-(IL-1R; TIR) domain, important for intracellular signal transduction upon binding of the respective PAMP or DAMP [22]. Depending on the type of TLR and the adaptor proteins bound to the intracellular domain, the signal transduction initiated by TLRs can largely be divided into myeloid differentiation-factor 88 (MyD88)-dependent and MyD88-independent (TLR3/TLR4-TIR domain-containing adaptor protein-inducing interferon β (TRIF)-dependent) pathways [23, 24] (Fig. 2). While the Myd88-indepenent pathways are mainly involved in interferon-signaling by recruitment of TRIF via association with the TRIF-adapter molecule (TRAM), the Myd88-dependent pathways induce the activation of the main pro-inflammatory NFκB and AP-1 transcription factors [25–27]. MyD88 constitutes the adaptor protein for most of the TLRs and upon pattern recognition, binds to the intracellular TIR domain of TLRs via its carboxy-terminal domain, while the amino-terminal domain recruits the IL-1R-related kinase 4 (IRAK4) [28]. IRAK4 activates and forms a complex with IRAK2, which further phosphorylates and recruits IRAK1. In complex, these kinases recruit and activate the tumor necrosis factor (TNF)-receptor associated factor 6 (TRAF6) [29]. The activated ubiquitin ligase TRAF6 subsequently polyubiquitinates itself, which recruits and activates the tumor growth factor (TGF)-β activated kinase 1 (TAK1) and two TAK-binding proteins (TAB1 and TAB4) [30]. The TAK1-TAB1-TAB4 complex itself can activate the NFκB and AP-1 signaling cascades via interaction with the IκB kinase of the NFκB signaling pathway and the activation of the c-Jun-N-terminal-kinase (JNK) and p38 kinase of the mitogen-activated protein kinase (MAPK) family, leading to AP-1 activation [31–33].

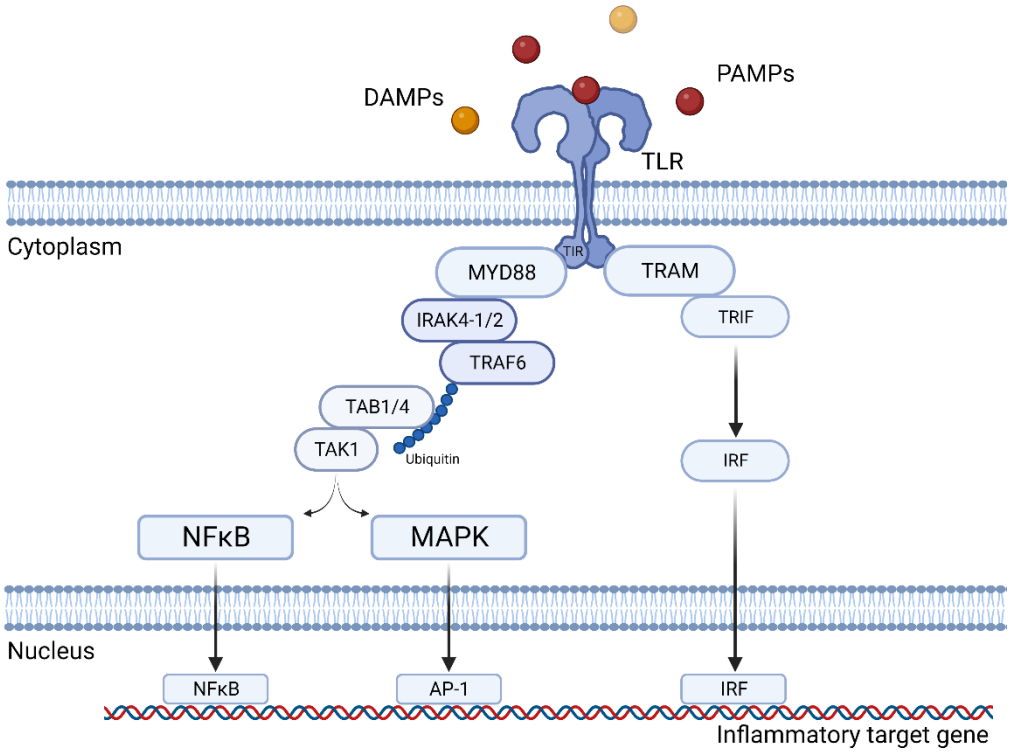

Figure 2. Recognition of PAMPs or DAMPs by TLRs leads to MyD88-dependent or -independent pro-inflammatory signaling cascades. Myd88-dependent signaling induces NFκB and MAPK signaling via TRAF6 and TAK1-TAB activation. Myd88-independent signaling involves TRIF recruitment via TRAM that leads to interferon regulatory factory (IRF) signaling.

Pattern recognition by the PRRs other than the TLRs is based on a variety of additional signaling cascades that will usually also induce NFκB and AP-1 via activation of TRAF6 or the TAK-TAB complex. While induction of the pro-inflammatory NFκB and AP-1 transcription factors generally leads to the expression of a multitude of pro-inflammatory target genes, recognition of PAMPs and DAMPs by tissue sentinel immune cells usually leads to the expression and secretion of pro-inflammatory chemokines and cytokines (Tab. 1), like TNF that induce the inflammatory response by recruitment and activation of immune effector cells.

Table 1. Pro-inflammatory cytokines, their source and resulting function. Taken from [18].

Cytokine	Family	Source	Function
IL-1β	IL-1	Macrophages	Pro-Infl; proliferation, differentiation
IL-6	IL-6	T-helper-cells	Pro-Infl; differentiation, cytokine production
IL-8	CXC	Macrophages, endothelial cells	Pro-Infl; chemotaxis, angiogenesis
IL-12	IL-12	T-cells, B-cells	Pro-Infl; differntiation, NK-cell activation
TNFα	TNF	Macrophages, NK-cells, T-helper-cells	Pro-Infl; cytokine production, proliferation, apoptosis, anti-infection
INF-γ	INF	T-cells, NK-cells	Pro-Infl; innate and adaptive anti-viral
GM-CSF	TGF	Macrophages, T-cells	Pro-Infl; macropohage activation

1.3.1 The NFκB signaling cascade

TNF (also called TNFα) constitutes one of the most important pro-inflammatory cytokines for induction of pro-inflammatory signaling cascades. TNF can either be expressed and secreted by cells in a soluble form or in a membrane-bound state [34]. While detection of soluble TNF is achieved by interaction with the TNF-receptor 1 (TNFR1), membrane bound TNF only binds and activates the TNF receptor 2 (TNFR2) [35–38]. The TNFR1 is expressed by most cell types, in contrast TNFR2 expression is limited to a subset of cell types including endothelial cells and some B- and T-cells [39, 40]. While binding of soluble vs. membrane bound TNF to the respective TNFR leads to different intracellular signaling pathways and according to the cell type to differing cellular responses, binding of soluble TNF usually leads to activation of the canonical NFκB signaling pathway, while binding of membrane-bound TNF usually leads to activation of the non-canonical NFκB pathway [32]. In addition, while the canonical NFκB pathway usually results in rapid activation of pro-inflammatory target genes, activation of the non-canonical pathway is slower and sustained and promotes cell survival and proliferation. Both TNFR belong to the type 1 membrane protein family and consist of an extracellular domain, a transmembrane domain and an intracellular domain [41]. However while the TNFR1 contains an intracellular death domain for interaction with adaptor proteins, the TNFR2 lacks this domain [39]. In the canonical NFκB signaling, binding of soluble TNF to TNR1 induces the trimerization of the receptor, leading to exposure of the intracellular death domain (DD; Fig. 3). The DD recruits the TNFR1-associated death domain (TRADD) protein. TRADD functions as an adaptor protein by recruiting the TNF receptor-associated factor 2 (TRAF2) or TRAF5, as well as the receptor-interacting serine/threonine protein-kinase 1 (RIPK1) [42, 43]. TRAF2/5 then recruits the cellular inhibitor of apoptosis protein (cIAP) 1 and cIAP2, completing the formation of the core NFκB signaling complex [44, 45]. The TRAF and cIAP proteins contain an E3 ubiquitin-ligase function and add ubiquitin chains to RIPK1, which, similar to the inflammatory response following pattern recognition, serve as scaffold for binding of the TAK1-TAB complex, leading to further pro-inflammatory signaling and cell survival [45, 46]. Incomplete ubiquitination of RIPK1 will, depending on the presence of caspases, induce apoptosis or necroptosis, terminating the inflammatory response [32, 47]. However, full ubiquitination of RIPK1 recruits and activates the TAK1-TAB2/3 complex via its ubiquitin-binding domain and also recruits the IκB kinase complex (IKK) consisting of IKKα, IKKβ and the regulatory subunit IKKγ, also called the essential NFκB modulator (NEMO), via the ubiquitin-binding function of the latter [48–50]. The IKK complex is then activated by the TAK1-TAB complex via phosphorylation of IKKβ [30, 50]. Activated IKK then phosphorylates and deactivates the proteins of the IκB family of proteins, i.e. IκBα, which sequester the NFκB dimer in cytosol by masking its nuclear translocation signal (NLS). After phosphorylation, the IκB protein are ubiquitinated and degraded by the proteasome and the NFκB transcription factor, usually consisting of the most transcriptionally active p65:p50 heterodimer, can enter the nucleus where it induces the transcription of pro-inflammatory target genes. In the non-canonical NFκB signaling pathway via the TNFR2 receptor that lacks the intracellular DD, signal propagation is still achieved via

interaction of TRAF2 and TRAF1 or TRAF3, as well as cIAP1 and 2, albeit with lower binding affinity [51–53]. In the basal state, TRAF2/3 and cIAP1/2 is in complex with the NFκB-inducible kinase (NIK), keeping NIK in an inactive state [54, 55]. Upon recruiting TRAF2, this complex is disrupted, and the active NIK can phosphorylate IKKα [56]. Active IKKα then induces the proteolytical procession of p100 to p52, which activates an alternative NFκB transcription factor consisting of p52:RelB. In addition

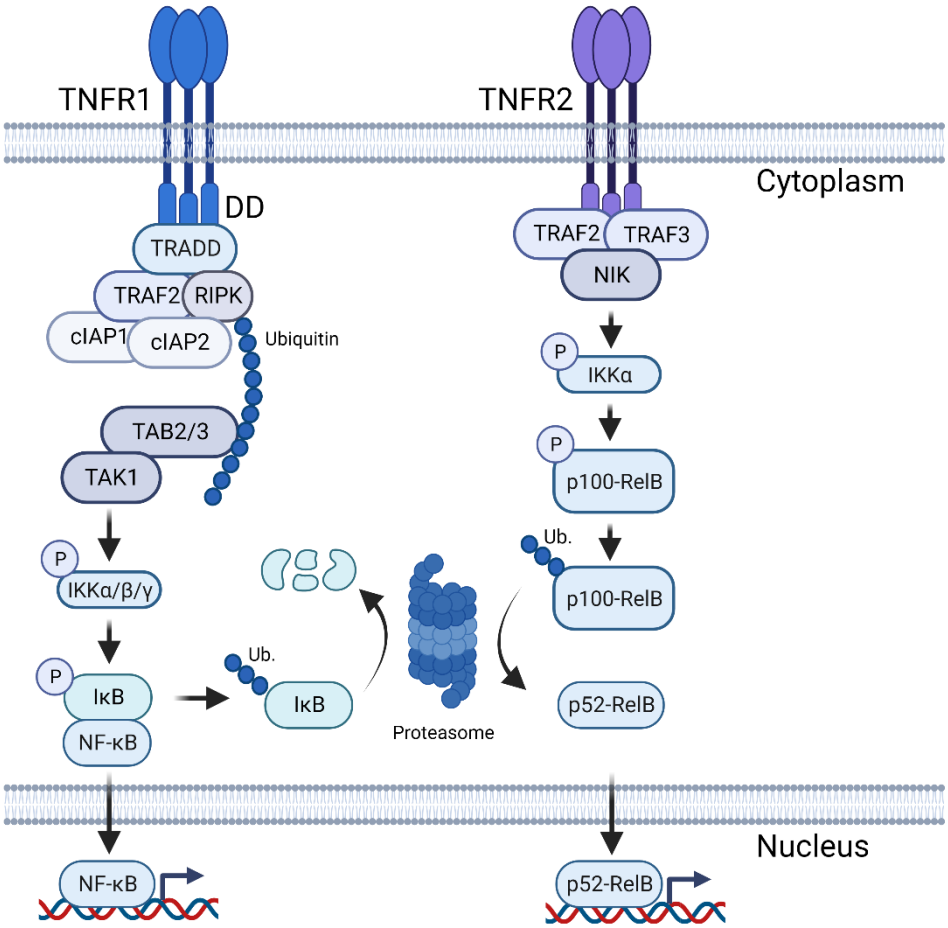

Figure 3. TNFR1-induced canonical NFκB signaling and TNFR2-induced non-canonical NFκB signaling cascades. Association of the DD of TNFR1 with adaptor proteins leads to the formation of the NFκB signaling complex consisting of TRADD, TRAFs, cIAPs and RIPK. TRAFs and cIAPs add ubiquitin chains to RIPK, which serve as binding platform for the TAK1-TAB complex. The TAK1-TAB complex activates IKK, which in turn deactivates IκB proteins leading to their ubiquitination and proteasomal degradation. Subsequently, NFκB is free to translocate into the nucleus and binds to target genes. In the non-canonical TNFR2 signaling, TRAF proteins interact with TNFR2 and recruit NIK, which activates IKKα leading to p100 phosphorylation, ubiquitination and proteasomal procession to p52. The p52-RelB dimer subsequently translocates to the nucleus to induce target genes. Adapted from [56].

to its kinase function during NFκB signaling, TAK1, also known as mitogen-activated protein 3 kinase 7, functions as a tier 3 MAPK leading to downstream activation of the pro-inflammatory MAPKs p38 and JNK. This demonstrates the crosstalk between different pro-inflammatory signaling cascades upon stimulation with TNF.

1.3.2 The MAPK signaling cascades

The MAPKs are a family of serine/threonine kinases that react to a wide variety of stimuli like inflammatory cytokines, but also osmotic stress, heat shock or mitogens leading to different cellular responses. This includes the propagation of inflammation, cell proliferation and differentiation and cell survival or apoptosis. The mammalian MAPKs primarily include the extracellular signal-regulated kinase 1 and 2 (ERK1/2), the different tissue and cell-type specific p38 MAP kinase isoforms p38α, p38β, p38γ and p38δ, as well as the JNK isoforms JNK1, 2 and 3 [57–59]. Each of the MAP kinase pathways consists of three tiers of MAPK modules, also termed MAPKKK (tier 3), MAPKK (tier 2) and the actual MAPKs (tier 1) ERK, p38 and JNK, with the higher tier MAPKs activating the lower tier MAPKs by phosphorylation [60, 61] (Fig. 4). ERKs are mainly involved in cell differentiation, while

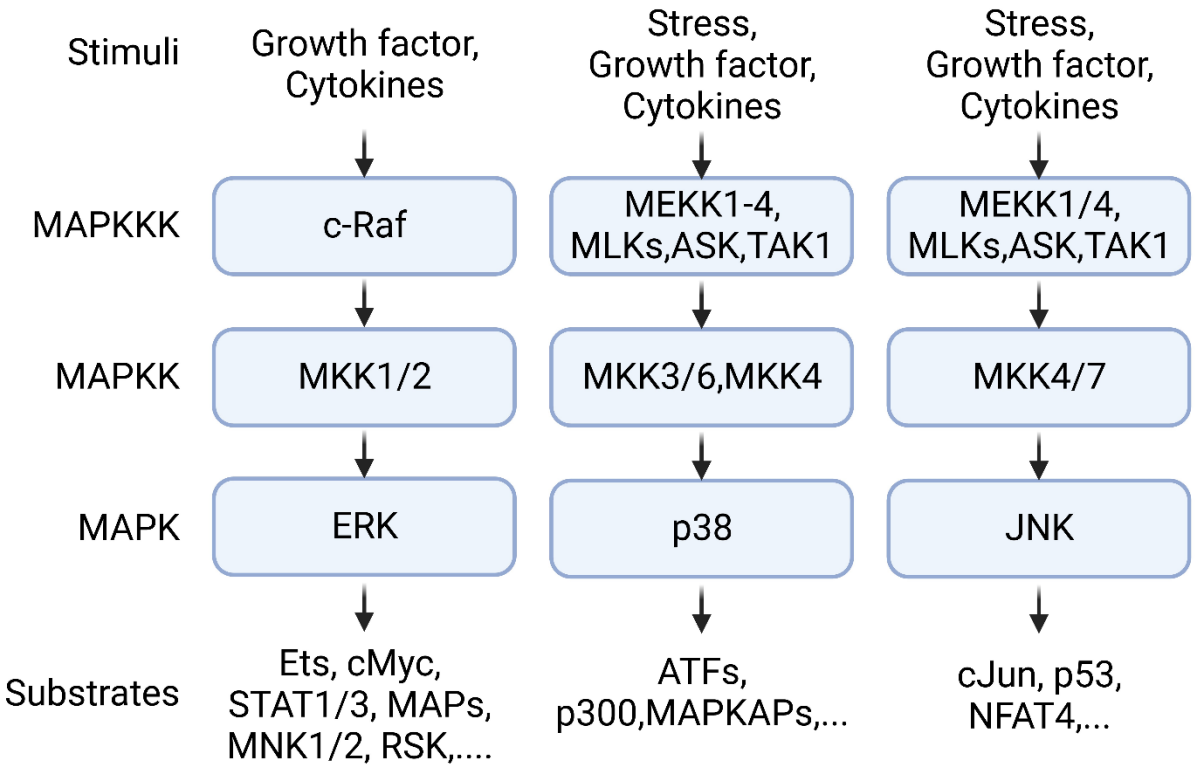

Figure 4. ERK, p38 and JNK MAPK signaling cascades in mammals. Each MAPK signaling cascades consists of three MAPK modules (MAPKKK, MAPKK and MAPK). Adapted from [61].

p38 and JNK mainly react to pro-inflammatory stimuli. Activation of the ERK pathway is usually coupled to growth factor detection via receptor tyrosine kinases (RTKs), leading to activation of the MAPKKK c-raf-1, which activates the downstream MAPKKs MAP kinase kinase 1 and 2 (MKK1/2), which in turn phosphorylate and activate the MAPKs ERK1/2 [62]. ERK1 and 2 activate a variety of substrates involved in cellular proliferation, differentiation and development, i.e. transcriptions factors of the erythroblast transformation specific (Ets) family like the ETS-like protein 1 (Elk1), MYC (c-Myc) or the signal transducer and activator of transcription 1 and 3 (STAT1/3), microtubule-associated proteins (MAPs), or kinases like the MAP kinase-interacting serine/threonine-protein kinase 1 and 2 (MNK1/2) and 90 kDa ribosomal S6 kinase ($p90^{rsk}$), which targets the transcription factors NFκB, cFos

as component of the AP-1 complex or the glycogen synthase kinase 3 (GSK3) [63]. The p38 MAPK pathway is usually activated by cell stress, i.e. osmotic stress, ultra-violet radiation, heat shock, cytokines (TNF), or growth factors, which activates the MAPKKKs, MEKK1-4, mixed-lineage kinases (MLKs), apoptosis-signal related kinases (ASKs), as well as TAK1 of the TAK1-TAB complex. These MAPKKKs activate the MAPKKs MKK3/6 and MKK4, which in turn activate the different p38 isoforms p38α/β/γ and δ [64]. Substrates of the p38 kinase include transcription factors like the activating-transcription factor 2 (ATF-2), but also NFκB via induction of the p300 histone acetyltransferase, or kinases of the MAPK-activated protein kinase (MAPKAPKs) family, which are involved in the regulation of RNA-binding proteins and hence, mRNA stability [65, 66]. The JNK pathways is similarly induced by cellular stress, cytokines or growth factors that induce the activity of the MAPKKKs MEKK1 and 4, MLKs, ASK and TAK1, demonstrating the cross-linkage of p38 and JNK pathway activation. The MAPKKs of the JNK pathway are MKK4 and MKK7, which activate the three different JNK isoforms JNK1/2 and 3 [67–69]. Substrates of the JNKs are the transcription factors cJun, ATF-2, p53 or the nuclear factors of activated T-cells 4 (NFAT4) [70]. In case of cJun, which together with cFos constitutes the main component of the AP-1 transcription factor, JNK induces the transactivatory activity by phosphorylation, enabling the transcription of pro-inflammatory target genes.

1.3.3 Additional pro-inflammatory signaling cascades

In addition to the pro-inflammatory NFκB and AP-1 signaling cascades, a variety of other signaling cascades exist that assist in the expression of pro-inflammatory target genes. This includes the Janus kinase (JAK)-induced activation of the STAT transcription factor family, the phosphoinositide 3-kinase (PI3K)-ASK-GSK3β-GATA6-transcription factor axis or the interferon-regulatory factor (IRF) signaling [71–73] (Fig. 5). Binding of an extracellular ligand in form of cytokines, i.e. IL-6 or growth

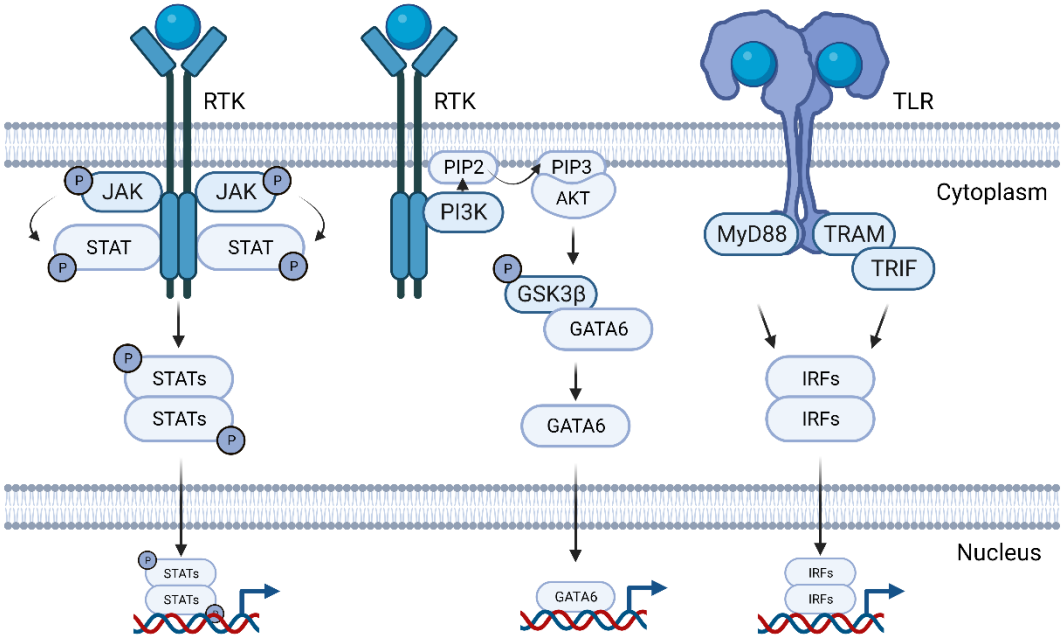

Figure 5. Pro-inflammatory JAK-STAT, PI3K-AKT-GATA6 and IRF signaling cascades. Signal recognition by an RTK leads to intracellular activation of JAKs, and STATs or activation of PI3K, which phosphorylates PIP2 to produce PIP3, leading to AKT activation and deactivation of GSK3β, releasing GATA6. Interferon signaling is usually integrated by TLRs, which activate IRFs in a Myd88-dependent or –independent manner.

factors to a JAK-associated receptor, induces conformational changes in the receptor that allows the intracellularly bound JAKs to phosphorylate and activate one another [74]. The activated JAKs then phosphorylate and activate the members of the STAT family, which subsequently dimerize and translocate to the nucleus to induce the activity of target genes [75]. In mammals, four different JAKs are known that induce the activity of seven STATs [76]. PI3K is similarly induced by binding of cytokines or hormones to PI3K-related receptors, inducing the phosphorylation of phosphatidylinositol-4,5-bisphosphate (PIP2) to produce phosphatidylinositol-3,4,5-triphosphate (PIP3) by PI3K leading to AKT activation [77–79]. AKT negatively regulates the activity of GSK3β, which in its active state binds to the pro-inflammatory transcription factor GATA-6, keeping it in an inactive state. Phosphorylation of GSK3β by AKT releases GATA-6 and induces its promoter activity [72]. Activation of IRF signaling is achieved by a large variety of different receptors like PRRs. Activation of IRFs can be achieved by MyD88-independent TLR signaling via activation of TRIF, but can also be MyD88-dependent via activation of IKKα [80–82]. To this date, nine different members of the IRF family are known to be expressed in mammals (IRF-1-9) [83]. Upon phosphorylation, these transcription factors dimerize and bind to the promoters of target genes. In general, the activity of many transcription factors is not only

achieved by post-translational modification, but also by transcriptional regulation. The *irf-1* gene for example contains bindings sites for IRF-1 and NFκB [84]. TNF induces the expression of many transcription factors that are involved in the induction of pro-inflammatory target genes by induction of NFκB or AP-1, which themselves are regulated by post-translational modifications (NFκB or AP-1) or transcriptional regulation (AP-1).

1.4. NFκB and AP-1 activity

1.4.1 Modulation of NFκB activity

The NFκB transcription factor mainly consists of the p65:p50 heterodimer, which has the highest DNA-binding affinity to the κB DNA binding motif of all NFκB constituents [85]. In addition, several other NFκB proteins exist that can form alternative NFκB complexes, like c-Rel and RelB, which can replace p65 in the NFκB dimer, or p52, which can replace p50 [86, 87]. While the p65:p50 heterodimer has the highest binding affinity to the to κB DNA consensus motif, the different NFκB forms have differing specificities to various κB binding sites [88, 89]. All of the Rel proteins share a Rel homology DNA-binding domain (RHD) in their amino-terminus, as well as a transactivation domain (TAD) for interaction with additional factors in their carboxy-terminal domain [90]. In contrast, p50 and p52 only contain a RHD and have no intrinsic transcriptional activity, and while the p65:p65 homodimer can still induce expression, the p50:p50 homodimers are thought to repress the transcription of target genes [91, 92]. The p50 and p52 proteins are expressed as the precursors p105 and p100, respectively, and are only activated after procession by the proteasome [93–95]. However, while p105 is constitutively processed to p50, p100 procession to p52 is largely regulated and affords the activation of NIK and IKKα [96, 97]. Upon activation of NFκB by release from IκB proteins, especially the p65 protein undergoes significant phosphorylation and acetylation events to further activate NFκB or 'fine-tune' the NFκB specificity to different target genes. To date, several p65 phosphorylation sites have been postulated including p65-S276 in the RHD and p65-S468, -S536 in the TAD of p65 (Fig. 6). Phosphorylation of p65 at S276 is

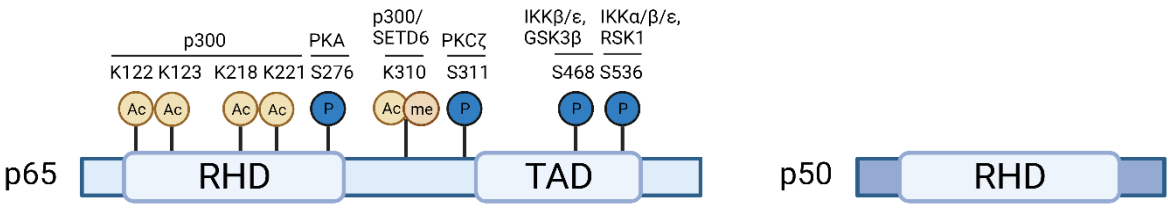

Figure 6. Representation of NFκB-p65 with phosphorylation sites and acetylation sites and correlated kinases, as well as NFκB-p50.

usually performed by protein kinase A (PKA), which is bound to the cytosolic IκB:NFκB complex in an inactive state [98, 99]. Release of NFκB during the inflammatory response also releases PKA, which subsequently phosphorylates p65 at S276. This phosphorylation induces conformational changes in p65 that facilitate the interaction with transcriptional co-activators such as the cAMP response element-binding protein (CREB)-binding protein (CBP) or the homologue p300, which are histone-acetyltransferases (HATs) that acetylate p65 or induce chromatin opening by acetylation of histones [100]. Several kinases have been identified in phosphorylation of S468 in the p65 TAD, which have differing impacts depending on the cellular context or cell-type. This includes GSK3β, which phosphorylates p65 in unstimulated cells to negatively regulate the p65 basal activity, as well as IKKβ, which has been shown to phosphorylate p65 leading to a slight inhibition of p65 activity [101, 102]. Inhibition of p65 transcriptional activity via S468 phosphorylation is sought to be related to increased

interaction with the histone deacetylase general control non-depressible protein 5 (GCN5), which deacetylates histones leading to chromatin closure. In addition, GCN5 has also been shown to facilitate the recruitment of an E3-ubiquitin ligase complex to the promoters of target genes, inducing p65 ubiquitination and degradation, limiting the p65 transcriptional response in a gene specific manner [103, 104]. However, p65-S468 phosphorylation by IKKε has also been shown to increase the transcriptional activity of p65 upon co-stimulation of T-cells, demonstrating the cell-type specificity of the functionality of p65 phosphorylation [105]. Similar to S468, phosphorylation of p65 at S536 also induces enhanced transactivation by increasing the interaction of p65 with CBP/p300, inducing chromatin opening and p65 acetylation [106]. However studies in mice have also correlated increased S536 phosphorylation in macrophages with reduced p65 stability, supporting the resolution of inflammation [107]. Phosphorylation of p65 at S536 has been linked to the activities of a variety of kinases including IKKα/β and ε and ribosomal S6 kinase 1 (RSK1) [108–111]. Similar to p65 phosphorylation, acetylation of p65 leads to different functional outcomes depending of the acetylation site [112, 113]. p65 is known to be acetylated at K122, K123, K218, K221 and K310 by CBP/p300. Acetylation on K310 is known to enable binding of the bromodomain-containing protein 4 (Brd4), which in turn serves as a transcriptional coactivator and recruits and activates the positive transcription elongation factor b (pTEFb), thereby having a particularly important function in the regulation of NFκB-dependent target genes [114]. However, p65 can also be monomethylated at K310 by the protein lysine methyltransferase SET-domain containing 6 (SETD6) [115]. Methylation of p65 on K310 recruits the euchromatic histone-lysine N-methyltransferases 1 (EHMT1 or GLP), which represses the NFκB transcriptional activity at target genes under basal conditions. Of note, activation of NFκB and the concomitant phosphorylation of S311 by the protein kinase C ζ-type (PKCζ) competes with methylation of K310 by SETD6 [116]. Acetylation of p65 at K218 and K221 has been shown to increase the NFκB response by inducing DNA-binding and decreasing the interaction with nuclear IκB proteins, inhibiting re-translocation of NFκB to the cytoplasm [117]. In contrast, acetylation of p65 at K122 and K123 has been shown to decrease the NFκB DNA-binding affinity, facilitating the re-capture of NFκB by IκB proteins and terminating the NFκB response [118].

1.4.2 Modulation of AP-1 activity

The AP-1 transcription factor is mainly composed of the members of the Jun and Fos family of transcription factors cJun and cFos. Additional members of the Jun and Fos family are JunB and JunD and FosB, FosL1 and FosL2, respectively. However, members of the Jun family can also interact with the activating transcription factor (ATF) family of proteins. Dimerizing occurs via the basic region leucine zipper (bZIP) domain of these proteins, which is also implied in DNA binding [119]. Similarly to the p65:p50 heterodimer, the cJun:cFos dimer has the highest DNA-binding activity and stability of the possible AP-1 complexes [120]. cJun can also form homodimers, albeit with lower DNA-binding activity [121, 122]. In contrast, Fos proteins cannot dimerize with themselves but need to be in complex with a Jun protein in order to bind to DNA. The activity of cJun is largely regulated by JNK via phosphorylation of residues in the transactivation domain of cJun [123–125] (Fig. 7). Upon binding to the JNK docking motif close to the amino-terminus of cJun, JNK phosphorylates S63, S73, T93 as well as T95 in order to increase interaction of cJun with transcriptional co-factors [126, 127]. As part of cJun turn-over, T239 and S243 form a phosphodegron motif, which is positioned close to the DNA-binding domain of cJun [128]. After priming of cJun S243 by JNK, GSK3β is thought to recognize this priming site and induce phosphorylation of T239 [129, 130]. After phosphorylation of both residues, this phosphodegron serves as a motif for the FBW7 ubiquitin ligase, which ubiquitinates cJun in order to induce its degradation. In addition, phosphorylation of these residues has been shown to reduce the DNA-binding affinity of cJun. Interestingly, while low levels of JNK activity lead to a strong cJun activation, high and sustained activation of JNK is known to negatively regulate cJun activity and protein levels by phosphorylating T239 and S243 independently of GSK3β activity [131]. In contrast to the NFκB transcription factor, cJun and cFos are present in the cell only in low levels under basal condition and are rapidly upregulated on an expressional level upon pro-inflammatory induction. Thus, the *cjun* and *cfos* genes are also termed immediate early response genes [132, 133]. cJun is known to auto-induce itself, in addition, the cFos promoter contains a NFκB binding motif, leading to a rapid and strong upregulation of cJun and cFos levels upon stimulation with TNF [134, 135]. Unlike p50 in NFκB, cFos contains a transactivatory potential, which is stimulated by phosphorylation of T232, T325, T331 and T374 by the ERK MAPK [136].

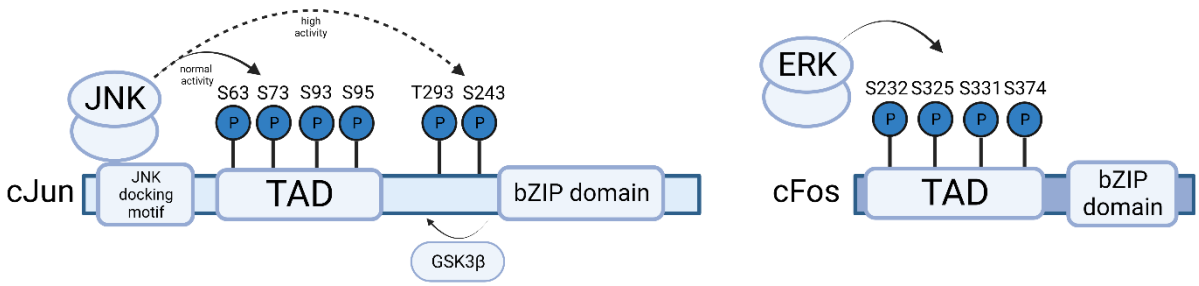

Figure 7. Representation of the domain structure of cJun and cFos with phosphorylation sites. Normal JNK activity leads to phosphorylation of TAD, thus activating cJun. High JNK activity can also phosphorylate a phosphodegron motif, leading to cJun inactivation and degradation.

Taken together, NFκB and AP-1 induce the expression of a multitude of pro-inflammatory target genes. During the initial inflammatory response, this entails the upregulation of chemokine and cytokine secretion by tissue sentinel cells, which attract leukocytes circulating in the blood stream to the site of inflammation and activate the immediate cellular environment in a pro-inflammatory manner.

1.5 The vascular endothelium and the leukocyte adhesion cascade

The vascular endothelium, which lines the insides of the blood vessels has a crucial role in the inflammatory response because it serves as a scaffold for interaction with leukocytes in order to enable leukocyte extravasation into the underlying inflamed tissues. Exposure of endothelial cells to cytokines such as TNF and the resulting pro-inflammatory signaling cascades induce the upregulation or redistribution of cell adhesion molecules (CAMs) on the endothelial surface for interaction with leukocytes. This includes members of the selectin family, E-selectin, L-selectin and P-selectin, members of the immunoglobulin superfamily such as the intracellular adhesion molecule 1 (ICAM-1), the vascular cell adhesion molecule 1 (VCAM-1), but also the platelet and endothelial cell adhesion molecule 1 (PECAM-1), the junction adhesion molecules A to C (JAM-A to JAM-C), the endothelial selective adhesion molecule (ESAM) and the non-immunoglobulin molecule CD99. These factors act together to enable the tightly regulated steps of the leukocyte adhesion cascade in the form of initial capture and rolling of the leukocytes on the endothelial surface, the firm arrest of leukocytes and the transmigration of leukocytes through the endothelial layer [137]. First capture and rolling of the leukocytes is enabled primarily by the selectins, which are rapidly expressed upon inflammatory

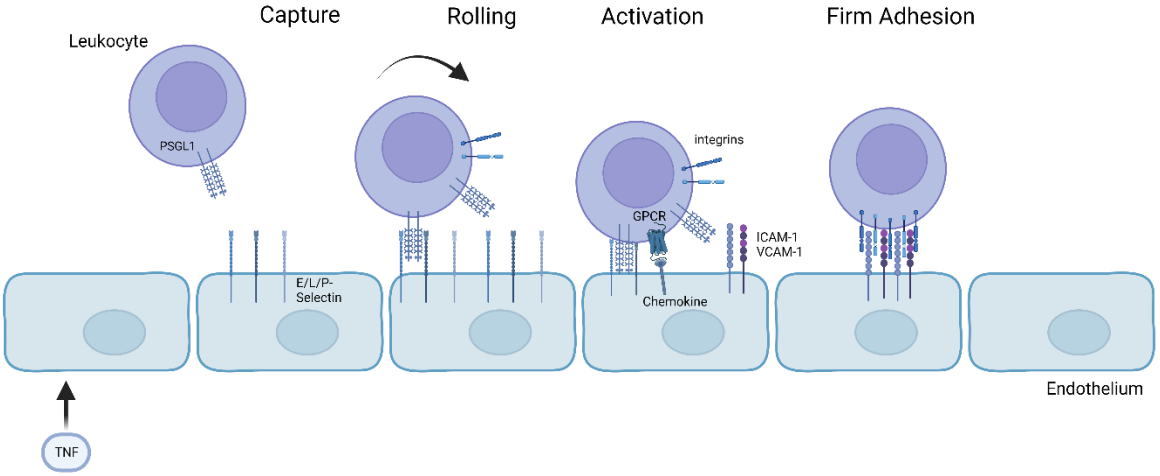

Figure 8. The leukocyte adhesion cascade represented by initial capture, rolling, activation and firm adhesion of leukocytes on the TNF-activated endothelium.

induction (Fig. 8). L-selectin is expressed by most leukocytes, but E-and P-selectin are exclusively expressed by activated endothelial cells [138]. These adhesion molecule interact with the P-selectin glycoprotein ligand 1 (PSGL1) on the surface of leukocytes, but also other glycosylated ligands [139]. The interaction of selectins with PSGL1 enables binding of the leukocyte under blood flow conditions, because of the high on/off rate character of this interaction, as well as the fact that binding of PSGL1 to L- and P-selectin is strengthened under shear stress [140–143]. The integrin binding partners of ICAM-1 and VCAM-1, termed lymphocyte function-associated antigen 1 (LFA-1, β_2 integrin) and very late antigen 4 (VLA-4, $\alpha_4\beta_1$ integrin), respectively, also participate in rolling of non-activated leukocytes [144–146]. Upon rolling on the endothelium, the leukocytes come in contact with chemokines expressed by the endothelial cells or deposited on the endothelial surface by immune cells, like CXCL or CCL

proteins, which bind to G protein-coupled receptors (GPCRs) on the surface of leukocytes, inducing a switch of the integrins LFA-1 and VLA-4 from a low-affinity state that enables rolling to a high-affinity states, which induces the firm arrest [147, 148]. The intracellular signaling events leading to the conformational changes in LFA1 and VLA4 are poorly understood, but entail GPCR induced activation of phospholipase C (PLC), the activation of small GTPases, as well as the induction of conformational changes in LFA1 and VLA4 by the intracellular association with actin-binding proteins like talin-1 [149–153]. Upon firm arrest of the leukocytes, the adhesion is further strengthened by signaling events in the leukocytes and endothelial cells, leading to a clustering of the integrins and ICAM-1 and VCAM-1 on the endothelium. The transmigration of leukocytes through the endothelium can either occur via a paracellular route (through cellular gaps) or a transcellular route (through endothelial cells; Fig. 9). The transmigration is preceded by the ICAM-1-dependent crawling of the leukocytes on the endothelium in

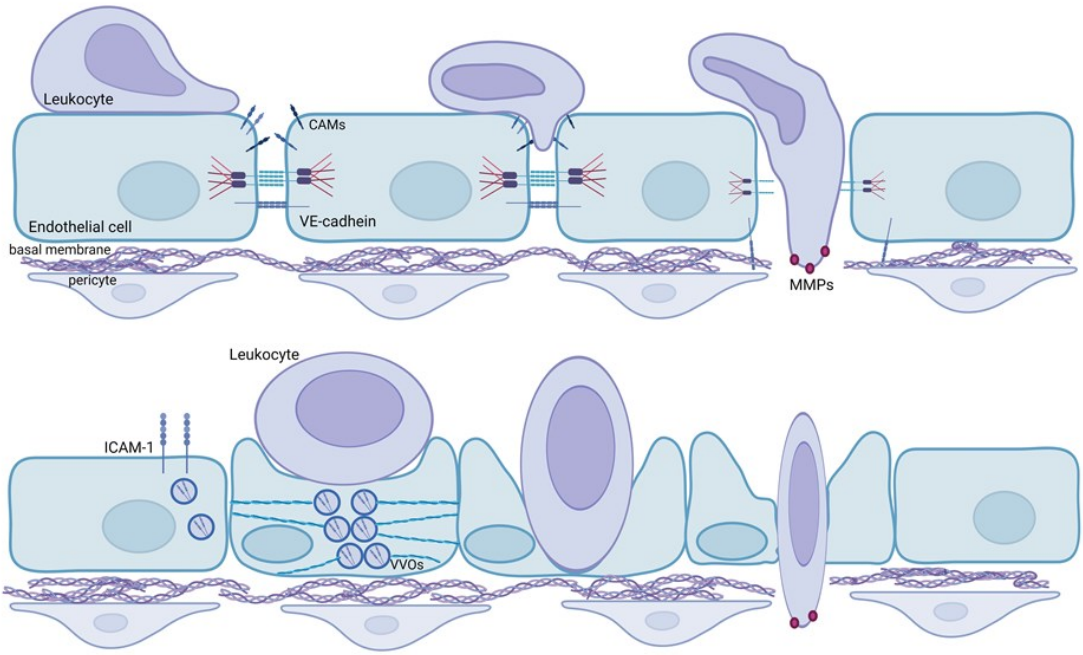

Figure 9. Paracellular (top) and transcellular (bottom) migration of leukocytes through the endothelium. In the paracellular migration, leukocytes follow a CAM gradient into the endothelial gap. Cadherins are transported off the gap, and the leukocyte migrates through the opened junction, where the underlying extracellular matrix (ECM) is thin due to the localization of pericytes. Transcellular migration is correlated with caveolin-based ICAM-1 uptake and the production of VVOs that form a channel trough the endothelial cell. ECM components are degraded by matrix metalloproteases (MMPs) on the leukocyte surface, facilitating the extravasation.

order to seek sites of preferred transmigration marked by chemoattractants, which induce transcellular migration, or the presence of endothelial gaps, which are rich in PECAM-1 and JAM-A, guiding the leukocytes to the endothelial junctions [154–158]. Many of the CAMs involved in the leukocyte adhesion cascade induce paracellular transmigration, like ICAM-1, JAM-A to JAM-C or ESAM and CD99 [158]. Upon binding to their ligands, these endothelial CAMs induce intracellular signaling events leading to the loosening of the endothelial cell junctional contacts, contraction of the endothelial cells and redistribution of surface markers such as VE-cadherin, which oppose leukocyte transmigration [159]. Compared to the paracellular migration through endothelial gaps, the transcellular migration occurs less frequently and is related to the presence of so called vesiculo-vacuolar organelles (VVO),

which are small passageways in endothelial cells suggested to act as a ‘gateway’ for transcellular migration [160, 161]. Clustering of ICAM-1 triggers intracellular signaling in endothelial cells that induce the caveolin-1-based uptake of ICAM-1 and redistribution of these vesicles to the VVOs, which subsequently form an F-actin stabilized channel through the endothelial cell [156, 162]. Upon passing the endothelial layer, leukocytes have to cross the underlying basement membrane and pericyte sheath. The endothelial basement is largely constituted by extracellular matrix (ECM) proteins like collagen and laminins. Pericytes contribute to the formation of the ECM and gaps between pericytes co-localize with decreased levels of collagen and laminins [163]. These sites represent the path of least resistance for the migrating leukocytes and might also facilitate the migration by permitting increased levels of chemoattractants produced in the underlying inflamed tissue. The expression of matrix metalloproteases (MMPs) on the surface of the leukocytes further facilitates migration of leukocytes through the endothelial basement membrane.

Due to their importance in the leukocyte adhesion cascade, the TNF-based upregulation of the CAMs E-selectin, ICAM-1 and VCAM-1 involved in first capture, rolling and firm adhesion are of crucial importance for enabling the inflammatory response via the leukocyte adhesion cascade. The genes of E-selectin, ICAM-1 and VCAM-1 all contain binding sites for NFκB and AP-1 in their promoters.

1.6 Cell adhesion molecule induction

1.6.1 Cell adhesion molecule promoters and transcriptional regulation

Induction of the *e-selectin* (*e-sele)*, *icam-1* and *vcam-1* genes is highly dependent on the activity of NFκB and AP-1. Consequently, the promoters of all of these genes contain binding motifs for NFκB and AP-1 and, depending on the gene, several other motifs for additional pro-inflammatory transcription factors [164–167] (Fig. 10). The promoter of *e-sele* contains one AP-1 binding site as well as three successive NFκB binding motifs. Compared to *icam-1* and *vcam-1*, the *e-sele* promoter is small, representing the fast response character of this gene upon pro-inflammatory induction. The *icam-1* promoter contains four AP-1 binding motifs that in part also serve as antioxidant-response elements (ARE), but only one NFκB binding site, indicating increased sensitivity to AP-1 induction. In addition, the *icam-1* promoter contains an interferon-response element (IRE) for binding of STAT transcription factors [168]. The *vcam-1* promoter only contains one AP-1 binding motif, but two adjacent NFκB binding site close to the TATA-box and an additional IRF-1 binding motif downstream of the TATA-box [169, 170]. In addition, the *vcam-1* promoter also contains two GATA transcription factor binding sites [171]. While the three CAM promoters show variable sensitivity to different transcription factors, binding of NFκB to its respective binding sites in the promoters of the CAMs has been shown to be of crucial importance for full CAM induction [165, 167, 172–176]. Of note, the promoters of the *e-sele* and *vcam-1* genes contain one TATA-box for transcriptional induction in their promoters, while the *icam-1* promoter contains an additional TATA-Box upstream of the TSS, indicating further means of transcriptional regulation. The presence of these transcription factors in the promoters of the CAMs (or

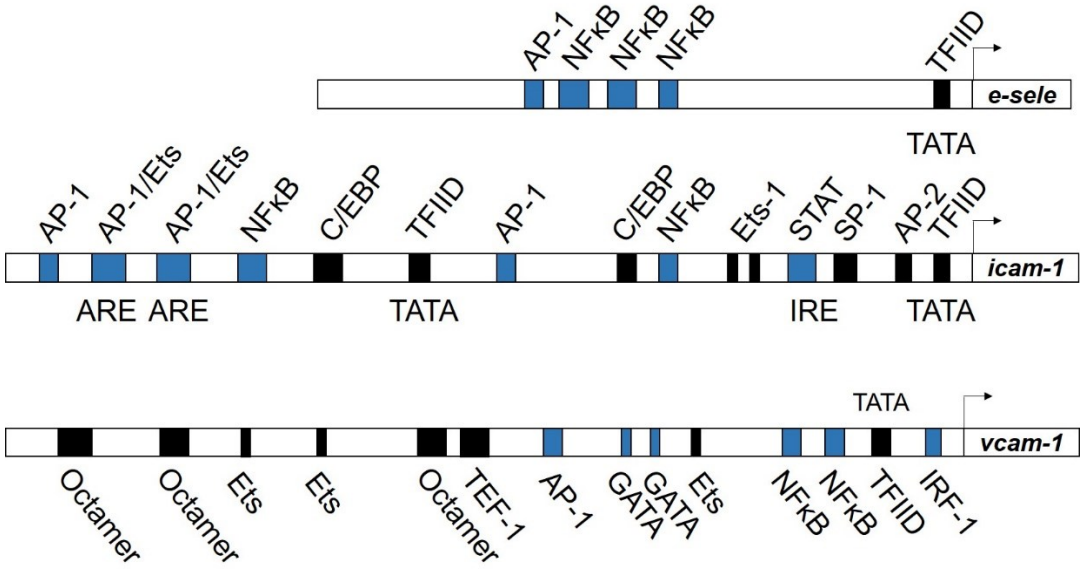

Figure 10. Schematic representation of the promoter structure of *e-sele*, *icam-1* and *vcam-1*. In addition to the pro-inflammatory transcription factor motifs, the *icam-1* and *vcam-1* promoters contains several additional motifs for C/EBP, Ets, SP-1, AP-2, octamer and TEF-1 factors.

in other genes) induce the formation of the pre-initiation complex (PIC), which consists of the RNA polymerase II (Pol II) and several general transcription factors, like the transcription factor II D (TFIID),

which directly binds to the TATA-box via its TATA-binding protein (TBP) subunit [177]. The PIC is also important for positioning the Pol II close to the transcription start site (TSS), denaturing the DNA and positioning of the DNA in the active center of the Pol II to enable transcription [178]. Successful initiation of transcription also involves association of the PIC with the mediator complex, which serves as a transcriptional co-activator and consists of a variety of different proteins that connect the transcription factors in the core promoter with the RNA polymerase and also binds to enhancer elements that regulate transcription far off the core promoter elements [179, 180]. Exit of the Pol II from the initiation site is induced by phosphorylation of the carboxy-terminal domain of Pol II in form of S5 phosphorylation by TFIIH (cyclin-dependent kinase 7; CDK7) [181]. Upon phosphorylation, the Pol II moves into the non-translated region following the TSS and is stalled, in order for additional regulatory mechanism to occur that induce productive elongation of the target gene.

1.6.2 Post-promoter regulation of transcription

The recruitment of the Pol II to the promoter of target genes has largely been believed to be the rate limiting step in transcription. However, more recent studies suggest that in many inducible mammalian genes, Pol II is kept in a stalled state approx. 20 to 70 nucleotides downstream of the TSS and that activation of the stalled Pol II represents the rate limiting step in transcription [182–186]. Several additional factors have been implied in stalling and release of the stalled Pol II, which either directly interact with the Pol II or participate in modification of the chromatin environment in form of HATs or histone methyltransferases (HMTs). In general, stalling of Pol II has been associated with the presence of active histone modifications like trimethylation of lysine 4 on histone 3 (H3K4me3) and acetylation of H3 lysine 9 and 14 (H3K9ac and H3K14ac), indicating that stalling might provide the basis for generation of an active chromatin environment [183]. Additional studies suggest that stalling of Pol II might assist in 5'-capping of the nascent mRNA [187]. Stalling is mainly induced by the interaction of Pol II with the negative elongation factor (NELF) and the DRB sensitivity-inducing factor (DSIF) [188, 189]. While NELF also binds to the nascent mRNA, DSIF only interacts with Pol II. The release of Pol II from its stalled state is induced by interaction with the positive elongation transcription factor b (pTEFb), consisting of CDK9 and cyclin T [190, 191]. Most of the pTEFb is present in an inactive state in the nucleus of cells by association with a 7SK RNA complex and HEXIM1 [192]. Certain signaling cues in form of nuclear phosphatases can inactivate this complex and release pTEFb. pTEFb is then recruited to the stalled Pol II and phosphorylates NELF and DSIF, which induces conformational changes that release the bound NELF and induces DSIF to become a positive transcription factor. In addition, CDK9 phosphorylates the S2 residues in the carboxy-terminal domain of Pol II, initiating the release of the stalled Pol II to enter productive elongation. The phosphorylated DSIF and pTEFb remain associated with the elongating Pol II to further stimulate productive transcription, which is assisted by the presence of additional factors like eleven-nineteen lysine-rich in leukemia (ELL) and elongin [182] (Fig. 11).

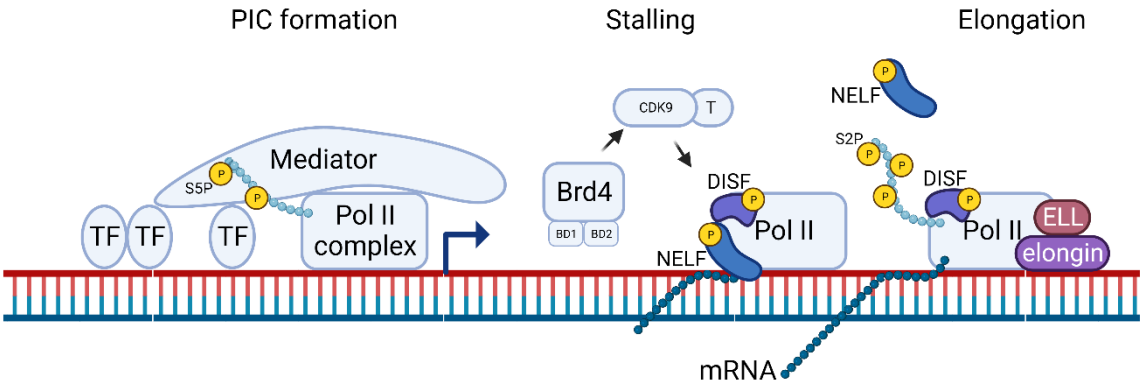

Figure 11. After formation of the PIC the Pol II will exit the promoter and stall in the untranslated region due to the actions of NELF and DSIF. pTEFb consisting of CDK9 and cyclin T is recruited and activated by Brd4, inducing phosphorylation of both proteins and initiation of productive elongation, which is marked by S2-phosphorylation of the Pol II carboxy-terminal domain.

Especially for NFκB-dependent target genes, the presence of additional factors like Brd4 has been shown to be of crucial importance for initiating transcription [193]. Brd4 is a member of the bromodomain and extra terminal domain (BET) family of proteins. Brd4 consists of two bromodomains (BD1 and BD2) that recognize and bind to acetylated lysin residues [194, 195]. Brd4 has been shown to directly recruit and activate pTEFb in order to induce the release of the stalled Pol II [196]. Additional studies have also implied Brd4 in directly phosphorylating the S2 residues in the stalled Pol II, as well as having an acetyltransferase function in order to evict nucleosomes from chromatin and induce chromatin opening [197, 198]. In general, Brd4 binds to acetylated histones and is thought to play a role in maintaining the epigenetic 'memory' [199]. However, newer studies have shown that Brd4 can directly interact with NFκB acetylated on K310 and induces transcriptional elongation by the recruitment and activation pTEFb at NFκB-dependent target genes [114]. In addition, Brd4 is also implied in interacting with several other co-factors that enable chromatin opening and constructive elongation during transcription, like the histone acetyltransferase p300, the histone demethylase jumonji domain containing 6 (JMJD6), as well as the chromodomain-helicase-DNA-binding protein 4 (CHD4), a member of the nuclear remodeling and deacetylase repressor complex [200–202].

1.7 Anti-inflammatory drugs

The occurrence of SCI and the resulting morbidities demonstrates the necessity for anti-inflammatory drugs. In general, such drugs can largely be divided into corticosteroids, nonsteroidal anti-inflammatory drugs (NSAIDs), disease-modifying anti-rheumatic drugs (DMARDs) and further anti-inflammatory natural products.

1.7.1 Corticosteroids

Corticosteroids are a class of steroid hormones that are released by the adrenal cortex and primarily have a role in the glucose, fat and protein metabolism in the body [203]. While the corticosteroids, which are released by the adrenal gland, comprises mineralocorticoids as well as glucocorticoids (GCs), the term corticosteroids is commonly used to refer to the latter [204]. GCs act by binding to the glucocorticoid receptor (GR) in the cytoplasm of cells. In the inactive state, the GR is localized in the cytoplasm of the cells as part of a multiprotein complex with chaperone proteins and immunophilins [205]. Binding of a GC induces conformational changes in the complex and phosphorylation of the GR leading to the release of the GR, exposure of nuclear translocation signals and subsequent translocation into the nucleus. The dimerized form of the GR binds to the palindromic GR element (GRE) and induces the expression of anti-inflammatory genes [206]. Apart from the GRE, a negative GRE (nGRE) DNA-binding element has been identified, which confers GC-dependent repression of pro-inflammatory target genes, by recruitment co-repressors and histone-deacetylases (HDACs) [207]. Genome-wide studies of the binding behavior of the GR have also shown a transrepressional influence on the NFκB and AP-1 induced expression of pro-inflammatory target genes. This genome wide repression of pro-inflammatory target genes is accomplished by either direct interaction of the GR with NFκB and AP-1 or by binding of the GR in close proximity to the NFκB and AP-1 DNA binding sites [208–210]. Since the first use of GCs in the treatment of rheumatic arthritis in 1949, efforts have been undertaken to minimize the site effects of the synthetic GCs (i.e. hydrocortisone, prednisolone) in treatment of SCIs. Nevertheless, the usage of GCs is associated with a large number of adverse effects (AEs), which minimize the clinical applicability of GCs. Commonly known AEs that correlate with the usage of GCs are weight-gaining, skin-thinning, insomnia, neuropsychiatric disorders and osteoporosis [211].

1.7.2 Nonsteroidal anti-inflammatory drugs (NSAIDs)

Another class of anti-inflammatory agents are the nonsteroidal anti-inflammatory drugs (NSAIDs), which circumvent many of the AEs associated with the use of GCs. While the first use of NSAIDs in the treatment of inflammation can be traced back thousands of years to the use of extracts of the willow bark and leaves, the active ingredient, today known to be salicin, has only been identified in the late 17th century [212–214] and has led to the development of acetylsalicylic acid (Aspirin) in the late 19th century [215]. However, the actual mechanism underlying the anti-inflammatory effects of aspirin are only known since the 1970s when Vane *et al*. discovered that aspirin inhibits the cyclooxygenase-1 (COX-1) enzyme, which induces the synthesis of the prostaglandins [216]. The lipids of the prostaglandin family are known to be involved in the induction of pain, fever and inflammation, as well as the prevention of gastric damage by protecting the gastric mucosa. These discoveries also explained the most common AE known to be associated with the usage of NSAIDs, which is gastric toxicity and the formation of stomach ulcers. The following discovery of the inducible COX isoform COX-2, which is functionally implicated to play a more important role in inflammation than in gastric protection, as well as the finding that aspirin non-specifically inhibits both isoforms, paved the way for selective COX-2 inhibitors, also termed coxibs (i.e. celecoxib) [217, 218]. These were thought to evade the gastric toxicity of the non-specifical NSAIDs. However, while clinical application of COX-2 inhibitors has shown that the selective targeting of COX-2 minimizes the risk of gastric toxicity, the risk for cardiovascular events (i.e. stroke and myocardial infarction) is increased. The increased risk for cardiovascular AEs due to COX-2 inhibitors is attributed to the inhibition of the endothelial production of COX-2 induced prostacyclins, while not inhibiting the COX-1 induced formation of thromboxane A2 in platelets, thereby increasing the risk for formation of blood clots [219, 220]. Today, NSAIDs are largely classified by their chemical structure and their selectivity for the COX isoforms. Apart from aspirin, further non-selective NSAIDs have been developed. These are comprised of non-acetylated salicylates (diflunisal, salsalate), propionic acids (naproxen, ibuprofen), acetic acids (diclofenac), enolic acids (meloxicam, piroxicam), anthranilic acids (meclofenamate, mefenamic acid) and naphthylalanine (nabumetone) [221]. Today, NSAIDs are the most commonly prescribed class of medications used for the treatment of pain and inflammation, responsible for up to 10 % of all medications prescribed worldwide [222, 223].

1.7.3 Disease-modifying anti-rheumatic drugs (DMARDs)

Disease-modifying anti-rheumatic drugs (DMARDs) are a class of immunomodulating and immunosuppressive agents. These drugs are mainly used in the treatment of inflammatory arthritides, like rheumatic arthritis (RA) and psoriatic arthritis as well as other inflammatory diseases like myositis, vasculitis, uveitis and inflammatory bowel disease (IBD). Each DMARD has a unique mechanism of action and influences specific inflammatory pathways. DMARDs can largely by subdivided into conventional and synthetic DMARDs (csDMARDs) and biological DMARDs (bDMARDs), which are selective for a molecular target. Commonly used csDMARDs used in treatment of RA include methotrexate (MTX) and hydroxychloroquine. MTX is a folic acid analog, which inhibits the 5-aminoimidazole-4-carboxamide ribonucleotide (AICAR) transformylase, involved in purine nucleotide synthesis. Inhibition of this enzyme leads to AICAR accumulation in the cell and a resulting inhibition of the adenosine deaminase. This in turn induces increased extracellular levels of adenosine [224–227]. The anti-inflammatory effect is thereby enacted by binding of adenosine to the leukocyte adenosine receptor reducing the chemotaxis of leukocytes, oxidative inflammation in neutrophils and monocytes and cytokine synthesis in monocytes and macrophages. In addition, MTX is known to inhibit the dihydrofolate reductase (DHFR), which catalyzes the reaction of dihydrofolate (DHF) to tetrahydrofolate (THF). THF acts as a methyl donor, which is essential for the formation of folate cofactors required for the purine and pyrimidine synthesis, with decreased THF levels leading to apoptosis of peripheral T-cells in RA [228]. The reduced levels of methyl donors by MTX are also thought to decrease the synthesis of polyamines (e.g. spermine and spermidine), involved in the induction of inflammatory pain and edema in RA, as wells as lymphotoxins, like ammonia and hydrogen peroxide [229, 230]. The anti-inflammatory mechanism of the antimalarial hydroxychloroquine (and also chloroquine) is poorly understood, but is thought to be correlated to regulation of cytokine production, stabilization of lysosomes and interference with antigen-presentation and TLR activation as well as beneficial metabolic and anti-atherosclerotic effects [231–233]. Additional csDMARDs that have shown to be effective in treatment of RA are leflunomide and sulfasalazine [234]. bDMARDs were first introduced in the 1990s and are used when the conventional therapy fails or in combination with csDMARDs. bDMARDs are comprised of monoclonal antibodies, chimeric humanized fusion antibodies or receptors that are fused to human immunoglobulins or small molecules. Due to their nature, these drugs are highly selective and usually interfere with cytokine production and function, as well as T-cell activation and B-cell depletion. These include TNF inhibitors (i.e. infliximab; a chimeric monoclonal antibody targeting TNF), IL-6 inhibitors (i.e. tocilizumab; a humanized monoclonal antibody targeting the IL-6 receptor), T-cell inhibitors (abatacept; a human fusion protein that targets CD80/86 costimulatory antigens, thereby inhibiting T-cell activation) and B-cell depleting agents (rituximab; a chimeric murine-human monoclonal antibody targeting CD20) [235]. Newer classes of synthetic, but specific small molecule DMARDs are the JAK inhibitors, like tofacitinib, a non-selective JAK inhibitor that inhibits STAT activity, or phosphodiesterase-4 (PDE-4) inhibitors, like apremilast

that is used in the treatment of psoriatic arthritis [236, 237]. Based on their diverse functions, DMARDs have several unique AEs. However, especially csDMARDs are known to increase the risk of infection, induce gastrointestinal distress, bone marrow suppression and hepatotoxicity.

In addition to the above-mentioned drugs, antibodies drugs have been established that directly target the leukocyte adhesion cascade in order to reduce leukocyte infiltration. This includes the monoclonal antibody drugs natalizumab, vedolizumab and crizanlizumab used for the treatment of multiple sclerosis, familial Mediterranean fever and Crohn's disease, ulcerative colitis or vaso-occlusive crisis in sickle-cell disease, respectively [238–241]. Natalizumab selectively binds to $\alpha_4\beta_1$ integrins, blocking the interaction with VCAM-1 or other $\alpha_4\beta_1$ binding molecules. Vedolizumab binds to $\alpha_4\beta_7$ integrins resulting in gut-selective inhibition of inflammation, and crizanlizumab binds to P-selectins reducing the effects of vaso-occlusive crisis during sickle-cell anemia.

1.7.4 Anti-inflammatory natural products (NPs)

The use of natural products (NPs) as a remedy for inflammation goes back to ancient times. Apart from the anti-inflammatory effects of salicins, a plethora of NPs with potential beneficial effects on health and in disease have been identified and have also set the basis for the synthesis of chemically synthesized analogues. These include plant derived anti-inflammatory NPs in the form of terpenoids, flavonoids, phenolic and polyphenolic compounds as well as sulphur-containing compounds [242], fungus-derived antibiotic compounds like penicillin [243] or marine-based NPs, like the saponines present in sponges [244]. The following gives a brief overview over some NPs involved in inhibiting the NFκB and MAPK based pro-inflammatory signaling cascades. One of the most studied and well-known plant-based and anti-inflammatory NP is curcumin, derived from the rhizome of the C*urcuma longa* plant. Curcumin has been shown to inhibit NFκB and MAPK signaling by directly targeting the IKK complex, as well as the MAPKs ERK, p38 and JNK, thereby reducing the inflammatory response [245–247]. Concomitantly, curcumin has been shown to inhibit the arachidonic metabolism, involved in pain response, COX activity as well as cytokine synthesis [248–252]. Another anti-inflammatory NP is the parthenolide, a sesqueterpene lactone found in Mexican medicinal plants and feverfew (*Tanacetum parthenium*) [253]. Parthenolide has been shown to have strong anti-inflammatory effects *in vivo* and is traditionally used as a treatment for fever, migraine and arthritis [254–257]. The anti-inflammatory effects of parthenolide have been shown to be based on inhibition of NFκB and MAPK activity, thereby reducing the expression of the pro-inflammatory nitric oxide (NO) synthase, CAMs as well as cytokines [258–262]. Another group of anti-inflammatory NPs are the flavonoids. These are phenolic compounds with variable structures that are distributed widely over the plant kingdom. These include flavones, flavanones, catechins and anthocyanins [263]. An example for a well-known and studied flavone is quercetin, found in plants like *Gingko biloba*. Quercetin has been shown to reduce interleukin levels and decrease the transcriptional activity of NFκB [264–266]. The diverse function and applicability of NPs is the result of the evolutionary adaption of organisms to their environment. Hence, while the essential metabolism of the biosynthesis and breakdown of carbohydrates, fats and proteins is very similar over different organisms (primary metabolism), NPs are usually the result of secondary metabolic pathways that organisms had to evolve to overcome the limitations in their surroundings [267]. Many of the most important secondary metabolites that give rise to NPs are derived from metabolic intermediates (also termed shunt metabolites) like acetyl coenzyme A, shikimic acid, mevalonic acid and 1-deoxyxylulose-5-phosphate. From an evolutionary perspective, it comes as no surprise that many secondary metabolites and hence NPs have been developed to defend an organism against other organisms. Some of the longest known and pharmaceutically used NPs that organisms produce for protection against other organism and that are widely distributed over the plant and prokaryotic kingdoms are the microtubule-targeting agents (MTAs), which target the eukaryotic microtubule cytoskeleton. MTAs have a long tradition in their usage against cancer as well as inflammatory diseases.

1.8 Microtubule-targeting agents (MTAs) and the microtubule cytoskeleton

Microtubule-targeting agents (MTAs) are a large and diverse family of chemical or biological agents that target the microtubule skeleton of eukaryotic cells. Based on their functionality, MTAs are subdivided into microtubule-stabilizing agents (MSAs) and microtubule-destabilizing agents (MDAs). Hence, these compounds alter the microtubule dynamics in favor of microtubule stabilization or destabilization.

1.8.1 Microtubule structure and dynamics

Microtubules are cytoplasmic based, hollow polymers, which consist of α- and β-tubulin heterodimers. They are involved in a variety of cellular functions like intracellular trafficking and positioning of organelles, cell shape and morphology, cell motility and migration as well as the assembly of the mitotic spindle apparatus and chromosome segregation during cell division [268, 269]. Tubulin is a 50 kDa GTP-binding protein with a globular structure. Each subunit in the heterodimer has the capability to bind GTP, but only the β-tubulin subunits have the ability to hydrolyze GTP during microtubule polymerization (Fig. 12). The soluble α- and β-tubulin heterodimers arrange into protofilaments, with

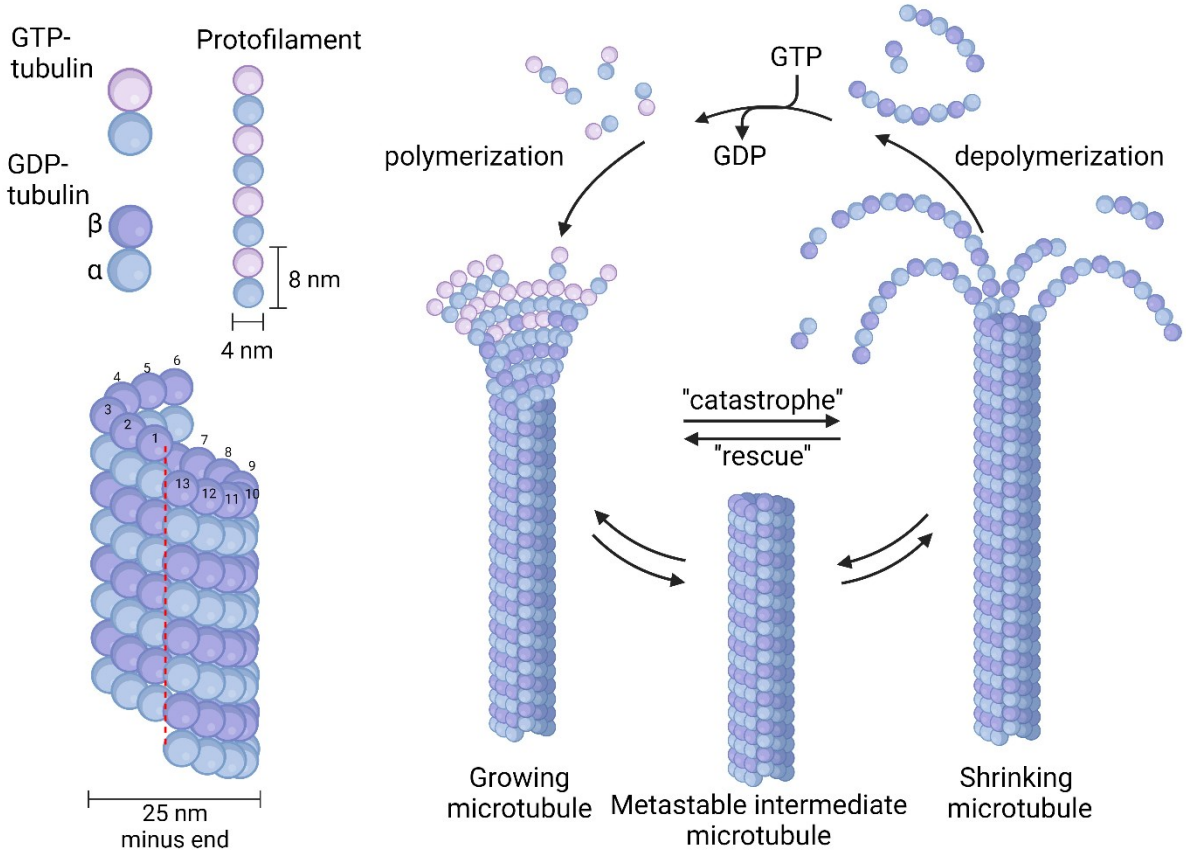

Figure 12. The structure of microtubules and microtubule dynamics. Both subunits in the α- and β-tubulin heterodimers can bind GTP, but only the β-subunits has a GTPase function. Tubulin heterodimers form protofilaments that arrange at the GTP-cap during microtubule polymerization to form a microtubule consisting of 13 protofilaments. During polymerization at the cap, GTP is hydrolyzed and the protofilaments arrange to the rigid, but unstable GDP-bound microtubule lattice. Low concentrations of free GTP-bound tubulin or increased hydrolysis of the cap lead to rapid microtubule depolymerization. The GDP in the β-tubulin subunits of the free heterodimers is exchange for GTP to again enable microtubule polymerization. Adapted from [269].

the prototypical microtubule having a width of approximately 25 nm and consisting of 13 filaments. Apart from the microtubule ”seam” (red dotted line in figure 12), each α- and β-tubulin subunit in the microtubule structure is positioned next the α- and β-tubulin subunit in the adjacent filament. Due to the polarity of the polymerized tubulin heterodimers, each microtubule has a minus end as well as a plus end, where polymerization and depolymerization occur. At their minus end, microtubules are usually stabilized by a microtubule-organizing center (MTOC). Microtubules are anchored to the MTOC via a ring of γ-tubulin, also termed γ-tubulin ring complex (γ-TuRC) that serves as a nucleator for tubulin polymerization. Additional proteins like the patronin family of proteins exist, which stabilize the microtubule around the MTOC, as well as anchoring proteins like ninein, which anchor the MTOC to compartments of the cell [270, 271]. According to the cap-model of microtubule dynamics and dynamic microtubule instability, GTP-bound tubulin heterodimers arrange at the plus end of the microtubule to form a GTP-tubulin-rich cap [272]. This cap stabilizes the more rigid, but under physiological tubulin concentration unstable underlying GDP-rich microtubule structure, also termed GPD lattice. If GTP in the cap is hydrolyzed too fast, or the GTP-bound tubulin heterodimers dissociate, the microtubule depolymerizes. This rapid depolymerization is also termed “catastrophe” and can be reversed by rearrangement of a GTP-tubulin cap, termed microtubule “rescue”. In case depolymerization occurs, the GDP in the β-tubulin subunits of the free tubulin heterodimers is replaced by GTP to enable further microtubule polymerization. Due to that, microtubules are under constant dynamics of polymerization and depolymerization, depending on the concentration of free GTP-bound tubulin heterodimers [273]. Two-models exist that aim at explaining the structural instability of the GDP-lattice based on conformational changes that occur in the tubulin heterodimers during GTP hydrolysis (Fig. 13). In the allosteric model, the GTP-bound heterodimers have a straight conformation. Hydrolysis of GTP during the microtubule polymerization induces conformational changes in the heterodimer, inducing a curved conformation. However, the structural incorporation of the filaments into the microtubules inhibits curvature of the heterodimers, thereby exerting allosteric strain and instability onto the microtubules [274]. In the lattice model, GTP- and GDP-bound tubulin heterodimers are both in a curved conformation and the incorporation into the microtubules during polymerization induces straitening of the dimers. In this model, conformational changes in the GTP-bound heterodimers in the GTP cap induce stronger lateral bonds or a lower bending stiffness between the filaments. GTP hydrolysis thereby induces conformational changes in the heterodimers that reduce the strength of the lateral bonds between the filaments or increase the overall bending stiffness, hence increasing microtubule instability [275–278].

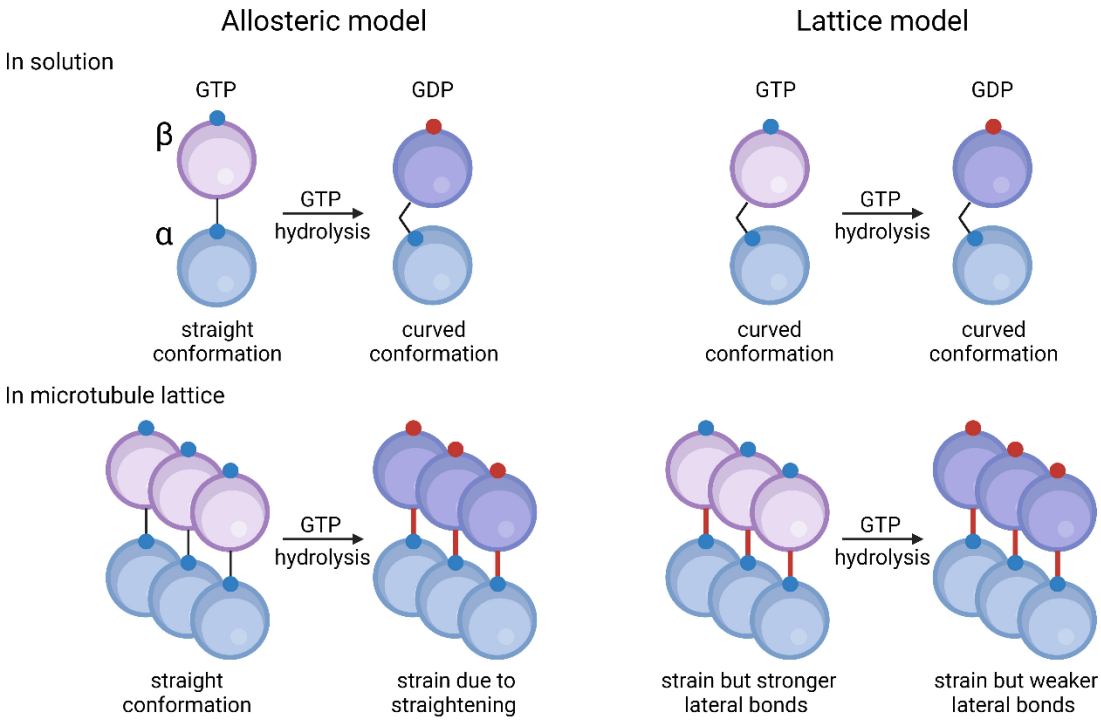

Figure 13. The allosteric and lattice model of conformational changes in the tubulin heterodimers that explain the instability of the microtubules. In the allosteric model, GTP hydrolysis induces a curved conformation in the heterodimers, which is straightened after incorporation into the microtubule lattice, thereby exerting strain (red line) and instability on the polymer. In the lattice model, GTP- and GDP-bound heterodimers both have a curved conformation. After incorporation into the lattice, both states are straightened, but conformational changes in the GTP-bound state increase lateral interactions between the filaments, which are lost after hydrolysis, thereby explaining the microtubule instability. Adapted from [273].

1.8.2 Microtubule-associated proteins (MAPs)

Several classes of proteins have been shown to interact directly with the microtubule skeleton. These microtubule –associated proteins (MAPs) can be involved in microtubule dynamics by either stabilizing or destabilizing the microtubules, capping proteins that stabilize the GTP cap, cross-linking proteins, which associate microtubules laterally, or cytoskeletal integrators that bind organelles to microtubules for spatial organization. In addition to proteins that are involved in microtubule dynamics, a variety of proteins are known to associate with the microtubule skeleton. This includes the microtubule motor proteins kinesin and dynein, which are involved in cellular transport, the associated dynactin complex as well as motor modulators like the tau and ensconcin proteins [279–282]. Several MAPKs like JNK have been shown to directly interact with the microtubule skeleton over JNK-interacting proteins (JIPs), which localize JNK to kinesin motor proteins [283]. JIP-1 has been shown to co-localize upstream MAPKs with JNK, thereby facilitating JNK activation [284]. Opposed to MAPK activation, many phosphatases have been shown to bind to the microtubules. This includes the general phosphatase 2 A (PP2A) or the JNK-specific phosphatase protein Ser/Thr metallophosphatase PPM1J (PP2Cζ) [285]. Association of many of the components involved in MAPK signaling is thought to provide the spatial localization important for proper signal integration as well as propagation.

1.8.3 The effects of MTAs on the microtubule dynamics

MTAs influence the microtubule dynamics by binding to the tubulin heterodimers. To this date, eight different binding sites for MTAs have been characterized depending on their position on the tubulin heterodimer. This includes the vinca site, the maytansine site, the laulimalide site, the taxane site, the colchicine site and the adjacent gatorbuline site as well as the pirotenin site and the adjacent todalam site (Fig. 14) [286]. Binding of an MSA to the taxane site either stabilizes the straight conformation of

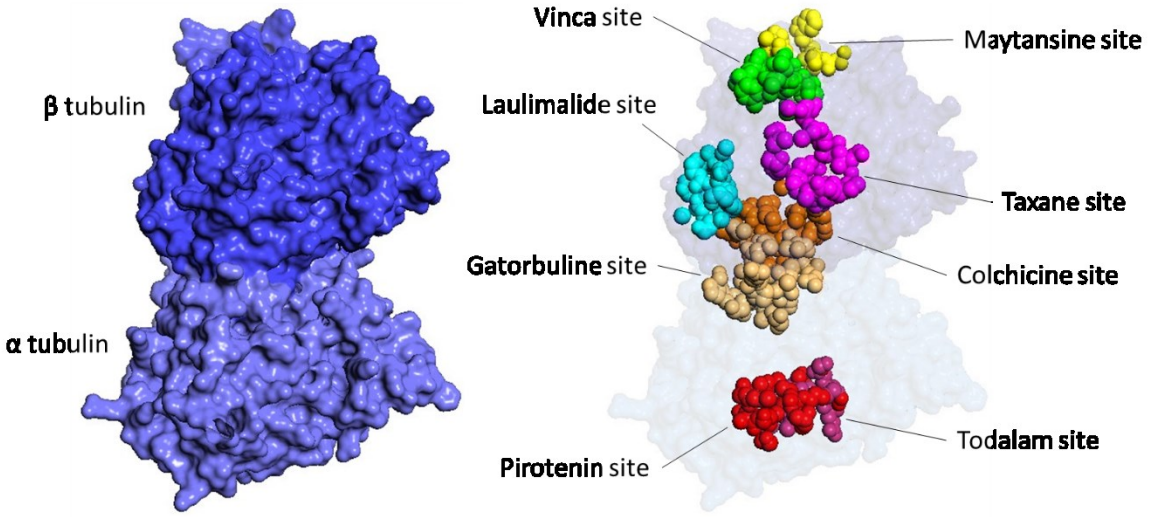

Figure 14. Sphere representation of the tubulin heterodimer (left) and transparent view of the heterodimer with colored contact surface involved in MTA interactions in sphere representation (right). Original structure; PDB: 1TUB, Maytansine site; PDB: 4TV8, vinca site; PDB: 5J2T, taxane site; PDB: 5LXT, laulimalide site; PDB: 4O4H, colchicine site; PDB: 4O2B, pironetin site; PDB: 5LA6, gatorbuline site; PDB: 7ALR, todalam site; PDB: 5SB5. Created with PyMOL.

the tubulin heterodimer (e.g. paclitaxel) or leads to conformational changes that promote the lateral interactions between the filaments in the microtubule (e.g. epothilone A), thereby stabilizing the microtubule cytoskeleton [287–290]. The laulimalide site is positioned at the lateral filament interface. Similar to the taxanes, binding of a laulimalide agent (e.g. laulimalide) also stabilizes the interaction between neighboring tubulin filaments [291, 292]. The colchicine site is positioned at the intra-dimer interface between the α- and β-tubulin subunits. Binding of a colchicine site-binding agent (e.g. colchicine) locks the tubulin heterodimer in the curved conformation by inhibiting conformational changes during the curved-to-straight transition [293, 294]. One of the best-studied MDA sites is the vinca site, which is positioned at the longitudinal interface between the tubulin heterodimers. Vinca site-binding agents (e.g. vinca alkaloids like vincristine) destabilize the microtubules by inducing a “wedge” at the top of the β-tubulin subunit, which prevents the straightening of the dimers and also promotes the formation of small helical tubulin polymers, thereby reducing the concentration of polymerization-competent free tubulin heterodimers [295]. In addition to these conformational changes, vinca site agents have also been shown to interfere with the GTP hydrolysis by hindering the alignment of the residues of the catalytic center necessary for hydrolyzation [296, 297]. The maytansine site is positioned

at the exposed inter-dimer interface on the β-tubulin subunit. Binding of a maytansine agent (e.g. maytansine) inhibits binding of additional tubulin heterodimers, thereby preventing polymerization [298]. Pirotenin is the only MTA that is known to exclusively interact with residues in the α-tubulin subunit. Pirotenin binds covalently to its binding pocket. Similar to the maytansine agents, pirotenin exerts its destabilizing effect by blocking the binding of the α-subunits to the β-tubulin subunit of another tubulin heterodimer [299, 300]. The gatorbuline and todalam sites are the newest MDA binding sites described on the tubulin heterodimer. Similar to the vinca agents, binding of gatorbuline or todalam is thought to induce a "wedge" in the heterodimer conformation, thereby preventing polymerization [301–303]. The gatorbuline site is position next to the colchicine site at the intra-dimer interface. Todalam is the first rationally designed MDA. The binding site of todalam is positioned on the β-tubulin subunit at the inter-dimer interface next to the pirotenin site and the maytansine site on the α-tubulin subunit of the following tubulin heterodimer.

1.8.4 The MTAs vincristine, paclitaxel and colchicine

The main mechanism of action of MTAs in the treatment of cancer is the interference with microtubule dynamics, the concomitant cell-cycle arrest and subsequent apoptosis that is especially affecting fast dividing cells, like cancer cells. However, especially colchicine has a long tradition in its use against inflammatory diseases.

1.8.4.1 The microtubule-destabilizer vincristine (VIN)

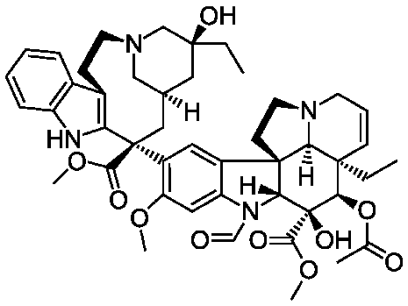

Figure 15. The structure of vincristine.

The secondary metabolite vincristine (VIN; Fig. 15) belongs to the family of the vinca alkaloids derived from the Madagascan periwinkle plant (*Catharanthus roseus*) [304, 305]. Like for all MTAs, the main mechanism of action for the MDA VIN is the interference with microtubule dynamics and the subsequent cell-cycle metaphase arrest [306]. VIN has been approved by the American food and drug agency (FDA) for the treatment of several malignancies like acute lymphatic leukemia (ALL), Burkitt lymphoma, B-cell ALL, lymphoid blast crisis of chronic myeloid leukemia, neuroblastoma, rhabdomyosarcoma, Wilms tumor, as well as Hodgkin and non-Hodgkin lymphomas. In addition, VIN is also used off-label for several further malignancies, i.e. central-nervous system tumors, sarcomas and lung cancer. Apart from their actions on cancer, vinca alkaloids have also been shown to affect malignant angiogenesis by inhibiting endothelial proliferation and chemotaxis necessary for new blood vessel formation [307]. Other vinca alkaloids that are in clinical use are the derivatives vinblastine, vinorelbine and vindesine. AEs that correlate with the usage of vinca alkaloids include peripheral neuropathy, due to the influence on axonal transport processes, as well as effects on physiological function that are related to fast cellular turn-over which lead to gastrointestinal toxicity, bone marrow suppression and alopecia [308].

1.8.4.2 The microtubule-stabilizer paclitaxel (PAC)

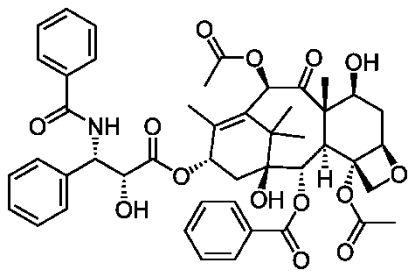

Figure 16. The structure of paclitaxel.

Paclitaxel (PAC; Fig. 16), which is sold under its trademark name Taxol is one of the most used anti-cancer agents. It is a secondary metabolite of the diterpene family originally isolated from the pacific yew (*Taxus brevifolia*) [309]. The main mechanism of action for PAC is the stabilization of the microtubule skeleton and the subsequent cell cycle arrest [310]. It is approved by the FDA for several malignancies like breast cancer, lung cancer and ovarian cancer and is also used for several other indications like esophageal and gastric cancers, as well as sarcoma and cervical cancers [311–315]. Apart from its effects on mitosis, PAC is assumed to also induce metabolic apoptosis by activation of p53, increase in reactive oxygen species (ROS) and

induction of proteins related to stress of the endoplasmic reticulum as well as a downregulation of the anti-apoptotic B-cell Leukemia 2 (Bcl-2) protein and upregulation of the pro-apoptotic Bcl-2-associated X protein (BAX) [316–321]. Like for other MTAs, AEs include neuropathy, bone marrow suppression, gastric toxicity and alopecia.

1.8.4.3 The microtubule-destabilizer colchicine (COL)

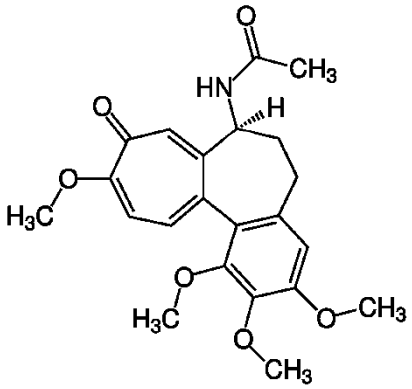

Figure 17. The structure of colchicine.

Colchicine (COL; Fig. 17) was first used in the form autumn crocus (*Colchicum autumnale*) to treat joint pain and swelling as early as 1500 B.C. [322]. While COL has been shown to have anti-cancer activity, its increased toxicity has historically excluded it from its pharmacological use in the treatment of cancer [323]. Nevertheless, COL is known for its therapeutical applicability in several inflammatory diseases like gout, familial Mediterranean fever (FMF), Behcet's disease, pericarditis as well as coronary artery diseases. On a molecular basis, COL has been shown to affect the formation of the inflammasome in leukocytes and to affect leukocyte migration by depolymerizing the microtubule skeleton necessary for migration and concomitant down-regulation of genes involved in the migration of leukocytes [324–327]. In addition, colchicine is known to affect the distribution of E-selectin in endothelial cells, thereby decreasing leukocyte adhesion [328]. Newer studies also show a reduced infarct incidence in atherosclerosis patients after colchicine treatment, by reducing the formation of aortic plaques due to decreased aortic inflammation in cells of the vascular endothelium [329, 330]. The AEs related to the use of COL are similar to those of other MTAs. However, COL is usually applied in lower concentrations compared to MTAs used during chemotherapy. The most common side effect is gastric toxicity, which usually leads to nausea, vomiting and diarrhea.

1.8.4.3.1 The anti-inflammatory effects of COL

COL is well known for its efficacy in the treatment of gout [331]. Hence, much of the knowledge concerning the biomolecular background of the anti-inflammatory effects of COL is the result of research on the effects of COL in the treatment of this disease. The central mechanism in acute gouty arthritis is the formation and precipitation of monosodium urate (MSU) crystals from uric acid in and around the joints of patients. MSU crystals have been shown to directly interact with the membrane of dendritic cells, leading to intracellular Syk kinase and dendritic cell activation [332]. In addition, MSU crystals have been shown to act as DAMPs and to directly bind to TLRs on the surface of immune and non-immune cells to induce MyD88-dependent NFκB-signaling cascades and the production of ROS [333–335]. TLR-induced activation of immune cells like neutrophils, macrophages, dendritic cells or mast cells usually leads to the expression of pro-inflammatory cytokines like TNFα, IL-1β or IL-6 [336, 337]. The expression of these cytokines induce the pro-inflammatory activation of endothelial cells in and around the joints, leading to the expression of the CAMs and leukocyte infiltration [338]. Additionally, MSU crystals can be internalized by immune cells via phagocytosis. Phagocytosis of MSU crystal induces phagolysosomal damage, leading to K^+ influx into cells. In the presence of the nucleotide-binding domain, leucine-rich repeat-containing 3 (NLR3) receptor, as well as the apoptosis-associated speck-like protein containing a caspase recruitment domain (ASC), the increased intracellular K^+ and ROS levels induce the formation of the NLRP3 inflammasome complex [339–341]. The active inflammasome complex processes the pro-caspase-1, leading to its activation and concomitant IL1β procession and activation. COL has been shown to inhibit the molecular mechanisms leading to MSU-crystal induced inflammation in gouty arthritis in a multimodular manner. Martinon *et al*. have shown that COL interferes with inflammasome activation via disruption of the microtubule skeleton, thereby preventing co-localization of mitochondria, where ASC is localized, with the endoplasmic reticulum, where NLR3 is localized [340]. While the primary effects of COL on leukocyte migration are thought to be based on microtubule disruption, Ben-Cherit *et al.* could show that long-term treatment with COL also inhibits the expression of factors involved in leukocyte migration [326], thereby minimizing systemic leukocyte chemotaxis. In addition, studies have shown that the effectiveness of the chemotactical inhibition in leukocytes after COL treatment are increased due to enrichment of COL in leukocytes [342]. Further studies by Ding *et al.* have correlated treatment with COL with decreased levels of the TNFR1 on macrophages and endothelial cells [343]. Jackman *et al.* reported that COL treatment and the concomitant microtubule disruption impeded the TNF-induced intracellular NFκB signaling, leading to decreased promoter activity of NFκB [344]. However, in this study, Jackman *et al.* showed that treatment of C2C12 muscle cells with 100 µM of COL for 4 h had no inhibitory effects on the NFκB promoter activity following 2 days of p65 overexpression and hence argued that COL must enact its effects prior to the release and degradation of IκBα. Roberge *et al.* and Chia *et al.* could show that COL reduced the MSU-induced production of ROS in neutrophils and hence impeded neutrophil activation [345, 346]. Cronstein *et al.* could show that treatment of neutrophils with COL decreased the

expression of L-selectin and in addition, that microtubule disruption in endothelial cells altered the qualitative display of E-selectin on the endothelial cell surface, thereby reducing leukocyte adhesion [328]. The beneficial effect of COL in patients with FMF has also been attributed to its inhibitory effects on the inflammasome. FMF is correlated to mutations in the MEFV gene on chromosome 16, which encodes the pyrin/marenostrin protein [347–349]. These mutations are known to induce a constitutively active form of the pyrin/marenostrin protein, hence leading to pathological inflammasome activation. The Behcet's disease is an inflammatory disorder that is characterized by auto-inflammation of blood vessels (vasculitis) leading to mucosal ulcers and arthritis [350]. COL is known to be effective in the treatment of Behcet's disease phenotypes involving pathological alteration of the skin, mucosa and joints [351–353]. However, the molecular basis for these effects is poorly researched. Newer clinical studies have shown beneficial effects of COL in patients with pericarditis, by minimizing the recurrence of pericarditis and post-pericardiotomy syndrome, as well as coronary artery disease and atrial fibrillation [354–357]. In addition, several clinical studies have shown the efficacy of COL in reducing the incidence of stroke in patients with high cardiovascular risk [329]. In one of the newest studies concerning the effects on COL on atherosclerosis, Meyer-Lindemann *et al.* could show that treatment with COL in mice with early atherosclerosis or post-myocardial infarction decreased the levels of leukocyte adhesion molecules and receptors for chemoattractants on neutrophils and macrophages, thereby reducing vascular inflammation [330]. Interestingly, Weng *et al.* showed that COL also acts selectively in the liver to increase the expression of anti-inflammatory hepatokines in hepatocytes, which systemically inhibit myeloid cell activation [358].

In conclusion, the main anti-inflammatory effects of COL are due to decreased chemotaxis of leukocytes, as well as an inhibition of the inflammasome complex and decreased intracellular NFκB signaling cascades, thereby reducing the expression of pro-inflammatory cytokines. Many clinical studies show beneficial effects of COL in treating inflammatory disorders. However, especially how COL or other microtubule-depolymerizers enact their effects on NFκB signaling and how MTAs affect the pro-inflammatory state in cells of the endothelium that act as a central interface for leukocyte infiltration in many inflammatory disorders, is still largely unknown.

1.8.5 The microtubule-destabilizer pretubulysin (PT)

The microtubule destabilizer pretubulysin (PT) constitutes a precursor of the tubulysins, which have initially been discovered in strains of the myxobaterium *Angiococcus disciformis*. It constitutes the first enzyme-free intermediate during biosynthesis of the tubulysins [359]. The tubulysins are synthesized by a polyketide synthase/non-ribosomal peptide synthetase pathway that produces linear tetrapeptides consisting of an amino-terminal N-methyl pipecolic acid, an isoleucine, as well as the unusual amino acid tubuvaline and an α-methylated aromatic γ-amino acid derived from tyrosine or phenylalanine. These tetrapeptides are known to bind to the vinca site of microtubules, thereby destabilizing the microtubule skeleton. However, the presence of a labile N,O-acetal group at the amino-terminus of tubuvaline limits the chemical accessibility of the tubulysins. In contrast, PT (Fig. 18) lacks this group

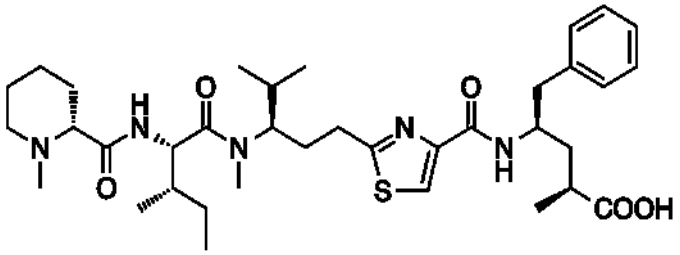

Figure 18. The structure of pretubulysin.

and can be synthesized in large quantities, while largely retaining the efficacy of the tubulysins in view of microtubule destabilization. PT has been shown to destabilize the microtubule cytoskeleton in endothelial cells already after 1 h treatment with 30 nM and to effectively depolymerize the entire endothelial microtubule network at a concentration of 300 nM [360].

1.8.5.1 Anti-cancer and anti-angiogenic effects of PT

In one of the first studies involving the effects of PT in view of its anti-cancer capabilities, Hermann *et al.* [361] could show that PT induces a significant mitotic G_2/M-phase arrest in human HepG2 hepatocellular carcinoma cells at concentrations starting at 50 nM following 24 h of treatment. Testing of the anti-proliferative effects of PT on human L3.6pl pancreatic cancer cells showed that already 5 nM of PT significantly reduces the clonogenic survival of the cells following 6 days of treatment. In addition, Hermann *et al.* proved that treatment of human U-2 OS osteosarcoma cells with 25 nM PT resulted in partial fragmentation of the nuclei and full depolymerization of the microtubule skeleton after treatment with concentrations of 50 nM of PT. The increased pro-apoptotic activity of PT in L3.6pl cells was shown to be partially based on the transiently increased phosphorylation and inhibition of the anti-apoptotic Bcl-2 protein, with significantly increased apoptosis already being observable after 48 h of treatment with 1 nM of PT. Additionally, PT was shown to significantly inhibit the fetal calf serum (FCS) induced migration of L3.6pl cells after treatment with a concentration of 1 nM and more. In a further study, Braig *et al.* [362] could show that the anti-proliferative effects of PT also extends to the

highly aggressive and metastatic T24 and MDA-MB-231 cancer cell lines, with PT inhibiting the proliferation of these cells after 72 h of treatment significantly with IC_{50} values of 1.6 nM and 2.4 nM, respectively. In addition, Braig *et al.* could show that the pro-apoptotic effects of PT in these cell lines are due to activation of caspase-8 and -3, as well as cleavage and activation of the BH3 interacting-domain death agonist (BID) protein and poly(ADP-ribose)-polymerase 1 (PARP), as well as increased Bax activity and cytochrome C release. By using an *in vivo* chicken chorioallantoic membrane (CHAM) model implanted with T24 cells as well as an *in vivo* mouse model with subcutaneously implanted MDA-MB-231 cells, Braig *et al.* could show that PT significantly inhibits the tumor growth and metastasis *in vivo* after treatment with 10 nM of PT over 3 days (CHAM model) or treatment with 0.1 mg/kg every second day for 4 weeks (mice xenograft model). In addition, Braig *et al.* found that the pro-apoptotic effects of PT also correlate to increased phosphorylation and degradation of the anti-apoptotic protein Mcl-1. Further studies concerning the anti-metastatic effects of PT by Schwenk *et al.* [363] showed that PT induces a retraction of endothelial cells leading to increased and β1-integrin-dependent interactions of MDA-MB-231 tumor cells with the underlying ECM, thereby reducing tumor cell transmigration and extravasation. Rath *et al.* [364] examined the anti-angiogenic effects of PT on human umbilical vein endothelial cells (HUVECs) and cells of the human dermal microvascular endothelial cell line-1 (HMEC-1) and found that PT inhibits the FCS induced migration and chemotaxis of HUVECs with an EC_{50} of 5.3 nM. Consequently, Rath *et al.* tested the Matrigel-based endothelial tube formation with HMEC-1 cells and found that treatment with 30 nM of PT over 16 h significantly reduced the formation of endothelial tubes compared to the control. In addition, by using an *in vivo* xenograft tumor model with hepatocellular carcinoma HUH7 cells, they could show that consecutive application of 0.1 mg/kg PT significantly reduced the mean tumor mass, as well as tumor neovascularization 16 days after xenograft implantation. In an up-following study, Kretzschmann *et al.* [360] extended on the anti-vascular properties of PT. They found that in addition to the depolymerization of the microtubules and the concomitant disassembly of cell–cell connections and retraction of endothelial cells, PT induces the formation of actin stress fibers by activation of the RhoA/Rho-associated protein kinase/myosin light chain pathway. Interestingly, they also found that extended treatment with PT induces slight, but fully reversible cytotoxic stress in endothelial cells. By employing an ectopic B16-F1 mouse melanoma tumor model, they could show that a single application of 10 mg/kg of PT and treatment for 24 h significantly reduced the tumor vessel perfusion and induces central necrosis in the tumor mass and that application of 10 mg/kg of PT every third day over 7 days significantly reduces the increase in tumor volume compared to the control animals.

1.9 Motivation and aims

The research on colchicine still leads to new finding of this very old drug in view of its anti-inflammatory potential. However, especially the effects that MTAs have on the interaction of leukocytes with the vascular endothelium during the leukocyte adhesion cascade as well as the underlying mechanisms that MTAs induce in the cells of the vascular endothelium are still largely unknown. The fact that clinical studies still find new therapeutical application areas for colchicine makes the research of the underlying mechanisms in endothelial cells worthwhile. On this basis, this study aimed at using the novel and potent MTA pretubulysin and the already clinically established MTAs colchicine, vincristine and paclitaxel, to elucidate the anti-inflammatory potential of these MTAs *in vivo* and to study their action *in vitro* in human umbilical vein endothelial cells (HUVECs) on the expression of the CAMs ICAM-1 and VCAM-1 as well as E-selectin. In addition, by utilizing pretubulysin, this study aimed at elucidating the underlying mechanisms that MTAs induce in endothelial cells to provide a baseline for future research of the anti-inflammatory effects of MTAs in the vascular endothelial cells.

To address these questions, the anti-inflammatory potential of PT is first tested in an *in vivo* psoriasiform dermatitis mouse model. To assess the influence of PT on the leukocyte adhesion *in vivo*, PT is tested towards its effects on the TNF induced adhesion of leukocytes in post-capillary venules of the mouse cremaster muscle. In addition, these results are confirmed in an *in vitro* leukocyte adhesion under flow model. Subsequently, PT and the additional MTAs VIN, COL and PAC are tested towards their potential influence on cell viability and protein translation in HUVECs in the *in vitro* cell culture setting. To analyze if the effects of PT and the additional MTAs are the result of an inhibition of the central and TNF-induced CAMs E-selectin, ICAM-1 and VCAM-1, flow cytometric experiments are performed and consolidated by western blot analysis and qRT-PCR analysis of the respective mRNA levels. Further analysis involves the assessment of the influence of PT on the main pro-inflammatory NFκB and AP-1 signaling pathways and MAPKs as well as the transcriptional activity of NFκB and AP-1 by utilizing western blot analysis and reporter gene assays. The influence of PT on the TNF-induced DNA binding behavior of NFκB and AP-1 to their respective binding sites in the CAM promoters are tested over time by chromatin immunoprecipitation and compared to the respective binding behavior of the RNA polymerase II. In addition, the effects of PT on the mRNA levels of the CAMs and several transcription factors are tested over time. Further analysis involves testing of the influence of the MAPK JNK on expression of the CAMs by utilizing the JNK inhibitor JNKIN8. Finally, the effects of PT on the presence of the bromodomain-containing protein 4 (Brd4) at the respective CAM promoters and genes are elucidated with and without inhibition of JNK by chromatin immunoprecipitation and the importance of Brd4 for the effects of PT on the CAM expression are analyzed by knock-down experiments.

2. Materials and Methods

2.1 Materials

2.1.1 Compounds

Pretubulysin was synthesized as previously described [PMID: 19431172] [365] and kindly provided by Prof. Dr. Uli Kazmaier. Colchicine (CAS 64-86-8), vincristine (CAS 2068-78-2) and paclitaxel (CAS 33069-62-4) were obtained from Biomol (Hamburg, Germany). The compounds were dissolved in DMSO to a concentration of 10 mM and stored at -20 °C. For experiments, compounds were further diluted in cell culture medium prior to application at the concentrations indicated in the figure legends, while not exceeding a final DMSO concentration of 0.01 % during treatment in *in vitro* assays.

2.1.2 Chemicals and reagents

Table 2. Chemicals and reagents used in this project.

Reagent	Supplier
1,4-Dithiothreitol (DTT)	Sigma-Aldrich Chemie GmbH, Taufkirchen, Germany
2-Mercaptoethanol	Sigma-Aldrich Chemie GmbH, Taufkirchen, Germany
Agarose Ultra-pure	ThermoFisher Scientific, Dreieich, Germany
Ammonium persulfate (APS)	Carl Roth GmbH, Karlsruhe, Germany
Bovine serum albumin (BSA)	Sigma-Aldrich Chemie GmbH, Taufkirchen, Germany
Bovine serum albumin (BSA, fraction V)	Sigma-Aldrich Chemie GmbH, Taufkirchen, Germany
Calcium chloride dihydrate, $CaCl_2 \cdot 2\ H_2O$	Carl Roth GmbH, Karlsruhe, Germany
CellTracker Green CMFDA dye	Life Technologies GmbH, Darmstadt, Germany
Dimethyl sulfoxid (DMSO)	Sigma-Aldrich Chemie GmbH, Taufkirchen, Germany
Disodium hydrogen phophate dihydrate, $Na_2HPO_4 \cdot 2\ H_2O$	Carl Roth GmbH, Karlsruhe, Germany
Disuccinimidyl glutarate (DSG)	SantaCruz Biotechnologies, Heidelberg, Germany
Ethylene glycol-bis(β-aminoethyl ether)-N,N,N′,N′-tetraacetic acid (EGTA)	Carl Roth GmbH, Karlsruhe, Germany
Ethylenediaminetetraacetic acid (EDTA)	Carl Roth GmbH, Karlsruhe, Germany
Formaldehyde (FA), 16 % ultrapure	Polysciences Europe GmbH, Hirschberg (Bergstraße), Germany

Table 2. Continuation of the chemicals and reagents used in this project.

Reagent	Supplier
Glycerol	Carl Roth GmbH, Karlsruhe, Germany
Glycine PUFFERAN ≥ 99 %, p.a.	Carl Roth GmbH, Karlsruhe, Germany
HEPES-potassium hydroxide (KOH)	Sigma-Aldrich Chemie GmbH, Taufkirchen, Germany
Herring sperm DNA	Promega GmbH, Mannheim, Germany
Hydrogen peroxide, H_2O_2 (30 % solution)	Sigma-Aldrich Chemie GmbH, Taufkirchen, Germany
Lithium chloride (LiCl)	Carl Roth GmbH, Karlsruhe, Germany
Luminol	Sigma-Aldrich Chemie GmbH, Taufkirchen, Germany
Magnesium chloride hexahydrate, $MgCl_2 \cdot 6\ H_2O$	Merck KGaA, Darmstadt, Germany
Sodium bicabonate, NaHCO3	Sigma-Aldrich Chemie GmbH, Taufkirchen, Germany
Nonidet P40 substitute (NP40)	Sigma-Aldrich Chemie GmbH, Taufkirchen, Germany
p-Coumaric acid ≥ 98.0 %	Sigma-Aldrich Chemie GmbH, Taufkirchen, Germany
peqGOLD dNTP-Set	VWR International GmbH, Darmstadt, Germany
peqGOLD Protein Marker IV, 10–170 kDa	VWR International GmbH, Darmstadt, Germany
Potassium chloride, KCl	Merck KGaA, Darmstadt, Germany
Potassium dihydrogen phosphate, KH_2PO_4	Carl Roth GmbH, Karlsruhe, Germany
Powdered milk (low fat, blotting grade)	Carl Roth GmbH, Karlsruhe, Germany
Propidium iodide (PI)	Sigma-Aldrich Chemie GmbH, Taufkirchen, Germany
Protein A/G magnetic beads	ThermoFisher Scientific, Dreieich, Germany
Pyronin Y	Sigma-Aldrich Chemie GmbH, Taufkirchen, Germany
Roti-Histofix 4 %	Carl Roth GmbH, Karlsruhe, Germany
Rotiphorese Gel 30	Carl Roth GmbH, Karlsruhe, Germany
Sodium chloride, NaCl	Carl Roth GmbH, Karlsruhe, Germany
Sodium deoxycholate ≥ 97 %	Sigma-Aldrich Chemie GmbH, Taufkirchen, Germany

Table 2. Continuation of the chemicals and reagents used in this project.

Reagent	Supplier
Sodium dodecyl sulfate (SDS)	Carl Roth GmbH, Karlsruhe, Germany
Spectra Multicolor High Range Protein Ladder 40-300 kDa	ThermoFisher Scientific, Dreieich, Germany
Tetramethylethylenediamine (TEMED)	Bio-Rad Laboratories GmbH, Munich, Germany
Tris hydrochloric acid (HCl)	Carl Roth GmbH, Karlsruhe, Germany
TRIS PUFFERAN ≥99.3 %	Carl Roth GmbH, Karlsruhe, Germany
Triton X-100	Merck KGaA, Darmstadt, Germany
Tween 20	Sigma-Aldrich Chemie GmbH, Taufkirchen, Germany

Table 3. Inhibitors used in this project.

Inhibitor	Supplier
Actinomycin D (ActD)	Sigma-Aldrich Chemie GmbH, Taufkirchen, Germany
cOmplete, Mini, EDTA-free Protease Inhibitor Cocktail	Roche Diagnostics Deutschland GmbH, Mannheim, Germany
Cycloheximide (CHX)	Sigma-Aldrich Chemie GmbH, Taufkirchen, Germany
JNK inhibitor, JNKIN8	Sigma-Aldrich Chemie GmbH, Taufkirchen, Germany
Phenylmethylsulfonyl fluoride (PMSF)	Sigma-Aldrich Chemie GmbH, Taufkirchen, Germany
Recombinant RNasin, Ribonuclease Inhibitor	Promega GmbH, Mannheim, Germany
Sodium fluoride, NaF	Merck KGaA, Darmstadt, Germany
Sodium orthovanadate, Na_3VO_4	Sigma-Aldrich Chemie GmbH, Taufkirchen, Germany
Sodium pyrophosphate	Sigma-Aldrich Chemie GmbH, Taufkirchen, Germany
Staurosporine	Sigma-Aldrich Chemie GmbH, Taufkirchen, Germany
β-Glycerophophate	Sigma-Aldrich Chemie GmbH, Taufkirchen, Germany

Table 4. Enzymes, enzyme mixes and protein reagents used in this project.

Reagent	Supplier
Interleukin-1β (IL-1β)	PeproTech GmbH, Hamburg, Germany
Proteinase K	Sigma-Aldrich Chemie GmbH, Taufkirchen, Germany
RNase A	Sigma-Aldrich Chemie GmbH, Taufkirchen, Germany
RNase-Free DNase Set	Qiagen GmbH, Hilden, Germany
SuperScript II Reverse Transcriptase	ThermoFisher Scientific, Dreieich, Germany
SYBR Green PCR Master Mix	ThermoFisher Scientific, Dreieich, Germany
Tumor necrosis factor-α (TNFα)	PeproTech GmbH, Hamburg, Germany

Table 5. Cell culture reagents and media used in this project.

Reagent	Supplier
Amphotericin B (250 µg/mL)	PAN-Biotech GmbH, Aidenbach, Germany
Brd4 siRNA (smart pool)	Dharmacon, Lafayette, Colorado, U.S.A
Collagen G	Biochrom AG, Berlin, Germany
Collagenase A	Merck KGaA, Darmstadt, Germany
EASY Endothelial cell growth medium (ECGM)	PELOBiotech GmbH, Planegg/Martinsried, Germany
Fetal Calf Serum (FCS), Superior	Biochrom AG, Berlin, Germany
HyClone RPMI-1640 medium	GE Healthcare Life Sciences, Freiburg, Germany
HyClone™ HyQTase Cell Detachment Reagent	GE Healthcare Life Sciences, Freiburg, Germany
Medium 199 (M199)	GE Healthcare Life Sciences, Freiburg, Germany
Non-targeting siRNA	Dharmacon, Lafayette, Colorado, U.S.A
Penicillin-Streptomycin (P: 10,000 U/mL, S: 10 mg/mL)	PAN-Biotech GmbH, Aidenbach, Germany
Trypsin/EDTA mix	Biochrom AG, Berlin, Germany

2.1.3 Buffers, solution and media

Table 6. Cell culture buffers and solutions used in this project.

Buffer or Solution	Composition
CellTracker Green solution	5 µM CellTracker Green CMFDA dye, in serum-free RPMI
ECGM	10 % FCS Superior, 2.5 % supplement Mix, 1 % penicillin, 1 % streptomycin, 1 % amphotericin B, in EASY ECGM
Freezing medium	10 % DMSO, in FCS
PBS (pH 7.4)	137 mM NaCl, 2.7 mM KCl, 10 mM $Na_2HPO_4 \cdot 2\ H_2O$, 2 mM KH_2PO_4, in dist. water
PBS^+ (pH 7.4)	137 mM NaCl, 2.7 mM KCl, 8.1 mM $Na_2HPO_4 \cdot 2\ H_2O$, 1.5 mM KH_2PO_4, 0.5 mM $MgCl_2 \cdot 6\ H_2O$, 0.7 mM $CaCl_2 \cdot 2\ H_2O$, in dist. water
PBSA (pH 7.4)	0.2 % BSA, in PBS
RPMI	10 % FCS Superior, 1 % penicillin, 1 % streptomycin, in HyClone RPMI-1640
Stopping medium	10 % FCS Superior, 1 % penicillin, 1 % streptomycin, in Medium 199
Trypsin/EDTA solution	0.05 % Trypsin, 0.02 % EDTA, in PBS

Table 7. Buffers and solutions used for *in vitro* assay.

Buffer or solution	Composition
1x sample buffer	125 mM Tris-HCl (pH 6.8), 20 % glycerol, 4 % SDS, 0.8 % DTT, 0.01 % Pyronin Y, in dist. water
5x sample buffer	312.5 mM Tris-HCl (pH 6.8), 50 % glycerol, 5 % SDS, 2 % DTT, 0.025 % Pyronin Y, in dist. water
Blotto-T (1 %/5 %)	1 %/5 % powdered milk, in TBS-T
BSA-T (1 %/5 %)	1 %/5 % BSA, in TBS-T
ChIP elution buffer	100 mM $NaHCO_3$, 1 % SDS, in dist. water
ChIP high salt wash buffer	500 mM NaCl, 20 mM TRIS-HCL (pH 8.0), 2 mM EDTA (pH 8.0), 1 % Triton X-100, 0.1 % SDS, in dist. water
ChIP LiCl wash buffer	250 mM LiCl, 10 mM TRIS-HCL (pH 8.0), 1 mM EDTA (pH 8.0), 1 % NP40, 1 % sodium deoxycholate, in dist. water
ChIP low salt wash buffer	150 mM NaCl, 20 mM TRIS-HCL (pH 8.0), 2 mM EDTA (pH 8.0), 1 % Triton X-100, 0.1 % SDS, in dist. water
ChIP Lysis buffer	140 mM NaCl, 50 mM HEPES-KOH (pH 7.5), 1 mM EDTA (pH 8.0), 1 % SDS, 1 % Titon X-100, 0.1 % sodium deoxycholate, in dist. water
cOmplet mini solution	1 tablet, in 1.5 mL dist. water

Table 7. Continuation of the buffers and solutions used for *in vitro* assay.

Buffer or solution	Composition
ECL solution	98.5 mM Tris-HCl (pH 8.5), 1 % luminol solution, 0.4 % *p*-coumaric acid solution, 0.02 % H2O2, in dist. water
Electrophoresis buffer	192 mM glycine, 25 mM Tris, 0.1 % SDS, in dist. water
HFS-PI solution	0.1 % Triton X-100, 0.1 % sodium citrate, 50 µg/mL propidium iodide, in PBS
Hypotonic buffer	20 mM Tris-HCl (pH 7.4), 10 mM KCl, 2 mM $MgCl_2^+$, 1 mM EGTA, 2 % cOmplete solution, 1 mM NaF, 1 mM PMSF, 1 mM Na_3VO_4, 1 mM β-glycerophosphate, 1 mM sodium-pyrophosphate, 0.5 mM DTT in dist. water
Isotonic buffer	20 mM Tris-HCl (pH 7.4), 150 mM KCl, 2 mM $MgCl_2^+$, 1 mM EGTA, 0.3 % NP40, 2 % cOmplete solution, 1 mM NaF, 1 mM PMSF, 1 mM Na_3VO_4, 1 mM β-glycerophosphate, 1 mM sodium-pyrophosphate, 0.5 mM DTT in dist. water
Luminol solution	250 mM luminol, in DMSO
p-Coumaric acid solution	90 mM *p*-coumaric acid, in DMSO
Protein reagent diluent	1 % BSA (fraction V), in PBS
RIPA	150 mM NaCl, 50 mM Tris HCL, 1 mM EDTA, 1 % NP40, 0.5 % sodium deoxycholate, 0.1 % SDS in dist. water
RIPA Lysis buffer	2 % cOmplete solution, 1 mM NaF, 1 mM PMSF, 1 mM Na_3VO_4, 1 mM β-glycerophosphate, 1 mM sodium-pyrophosphate in RIPA
Separation gel (5 %)	17.3 % Rotiphorese Gel 30, 375 mM Tris-HCl (pH 8.8), 0.1 % SDS, 0.1 % TEMED, 0.05 % APS, in dist. water
Separation gel (10 %)	33.4 % Rotiphorese Gel 30, 375 mM Tris-HCl (pH 8.8), 0.1 % SDS, 0.1 % TEMED, 0.05 % APS, in dist. water
Separation gel (15 %)	49.6 % Rotiphorese Gel 30, 375 mM Tris-HCl (pH 8.8), 0.1 % SDS, 0.1 % TEMED, 0.05 % APS, in dist. water
Stacking gel (4 %)	16.7 % Rotiphorese Gel 30, 125 mM Tris-HCl (pH 6.8), 0.1 % SDS, 0.2 % TEMED, 0.1 % APS, in dist. water
Stripping buffer, pH-based	200 mM Glycine (pH 2.2), 1 % Tween 20, 1 % SDS, in dist. water
Stripping buffer, stringent	62.5 mM Tris, 2 % SDS, 0.8 % 2-mercaptoethanol, in dist. water
TBS-T (pH 7.4–7.5)	25 mM Tris, 150 mM NaCl, 0.05 % Tween 20, in dist. water
Tris-EDTA buffer	10 mM Tris (pH 8.0), 1 mM EDTA (pH 8.0), in dist. water
Triton X-100 (0.2 %)	0.2 % Triton X-100, in PBS, in dist. water
Western blot transfer buffer	192 mM glycine, 25 mM Tris, 20 % methanol, in dist. water

2.1.4 Commercial Kits

Table 8. Commercially obtained Kits used in this project.

Kit	Supplier
CellTiter-Blue Cell Viability Assay	Promega GmbH, Mannheim, Germany
ChIP DNA-clean and concentrator	Zymo Research Europe GmbH, Freiburg, Germany
CytoTox 96 Non-Radioactive Cytotoxicity Assay	Promega GmbH, Mannheim, Germany
Dual-Luciferase Reporter Assay System	Promega GmbH, Mannheim, Germany
GeneTrans II transfection reagent	MoBiTec, Goettingen, Germany
HUVEC Nucleofector Kit	Lonza Cologne GmbH, Cologne, Germany
MiraCLEAN Endotoxin Removal Kit	Mirus Bio LLC, Madison, WI, USA
Pierce BCA Protein Assay Kit	Thermo Fisher Scientific GmbH, Dreieich, Germany
PureYield Plasmid Maxiprep System	Promega GmbH, Mannheim, Germany
RNeasy Mini Kit	Qiagen GmbH, Hilden, Germany

2.1.5 Antibodies

The following tables list the antibodies used for different application. For western blot analysis, antibodies were routinely used in a 1:1000 dilution. For chromatin immunoprecipitation assays, 1 µg of the respective binding or non-binding antibody was used.

Table 9. Primary antibodies used for western blot analysis.

Immunogen, Ref. number	Type	Supplier	Solution
CD54/ICAM-1, 4915	rabbit, polyclonal	Cell Signaling Technology Europe B.V., Frankfurt am Main, Germany	5 % BSA-T
Akt, 9272	rabbit, polyclonal	Cell Signaling Technology Europe B.V., Frankfurt am Main, Germany	5 % BSA-T
AP-1-cJun, sc-74543	mouse, monoclonal	SantaCruz Biotechnologies, Heidelberg, Germany	5 % Blotto-T
Brd4, sc-48772	rabbit, polyclonal	SantaCruz Biotechnologies, Heidelberg, Germany	5 % Blotto-T

Table 9. Continuation of the primary antibodies used for western blot analysis.

Immunogen, Ref. number	Type	Supplier	Solution
eIF2α, 9722	rabbit, polyclonal	Cell Signaling Technology Europe B.V., Frankfurt am Main, Germany	5 % BSA-T
E-selectin, sc-137054	mouse, monoclonal	SantaCruz Biotechnologies, Heidelberg, Germany	5 % Blotto-T
Histone 3 (H3), 9751	rabbit, monoclonal	Cell Signaling Technology Europe B.V., Frankfurt am Main, Germany	5 % BSA-T
IKKβ, 8943	rabbit, monoclonal	Cell Signaling Technology Europe B.V., Frankfurt am Main, Germany	5 % BSA-T
IRF-1, sc-514544	mouse, monoclonal	SantaCruz Biotechnologies, Heidelberg, Germany	5 % Blotto-T
IκBα, 4812	rabbit, monoclonal	Cell Signaling Technology Europe B.V., Frankfurt am Main, Germany	5 % BSA-T
NFκB1 p105/p50, 13586	rabbit, monoclonal	Cell Signaling Technology Europe B.V., Frankfurt am Main, Germany	5 % BSA-T
NFκB-p65, sc-8008	mouse, monoclonal	SantaCruz Biotechnologies, Heidelberg, Germany	5 % Blotto-T
p38 MAPK, 9212	rabbit, polyclonal	Cell Signaling Technology Europe B.V., Frankfurt am Main, Germany	5 % BSA-T
p44/42 (Erk1/2), 9106	mouse, monoclonal	Cell Signaling Technology Europe B.V., Frankfurt am Main, Germany	5 % BSA-T
Phospho-Akt (Ser473), 9271	rabbit, polyclonal	Cell Signaling Technology Europe B.V., Frankfurt am Main, Germany	5 % BSA-T
Phospho-AP-1-cJun (Ser243), A27328	rabbit, polyclonal	Bioworld Technology,Inc., Minessota, U.S.A	5 % BSA-T
Phospho-IKKα/β (Ser176/180), 2697	rabbit, monoclonal	Cell Signaling Technology Europe B.V., Frankfurt am Main, Germany	5 % BSA-T
Phospho-IκBα (Ser32), 2859	rabbit, monoclonal	Cell Signaling Technology Europe B.V., Frankfurt am Main, Germany	5 % BSA-T
Phospho-NFκB p65 (Ser468), 3039	rabbit, polyclonal	Cell Signaling Technology Europe B.V., Frankfurt am Main, Germany	5 % BSA-T
Phospho-NFκB p65 (Ser536), 3033	rabbit, polyclonal	Cell Signaling Technology Europe B.V., Frankfurt am Main, Germany	5 % BSA-T
Phospho-p38 MAPK (Thr180/Tyr182), 9211	rabbit, polyclonal	Cell Signaling Technology Europe B.V., Frankfurt am Main, Germany	5 % BSA-T
Phospho-p44/42 (Erk1/2) (Thr202/ Tyr204), 9106	rabbit, polyclonal	Cell Signaling Technology Europe B.V., Frankfurt am Main, Germany	5 % BSA-T

Table 9. Continuation of the primary antibodies used for western blot analysis.

Immunogen, Ref. number	Type	Supplier	Solution
Phospho-SAPK/JNK (Thr183/Tyr185), 4668	rabbit, polyclonal	Cell Signaling Technology Europe B.V., Frankfurt am Main, Germany	5 % BSA-T
SAPK/JNK, 9252	rabbit, polyclonal	Cell Signaling Technology Europe B.V., Frankfurt am Main, Germany	5 % BSA-T
VCAM-1 , sc-13160	mouse, monoclonal	SantaCruz Biotechnologies, Heidelberg, Germany	5 % Blotto-T

Table 10. Secondary antibodies used for western blot analysis.

Antibody, Ref. number	Supplier	Solution
Goat-anti-rabbit IgG-HRP, sc-2004	SantaCruz Biotechnologies, Heidelberg, Germany	5 % Blotto-T
Goat-anti-mouse IgG-HRP, sc-2005	SantaCruz Biotechnologies, Heidelberg, Germany	5 % Blotto-T

Table 11. Antibodies used for flow cytometry.

Antibody, Ref. number	Label	Type	Supplier	Dilution
FITC-CD54 (ICAM-1), MCA1615F	FITC	mouse, monoclonal	Bio-Rad Laboratories GmbH, Munich, Germany	1:20
PE-CD106 (VCAM-1), 555647	PE	mouse, monoclonal	BD Biosciences, Heidelberg, Germany	1:20
PE-CD62 antigen-like family member E (E-selectin), 551145	PE	mouse, monoclonal	BD Biosciences, Heidelberg, Germany	1:20

Table 12. Antibodies used for chromatin immunoprecipitation.

Antibody, Ref. number	Type	Supplier
NFκB-p65, C15310256	rabbit, polyclonal	Diagenode, Seraing, Belgium
RNA polymerase II , C15200004	mouse, monolonal	Diagenode, Seraing, Belgium
Brd4, C15410337	rabbit, polyclonal	Diagenode, Seraing, Belgium
IgG non-binding mouse, C15400001	mouse, monolonal	Diagenode, Seraing, Belgium
IgG non-binding rabbit, C15410206	rabbit, polyclonal	Diagenode, Seraing, Belgium
AP-1-cJun, 24909-1-AP	rabbit, polyclonal	Proteintech Germany GmbH, Planegg-Martinsried, Germany
H3K9me3, ab8898	rabbit, monoclonal	Abcam, Cambrige, UK

2.1.6 Oligonucleotides

All oligonucleotides in form of primers used for this project were purchased by Eurofins Genomics Europe Shared Services GmbH (Ebersberg, Germany)

Table 13. Primers used for quantitative real-time polymerase chain reaction analysis.

Gene	Sequence forward	Sequence reverse
Brd4	AAT AGC AGC AAC AGC AAT GTG AG	CTT CCT CCG ACT CAT ACG TG G
cFos	GGG GCA AGG TGG AAC AGT TA	AGG TTG GCA ATC TCG GTC TG
cJun	ATC AAG GCG GAG AGG AAG CG	TGA GCA TGT TGG CCG TGG AC
E-selectin	AGA TGA GGA CTG CGT GGA GA	GTG GCC ACT GCA GGA TGT AT
GAPDH	CCA CAT CGC TCA GAC ACC AT	TGA AGG GGT CAT TGA TGG CAA
ICAM-1	CTG CTC GGG GCT CTG TTC	AAC AAC TTG GGC TGG TCA CA
IRF-1	ACA AGG ATG CCT GTT TGT TCC	TGG AAG CAT CCG GTA CAC TC
IκBα	GTG ACC CTA GTG GCT CA TCG	GGC GCC CTA TAA ACG CTG G
p105	CAT CCC ATG GTG GAC TAC CT	GGG CAT GCA GGT GGA TAT TT
p65	GGG GAC TAC GAC CTG AAT GC	GAT CTT GAG CTC GGC AGT GT
VCAM-1	CCA CAG TAA GGC AGG CTG TAA	GCT GGA ACA GGT CAT GGT CA

Table 14. Primers used for chromatin immunoprecipitation-quantitative real-time polymerase chain reaction analysis.

Gene	Sequence forward	Sequence reverse
E-selectin cJun	TAC GAT ATA AAG GCA TGG ACA AAG G	GGA GGG ATT GCT TCC TGT GAA
E-selectin p65	TAC GAT ATA AAG GCA TGG ACA AAG G	GGA GGG ATT GCT TCC TGT GAA
E-selectin Pol II promoter	CCC GGG AAA GTT TTT GGA TGC	AGC GTT CTG CAC TTA CCG TT
E-selectin Pol II stalling region	TCC TAT AAA AGG GCC TCA GCC G	GCC CTT ATA AAG CGT TCT GCA CT
ICAM-1 cJun	ACA ATA ACA GTC TCC ACT CTC CG	AGG GCG ATG ACC CCG
ICAM-1 p65	GGA AAC GGG AGG CGT GG	GAG AGG GTC ATC CTC CCT CG

Table 14. Continuation of the primers used for chromatin immunoprecipitation-quantitative real-time polymerase chain reaction analysis.

Gene	Sequence forward	Sequence reverse
ICAM-1 Pol II promoter	GGG AAG GCG CGA GGT TT	CGG GGC TTC GGA GAA CTG
ICAM-1 Pol II stalling region	ATA AAG GAT CAC GCG CCC CA	CTT CGG AGA ACT GGC CCG AC
VCAM-1 cJun	GTT GAT GTT TGT TGC TAA AAG AAC T	ACG ACT ATG CCA TGT GAA TTG AT
VCAM-1 p65	GAA CTT GGC TGG GTG TCT GT	AAG GGT CTT GTT GCA GAG GC
VCAM-1 Pol II promoter	GAG GAG CTT CAG CAG TGA GAG	GAGGCCCGATGCAGATACC
VCAM-1 Pol II stalling region	AAA GCA CAG ACT TTC TAT TTC ACT C	TTT GAG GCT CCA AGG ATC ACG
rpl13a 3'-UTR	CCA GGT CTC CAC GCT AAA CA	AAT CTT GGC ATC CAA CCG CA

2.1.7 Primary cells and cell lines

Table 15. Primary cells and cell lines used in this project.

Primary cells/ cell line	Supplier	Reference number
HUVECs	PELOBiotech GmbH, Planegg/Martinsried, Germany	PB-CH-190-8013
HMEC-1	American Type Culture Collection (ATCC), LGC Standards GmbH, Wesel, Germany	ATCC CRL-3243
THP-1	Leibniz Institute for German Collection of Microorganisms and Cell Cultures (DSMZ), Braunschweig, Germany	ACC-16

2.1.8 Technical equipment

Table 16. Technical equipment used in this project.

Device	Supplier
Autoclave: Systec VX-95	Systec GmbH, Linden, Germany
Bioruptor Puls System	Diagenode, Seraing, Belgium

Table 16. Continuation of the technical equipment used in this project.

Device	Supplier
Blotter: Criterion Blotter	Bio-Rad Laboratories GmbH, Munich, Germany
Centrifuge: Heraeus Megafuge 16R	Thermo Fisher Scientific, Dreieich, Germany
Centrifuge: MICRO STAR 17R	VWR International GmbH, Darmstadt, Germany
Centrifuge: Mini Star silverline	VWR International GmbH, Darmstadt, Germany
Current source: PowerPacTM HC	Bio-Rad Laboratories GmbH, Munich, Germany
Electrophoresis system: Mini-PROTEAN Tetra System	Bio-Rad Laboratories GmbH, Munich, Germany
Electroporator: Nucleofector 2b	Lonza Cologne GmbH, Cologne, Germany
Flow cytometer: FACSVerse	BD Biosciences, Heidelberg, Germany
Fluorescence microscope: LSM 510	Carl Zeiss AG, Jena, Germany
Heatblock	VWR International GmbH, Darmstadt, Germany
Hemocytometer: Neubauer-improved	Paul Marienfeld GmbH & Co. KG, Lauda-Königshofen, Germany
Incubator: HERACell 150i	Thermo Fisher Scientific, Dreieich, Germany
Inverted microscope: DM IL LED	Leica Microsystems, Wetzlar, Germany
Liquid nitrogen storage system: ARPEGE 110	Air Liquide S.A., Paris, France
Magnetic stirrer: IKA RH basic 2	IKA-Werke GmbH & Co. KG, Staufen, Germany
Microplate reader: Infinite F200 pro	Tecan Trading AG, Männedorf, Switzerland
Microplate reader: Varioskan Flash	Thermo Fisher Scientific, Dreieich, Germany
Nanophotometer: P 330	Implen GmbH, Munich, Germany
Orbital shaker: Sea Star	Heathrow Scientific, Vernon Hills, IL, USA
pH meter: FE20	Mettler-Toledo GmbH, Gießen, Germany
Pipette: Eppendorf Multipette plus	Eppendorf AG, Hamburg, Germany
Pipettes: Eppendorf Research plus	Eppendorf AG, Hamburg, Germany

Table 16. Continuation of the technical equipment used in this project.

Device	Supplier
Pipettor: Pipetus	Hirschmann Laborgeräte GmbH & Co. KG, Eberstadt, Germany
qRT-PCR system: StepOnePlus System	Applied Biosystems GmbH, Darmstadt, Germany
Scale: Mettler-Toledo (0.1–200 mg)	Mettler-Toledo GmbH, Gießen, Germany
Scale: PIONEER (10–1000 g)	Ohaus Europe GmbH, Greifensee, Switzerland
Sterile bench: SAFE 2020	Thermo Fisher Scientific, Dreieich, Germany
Tube roller: Stuart SRT9D	Bibby Scientific Limited, Staffordshire, UK
Ultra-pure water system: Astacus	MembraPure GmbH, Berlin, Germany
Ultrasonic cleaner: USC300TH	VWR International GmbH, Darmstadt, Germany
Vacuum pump: Integra Vacusafe	INTEGRA Biosciences GmbH, Biebertal, Germany
Vortexer: Vortex Genie 2	Scientific Industries, Inc., Bohemia, NY, USA
Water bath: Julabo ED	JULABO GmbH, Seelbach, Germany
X-ray Film processor: Agfa CP 1000	AGFA, Cologne, Germany

2.1.9 Consumables

Table 17. Consumables used in this project.

Consumable	Supplier
8-well µ-slides: µ-Slide 8 well, ibiTreat	ibidi GmbH, Planegg-Martinsried, Germany
Microplates for absorbance measurements: Nunc MicroWell 96-Well (269620)	Thermo Fisher Scientific GmbH, Dreieich, Germany
Cell culture dishes (10 cm)	Sarstedt AG & Co., Nümbrecht, Germany
Cell culture flasks (25 cm^2, 75 cm^2)	Greiner Bio-One GmbH, Frickenhausen, Germany
Cell culture plates (6-, 12-, 24-, 48-, 96-well)	Greiner Bio-One GmbH, Frickenhausen, Germany
Cell scraper	TPP Techno Plastic Products AG, Trasadingen, Switzerland

Table 17. Continuation of the consumables used in this project.

Consumable	Supplier
Centrifuge tubes (15 mL, 50 mL)	Greiner Bio-One GmbH, Frickenhausen, Germany
Cover slips	Helmut Saur, Reutlingen, Germany
Cryo vials	Greiner Bio-One GmbH, Frickenhausen, Germany
Eppendorf Combitips advanced	Eppendorf AG, Hamburg, Germany
Low-binding tubes (1.5 mL)	Sarstedt AG & Co., Nümbrecht, Germany
Microplates for fluorescence measurements: Nunc MicroWell 96-Well (265301)	Thermo Fisher Scientific GmbH, Dreieich, Germany
Microplates for luminescence measurements: Corning 96 well NBS Microplate	Sigma-Aldrich Chemie GmbH, Taufkirchen, Germany
Microplates for qRT-PCR: MicroAmp Fast Optical 96-Well Reaction Plate	Applied Biosystems GmbH, Darmstadt, Germany
Pipette tips (standard, 10 µL, 100 µL, 300 µL, 1000 µL)	Greiner Bio-One GmbH, Frickenhausen, Germany
Pipette tips with filter: ART Aerosol Resistant Tips (10 µL)	Thermo Fisher Scientific GmbH, Dreieich, Germany
Pipette tips with filter: Biosphere (200 µL, 1000 µL)	Sarstedt AG & Co., Nümbrecht, Germany
PVDF membrane: Immun-Blot PVDF	Bio-Rad Laboratories GmbH, Munich, Germany
Reaction tubes (0.2 mL, 1.5 mL, 2 mL)	Greiner Bio-One GmbH, Frickenhausen, Germany
Sealing tape for qRT-PCR: StarSeal Sealing Tape Polyolefin Film (E2796-9795)	STARLAB INTERNATIONAL GmbH, Hamburg, Germany
Serological pipettes (5 mL, 10 mL, 25 mL)	Greiner Bio-One GmbH, Frickenhausen, Germany
TPX-tubes	Diagenode, Serainge, Belgium
Transwell Insert (polycarbonate membrane, diameter 6.5 mm, pore size 8 µm)	Corning, New York, USA
Whatman filter paper	Bio-Rad Laboratories GmbH, Munich, Germany
X-ray films: Super RX-N	FUJIFILM Europe GmbH, Düsseldorf, Germany

2.2 Methods

2.2.1 Cell culture

Primary cells and cell lines were cultured in cell culture incubators under constant humidity at 37 °C and 5 % CO_2. Growth and morphology of the cells was routinely observed microscopically by using an inverted Leica DM IL LED microscope (Leica Microsystems, Wetzlar, Germany). Unless otherwise stated, all buffers, solution and media were pre-warmed to 37 °C before application to the cells.

2.2.2 Primary cells and cell lines

All adherent cells were cultivated in culture flasks pre-coated with collagen G (10 µg/mL) in PBS for 30 min at 37 °C before use.

2.2.2.1 Human umbilical vein endothelial cells (HUVECs)

Primary human umbilical vein endothelial cells (HUVECs) were obtained commercially or prepared from umbilical cords (2.2.3). HUVECs were cultivated in endothelial cell growth medium (ECGM) and were used to study the influence of MTAs on the leukocyte-endothelial cell interactions as well as the underlying mechanisms.

2.2.2.2 Human dermal microvascular cell line 1 (HMEC-1)

The cells of the human dermal microvascular cell line 1 (HMEC-1) constitute an immortalized cell line created by transfecting human dermal microvascular endothelial cells with a PBR-322-based plasmid containing the simian virus 40 A, large T antigen [366]. The resulting cell line (CDC/EU.HMEC-1) has been shown to retain the morphology, phenotype and functional characteristics of normal human dermal microvascular endothelial cells. HMEC-1 cells were used in this project to confirm the effects observed in primary HUVECs.

2.2.2.3 Human monocytic leukemia cell line 1 (THP-1)

The human monocyte-like cell line THP-1 constitutes cells that were initially isolated from the peripheral blood of an acute monocytic leukemia (AML) patient [367]. THP-1 cell were exclusively used for testing the adhesion of the cells to endothelial monolayers. The cells were cultivated in RPMI.

2.2.2.4 Passaging of cells

To passage confluent adherent HUVECs or HMECs, the cell culture medium was subtracted, and the cells were washed twice with phosphate-buffered saline (PBS, pH 7.4) and incubated with 2 mL of Trypsin/EDTA solution at 37 °C until the cells were detached. After detachment, the enzymatic reaction was stopped by addition of stopping medium. The cells were sedimented by centrifugation (300 g, 5 min at RT) and resuspended in ECGM and either transferred into new culture flasks (75 cm^2) or seeded into cell culture dishes or plates. Endothelial cells were passaged three times a week in a 1:3 ratio.

For passaging of THP-1 cells growing in suspension, the cell number was determined using a hemocytometer and the cell count was adjusted to 3 x 10^5 cells per mL. The appropriate number of cells was sedimented (300 g, 5 min at RT), resuspended in RPMI and transferred into a new cell culture flask. The THP-1 cells were passaged three times a week.

2.2.2.5 Freezing and thawing of cells

For freezing of cells, confluent adherent HUVECs or HMECs were detached as described above and sedimented by centrifugation (300 g, 5 min at RT). The cells were resuspended in freezing medium (2 mL per 75 cm^2 flask or 6 x 10^6 cells) and transferred into cryovials and frozen at -80 °C overnight. Subsequently, the frozen cells were transferred into liquid nitrogen for long-term storage.

For thawing, frozen cells were rapidly thawed at 37 °C and immediately transferred into 10 mL ice-cold culture medium to dilute the DMSO in the freezing medium. The cells were harvested by centrifugation (300 g, 5 min at RT) and seeded into 75 cm^2 (endothelial cells) or 25 cm^2 (THP-1 cells) culture flasks.

2.2.3 Preparation of primary human umbilical vein endothelial cells (HUVECs)

Primary HUVECs were isolated from the veins of umbilical cords of healthy donors based on the method developed by Jaffe *et al.* [368]. A waiver (no. W1/21Fü) has been granted for the use of anonymized human material on September 15th, 2021, issued by the head of the Research Ethics Committee/Institutional Review Board. For isolation, the cord vein was cannulated from both sites with injection needles. The needles were clamped with ties, and the veins were washed from both sites with pre-warmed PBS containing Ca^{2+} and Mg^{2+} (PBS^+) to wash out blood. The cords were allowed to drain and filled tightly with collagenase A (0.1 mg/mL in PBS^+), sealed with a multi-way valve and were incubated for 45 min at 37 °C. After incubation, the veins were flushed from both sites with medium 199 (M199) supplemented with 10 % FCS, 100 U/mL penicillin and 100 µg/mL streptomycin. After centrifugation, the isolated cells were resuspended in pre-warmed ECGM, seeded into a T25 flask and were incubated for 24 h. The adherent cells were washed twice with PBS^+ and were supplied with fresh

ECGM. After reaching confluency, HUVECs were passaged and used for experiments in the third passage.

2.2.4. Protein translation inhibition assay

The protein translation inhibition assay was used to test the influence of MTAs on the translation machinery of HUVECs. This assay was performed with the ClickIT Plus OPP Protein Synthesis assay Kit (Thermo Fisher, Dreieich, Germany). In this assay, translation is detected by addition of *O*-propargyl-puromycin (OPP) to the culture medium, which is taken up by the cell and incorporated into nascent polypeptide chains, disrupting peptide transfer on the ribosome and inducing premature chain termination. Addition of an AlexaFluor 488 picolyl azide dye together with different reagents allows for chemoselective ligation of the dye with the alkyne group of OPP and enables fluorescence-based imaging for detection.

The assay was performed according to the manufacturer's instructions. Briefly, HUVECs were seeded into 8-well µ-ibidi slides (ibidi GmbH, Germany), grown to confluency and treated as indicated in the figure legends. After treatment, the OPP reagent was added, and the cells were incubated for 30 min at 37 °C. After the incubation, the cells were washed once with PBS^+ and fixated with 4 % Histofix (Roth, Germany) formaldehyde solution for 15 min at RT. The fixed cells were washed once with PBS and permeabilized using 0.2 % Triton X-100 (Merck, Germany) in PBS for 15 min. Subsequently, the cells were washed twice with PBS and the ClickIT OPP reaction cocktail was added and let to incubate for 30 min at RT under exclusion of light. The cells were washed once with ClickIT Reaction rinse buffer. To stain the nuclei, HCS NuclearMask blue stain was diluted 1:2000 in PBS, applied to the cells and incubated for 30 min at RT and protected from light. Subsequently, the cells were washed twice with PBS and sealed by the addition of one drop of FluorSave Reagent (Merck) and a coverslip.

Images were taken with a DMI 6000B (Leica Microsystems, Wetzlar, Germany) fluorescence microscope. Analysis of fluorescence signals was performed using ImageJ (National Institutes of Health, USA), by measuring the fluorescence of the nuclei in the AlexaFluor 488 channel and normalizing it on the core fluorescence in the HCS NuclearMask channel.

2.2.5 Cytotoxicity assays

Cytotoxicity assays were performed to test the influence of the MTAs on the viability of HUVECs. Metabolic activity was analyzed with the CellTiter-Blue cell viability assay, membrane integrity was analyzed based on the release of lactate dehydrogenase (LDH) by the CytoTox 96 non-radioactive cytotoxicity assay and the rate of apoptosis was determined based on the sub-diploidy state of the DNA by the method described by Nicoletti *et al.* [369].

2.2.5.1 Metabolic activity assay

The effects of the MTAs on the metabolic activity of HUVECs was analyzed by the CellTiter-Blue cell viability assay (Promega GmbH, Mannheim, Germany). This assay is based on the principle that viable cells retain the ability to reduce the dye resazurin into the fluorescent product resorufin. Non-viable cells lose the ability to reduce the resazurin dye and hence, do not generate a fluorescent signal.

The assay was performed based on the manufacturer's instructions. HUVECs were grown to confluence in 96-well cell culture plates. The CellTiter-Blue agent was added to the culture medium in a 1:10 ratio for the last 4 h of treatment and the reduction of resazurin into resorufin was determined by fluorescence measurements (ex.: 579 nm, em.: 584 nm) using an Infinite F200 pro microplate reader (Tecan Trading AG, Männedorf, Switzerland).

2.2.5.2 Lactate dehydrogenase release assay

The membrane integrity was measured based on the release of lactate dehydrogenase (LDH) into the cell culture supernatant by using the CytoTox 96 non-radioactive cytotoxicity assay (Promega GmbH). This assay is based on the LDH-catalyzed conversion of oxidized nicotinamide adenine dinucleotide (NAD^+) into the reduced NADH and the coupled conversion of an iodonitrotetrazolium salt into an absorbance active formazan product and NAD^+. Since the amount of the generated formazan product is proportional to the amount of released LDH, it can be used to analyze the membrane integrity and hence, viability of the cells.

The assay was performed based on the manufacturer's instructions. Briefly, HUVECs were seeded into 96-well cell culture plates, grown to confluency and treated with MTAs as described. For positive control, lysis solution was added to the cells in a 1:10 ratio and incubated for the last 45 min of treatment. 50 µL of the respective supernatant were transferred into a new 96-well cell culture plate, and 50 µL of CytoTox 96 reagent was added and incubated for 30 min at RT. The reaction was stopped by the addition of 50 µL of stopping solution and the absorbance of the formazan product was measured at 490 nm using a Varioskan Flash microplate reader (Thermo Fisher Scientific, Dreieich, Germany).

2.2.5.3 Cell apoptosis assay

The rate of apoptosis was measured by the method described by Nicoletti *et al.* This method is based on the principle that the apoptosis of cells is accompanied by fragmentation of the DNA due to the activity of endonucleases. The fragmentation state of the DNA can be visualized by the addition of DNA intercalating agents like propidium iodide (PI) and measured by flow cytometry.

HUVECs were grown to confluency in 24-well cell culture plates and treated with MTAs as indicated. The cell culture supernatants were collected, and the cells were washed twice with PBS. The wash fractions were combined with the supernatants and the cells were detached as described. The detached cells were added to the collected supernatant and wash fractions and sedimented by centrifugation (300 g, 10 min at 4 °C). The cells were washed once by resuspension in ice-cold PBS and harvested by centrifugation (300 g, 10 min at 4 °C) and were resuspended in hypotonic fluorochrome solution (HFS) containing PI (HFS-PI) and incubated overnight at 4 °C protected from light. The fragmentation state was measured based on the PI fluorescence signal by flow cytometry using a FACSVerse (BD Biosciences, Heidelberg, Germany).

2.2.6 Animal experiments

2.2.6.1 Animals

In vivo experiments were performed using 8-10 week-old male or female C57BL/6N mice obtained from Charles River Laboratories (Wilmington, Ma, USA). Mice were housed based on a 12 h light/dark cycle with free access to food and water.

2.2.6.2 Imiquimod-induced psoriasiform dermatitis mouse model

The imiquimod (IMQ)-induced psoriasis mouse model was performed and skin severity was assessed as previously described by van der Fits *et al.* [370]. IMQ is a TLR7 agonist and used to initiate the inflammatory response and to induce the psoriasiform dermatitis in mice [371, 372]. Therefore, the mouse back skin was shaved one day before starting the experiment. 62.5 mg commercially available cream containing 5% IMQ (Aldara; 3M Pharmaceuticals, Neuss, Germany) was daily applied on the back skin of 8–10 weeks old male or female mice for 6 consecutive days. Skin severity was evaluated according to the psoriasis area and severity index (PASI) scoring system based on the extent of skin thickness, redness and scaling for up to 10 days. Additionally, the mice received s.c. injections of 1 mg/kg PT or vehicle (PBS) on day 1, 3, and 5. All mouse experiments were approved by and followed the guidelines of the Hessian animal care and use committee (FU/2064).

2.2.6.3 Intravital microscopy of the mouse cremaster muscle

Intravital microscopy was used to assay the effects of PT on the classical steps of the leukocyte adhesion cascade, i.e. rolling, firm adhesion and transmigration, *in vivo*. The interaction of the endothelium with leukocytes (Gr-1$^+$ and classical monocytes) in the TNF-activated mouse cremaster muscle was analyzed based on the technic developed by Baez *et al*. [373, 374]. 30 min after intraperitoneal application of pretubulysin (1 mg/kg) or drug vehicle, TNF (25 µg/kg) was injected intrascrotally to induce leukocyte recruitment to the cremaster muscle. After 4 h, mice were anesthetized (ketamine/xylazine) and the right cremaster muscle was prepared. Intravital microscopy of the cremaster muscle was performed using an Olympus BX 50 upright microscope (Olympus, Tokyo, Japan). Analysis was conducted with the Cap-Image analysis software (Dr. Zeintl, Heidelberg, Germany). All experiments were approved by the local governmental authorities under the reference number 55.2-1-54-2531-84-09, Regierung von Oberbayern.

2.2.7 Cell adhesion assay under flow conditions

The cell adhesion assay under flow condition constitutes an advanced method of assaying the adhesion of cells under more physiological conditions, compared to the static assay environment. The adhesion of THP-1 cells to MTA-treated HUVEC monolayers under flow condition was analyzed by using an ibidi pump system (ibidi, Gräfelfing, Germany) that mimics the flow conditions of the blood.

HUVECs (1.6 x 10^6 cells/mL) were seeded into collagen G-precoated µ-slide I$^{0.8}$ Luer channel slides (ibidi, Germany), let to attach for 2 h and subjected to 1 h of 1 dyn/cm^2, 1 h of 3 dyn/cm^2 and constant 5 dyn/cm^2 shear pressure overnight under cell culture conditions. After overnight cultivation and subsequent treatment, the monolayers were tested for the adhesion of THP-1 cells (8 x 10^5 cells/mL), which were stained with 5 µM CellTracker Green (CTG) in serum-free RPMI for 30 min according to the manufacturer's instructions. Adhesion was performed for 10 min at 0.5 dyn/cm^2 under cell culture conditions. Non-adherent THP-1 cells were removed by washing once with PBS$^+$ and the cells were lysed using RIPA lysis buffer and frozen at -80 °C. Quantification of the THP-1 cell adhesion was performed by fluorescence measurement (ex.: 485 nm, em.: 535 nm) of the obtained lysates by using an Infinite F200 pro microplate reader (Tecan Trading AG, Switzerland).

2.2.8 Flow cytometric analysis

Flow cytometry constitutes a technic for measuring the physical and chemical characteristics such as the morphology of cells or the presence of cell surface markers of different cell populations. The cells are thereby injected in the flow cytometer and funneled into a laminar flow that enables measurement of singular cells based on light scattering. In case of labeling the cells with fluorescent markers, flow-cytometry can also be used to analyze the cell surface levels of membrane proteins such as cell adhesion molecules.

For preparation of cells prior to the flow cytometry measurement, MTA-treated HUVECs were washed twice with PBS and detached with HyQTase (GE Healthcare, Solingen, Germany) by incubation at 37 °C. The detachment reaction was stopped by addition of ice-cold stopping medium, and PBS with 0.2 % BSA (PBSA) was added in an equal amount to the cell suspension. The cells were sedimented at 4 °C and resuspended in ice-cold PBSA containing either FITC-labeled anti-human CD54 (ICAM-1) antibody (MCA1615F, Biozol, Eching, Germany), PE-labeled anti-human CD106 (VCAM-1) antibody (555647, Becton Dickinson, Heidelberg, Germany) or PE-labeled anti-human CD62 antigen-like family member E (E-selectin) antibody (551145, Becton Dickinson, Germany) and were incubated on ice for 45 min. For more details on the used antibody solutions see section 2.1.5; Tab. 11. Unbound antibody was removed by washing twice with PBSA. The protein levels on the endothelial cell surface were analyzed by using a FACSVerse flow cytometer (Becton Dickinson).

2.2.9 Western blot analysis

Western blot analysis was used to detect and quantify the content of proteins in endothelial cells after treatment with MTAs. The immunogenic detection of proteins is preceded by the sodium dodecyl sulfate polyacrylamide gel electrophoresis (SDS-PAGE), in which proteins are separated based on their molecular weight. Then, the separated proteins are transferred onto a membrane for detection. The western blot technique, also termed immunoblotting, was first described by Towbin *et al.* [375].

2.2.9.1 Sample preparation

For preparation of lysates for western blot analysis, HUVECs or HMECs were grown to confluency in 6-well plates and treated with MTA as described. The cells were washed once with PBS and lysed with RIPA lysis buffer and frozen at -80 °C for at least 1 h.

2.2.9.2 Protein quantification and sample adjustment

The total protein amount of the obtained lysates was determined using the Pierce BCA Protein Assay Kit (Thermo Fisher Scientific GmbH). This assay is based on the reduction of Cu^{2+} to Cu^{+} by the peptide bonds of polypeptides in an alkaline environment and the complexation with bicinchoninic acid (BCA) to form purple complexes. These complexes can be measured by absorbance reading and compared to a protein standard to determine the total protein content of the lysates.

The quantification of the total protein content was performed based on the manufacturer's instruction. Briefly, lysates were thawed on ice, scraped off the plates and transferred to pre-cooled tubes. For immunodetection of proteins contained in the RIPA-insoluble fraction, lysates were transferred to TPX-tubes (Diagenode, Seraing, Belgium) and sonicated at 'high' setting in a Bioruptor plus system (Diagenode, Belgium) for 2 cycles with 30 s on- and 30 s off-intervals at 4 °C. Subsequently, the cells were centrifuged at 17,000 g for 10 min at 4 °C, and the supernatant was transferred to a new tube. For protein quantification, the lysates were diluted in a 1:10 ratio in distilled water. The protein content was calculated based on linear regression of a bovine serum albumin (BSA) standard concentration row (0, 50, 100, 150, 200, 300, 400, 500 µg/mL) which was diluted from a 2 mg/mL stock solution. 10 µL of the respective standard or lysate solution was supplemented with 190 µL of the BCA working solution and incubated at 37 °C for 30 min. The absorbance was measured at 562 nm using an Infinite F200 pro microplate reader (Tecan Trading AG). After determination of the total protein content, the lysates were supplemented with 5x SDS-PAGE sample buffer and corrected with 1x SDS-PAGE sample buffer to the concentration of the lowest concentrated sample. Samples were boiled at 95 °C for 5 min to promote solubilization and were stored at -20 °C until usage.

2.2.9.3 Sodium dodecyl sulfate gel electrophoresis (SDS-PAGE)

The SDS-PAGE is a technique for separation of proteins based on their size in an electric field. SDS solubilizes the proteins and binds to nonpolar amino acid residues via its alkyl function, introducing negative charges to the proteins. This enables migration of the protein in an electric field and a size-dependent separation based on the density of the polyacrylamide mesh in the gel. In the discontinuous SDS-PAGE according to Lämmli *et al.* [376] the gel is separated into a focusing gel and a separation gel. In the focusing gel, the pH of 6.8 introduces a positive charge to glycine, which weakly migrates in the applied electric field. Proteins are focused based on their negative electric charge due to the field-gradient between the fast-migrating chloride ions and the slow-migrating positively charged glycine. Stacking of proteins enables better entry and separation of proteins in the separating gel. Due to the higher pH (8.8) glycine is deprotonated and the proteins are separated based on their size due to the increased polyacrylamide concentration in the separation gel.

Discontinuous SDS-PAGE was performed with a vertical electrophoresis system (Mini-PROTEAN Tetra System, Bio-Rad Laboratories GmbH, Munich, Germany). The polyacrylamide (Rotiphorese Gel 30, Carl Roth GmbH, Karlsruhe, Germany) concentration was adapted based on the molecular weight of the separated proteins to 5, 10 or 15 % polyacrylamide. Gels were run at 80 V and constant current for focusing and above 120 V for separation.

2.2.9.4 Immunoblotting

During immunoblotting, the separated and negatively charged proteins are transferred from the gel by an electric field onto a carrier membrane that enables immunodetection. Binding of the proteins via interaction of nonpolar residues with the membrane requires alcohol (methanol)-based separation of SDS from the proteins during the transfer.

Proteins separated by SDS-PAGE were transferred to a polyvinylidene difluoride (PVDF) membrane (Immun-Blot PVDF, Bio-Rad Laboratories GmbH) in a vertical blotting system (Criterion Blotter, Bio-Rad Laboratories GmbH). Therefore, membranes were activated in methanol, applied to the gels, and transfer was performed at 100 V and constant current for 1 h at 4 °C or overnight at 30 V and 4 °C.

2.2.9.5 Immunodetection

The immunodetection of proteins during western blot analysis is usually achieved by a horse-radish peroxidase (HRP)-catalyzed luminescence reaction. HRP catalyzes the chemiluminescent oxidation of luminol under consumption of H_2O_2. The chemiluminescence reaction can be imaged by usage of radiographic films (RX-N, FUJIFILM Europe GmbH, Düsseldorf, Germany), which in turn can be developed photographically (Agfa CP 1000 X-ray film processor; AGFA, Cologne, Germany).

After immunoblotting, the membranes were blocked towards unspecific antibody binding with either 5 % non-fat dry milk in Tris-buffered saline with Tween 20 (TBS-T) or 5 % BSA in TBS-T for 1 h at RT while rolling or overnight at 4 °C. Subsequently, the blocked membranes were incubated with primary antibody solution (2.1.5; Tab. 9) overnight at 4 °C, washed three times with TBS-T and incubated with the respective HRP-coupled secondary antibody (2.1.5; Tab. 10) for 2 h at RT while rolling. The membranes were again washed with TBS-T and enhanced chemiluminescence (ECL) was applied to enable detection. Western blot results were analyzed by densitometric analysis using the software ImageJ (National Institutes of Health, USA) and were normalized on the respective levels of a housekeeping gene for normalization.

2.2.9.6 Stripping of membranes

Membranes were stripped from proteins to enable subsequent immunodetection of proteins with a similar size. Depending on the protein and purity requirements for stripping, membranes were either stripped pH-based by application of a low pH buffer or stringently by usage of SDS for solubilization and 2-mercaptoethanol to denature the antibodies.

In case of stringent stripping, membranes were incubated in stringent stripping buffer at 50 °C for 30 min and subsequently washed extensively in TBS-T to remove the 2-mercaptoethanol. After the wash, the membranes were blocked again as already described and used for further immunodetection. For pH-based stripping, membranes were incubated in pH-based stripping buffer (pH 2.2) and incubated for 10 min at RT while shaking. The buffer was replaced, and the incubation step was repeated. Subsequently, the membranes were washed twice in PBS for 10 min at RT, washed twice in TBS-T for 5 min at RT and were again blocked and re-used for immunodetection as already described.

2.2.9.7 Western blot analysis of cell fractions

To analyze the protein content in the cytoplasmic fraction and the nuclear fraction of endothelial cells, cell fractionation was performed based on the application of detergents that solubilize the outer membrane of cells in combination with shearing of the obtained nuclei to enable total detection of proteins in the nuclear compartment.

HUVECs were seeded into 10 cm cell culture dishes, grown to confluency and treated with PT as indicated. After treatment, the cells were washed once with ice-cold PBS, transferred into pre-cooled tubes and sedimented by centrifugation at 500 g for 5 min at 4 °C. The pellets were resuspended in hypotonic buffer and incubated on ice for 15 min. Subsequently, the cells were supplemented with 0.75 % NP40 and directly vortexed at maximum setting for 10 s. The nuclei were separated from the cytoplasm by centrifugation at 17,000 g for 1 min at 4 °C. The supernatant (cytoplasm) was transferred to fresh tubes, and the nuclei were washed once by resuspension in isotonic buffer and incubated for 5 min at 4 °C and were sedimented by centrifugation at 3,000 g for 3 min at 4 °C. The supernatant was subtracted, and the nuclei were resuspended in 50 µL of RIPA lysis buffer supplemented with 0.5 mM DTT, transferred into TPX-tubes (Diagenode, Belgium) and sonicated at ‘high’ setting in a Bioruptor plus system (Diagenode, Belgium) for 2–4 cycles with 30 s on- and 30 s off-intervals at 4 °C. The obtained lysates were centrifuged at 17,000 g for 5 min at 4 °C and transferred to fresh tubes. The total protein content for each fraction was analyzed as already described and the samples were supplemented with 5x SDS-PAGE sample buffer, boiled at 95 °C for 5 min and used for western blot analysis.

2.2.10 Quantitative real-time polymerase chain reaction (qRT-PCR) analysis

The quantitative real-time polymerase chain reaction (qRT-PCR) was used to compare the mRNA content of different proteins in endothelial cells after treatment with MTAs. This method utilizes the ability of fluorescent DNA-binding dyes to intercalate into DNA and hence, can be used as a measure to compare the DNA content in different samples. Since qRT-PCR utilizes DNA, the initially isolated RNA has to be transcribed into complementary DNA (cDNA) by a reverse transcriptase reaction. Quantification of the qRT-PCR results was performed based on the $2^{-\Delta\Delta Ct}$ method [377].

2.2.10.1 Sample preparation and RNA isolation

HUVECs or HMECs were grown to confluency in 6-well cell culture plates and treated with MTAs as indicated. After treatment, the cells were washed once with PBS and lysed by the addition of 350 µL of RLT buffer (RNeasy Mini Kit, Qiagen GmbH, Hilden, Germany) supplemented with 2-mercaptoethanol (1:100) and frozen at -80 °C for at least 1 h. Isolation of the total RNA was performed with the RNeasy Mini Kit (Qiagen GmbH) including on-column-based DNA digestion with the RNase-free DNase Set (Qiagen GmbH) according to the manufacturer's instruction. Briefly, the lysates were thawed on ice, scraped off the plates and transferred into fresh tubes. An equal amount of 70 % ethanol was added, mixed by pipetting and the solution was transferred into an RNeasy spin-column and centrifuged. The flow-though was discarded, and the column was washed once with 500 µL of RW1 buffer, centrifuged again and supplemented with 80 µL of DNase I mix for 15 min at RT. After the incubation, the columns were washed again with RW1 buffer and subsequently washed twice with 500 µL of RPE buffer. RNA was eluted by addition of 30 µL of RNase-free water and the RNA concentration in each sample was measured by absorbance at 260 nm using a P 330 nanophotometer (Implen GmbH, Munich, Germany).

2.2.10.2 Reverse transcription reaction

Isolated RNA was reversely transcribed into cDNA using the SuperScript II Reverse Transcriptase (Thermo Fisher Scientific GmbH). For this, 1 µg of the respective RNA was adjusted to 7 µL with RNase-free water and supplemented with 1 µL of random primer N6 (100 pmol) and 4 µL of a dNTP mix (2 mM).The samples were heated for 10 min at 70 °C and cooled on ice for 2 min. Subsequently, 4 µL of 5x reverse transcriptase reaction buffer, 2 µL of DTT (100 mM), 1 µL RNasine and 1 µL of reverse transcriptase were added to each sample and incubated at RT for 10 min. Reverse transcription was performed at 42 °C for 1 h. The reaction was stopped by the addition of 80 µL of dist. water and incubation at 70 °C for 10 min. The obtained cDNA was stored at -20 °C until further use.

2.2.10.3 qRT-PCR

qRT-PCR based on the $2^{-\Delta\Delta Ct}$ method was performed with a StepOnePlus System (Applied Biosystems GmbH) and the Power SYBR Green PCR Master Mix (Life Technologies GmbH, Darmstadt, Germany). All standard qRT-PCR reaction were performed with 10 µL of sample volume. For this, the respective primer pair (2.1.6, Tab. 13) was diluted to 4 µM in 2.5 µL to reach a final concentration of 1 µM. 2.5 µL of the primer dilution was mixed with 2.5 µL of a 1:5 cDNA dilution and 5 µL of SYBR Green PCR master mix was added. The qRT-PCR plate was sealed with a plate sealer for optical analysis and centrifuged briefly to sediment all liquid. Results were normalized on the respective levels of the GAPDH mRNA. Table 18 shows the qRT-PCR program that was used.

Table 18. Program for the quantitative real-time polymerase chain reaction.

Reaction step	Temperature	Time period	Cycle number
Initial heating	95 °C	10 min	1
Denaturing, annealing and elongation	95 °C 60 °C	15 s 60 s	40
Melt curve stage	95 °C 60 °C 95 °C	15 s 60 s 15 s	1

2.2.10.4 mRNA decay

mRNA decay experiments were performed to test the decay rate of VCAM-1 mRNA after treatment of HUVECs with the MTAs. This assay utilizes the ability of actinomycin D (ActD) to inhibit transcription, thus enabling analysis of the given VCAM-1 mRNA levels over time.

To test the decay rate of the VCAM-1 mRNA, HUVECs were seeded into 6-well cell culture plates, grown to confluency and activated with TNF (10 ng/mL) for 12 h. Subsequently, the TNF containing medium was replaced and 1.6 µM of ActD (Sigma-Aldrich Chemie GmbH, Taufkirchen, Germany) was added to inhibit transcription. The respective MTA was added to 300 nM and samples were taken at different treatment times. Isolation of RNA and subsequent qRT-PCR analysis was performed as described above. Results were normalized on the GAPDH content of the TNF-only treated samples.

2.2.11 Chromatin immunoprecipitation (ChIP) – qRT-PCR

To test the enrichment of different proteins at target genes, chromatin immunoprecipitation (ChIP) was used. In this method, proteins such as transcription factors are cross-linked to the DNA by chemical agents and subsequently sheared by sonication to generate DNA fragments with a size distribution of approx. 200–600 bp length. The chromatin fragments can then be immunoprecipitated with a respective target-binding antibody and isolated using beads. After elution, the immunoprecipitated DNA fragments can be used to analyze the enrichment of the target proteins for different samples via qRT-PCR analysis by the use of primers encompassing the respective protein-binding sites.

2.2.11.1 Sample preparation, cross-linking reaction and chromatin shearing

HUVECs were grown to confluency in 10 cm dishes and treated as indicated. After treatment, the cells were washed once with ice-cold PBS and protein complexes were cross-linked using 2 mM disuccinimidyl glutarate (DSG; SantaCruz Biotechnologies, Germany) in PBS for 45 min at room temperature while shaking. Subsequently, the cells were washed three times with PBS and proteins were cross-linked to the DNA by adding 1 % (v/v) methanol-free formaldehyde (Polysciences, Hirschberg an der Bergstraße, Germany) in PBS for 10 min at room temperature. The cross-linking reaction was quenched by addition of 125 mM glycine for 5 min at room temperature. The cross-linked cells were washed twice with ice-cold PBS, scraped off and sedimented at 1,000 g and 4 °C for 5 min and resuspended in 375 µL of ChIP lysis buffer supplemented with PMSF and Complete Mini and incubated on ice for 10 min while shaking. Subsequently, 187.5 µL of lysates were transferred into 1.5 mL TPX-tubes (Diagenode, Belgium) and the chromatin was sheared at the ‘high’ setting with a Bioruptor plus system (Diagenode, Belgium) at 4 °C for three times with 10 cycles at 30 s on- and 30 s off-intervals to obtain chromatin fragments of 200–600 bp length.

2.2.11.2 Immunoprecipitation

After shearing, cell debris was sedimented by centrifugation at 8,000 g for 10 min at 4 °C and 100 µL of the obtained supernatant was diluted 1:10 in RIPA supplemented with 1 mM PMSF and Complete Mini. 1 µg of the respective antigen-binding or negative control antibody (2.1.5; Tab. 12) was added and samples were incubated overnight at 4 °C while rotating. Prior to the immunoprecipitation, Protein A/G magnetic beads (Thermo Fisher, Germany) were pre-blocked with 75 ng/µL herring sperm DNA (Promega GmbH) per µL of beads and 0.1 µg/µL BSA per µL of beads in RIPA for 30 min at 4 °C while rotating. Subsequently, the beads were washed twice with RIPA to remove access blocking reagent. The beads were resuspended in RIPA to their initial volume, and 20 µL of bead solution was added to each chromatin sample and incubated for 4 h at 4 °C while rotating in order to immunoprecipitate chromatin-antibody complexes. Subsequently, the beads were washed once with ChIP low salt washing buffer,

high salt washing buffer and lithium chloride-containing washing buffer by resuspension and eluted in 120 µL of ChIP elution buffer at 30 °C for 15 min while shaking. After removal of the beads, 4.8 µL of 5 M NaCl and 2 µL of 10 mg/mL RNase A (Roche, Germany) was added and incubated overnight at 65 °C. On the next day, 2 µL of 20 mg/mL proteinase K (Thermo Fisher Scientific) was added and incubated for 1 h at 60 °C. In case of percent-input ChIP, 50 µL of the initially sheared chromatin lysate were supplemented with 70 µL of elution buffer and subjected to the same treatment as described above.

2.2.11.3 Isolation of immunoprecipitated chromatin

The immunoprecipitated DNA was isolated using the ChIP DNA Clean and Concentrator Kit (Zymo Research, Freiburg, Germany) according to the manufacturer's instructions and used for qRT-PCR analysis. Briefly, the samples were supplemented with 600 µL of ChIP DNA binding buffer, vortexed and transferred into the ChIP DNA Clean and Concentrator tubes. After centrifugation, the flow-through was discarded and the columns were washed twice with 200 µL of ChIP washing buffer. After centrifugation, the DNA fragments were eluted with ChIP DNA elution buffer. To generate samples containing 2 % of the total immunoprecipitated DNA for percent-input ChIP. The respective input sample was eluted in 125 µL of elution buffer. All remaining samples were eluted in 100 µL of elution buffer.

2.2.11.4 ChIP-qRT-PCR

ChIP-qRT-PCR was performed as described above. However, ChIP-qRT-PCR runs were performed with a 20 µL reaction volume to enable higher accuracy. ChIP-qRT-PCR was performed with primers encompassing the most proximal transcription factor binding sites in the promoters of target genes (p65, cJun) or untranslated regions downstream of the transcription start site, where RNA polymerase stalling occurs (RNA polymerase II and Brd4). The ChIP primers are listed in section 2.1.6; Tab. 14. For analysis of transcription factor and RNA polymerase enrichment, data was normalized on the background levels of a sequence of the *rpl13a* 3'-untranslated region. Brd4 enrichment data was analyzed based on the percent-input method using the equation: $100 \times 2^{(Ct_{input} - Ct_{IP})}$.

2.2.12 Reporter gene assay

The reporter gene assay is a sensitive method used to examine the gene expression activity of a target gene. In this study, the Dual-Luciferase reporter assay system (Promega GmbH) was used to study the influence of the MTAs on the NFκB- and AP-1-induced promoter activity. This assay utilizes the fluorescence activity of the firefly luciferase (*Photinus pyralis*) gene under control of the NFκB or AP-1 response elements in combination with the *Renilla* luciferase (*Renilla reniformis*) gene downstream of the constitutionally expressed herpes simplex virus (HSV) thymidine kinase (TK) promoter as an internal control. Figure 19 shows the respective plasmids containing the NFκB-induced firefly luciferase (left) and the AP-1-induced firefly luciferase (right) as well as the *Renilla* luciferase (bottom):

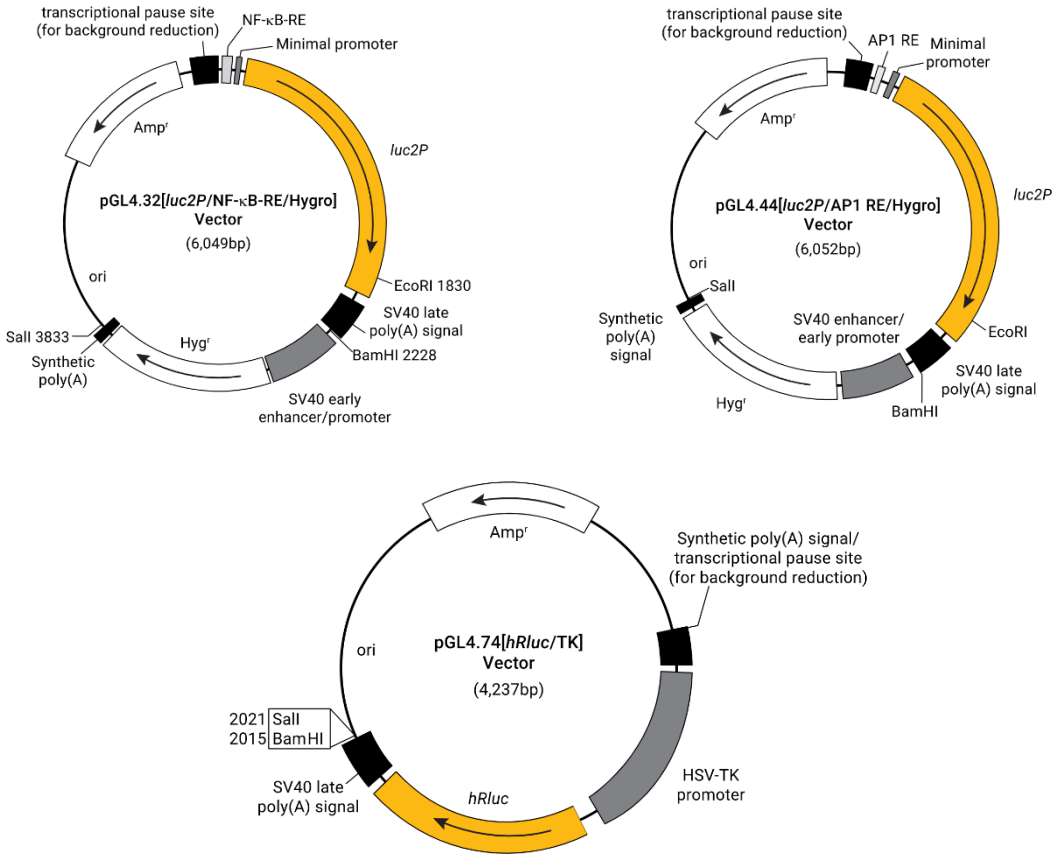

Figure 19. Map of pGL4.32[*luc2p*/NFκB-RE/Hygro] (left) and pGL4.44[*luc2P*/AP1-RE/Hygro] (right) vectors containing the *Photinus* luciferase gene *luc2P* under control of the NFκB or AP-1 response element (RE), respectively. In addition, these vectors contain two additional resistance markers for ampicillin and hygromycin. (bottom) Map of the pGL4.74[*hRluc*/TK] vector containing the *Renilla* luciferase under control of the HSV-TK promoter used for normalization. Vector maps taken from Promega.

The respective plasmids (obtained from Promega) were amplified in *E. coli* DH5α, isolated and purified and used to transfect endothelial cells prior to the reporter gene assay.

2.2.12.1 Transformation of *E. coli* DH5α

Chemically competent *E. coli* DH5α cells were thawed on ice, and 0.5 µL (approx. 500 ng) of the respective plasmid was added and the cells were incubated on ice for 30 min. The cells were subjected to heat shock at 42 °C for 45 s and cooled down on ice for 2 min. Subsequently, cells were supplemented with 500 µL of LB medium. For recuperation, cells were incubated at 37 °C, shaking for 1 h. After incubation, the transformed cells were plated on LB agar plates containing the respective antibiotic (100 µg/mL ampicillin) and incubated overnight at 37 °C.

2.2.12.2 Plasmid preparation and endotoxin removal

Plasmids were prepared from 100 mL overnight cultures with the PureYield Plasmid Midiprep System (Promega GmbH) according to the manufacturer's manual. After the plasmid preparation, residual endotoxins were removed using the MiraCleanKit (Mirus Bio LLC, Medison, Wisconsin, USA) according to the manufacturer's instructions. Briefly, the plasmids were supplemented with the EndoGO Reagent and incubated on ice for 5 min and subsequently incubated for 30 min at 50 °C. The mixture was again incubated for 5 min on ice and centrifuged at 14,000 g for 1 min at RT. The upper phase, containing the endotoxins was removed and the procedure was repeated at least twice to sufficiently remove any endotoxin. Subsequently, the DNA was precipitated by adding pure ethanol cooled to -20 °C, and the samples were incubated at -20 °C for 30 min. The DNA was pelleted by centrifugation at 17,000 g for 20 min at 4 °C and allowed to air-dry and resuspended in DNase/RNase-free water.

2.2.12.3 Plasmid transfection and sample preparation

For reporter gene assays, endothelial cells were transfected with the purified reporter gene plasmids using the HUVEC Nucleofactor Kit (Lonza Cologne GmbH, Cologne, Germany), which is based on electroporation of the target cells, according to the manufacturer's instructions. Therefore, confluent endothelial cells were detached, and the number of cells was determined using a hemocytometer. $1x10^6$ cells were pelleted at 300 g for 5 min at RT and resuspended in 100 µL of Nucleofactor solution. Subsequently, 3.5 µg of the firefly reporter plasmid and 1.4 µg of the *Renilla* reporter plasmid were added to the suspension, and the mixture was directly transferred into Nucleofactor cuvettes and electroporated using the Nucleofactor program A034 of the electroporator Nucleofactor 2b (Lonza Cologne GmbH). After electroporation, 560 µL of ECGM was added, and the cells were seeded into collagen pre-coated 48 well plates ($1.25x10^5$ cells per well), prefilled with 500 µL ECGM and incubated at 37 °C and 5 % CO_2. After 5 h, the medium was changed to remove the Nucleofactor solution. Approximately 24 h after transfection, the cells were treated as indicated and were washed once with 500 µL of PBS, lysed with 65 µL of passive lysis buffer (PLB) and stored at -80 °C until usage in the Dual-Luciferase reporter assay.

2.2.12.4 Dual-Luciferase reporter assay

The Dual-Luciferase reporter assay is based on the co-transfection of two separately expressed reporter genes in one sample. While one of the reporter genes, in this case the *Phontinus* firefly luciferase, is under control of the NFκB or AP-1 promoter of interest (pGL4.32[*luc2p*/NFκB-RE/Hygro] or pGL4.44[*luc2P*/AP-1-RE/Hygro]), the other reporter gene, namely the *Renilla* luciferase, is under control of a constitutively expressed HSV-TK promotor (pGL4.74[*hRluc*/TK]). This assay correlates the activity of the promoter of interest to the light emitting reaction catalyzed by the firefly luciferase. Since the reporter gene is located downstream to the promoter of interest, any light emission is directly proportional to the activity of the promoter. While the firefly luciferase catalyzes the ATP-dependent reaction of luciferin to oxyluciferin, the *Renilla* luciferase catalyzes the oxygen-dependent reaction of coelenterazine to coelenteramide, both of which emit light at their respective wavelength (550–580 nm for firefly and 480 nm for Renilla). The addition of a second constitutively expressed *Renilla* luciferase serves as an internal control, on which the experimentally obtained values can be normalized to achieve higher accuracy.

The assay was performed according to the manufacturer's instructions. Therefore, the cell lysates were thawed at RT while gently shaking. To remove cell debris, lysates were centrifuged at 17,000 g for 1 min at RT and 10 µL of the supernatant were transferred into a 96 well plate suitable for luminescence measurements. The luciferase substrate solutions LARII and Stop&Glo were freshly prepared and separately transferred into the injectors of an Infinite Pro F200 plate reader (Tecan Trading AG). The injectors were primed with the respective substrate solution and the light emitting reaction of the *Photinus* luciferase was induced by addition of 50 µL of LARII to each well and the luminescence activity was measured. Subsequently, 50 µL of Stop&Glo were added to each well to quench the *Photinus* luciferase luminescence reaction and induce the *Renilla* luciferase luminescence reaction followed by luminescence measurements. All measurements were performed with a 2 s delay after substrate injection with a read time of 10 s. The obtained values for the AP-1-induced *Photinus* luciferase luminescence were normalized to the obtained *Renilla* luciferase luminescence values.

2.2.13 Small interfering RNA transfection

Transfection of HUVECs with small interfering RNA (siRNA) was used to test the effects of Brd4 knock-down on the cell surface expression of ICAM-1 and VCAM-1. The transfection of HUVECs with siRNA was performed chemically with the GeneTrans II transfection reagent (MoBiTec, Goettingen, Germany). The chemical transfection of cells is usually performed by adding plasmids to a positively charged transfection reagent that enables adhesion to the negatively charged cell surface and subsequent endocytosis of the DNA-reagent complexes.

Transfection of HUVECs was performed with the GeneTrans II transfection reagent (MoBiTec) based on the manufacturer's instructions. Briefly, HUVECs were seeded into 6-well plates (25,000 cells/cm^2) and cultivated overnight. Transfection was performed at a confluency of 70–80 % with either smart-pool non-targeting siRNA or smart-pool siRNA targeting Brd4 purchased from Dharmacon (Lafayette, Colorado, USA) in FCS-free ECGM supplemented with 2 mM of L-glutamine (Thermo Fisher Scientific) under cell culture conditions. After 4 h, the transfected cells were supplied with fresh ECGM and were incubated overnight. On the next day, transfected cells were again supplied with fresh medium. The knock-down efficiency was tested by western blot analysis of Brd4. Experiments were performed 48 h after the initial transfection, and transfected cells were used for flow cytometric analysis of the ICAM-1 and VCAM-1 cell surface levels as described.

2.2.14 Statistic analysis

Data analysis was performed with the software GraphPad Prism 7.0 (GraphPad Software, USA). The One-way ANOVA and Tukey's post-hoc test was used for evaluation of data resulting from three or more independently performed experiments. The numbers of performed replicates (n) are shown in the figure legends. Results were considered as statistically significant when $P \leq 0.05$.

2.2.15 Images and schematics

Images in the introduction, results and discussion sections were created with BioRender.com.

3. Results

3.1 Evaluation of the anti-inflammatory potential of PT *in vivo*

3.1.1 The influence of PT on inflammation in a murine psoriasiform dermatitis model

To initially assess the anti-inflammatory potential of PT *in vivo*, the compound was tested towards it effects on the imiquimod (IMQ)-induced psoriasiform dermatitis in mice. The topically applied IMQ, which is a TLR7 ligand (2.2.6.2), induces an inflammatory response and leads to alterations of the epidermis, skin erythema, thickening and scaling of the skin as well as infiltration of leukocytes. Evaluation of the anti-inflammatory effects in the psoriasiform dermatitis mouse model is achieved *via* analyzation of the redness, thickness and scaling of the skin, represented by a score, the cumulative Psoriasiform Area Severity Index (PASI; Fig. 20).

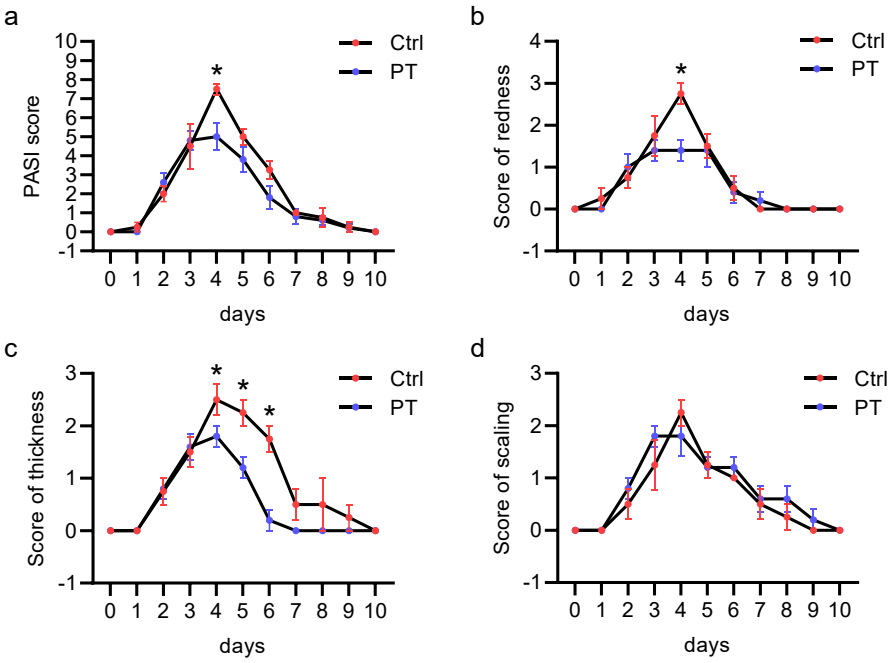

Figure 20. Pretubulysin reduces inflammation in a murine psoriasiform dermatitis model. Mice were treated by topical application of 62.5 mg of IMQ for 4 consecutive days (starting at day 1). PT (1 mg/kg) was administered s.c. at day 1, 3 and 5, and the redness, thickness and scaling were analyzed daily and combined to the cumulative PASI score. Data derived are expressed as mean ± SEM. *p ≤ 0.05 versus IMQ control for 5 individual animals.

The psoriasiform dermatitis peaked at day 4 after IMQ application, as seen by the scores for redness, thickness and scaling of the skin as well as the resulting PASI (Fig. 20). Treatment of mice with PT (1 mg/kg) significantly reduced the redness and thickness of the skin at day 4 by approx. 50 % and 30 %, respectively, while not influencing the skin scaling. This led to a reduction of the PASI for the PT-treated animals by approx. 33 %. Interestingly, while PT reduced the amplitude of skin redness, formation and resolution were not influenced. In contrast, the resolution of the increased skin thickness was accelerated for the PT-treated animals, represented by the decreased scores at day 5 and 6 as well the fact that the skin thickness already approached baseline levels 7 days after initial IMQ application.

3.1.2 The influence of PT on the inflammatory leukocyte adhesion cascade in the mouse cremaster muscle

To further analyze if the anti-inflammatory effects of PT are related to an inhibition of the leukocyte adhesion cascade, the compound was tested towards its influence on the interaction of leukocytes with the endothelium *via* intravital microscopy of the TNF-activated mouse cremaster muscle. The classic steps of the leukocyte adhesion cascade were analyzed, i.e. rolling, firm adhesion and transmigration (Fig. 21).

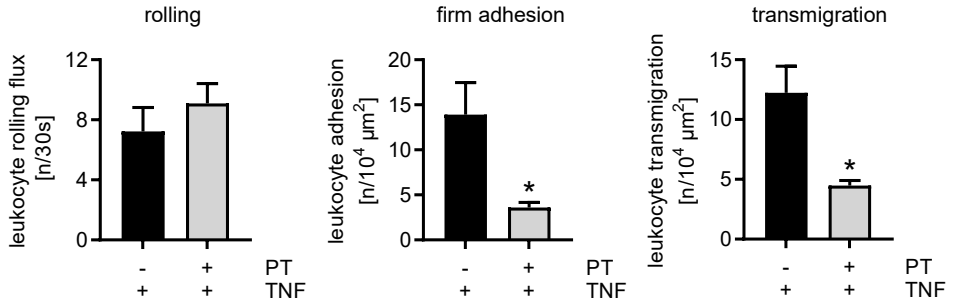

Figure 21. Pretubulysin reduces the interaction of leukocytes with the endothelium *in vivo.* Intravital microscopy of the cremaster muscle. Mice were injected with PT (1 mg/kg i.p.) or vehicle. After 30 min, TNF (25 µg/kg) was injected intrascrotally for 4 h, and intravital microscopy was performed to detect intravascular rolling, adhesion and transmigration of leukocytes to the activated endothelium in postcapillary venules of the mouse cremaster muscle. (n=3) Data are expressed as mean ± SEM. $^{\#}p \leq 0.05$ versus control, $^{*}p \leq 0.05$ versus TNF control.

Pre-treatment of mice with PT (1 mg/kg) induced a slight, non-significant increase in the TNF-induced rolling flux of leukocytes on the endothelium by approx. 25 %, but strongly decreased the firm adhesion and transmigration of leukocytes onto and through the endothelium of postcapillary mouse venules by approx. 75 % and 65 %, respectively (Fig. 21).

These results show that the anti-inflammatory effects observed for PT can be related to an inhibition of the leukocyte adhesion cascade as well as the resulting transmigration *in vivo*. In order to extend the analysis of PT and the clinically used MTAs vincristine (VIN), colchicine (COL) and paclitaxel (PAC) to the *in vitro* setting, the compounds were first tested in cell viability assays.

3.2 The influence of MTAs on cell viability and protein translation

To exclude the possibility that the effects of PT (and of the other MTAs) are associated with any cytotoxic activity, PT, VIN, COL and PAC were tested in cell viability assays in HUVECs. The metabolic activity was analyzed based on the metabolism-dependent reduction of the dye resazurin into the fluorescent dye resorufin. The membrane-integrity of the cells was analyzed based on the release of lactate dehydrogenase (LDH) and the concomitant reduction of an iodonitrotetrazolium salt to an absorbance active formazan product (Fig. 22).

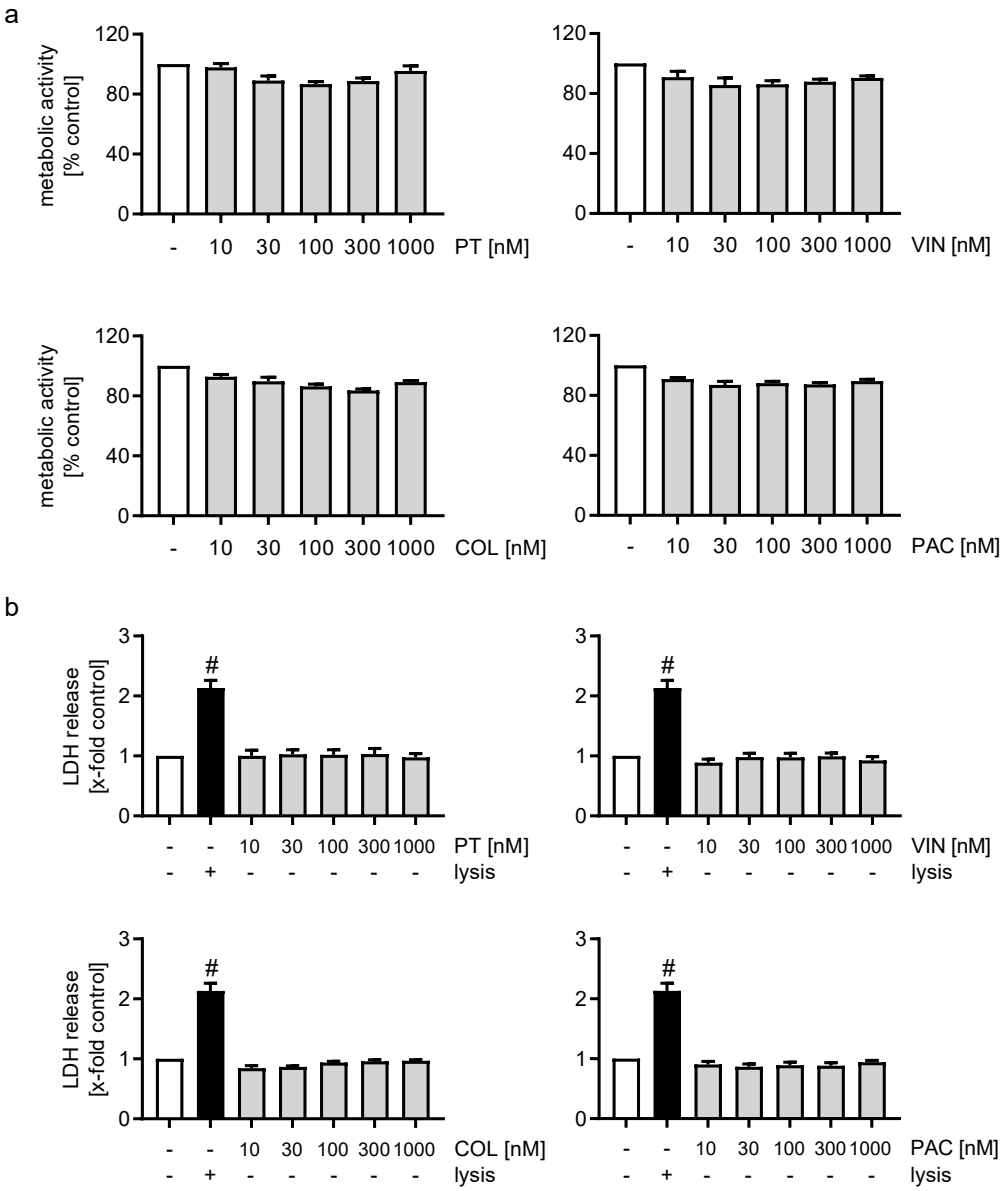

Figure 22. Pretubulysin and the other MTAs do not significantly impact the metabolic activity and membrane integrity of HUVECs. Confluent HUVECs were treated with different concentrations (10, 30, 100, 300, 1000 nM) of PT, VIN, COL or PAC for 24 h. (a) Metabolic activity measured by fluorescence reading and (b) the membrane integrity as measured by absorbance reading. For control, cells were lysed with detergent (n=4). Data are expressed as mean ± SEM. $^{\#}p \leq 0.05$ versus control.

Treatment of HUVECs with PT, VIN, COL or PAC for 24 h did not negatively influence the metabolic activity (Fig. 22a) or membrane integrity (Fig. 22b) of HUVECs compared to the control cells at any tested concentration.

Due to the known characteristics of MTAs to induce mitotic arrest, the compounds were also tested for an increased apoptosis rate by measuring the number of HUVECs with a sub-diploidic state after treatment by flow cytometry (Nicoletti assay, Fig. 23).

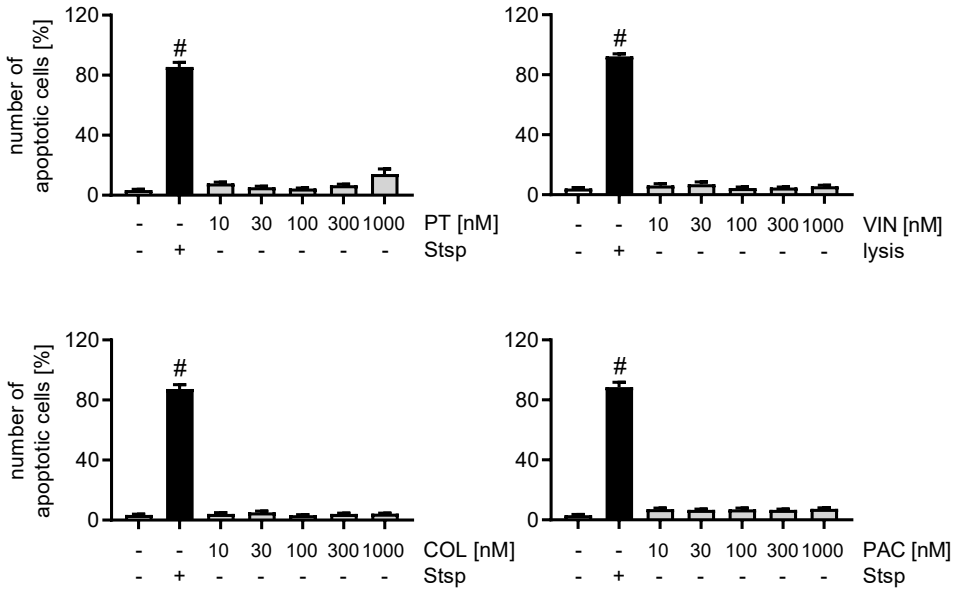

Figure 23. MTAs do not significantly increase apoptosis in HUVECs. Flow cytometric analysis of the number of subdiploidic cells. Confluent HUVECs were treated with different concentrations (10, 30, 100, 300, 1000 nM) of PT, VIN, COL or PAC for 24 h or were treated with 10 µM staurosporine for 24 h. (n=4) Data are expressed as mean ± SEM. $^{\#}p \leq 0.05$ versus control.

Compared to the staurosporine control, treatment of HUVECs for 24 h with any of the MTAs did not induce a significant increase in the rate of apoptosis for any of the concentration tested here (Fig. 23). Only in case of PT, treatment with 1000 nM induced a slight increase in the number of apoptotic cells, albeit without statistical significance. Based on these results, it is evident that PT and the other MTAs have no significant cytotoxic effects on HUVECs at the treatment conditions tested here. Due to the observed slight increase in the rate of apoptosis after treatment with 1000 nM of PT, further testing of the compounds was mainly performed with a concentration of 300 nM to exclude any cytotoxicity.

To exclude the possibility of an MTA-induced impairment of the translation machinery, the *de novo* polypeptide synthesis was analyzed microscopically. This assay is based on the incorporation of an *O*-propargyl-puromycin (OPP), which is incorporated into nascent polypetides chains, leading to chain termination and the chemoselective coupling of a fluorescent picolyl azide dye, which enables visualization of the nascent polypeptide synthesis (2.2.4) (Fig. 24).

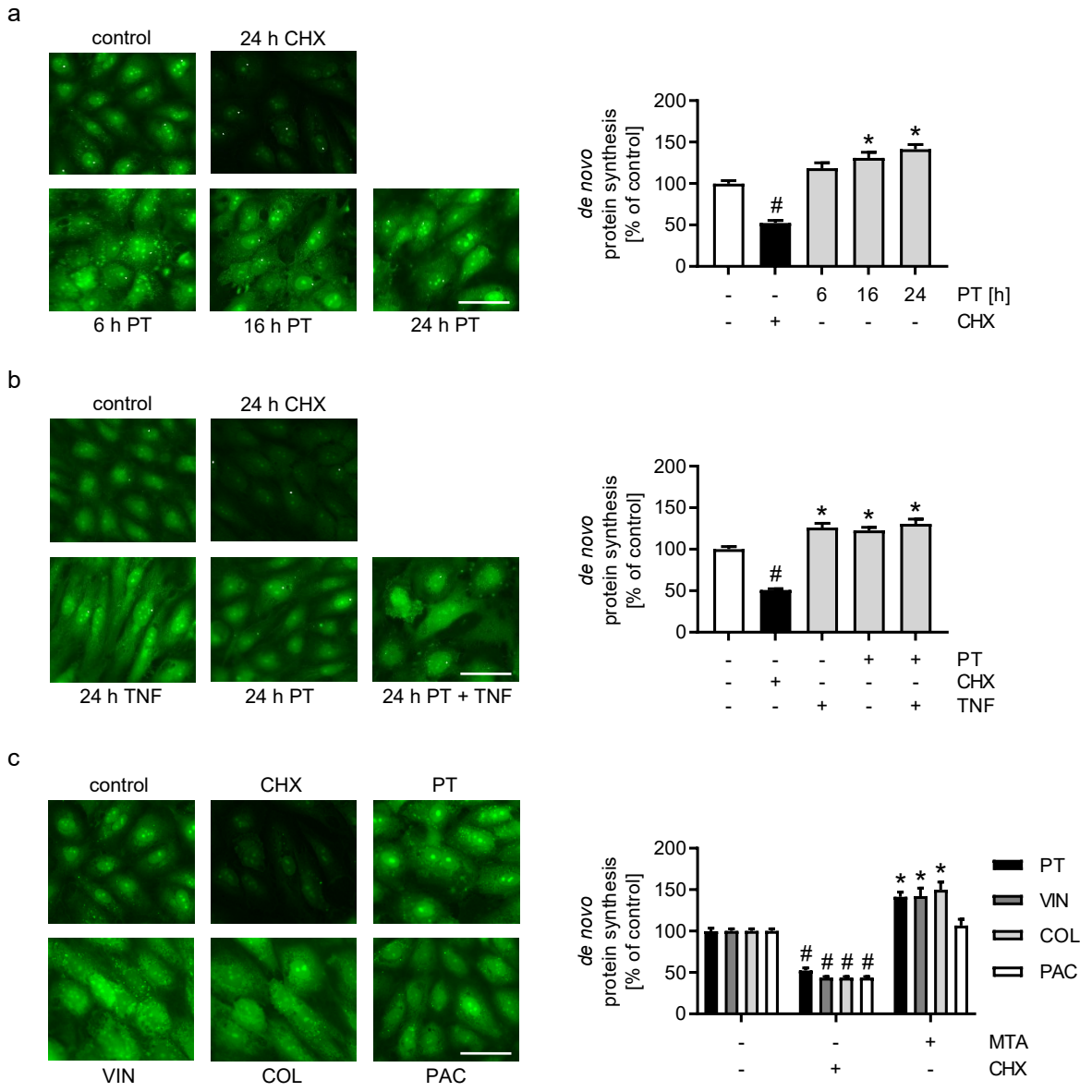

Figure 24. Pretubulysin and the other MTAs do not negatively impact *de novo* protein synthesis. Microscopical analysis of *de novo* protein synthesis *via* immunostaining of HUVECs. Confluent HUVECS were treated with PT for different durations (6, 16, 24 h; a) or pre-treated with PT for 30 min and/or activated with TNF (10 ng/mL) for 24 h (b) or treated with PT, VIN, COL or PAC for 24 h (c). 24 h of cycloheximide (1 µg/mL) treatment was used as positive control. (n=3) Data are expressed as mean ± SEM. $^{\#}p \leq 0.05$ versus control, *$p \leq 0.05$ versus TNF control. The bar represents 20 µm distance.

Treatment of HUVECs with 300 nM of PT did not negatively impact the total protein synthesis, as compared to the cycloheximide-treated cells (Fig. 24a). In contrast, treatment induced a time-dependent increase in the *de novo* protein synthesis over the control HUVECs. This behaviour was also observed

independent of the addition of TNF (Fig. 24b). Notably, stimulation of HUVECs with PT alone induced an increase in the overall polypetide synthesis comparabel to the TNF treatment. The other microtubule-destabilizers VIN and COL also led to an increase in the overall polypetide synthesis comparabel to PT (Fig. 24c). In contrast, the microtubule stabilizer PAC did not influence the protein synthesis.

3.3. Evaluation of the anti-inflammatory potential of PT concerning the leukocyte adhesion *in vitro*

3.3.1 The influence of PT on the leukocyte adhesion cascade *in vitro*

Neither PT nor any of the other MTAs showed any detrimental effects on the cell viability or protein translation machinery. In order to confirm the inhibitory effects of PT on leukocyte adhesion *in vitro*, PT was analyzed regarding its influence on the adhesion of the human monocytic cell line THP-1 to a PT-treated and TNF-stimulated HUVEC monolayer under flow conditions (Fig. 25).

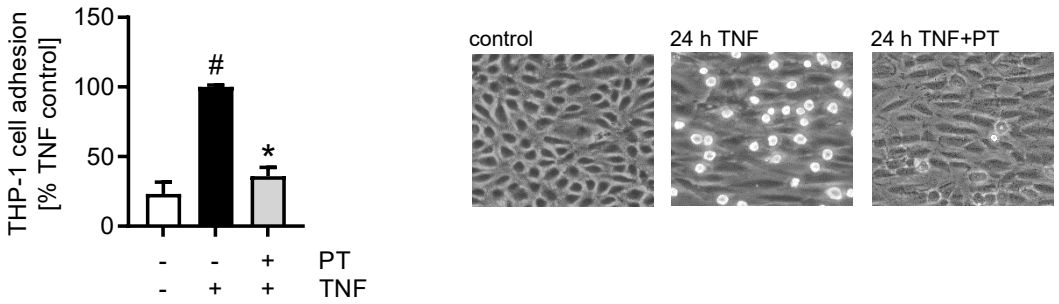

Figure 25. Pretubulysin reduces the interaction of leukocytes with the endothelium *in vitro*. THP-1 cell adhesion to endothelial cells under flow condition. HUVECs were cultivated under constant flow (5 dyn/cm^2) and pre-treated with PT (300 nM) for 30 min. TNF (10 ng/mL) was added for 24 h and fluorescence-labeled THP-1 cells were let to adhere at constant shear pressure (0.5 dyn/cm^2) for 10 min. Phase-contrast images were taken and the fluorescence signal of the adherent THP-1 cells was measured after cell lysis. (n=3) Data are expressed as mean ± SEM. $^{\#}p \leq 0.05$ versus control, $*p \leq 0.05$ versus TNF control.

24 h of TNF stimulation strongly induced the adhesion of the THP-1 cells to the endothelial cell monolayer (EC; Fig. 25). In contrast, pre-treatment of the HUVECs with 300 nM of PT significantly reduced the TNF-induced adhesion of the THP-1 cells to the ECs by approx. 65 % compared to the TNF control cells.

PT reduced the TNF-induced adhesion of leukocytes *in vivo* and *in vitro*. The upregulation of CAM expression in endothelial cells is a pre-requisite for the interaction with leukocytes during the leukocyte adhesion cascade. Due to that, PT and the other MTAs were subsequently tested towards a potential influence on the endothelial CAMs.

3.4 The Influence of PT on endothelial components of the leukocyte adhesion cascade

3.4.1 The influence of PT on the cell surface levels of endothelial cell adhesion molecules

The cytokine-induced expression and upregulation of the cell surface protein levels of the endothelial CAMs ICAM-1, VCAM-1 and E-selectin are integral parts of the leukocyte adhesion cascade (1.5). Therefore, the influence of PT on the cell surface levels of ICAM-1, VCAM-1 and E-selectin was tested by flow cytometry in TNF-activated HUVECs (Fig. 26).

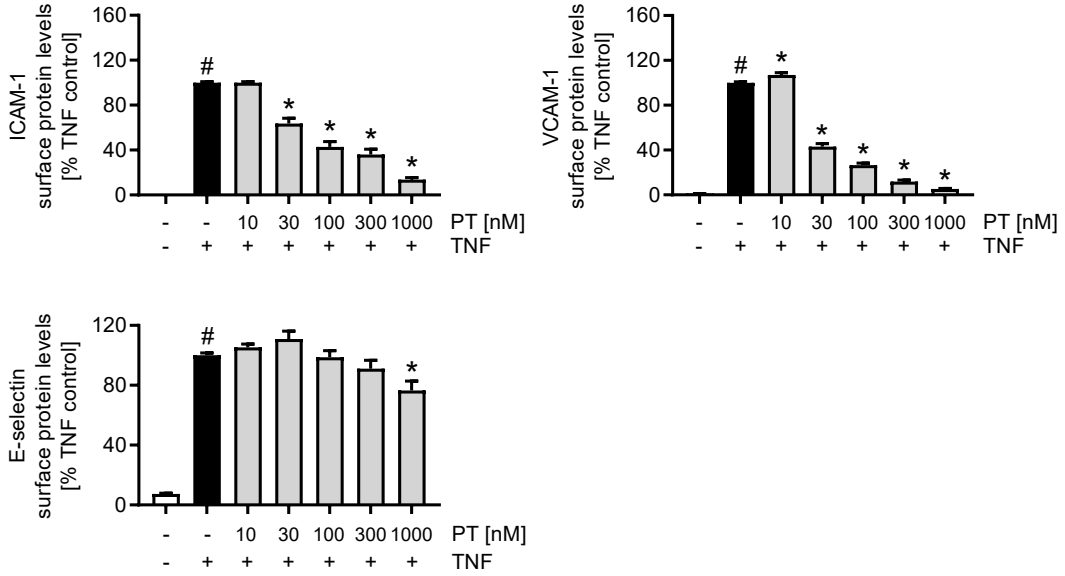

Figure 26. Pretubulysin decreases the cell surface levels of CAMs. Flow cytometric analysis of the cell surface protein levels of ICAM-1, VCAM-1 and E-selectin. Confluent HUVECs were pre-treated with different concentrations of PT (10, 30, 100, 300, 1000 nM) for 30 min and activated with TNF (10 ng/mL) for 24 h (ICAM-1 and VCAM-1) or pre-treated with PT for 20 h and activated with TNF for 4 h (E-selectin). ($n \geq 3$) Data are expressed as mean ± SEM. $^{\#}p \leq 0.05$ versus control, $^{*}p \leq 0.05$ versus TNF control.

Low concentrations of PT (10 nM) had no apparent effect on the TNF-induced ICAM-1 cell surface levels (Fig. 26). In contrast, the VCAM-1 levels were slightly, but significantly increased. At higher concentrations (30, 100, 300, 1000 nM) PT treatment led to a significant and concentration-dependent reduction of the cell surface levels of ICAM-1 and VCAM-1. The ICAM-1 levels were reduced to approx. 35 % at 300 nM and 15 % at 1000 nM of PT, while the VCAM-1 levels were reduced to approx. 10 % at 300 nM and 5 % at 1000 nM of PT. For E-selectin, low concentrations of PT of 10 and 30 nM marginally increased the TNF-induced E-selectin levels, while PT concentration-dependently decreased the levels from 100 to 1000 nM. PT only slightly reduced the E-selectin levels by approx. 10 % at a concentration of 300 nM and by approx. 25 % at a concentration of 1000 nM.

The effects of PT on the cell surface expression of VCAM-1 have also been tested upon stimulation with IL-1β, to prove the effectiveness of PT outside of TNF-induced pro-inflammatory signaling (Fig. 27).

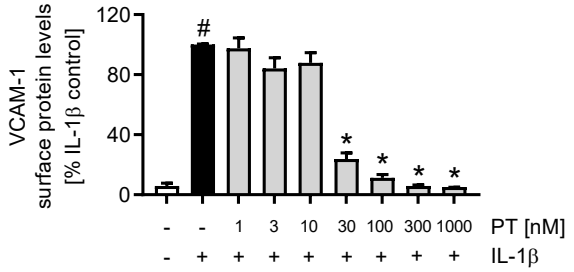

Figure 27. PT decreases the cell surface levels of VCAM-1 in a concentration-dependent manner upon stimulation with IL-1β. Flow cytometric analysis of the cell surface levels of VCAM-1 after treatment with PT. Confluent HUVECs were pre-treated with different concentrations (1, 3, 10, 30, 100, 300, 1000 nM) of PT for 30 min and activated with IL-1β (5 ng/mL) for 24 h. (n=3) Data are expressed as mean ± SEM. $^{\#}p \leq 0.05$ versus control, $^{*}p \leq 0.05$ versus IL-1β control.

PT was shown to be equally effective in inhibiting the VCAM-1 synthesis upon stimulation with IL-1β (Fig. 27). Treatment with 1 to 10 nM of PT had no significant influence on the IL-1β induced VCAM-1 levels. However, concentration of 30 nM of PT and more led to a significant inhibition of VCAM-1 on the cell surface of HUVECs with 30 nM reducing the VCAM-1 levels to approx. 24 %, 100 nM to approx. 11 % and concentrations of 300 nM and 1000 nM reducing the cell surface levels of VCAM-1 to baseline levels with 6 % and 5 % compared to the TNF control, respectively.

3.4.2 The influence of VIN, COL and PAC on the cell surface levels of the endothelial cell adhesion molecules ICAM-1 and VCAM-1

To compare the effects of PT with other MTAs, the influence of VIN, COL and PAC on the cell surface levels of ICAM-1 and VCAM-1 were tested by flow cytometry (Fig. 28).

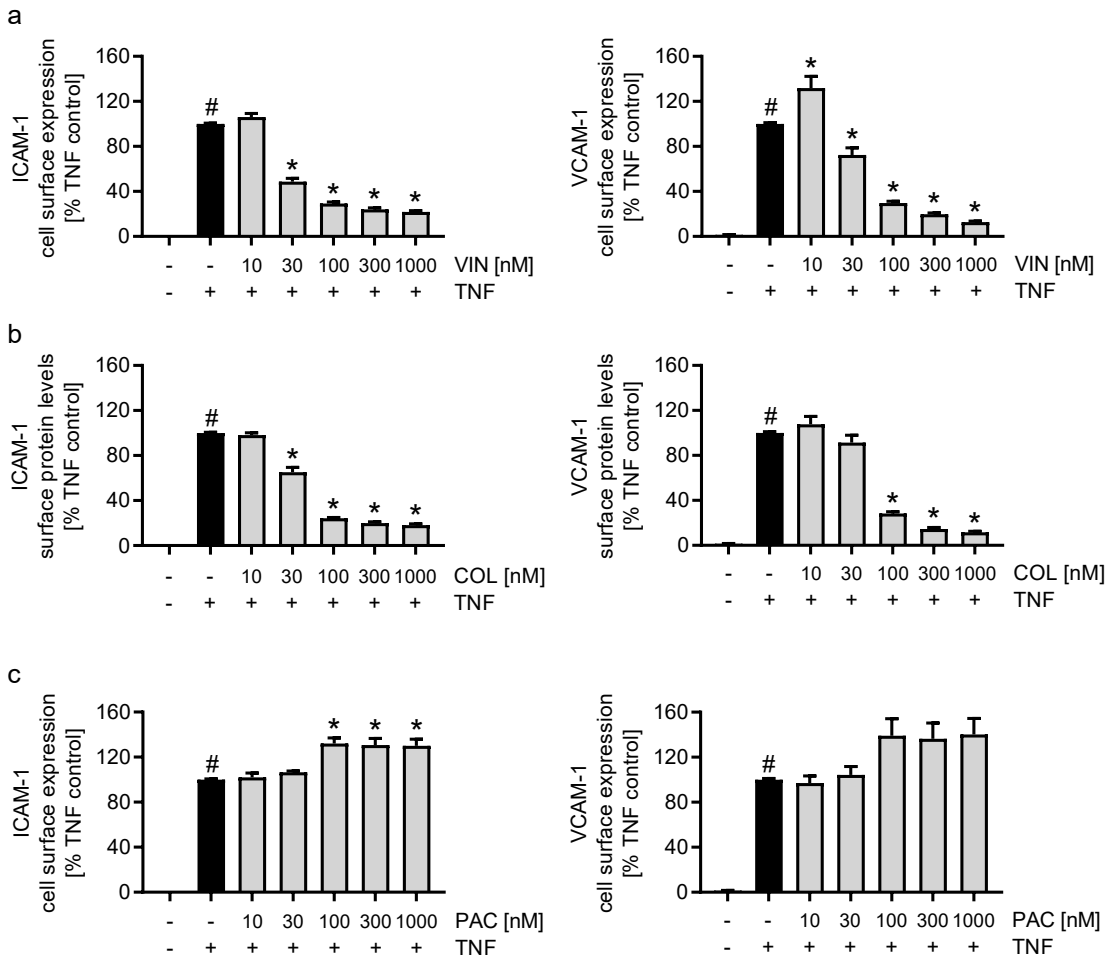

Figure 28. The depolymerizing MTAs decrease the cell surface levels of ICAM-1 and VCAM-1 in a concentration-dependent manner. Flow cytometric analysis of the cell surface levels of ICAM-1 (a, b, c; left) and VCAM-1 (a, b, c; right) after treatment with depolymerizing or stabilizing MTAs. Confluent HUVECs were pre-treated with different concentrations (10, 30, 100, 300, 1000 nM) of VIN, COL or PAC for 30 min and activated with TNF (10 ng/mL) for 24 h. (n=3) Data are expressed as mean ± SEM. $^{\#}p \leq 0.05$ versus control, $^{*}p \leq 0.05$ versus TNF control.

Treatment of HUVECs with VIN and COL led to a concentration-dependent inhibition of the ICAM-1 and VCAM-1 cell surface levels similar to PT (Fig. 28). In contrast, treatment with concentrations of 100 nM or more of the microtubule stabilizer PAC increased the ICAM-1 and VCAM-1 cell surface levels after 24 h of TNF stimulation by approx. 30 % compared to the TNF control cells.

3.4.3 Influence of MTAs on protein and mRNA levels of endothelial cell adhesion molecules

Treatment with PT or the other destabilizing MTAs significantly reduced the cell surface levels of ICAM-1 and VCAM-1. To exclude the possibility that the observed effects are due to an impairment of the secretory pathway after microtubule depolymerization, the MTAs were tested for their influence on the CAM total protein and mRNA levels (Fig. 29).

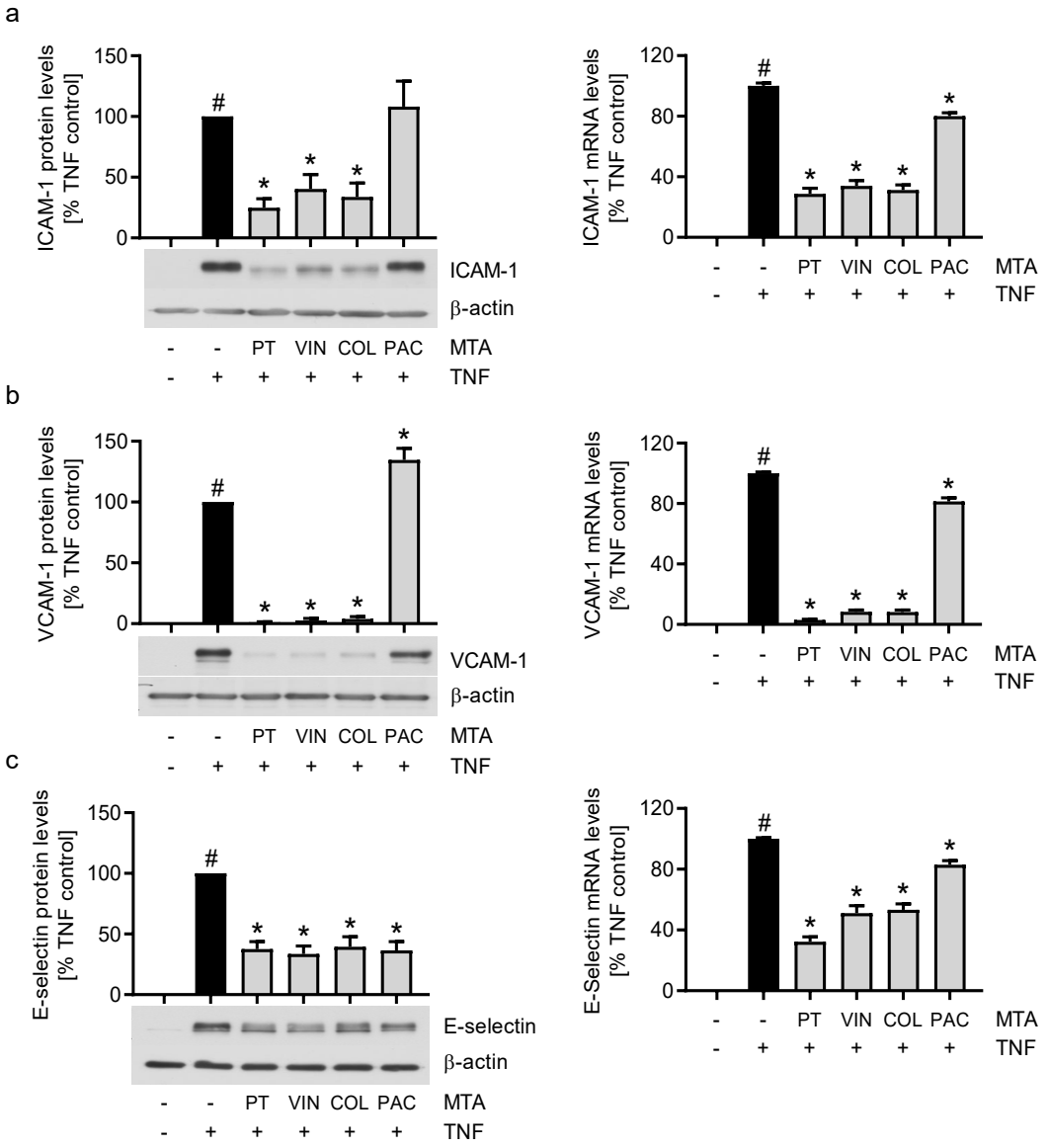

Figure 29. The destabilizing MTAs reduce the protein levels and mRNA levels of ICAM-1 and VCAM-1 and E-selectin. Western blot analysis of the total ICAM-, VCAM-1 and E-selectin protein levels (a, b and c, left) and qRT-PCR analysis of the mRNA levels (a, b and c, right). Confluent HUVECs were pre-treated with 300 nM of PT, VIN, COL or PAC and activated with TNF (10 ng/mL) for 24 h (a and b, left) or 12 h (a and b, right) or pre-treated with 300 nM MTA for 20 h and activated with TNF for 4 h (c, left) or pre-treated with MTA for 10 h and activated with TNF for 2 h (c, right). Western blot results were normalized to the respective β-actin levels, and qRT-PCR results were normalized on the respective GAPDH mRNA levels. (n=3) Data are expressed as mean ± SEM. $^{\#}p \leq 0.05$ versus control, $*p \leq 0.05$ versus TNF control.

Treatment with PT reduced the ICAM-1 protein and mRNA levels by approx. 75 % compared to the TNF control cells (Fig. 29a). The TNF-induced VCAM-1 protein and mRNA levels were reduced to baseline values, suggesting near complete inhibition of the TNF-induced VCAM-1 synthesis (Fig. 29b). Interestingly, PT also significantly reduced the E-selectin protein and mRNA levels by approx. 60 % (Fig. 29c). Compared to PT, treatment with VIN and COL lead to a similar, albeit slightly weaker reduction of the CAM protein and mRNA levels. The microtubule stabilizer PAC had no effect on the ICAM-1 protein levels, slightly induced the protein levels of VCAM-1, but reduced the E-selectin protein levels to a similar extent as the depolymerizing agents. In contrast, the mRNA levels of ICAM-1, VCAM-1 and E-selectin were reduced by approx. 10 % after treatment with PAC.

Taken together, these results show that the PT-induced inhibition of the cell surface levels of the CAMs in HUVECs also extends to the total protein and mRNA levels and are hence not the result of an impairment of the secretory pathways. To consolidate these results, the influence of the MTAs on the components of the leukocyte adhesion cascade ICAM-1 and VCAM-1 were also tested in microvascular endothelial cells.

3.4.4 Effects of PT, VIN, COL and PAC on the adhesion molecules ICAM-1 and VCAM-1 in cells of the human dermal microvascular endothelial cell line 1 (HMEC-1)

In order to confirm the results of the actions of the MTAs on the components of the leukocyte adhesion cascade obtained from HUVECs, the MTAs were also tested towards their influence on the cell surface levels (Fig. 30) and total protein levels, as well as mRNA levels (Fig. 31) of ICAM-1 and VCAM-1 in cells of the human dermal microvascular cell line-1 (HMEC-1).

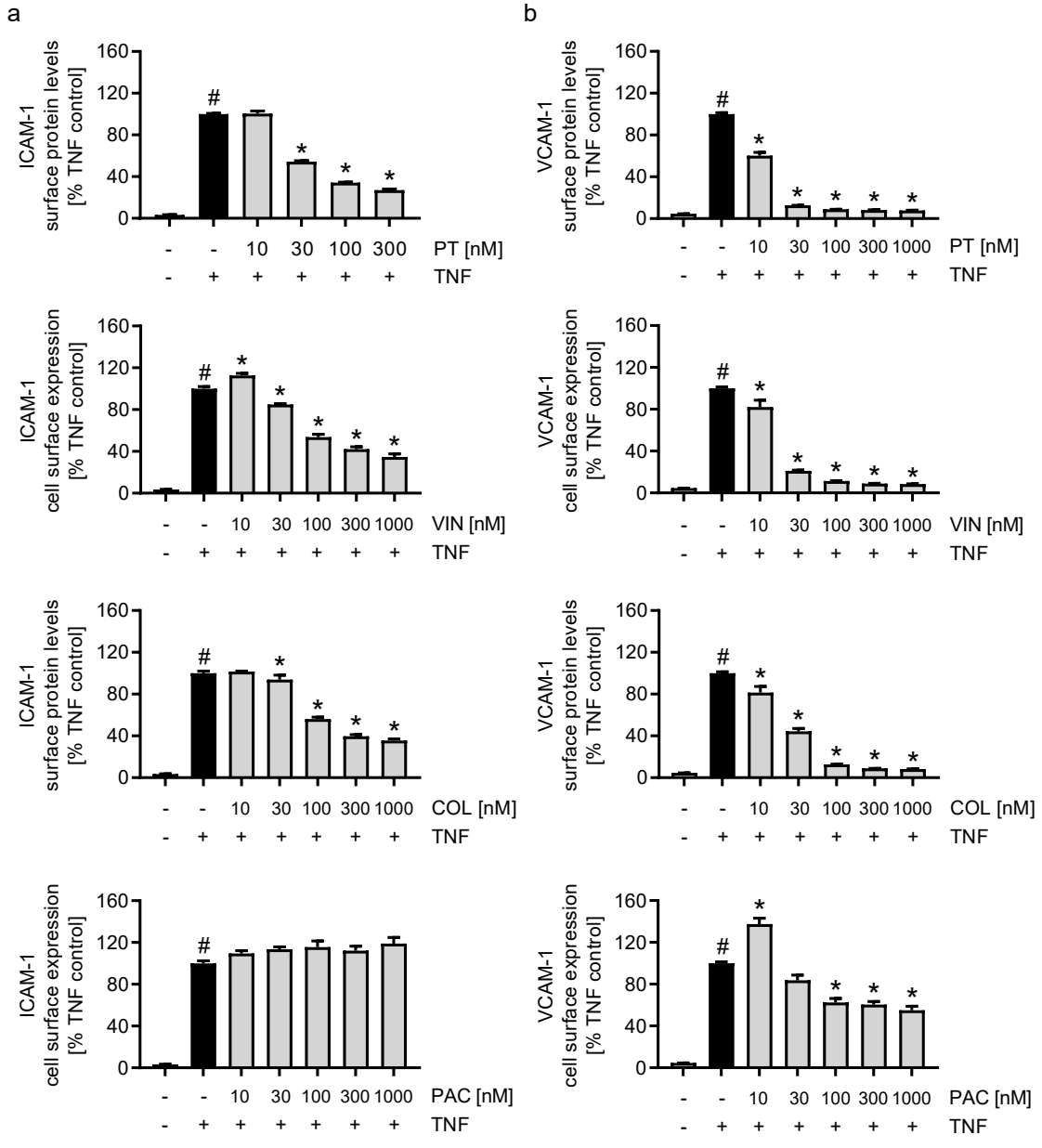

Figure 30. The depolymerizing MTAs decrease the cell surface levels of ICAM-1 and VCAM-1 in a concentration-dependent manner in HMEC-1. Flow cytometric analysis of the cell surface levels of ICAM-1 (a) and VCAM-1 (b) after treatment with depolymerizing or stabilizing MTAs. Confluent HMECs were pre-treated with different concentrations (10, 30, 100, 300, 1000 nM) of PT, VIN, COL or PAC for 30 min and activated with TNF (10 ng/mL) for 24 h. (n=3) Data are expressed as mean ± SEM. $^{\#}p \leq 0.05$ versus control, $^{*}p \leq 0.05$ versus TNF control.

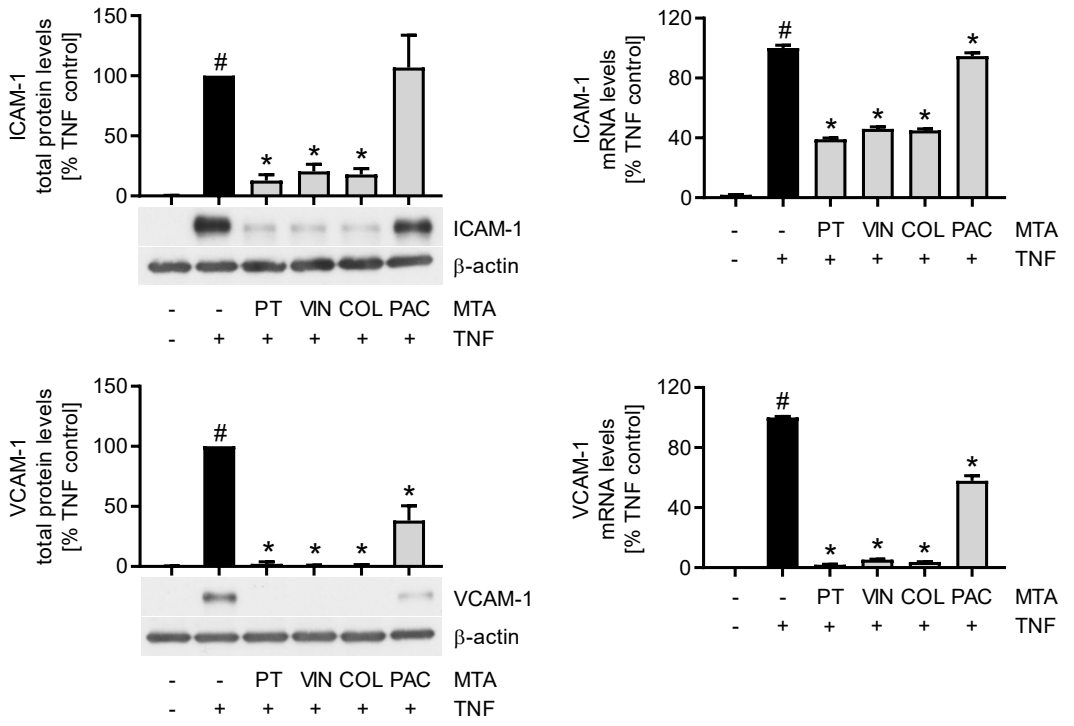

Figure 31. The destabilizing MTAs reduce the protein levels and mRNA levels of ICAM-1 and VCAM-1 in HMEC-1. Western blot analysis of the total ICAM-1 and VCAM-1 protein levels and qRT-PCR analysis of the respective mRNA levels. Confluent HMECs were pre-treated with 300 nM of PT, VIN, COL or PAC and activated with TNF (10 ng/mL) for 24 h (left) or 12 h (right). Western blot results were normalized on the respective β-actin and qRT-PCR results were normalized on the respective GAPDH mRNA levels. (n=3) Data are expressed as mean ± SEM. $^{\#}p \leq 0.05$ versus control, $^{*}p \leq 0.05$ versus TNF control.

Analysis of the cell surface levels of ICAM-1 and VCAM-1 in HMEC-1 cells after treatment with the depolymerizing MTAs revealed a concentration-dependent downregulation of the TNF-induced CAMs comparable to HUVECs (Fig. 30). Compared to the TNF controls, treatment with 300 nM of PT, VIN or COL led to an approx. 60 % reduction of the ICAM-1 and an approx. 90 % reduction of the VCAM-1 cell surface levels following 24 h of treatment. The inhibitory effects of treatment with 300 nM of the destabilizers also extended to the total protein and mRNA level (Fig. 31). In case of the microtubule-stabilizer PAC, treatment of HMECs with concentrations of 100 nM and more did not induce a significant increase in ICAM-1 cell surface levels comparable to HUVECs, with ICAM-1 total protein and mRNA levels being largely not influenced by PAC. Interestingly, treatment with 10 nM of PAC increased the cell surface levels of VCAM-1 by approx. 40 % compared to the TNF control. However, treatment with 30 nM to 1000 nM of PAC induced a concentration-dependent downregulation of the VCAM-1 cell surface levels, with VCAM-1 levels being reduced by approx. 60 % compared to the TNF control cells, which could not be observed in HUVECs. In addition, treatment of HMECs with 300 nM of PAC also led to a reduction of the VCAM-1 total protein levels and reduced the VCAM-1 mRNA levels comparable to HUVECs.

3.5 The influence of PT on pro-inflammatory signaling cascades

PT did not impair the secretory pathway, but significantly reduced the expression of the CAMs ICAM-1 and VCAM-1. Due to that, the influence of PT on the pro-inflammatory NFκB and AP-1 signaling cascades and also additional pro-inflammatory factors that are involved in CAM induction was tested.

3.5.1 The NFκB signaling cascade

3.5.1.1 The TNF receptor 1

The NFκB signaling cascade constitutes one of the most important pro-inflammatory signaling cascades for CAM induction (1.6.1). The first step is thereby the integration of external stimuli by binding of TNF to the TNFR1. Earlier studies have correlated treatment of endothelial cells with colchicine with a down-regulation of TNFR1 and a resulting desensitization of endothelial cells to TNF (1.8.4.3.1). Therefore, the protein levels of the TNFR1 were analyzed after short and long treatment with PT (Fig. 32).

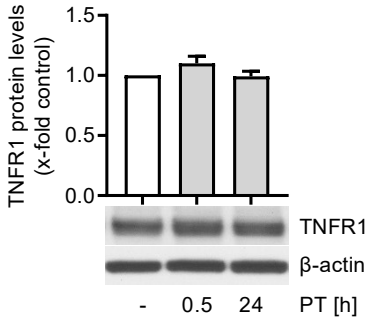

Figure 32. Pretubulysin does not affect the total TNFR1 protein levels. Western blot analysis of the TNFR1 protein levels. Confluent HUVECs were treated with PT (300 nM) for 0.5 h or 24 h. Results were normalized on the respective β-actin levels. (n=3)

PT did not affect the TNFR1 protein levels after short (0.5 h) or long (24 h) treatment in a negative manner (Fig. 32). Based on this, it is to argue that neither short nor long pre-stimulation with PT affects the TNFR1 levels in a way that could negatively influence the induction of the pro-inflammatory signaling cascades.

3.5.1.2 Influence of PT on the activity of the IκB kinase and IκB degradation

Due to its function in deactivating the proteins of the IκB family, the IKK plays a central role in the activation of NFκB (1.3.1). The influence of PT on the activity of IKK and the resulting degradation of IκBα was tested by western blot analysis (Fig. 33).

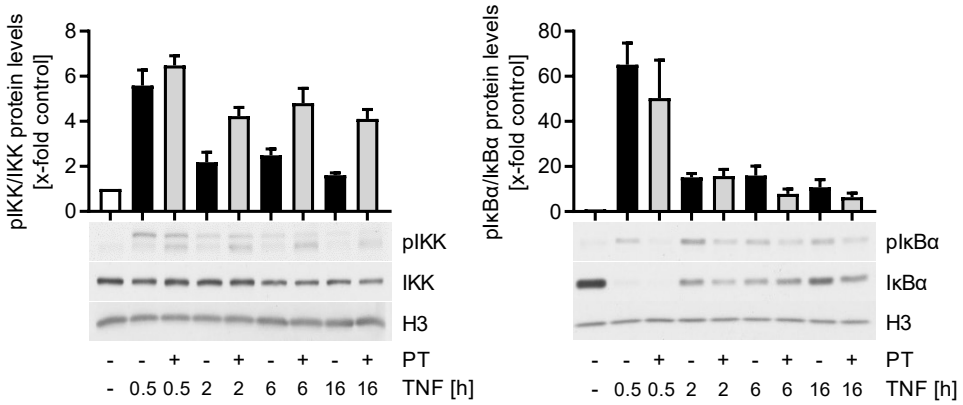

Figure 33. Pretubulysin treatment leads to increased IKK activity and IκBα degradation. Western blot analysis of the IKK (left) and IκBα phosphorylation ratio (right). Confluent HUVECs were pre-treated with PT (300 nM) for 30 min and activated with TNF (10 ng/mL) for different durations (0.5, 2, 6, 16 h). Results were normalized on the respective histone 3 (H3) levels. (n=3)

Stimulation with TNF for 0.5 h strongly induced the phosphorylation and hence activity of the IκB kinase (IKK) approx. 5-fold over the control cells, which subsequently diminished over extended treatment times to approx. 2-fold after 2 and 6 h and 1.5-fold after 16 h. In contrast, PT-treatment increased the phosphorylation of IKK compared to the TNF-treated control cells at all tested treatment times (Fig. 33, left). PT slightly increased the IKK phosphorylation after short TNF stimulation times of 0.5 h, but notably induced the IKK phosphorylation after extended stimulation times of 2, 6 and 16 h, when the IKK phosphorylation in the TNF-control cells already diminished. Extended stimulation with TNF also induced a small decrease in the total IKK protein levels independent of PT treatment. TNF stimulation strongly increased the IKK-dependent phosphorylation and strongly reduced the total protein levels of IκBα after 0.5 h, which increased again following longer stimulation times of 2, 6 and 16 h (Fig. 33, right). Treatment with PT induced an even stronger degradation of IκBα at 0.5, 2 and 16 h of TNF stimulation, but led to a slight induction of the IκBα total protein levels after 6 h of stimulation, compared to the TNF control.

Based on this, the influence of PT on the IκBα protein levels at mean treatment times of 10 h and 12 h was measured by western blot analysis (Fig. 34).

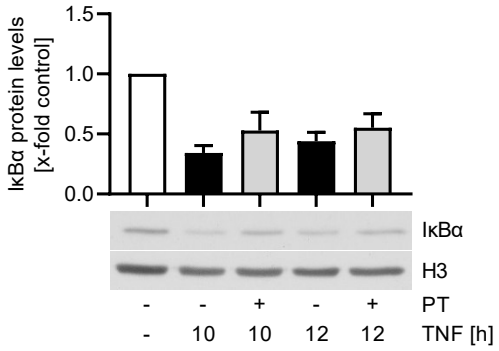

Figure 34. Pretubulysin increases the IκBα total protein levels at mean treatment times. Western blot analysis of the IκBα protein levels. Confluent HUVECs were pre-treated with PT for 30 min and activated with TNF (10 ng/mL) for 10 or 12 h. Results were normalized on the respective histone 3 (H3) levels. (n=3)

10 and 12 h of TNF stimulation led to a strong decrease of the IκBα protein levels. In comparison, treatment with PT increased the IκBα protein levels by approx. 55 % after 10 h and by 25 % after 12 h of TNF stimulation compared to the TNF control (Fig. 34). Due to the apparent increase in the IκBα protein levels, it is likely that PT induces a time-dependent differential expressional pattern of IκBα, which might negatively impact the NFκB response at these treatment times. However, due to the lasting activation of IKK and the again increased degradation of IκBα after longer treatment with PT, it can be assumed that the overall influence of PT on the IKK signaling and resulting IκB degradation is not the main cause for the decreased CAM synthesis.

3.5.1.3 Translocation of NFκB-p65 into the nucleus and p65 mRNA levels

PT did not negatively affect the activity of IKK and the resulting degradation of IκBα. Hence, the NFκB-p65 protein levels in the cytoplasm and nucleus were analyzed by western blot analysis of cell fractions. In addition, PT was tested for its influence on the NFκB-p65 mRNA levels by qRT-PCR analysis (Fig. 35).

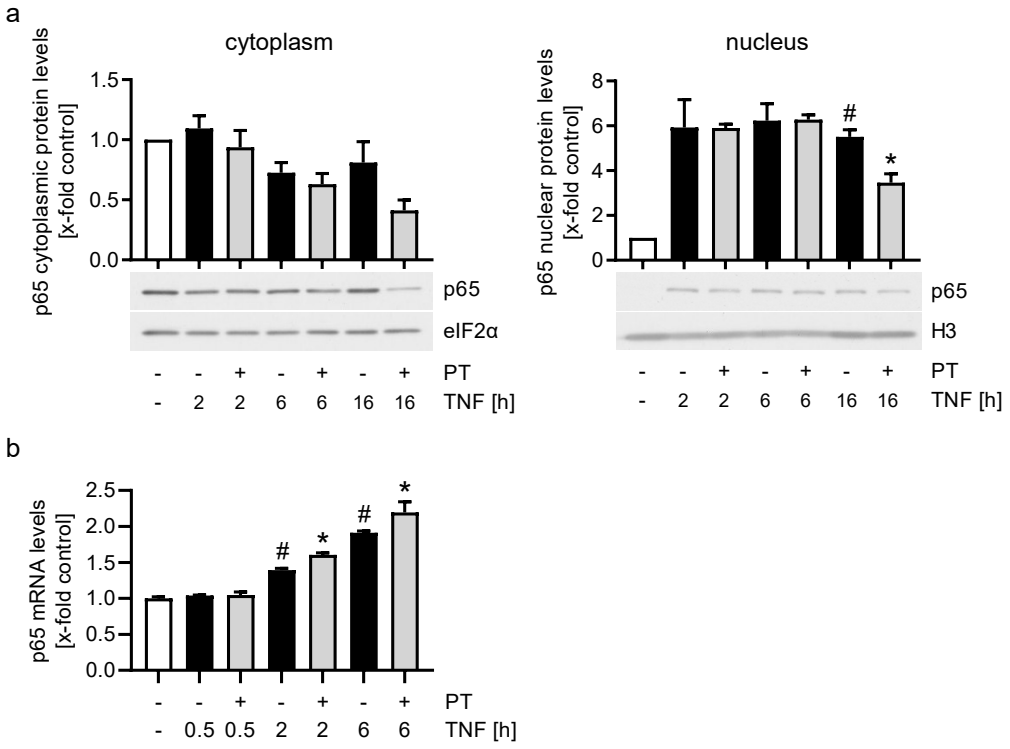

Figure 35. PT does only affect the NFκB-p65 levels after extended treatment times and has no negative impact on the p65 mRNA levels. (a) Western blot analysis of the NFκB-p65 levels in cell fractions. Confluent HUVECs were pre-treated with PT (300 nM) and activated with TNF (10 ng/mL) for different duration (2, 6, 16 h). Results were normalized on the respective elongation initiation factor 2α (eIF2α) levels (cytoplasmic fraction) or H3 levels (nuclear fraction). (b) qRT-PCR analysis of the p65 mRNA levels. Confluent HUVECs were pre-treated with pretubulysin (300 nM) for 30 min and activated with TNF (10 ng/mL) for different durations (0.5, 2, 6 h). Results were normalized on the respective GAPDH mRNA levels. (n=3) Data are expressed as mean ± SEM. $^{\#}p \leq 0.05$ versus control, $^{*}p \leq 0.05$ versus TNF control.

2 h of TNF stimulation led to a strong translocation of NFκB-p65 into the nucleus of HUVECs, which only slightly diminished after 16 h of TNF stimulation (Fig. 35a). In comparison, treatment with PT did not negatively influence the nuclear p65 levels after 2 or 6 h of treatment, but lead to a noticeable decrease of the p65 levels in the cytoplasmic and nuclear fractions after 16 h of treatment. Concerning the p65 mRNA levels, stimulation with TNF only increased the mRNA levels of p65 after 2 h, which were further increased after 6 h of stimulation (Fig. 35b). Additional treatment with PT further induced the mRNA levels compared to the TNF controls.

3.5.1.4 The influence of PT on NFκB-p50 protein and mRNA levels

NFκB is mainly comprised of the transcriptionally most active p65:p50 heterodimer (1.4.1). Due to that, the influence of PT on the p50 protein and the mRNA levels of the p50 precursor p105 was tested (Fig. 36).

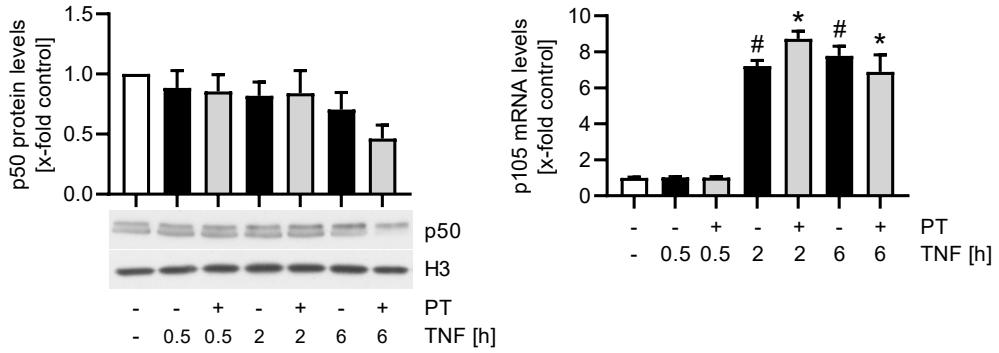

Figure 36. Pretubulysin negatively influences the total NFκB-p50 levels. Western blot analysis of the total p50 protein levels and (left) qRT-PCR analysis of the p105 mRNA levels (right) .Confluent HUVECs were pre-treated with PT (300 nM) for 30 min and activated with TNF (10 ng/mL) for different duration (0.5, 2, 6 h). Results were normalized on the respective histone 3 (H3; left) or GAPDH mRNA levels (right). (n=3) Data are expressed as mean ± SEM. $^{\#}p \leq 0.05$ versus control, $*p \leq 0.05$ versus TNF control.

TNF stimulation did not alter the p50 protein levels after 0.5 h or 2 h of stimulation, but slightly reduced the p50 levels after 6 h (Fig. 36, left). PT treatment also had no influence on the p50 protein levels after 0.5 h and 2 h, but reduced the p50 levels after 6 h of treatment by approx. 40 % compared to the TNF control. The mRNA levels of the p50 precursor p105 were only induced after 2 h of TNF stimulation (Fig. 36, right). PT slightly induced the p105 levels after 2 h compared to the TNF control cells and slightly reduced the mRNA levels after 6 h of treatment.

The decrease in p50 protein levels after 6 h of treatment with PT suggests a deregulation of the relative p65:p50 levels over time. To analyze the transcriptional activity of NFκB, the influence of PT on the NFκB transcriptional activity was tested in a reporter gene assay.

3.5.1.5 The influence of MTAs on the transcriptional activity of NFκB

The influence of PT and the other MTAs on the transcriptional activity of NFκB was tested by a dual-luciferase reporter gene assay. To exclusively analyze the transcriptional activity of NFκB, the reporter gene assay was performed after 6 h of PT treatment, when the p65 protein levels are not negatively influenced by PT (Fig. 37).

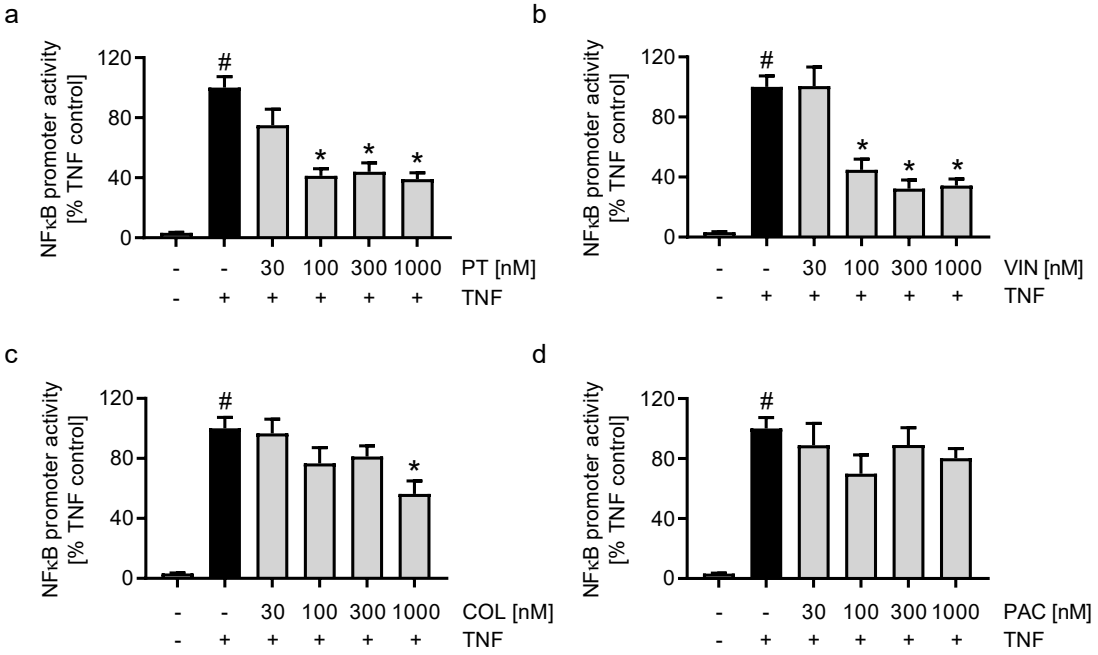

Figure 37. MTAs decrease the NFκB promoter activity. Reporter gene assay of the NFκB promoter activity after treatment with PT (a), VIN (b), COL (c) and PAC (d). HUVECs were transfected with pGL4.32[*luc2p*/NFκB-RE/Hygro] or pGL4.44[*luc2p*/AP-1-RE/Hygro] and pGL4.74[*hRluc*/TK] for normalization and were pre-treated with different concentrations (30, 100, 300, 1000 nM) of VIN, COL or PAC for 30 min and then activated with TNF (10 ng/mL) for 6 h. (n=3) Data are expressed as mean ± SEM. $^{\#}p \leq 0.05$ versus control, $^{*}p \leq 0.05$ versus TNF control.

PT treatment of HUVECs with concentrations of 100 nM or more significantly decreased the transcriptional activity of NFκB by approx. 60 % (Fig. 37). Treatment with VIN lead to a reduction of the NFκB transcriptional activity comparable to PT. The effects of COL were much weaker, with only 1000 nM significantly reducing the transcriptional activity of NFκB by approx. 40 % compared to the TNF control. Treatment with PAC also slightly influenced the transcriptional activity of NFκB, albeit without statistical significance.

The NFκB-p65 S468 and S536 phosphorylation sites are implied in regulating the transactivatory potential and hence, the transcriptional activity of NFκB (1.4.1). Thus, PT was tested for its influence on S468 and S536 phosphorylation.

3.5.1.6 The impact of PT on phosphorylation of NFκB-p65

Several studies have correlated an increased IKK activity with a decreased NFκB-p65 transactivatory potential at the promoters of ICAM-1 and VCAM-1 *via* an increased phosphorylation of NFκB-p65 at serine 468 (1.4.1). In addition, other studies have implied the NFκB-p65 phosphorylation at serine 536 to negatively influence the stability of NFκB-p65 (1.4.1). Based on the increased IKK activity after treatment with PT, the influence of PT on the p65-S468 and p65-S536 phosphorylation levels were analyzed by western blotting (Fig. 38).

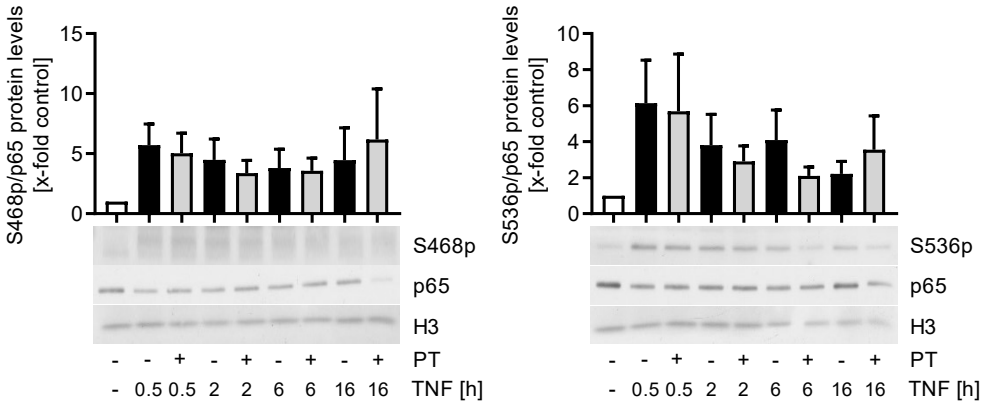

Figure 38. Pretubulysin has no significant influence on the NFκB p65-S468 (left) and p65-S536 (right) phosphorylation levels. Confluent HUVECs were pre-treated with PT (300 nM) for 30 min and activated with TNF (10 ng/mL) for different duration (0.5, 2, 6, 16 h). Results were normalized on the respective histone 3 (H3) levels. (n=3)

The levels of both phosphorylation sites were only marginally influenced by PT treatment (Fig. 38). The increase in the phosphorylation ratio after 16 h of treatment is largely based on the decreased levels of p65 after extended treatment times.

3.5.2 The JNK-AP-1 signaling cascade

3.5.2.1 Influence of PT on the c-Jun-N-terminal kinase

To evaluate the influence of PT and the other MTAs on the JNK-AP-1 signaling cascade, the activity of the cJun-upstream kinase JNK was tested by western blot analysis (Fig. 39).

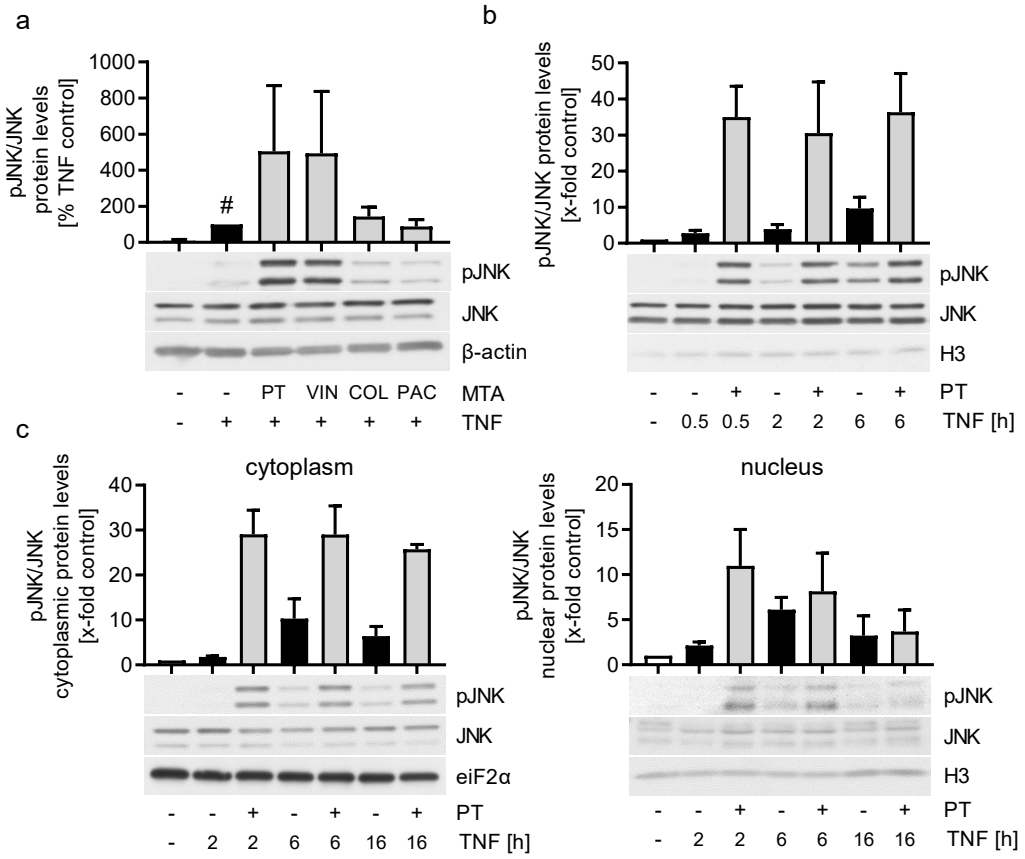

Figure 39. Pretubulysin treatment leads to a strong induction of JNK activity. Western blot analysis of the JNK phosphorylation ratio. (a) Western blot analysis of the total JNK phosphorylation ratio after MTA treatment. Confluent HUVECs were pre-treated with MTA for 30 min and activate with TNF (10 ng/mL) for 2 h. Results were normalized to the β-actin content. (b) Western blot analysis of the total JNK phosphorylation ratio after different treatment times. Confluent HUVECs were pre-treated with pretubulysin (PT) for 30 min and activate with TNF (10 ng/mL) for different durations (0.5, 2, 6, 16 h). Results were normalized to the respective histone 3 (H3) levels. (c) Western blot analysis of the JNK phosphorylation ratio in cell fractions. Confluent HUVECs were pre-treated with pretubulysin (300 nM) for 30 min and activated with TNF (10 ng/mL) for different duration (2, 6, 16 h). Results were normalized on the respective elongation initiation factor 2α (eIF2α) levels (cytoplasmic fraction) or H3 levels (nuclear fraction). (n=3)

Analysis of the effects of the MTAs revealed that upon 2 h of treatment especially PT and VIN led to a significant induction of JNK activity to approx. 500 %, while treatment with COL and PAC had little influence (Fig. 39a). Analyzing the phosphorylation and hence, activity of JNK upon 0.5 h of TNF stimulation revealed an approx. 4-fold increase in phosphorylation compared to the control cells (Fig. 39b). Longer stimulation increased the phosphorylation ratio to 5-fold after 2 h and approx. 10-fold after 16 h. The JNK activity in the PT-treated cells was again significantly higher, with PT inducing the activity of JNK to approx. 30- to 40-fold compared to the control cells at all treatment times tested.

Highly active JNK was also present in the nucleus of HUVECs (Fig. 39c). Notably, the JNK activity in the TNF-stimulated cells reached its maximum after 6 h of stimulation and declined again after 16 h of stimulation with TNF.

To further analyze the intensity of JNK activation after extended pre-treatment with the MTAs, HUVECs were pre-treated for 24 h with PT, VIN, COL and PAC (Fig. 40).

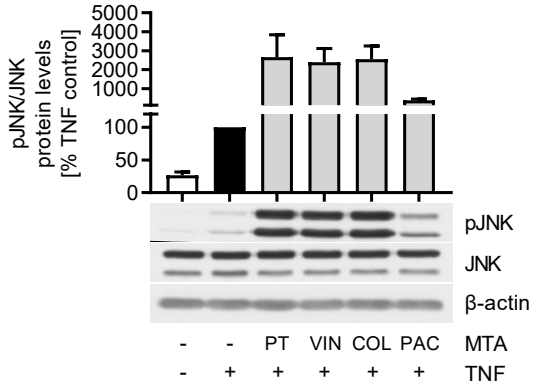

Figure 40. The MTAs induce the activity of JNK after extended pre-treatment. Western blot analysis of the total JNK phosphorylation ratio after long pre-treatment with MTAs. Confluent HUVECs were pre-treated with 300 nM of PT, VIN, COL or PAC for 24 h and activated with TNF (10 ng/mL) for 30 min. Western blot results were normalized on the respective β-actin levels. (n=3)

Extended pre-treatment with the MTAs for 24 h and 0.5 h of TNF stimulation led to a further increase in JNK phosphorylation compared to 2 h of treatment (Fig. 40). Treatment with the destabilizing MTAs induced the phosphorylation of JNK to approx. 2500 % compared to the TNF control. Interestingly, extended pre-treatment with PAC also increased the JNK phosphorylation significantly, compared to only 2 h of treatment, with JNK phosphorylation being increased to approx. 500 %.

3.5.2.2 Influence of PT on AP-1-cJun protein and mRNA levels

Based on the significantly increased activity of JNK after treatment and the fact that high and lasting JNK activity is known to deregulate cJun activity (1.4.2), PT was tested towards its influence on the cJun protein and mRNA levels (Fig. 41).

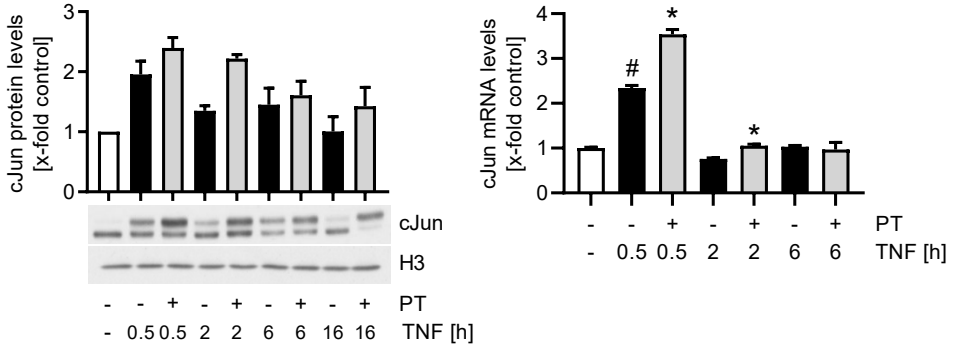

Figure 41. Pretubulysin treatment leads to increased cJun protein and mRNA levels. Western blot analysis of the total cJun protein levels (left) and qRT-PCR analysis of the cJun mRNA levels (right). Confluent HUVECs were pre-treated with PT for 30 min and activate with TNF (10 ng/mL) for 0.5, 2, 6, 16 h (left) or 0.5, 2, 6 h (right). Western blot results were normalized on the respective histone 3 (H3) levels and qRT-PCR Results were normalized on the respective GAPDH mRNA levels. (n=3) Data are expressed as mean ± SEM. $^{\#}p \leq 0.05$ versus control, $^{*}p \leq 0.05$ versus TNF control.

Treatment with PT increased the cJun protein levels compared to the TNF controls after all stimulation times tested (Fig. 41, left). Stimulation with TNF for 0.5 h induced a phosphorylation-dependent electromobility shift of cJun, as seen by the emergence of an additional cJun protein fraction. Treatment with PT led to a further increase of the apparent electromobility-shift, which is also present following 16 h of TNF stimulation, when it is almost fully lost in the TNF control cells. This indicates the induction of high and lasting cJun activity due to PT. cJun is known to auto-induce itself by binding to the *cjun* promoter (1.4.2). Due to that, the relative cJun mRNA levels were tested upon treatment with PT (Fig. 41, right). In accordance with the elevated cJun protein levels, PT treatment induced the cJun mRNA levels by approx. 50 % after 0.5 h of TNF stimulation, compared to the TNF control. Longer stimulation periods did not induce the cJun mRNA levels above the values of the negative control under any of the treatment conditions tested.

3.5.2.3 The influence of MTAs on the transcriptional activity of AP-1

To further analyze the effects of PT and the other MTAs on AP-1, the transcriptional activity of AP-1 was determined in a reporter gene assay (Fig. 42).

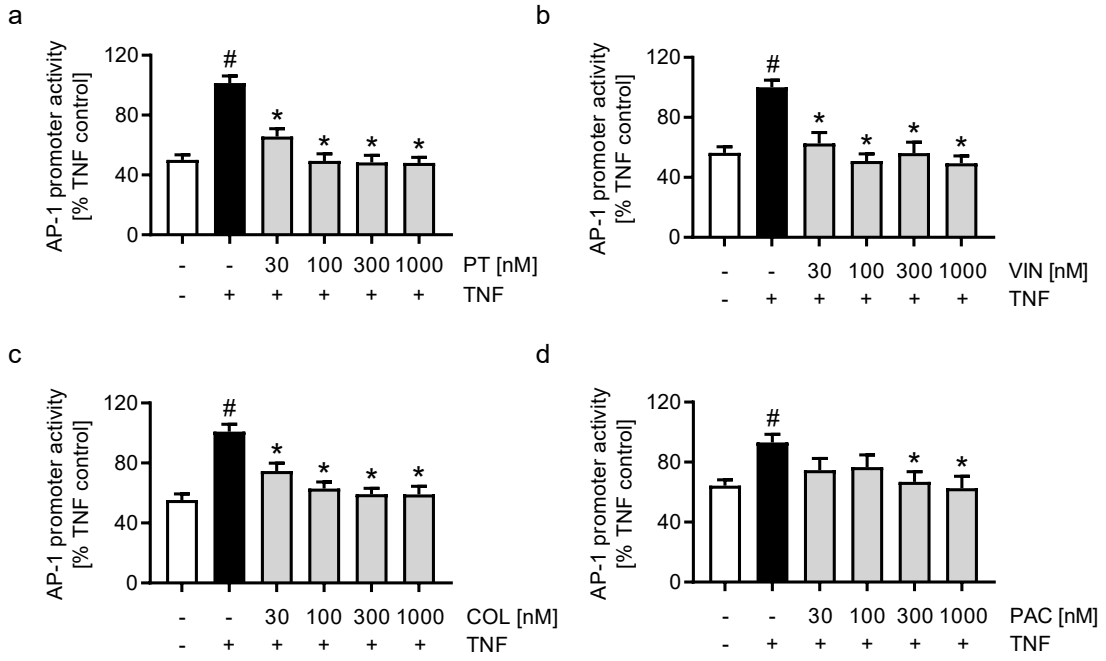

Figure 42. MTAs decrease the AP-1 promoter activity. Reporter gene assay of the AP-1 promoter activity after treatment with PT (a), VIN (b), COL (c) and PAC (d). HUVECs were transfected with pGL4.44[*luc2p*/AP-1-RE/Hygro] and pGL4.74[*hRluc*/TK] for normalization and were pre-treated with different concentrations (30, 100, 300, 1000 nM) of MTA for 30 min and then activated with TNF (10 ng/mL) for 6 h. (n=3) Data are expressed as mean ± SEM. $^{\#}p \leq 0.05$ versus control, $^{*}p \leq 0.05$ versus TNF control.

PT treatment significantly reduced the promoter activity of AP-1 (Fig. 42a). Similar to NFκB, concentrations of 100 nM or more reduced the AP-1 promoter activity by approx. 50 %. Treatment with VIN and COL led to a reduction of the AP-1 promoter activity similar to PT (Fig. 42b/c). The microtubule stabilizer PAC also reduced AP-1 activity, albeit to a weaker extent than the destabilizers, with 1000 nM of PAC reducing the activity by approx. 40 % compared to the TNF control (Fig. 42d).

JNK is known to induce the transactivatory potential of cJun by phosphorylating residues in the cJun transactivation domain (1.4.2). High and lasting JNK activity is thought to also induce phosphorylation in the phosphodegron motif of cJun, reducing its DNA-binding activity (1.4.2).

3.5.2.4 The impact of PT on phosphorylation of AP-1-cJun

The S243 site constitutes one of the phosphorylation sites in the phosphodegron motif of cJun that induces cJun degradation and reduces the DNA-binding affinity of cJun (1.4.2). The influence of PT on the cJun-S243 phosphorylation levels was analyzed by western blotting. In addition, the nuclear protein levels of GSK3β, which is implied in phosphorylating the cJun phosphodegron under normal cJun turn-over conditions (1.4.2), was analyzed (Fig. 43).

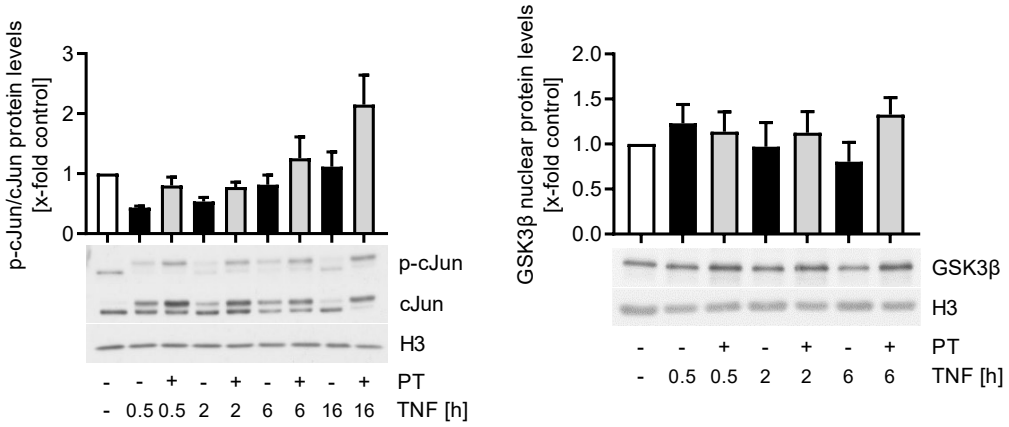

Figure 43. Pretubulysin slightly increases cJun S243 phosphorylation and nuclear GSK3β levels. Western blot analysis of the cJun S243 phosphorylation ratio (left) and nuclear protein levels of GSK3β (right). Confluent HUVECs were pre-treated with PT (300 nM) for 30 min and activated with TNF (10 ng/mL) for 0.5, 2, 6, 16 h (left) or 0.5, 2 and 6 h and cell fraction was performed (right). Results were normalized on the respective histone 3 (H3) levels. (n=3)

TNF stimulation for 0.5 h reduced the levels of the inhibitory S243 phosphorylation, which subsequently increased over the treatment time, until approaching the phosphorylation ratio of the control cells after 16 h of stimulation (Fig. 43, left). PT increased the inhibitory S243 phosphorylation compared to the respective TNF control at all treatment times tested, reaching twice the phosphorylation ratio after 16 h of treatment. In case of GSK3β, initial TNF stimulation for 0.5 h increased the nuclear protein levels slightly, which decreased to approx. 75 % after 6 h of stimulation (Fig. 43, right). In contrast, treatment with PT increased the nuclear levels of GSK3β, which were elevated by approx. 25 % after 6 h of treatment, compared to the respective TNF control.

3.5.2.5 Summary for the PT-induced effects on NFκB and AP-1 signaling and the resulting CAM expression

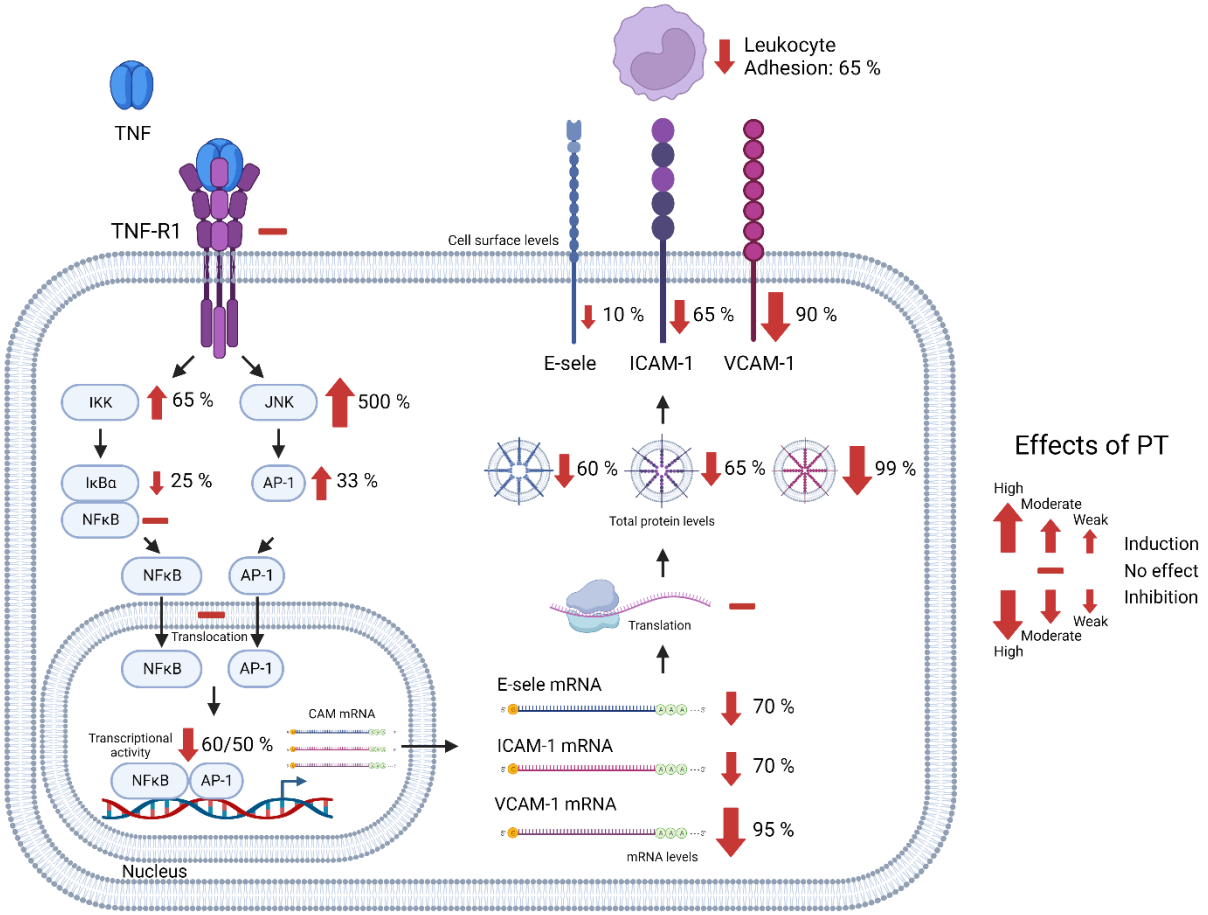

Figure 44. Graphical summary for the effects on NFκB and AP-1 signaling and the resulting CAM expression after treatment with 300 nM of PT. Percentual representation of induction or inhibition due to PT. For time rows, the percentual increase or decrease represents the mean value over the treatment time.

Treatment of HUVECs with PT did not affect the total protein levels of the TNFR1, but induced the activity IKK and significantly induced the activity of JNK (Fig. 44). The increase in IKK activity resulted in an increase in IκBα degradation. The steady-state levels of NFκB were largely uninfluenced. However, in case of AP-1-cJun, the increased JNK activity resulted in an overall increase of cJun protein levels. While the translocation of NFκB and AP-1 appeared to be not influenced by PT, the transcriptional activity of NFκB and AP-1 were reduced. This led to decreased levels of CAM mRNAs, total protein levels and cell surface levels, while not negatively influencing the overall polypeptide synthesis. The reduced cell surface levels of the CAMs resulted in a decreased leukocyte adhesion.

3.5.3 Additional pro-inflammatory signaling kinases and factors

In addition to the main pro-inflammatory NFκB and AP-1 signaling, PT was also tested towards its influence on other kinases like AKT and the MAPKs p38 and ERK as well as the IRF-1 transcription factor, which is involved in the induction of VCAM-1 (1.6.1).

3.5.3.1 AKT activity

AKT or protein kinase B (PKB) is involved in pro-inflammatory signaling by activation of GATA6 (1.3.3). The activity of AKT after PT treatment was tested by western blot analysis (Fig. 45).

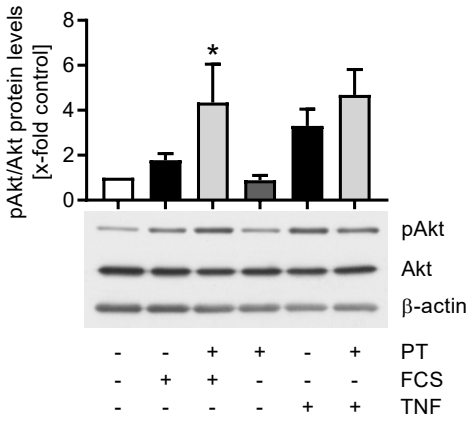

Figure 45. Pretubulysin increases AKT activity. AKT phosphorylation ratio after treatment with PT analyzed by western blot analysis. Confluent HUVECs were treated with PT (300 nM) for 8 h under starvation conditions and activated with FCS (10 %) or TNF (10 ng/mL) for 15 min. Results were normalized to the respective β-actin levels. (n=3) Data are expressed as mean ± SEM. $^{\#}p \leq 0.05$ versus control, $^{*}p \leq 0.05$ versus TNF control.

Stimulation of HUVECs with FCS for 15 min increased AKT phosphorylation approx. 2-fold compared to the control cells (Fig. 45). Stimulation with TNF led to a stronger induction, with AKT phosphorylation being increased approx. 3.5-fold. While treatment with only PT had no effect on AKT phosphorylation, combination with FCS or TNF induced AKT activity approx. 4-fold, compared to the untreated control HUVECs.

3.5.3.2 IRF-1 activity

The activity of IRFs like IRF-1 is largely connected to a TLR-induced MyD88-dependent activation (1.3.3). However, the activity of IRF-1 is also highly regulated on an expressional level upon NFκB induction (1.3.3). Based on this, the nuclear protein levels of IRF-1 and the IRF-1 mRNA levels were investigated by western blot analysis of the nuclear fraction and qRT-PCR analysis, respectively (Fig. 46).

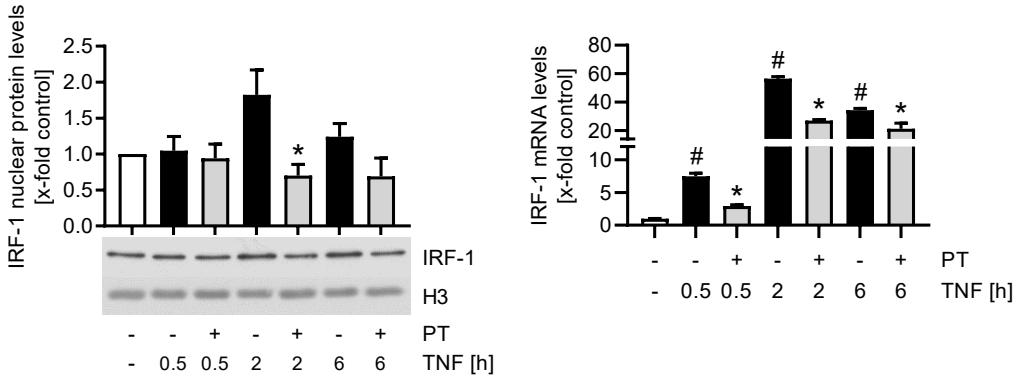

Figure 46. Pretubulysin reduces the nuclear IRF-1 protein and overall mRNA levels. Western blot analysis of the nuclear IRF-1 protein levels (left) and qRT-PCR analysis of the IRF-1 mRNA levels (right) after PT treatment. Confluent HUVECs were pre-treated with PT (300 nM) for 30 min and activated with TNF (10 ng/mL) for 0.5, 2 or 6 h. Western blot results were normalized on the respective histone 3 (H3) levels and qRT-PCR results were normalized on the respective GAPDH mRNA levels. (n=3) Data are expressed as mean ± SEM. $^{\#}p \leq 0.05$ versus control, $^{*}p \leq 0.05$ versus TNF control.

PT had no effect on the nuclear IRF-1 levels after 0.5 h of treatment, but significantly reduced the nuclear levels after 2 h of treatment by approx. 60 % (Fig. 46, left). The PT-induced effects on IRF-1 also extended to the mRNA level (Fig. 46, right), with PT significantly reducing the IRF-1 mRNA levels at all treatment times tested.

3.5.3.3. p38 MAPK activity

As part of the MAPK signaling pathways, the activity of the p38 kinase also participates in pro-inflammatory signaling, but also regulates the activity of mRNA binding proteins and hence transcript stability (1.3.2). The activity of the p38 kinase was analyzed by western blotting of cell fractions (Fig. 47).

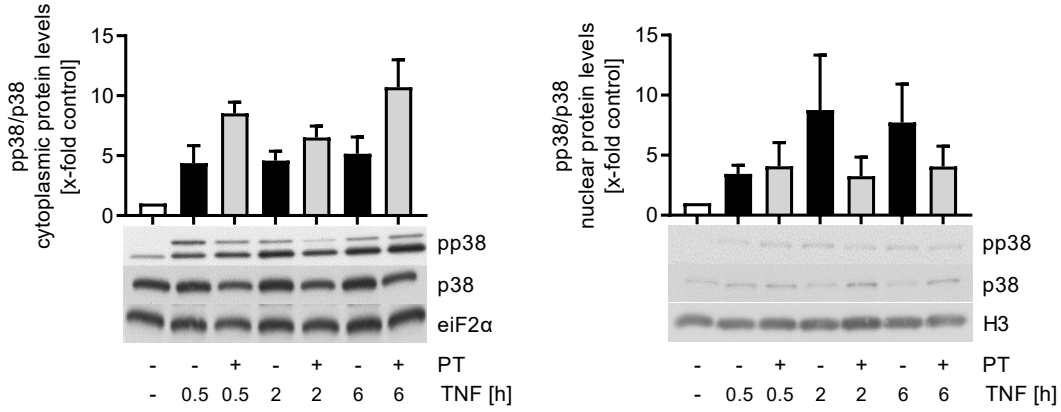

Figure 47. Pretubulysin induces nuclear translocation of p38 but reduces nuclear p38 phosphorylation. Western blot analysis of the p38 phosphorylation ratio in the cytoplasmic fraction (left) and nuclear fraction (right). Confluent HUVECs were pre-treated with PT (300 nM) and activated with TNF for different durations (0.5, 2, 6 h). Results were normalized on the respective elongation initiation factor 2 α (eIF2α, cytoplasmic fraction) or histone 3 (H3, nuclear fraction). (n≥3)

Treatment with PT induced the translocation of the p38 kinase into the nucleus of HUVECs (Fig. 47), as based on the reduced cytoplasmic p38 protein levels and the increased levels in the nuclear fraction. The phosphorylation levels of the cytoplasmic fraction appeared to be increased. In contrast, the nuclear phosphorylation levels were decreased, demonstrating the nuclear presence of inactive p38 upon treatment with PT.

3.5.3.3.1 The influence of PT on VCAM-1 mRNA stability

Since the p38 kinase is involved in regulating mRNA transcript stability *via* induction of MAPKAPKs that induce phosphorylation of mRNA-binding proteins (1.3.2), PT and the other MTAs were investigated for their influence on the decay rate of the VCAM-1 mRNA (Fig. 48).

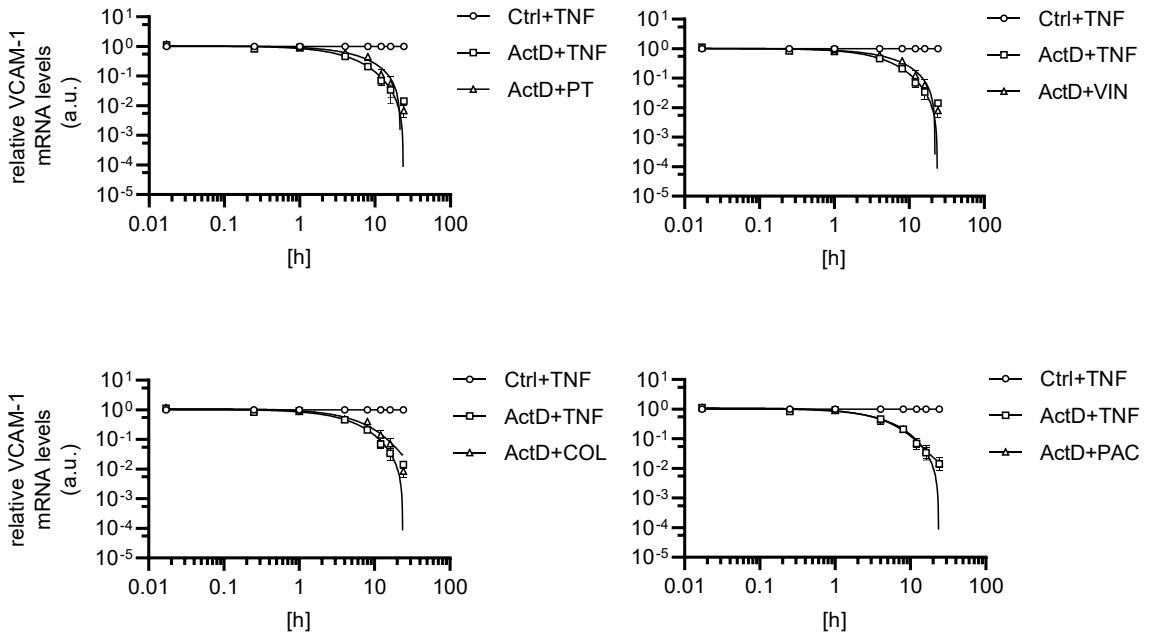

Half-life (h)	PT	VIN	COL	PAC
ActD+TNF	3.6 (0.9234)	3.6 (0.9234)	3.6 (0.9234)	3.6 (0.9234)
ActD+MTA	5.9 (0.8914)	5.7 (0.9596)	4.1 (0.9324)	3.0 (0.9642)

Figure 48. Pretubulysin and the other destabilizing MTAs increase the half-live ($t_{1/2}$) of the VCAM-1 mRNA. qRT-PCR analysis of the VCAM-1 mRNA levels after actinomycin D addition. Confluent HUVECs were treated with TNF (10 ng/mL) for 12 h. Actinomycin D (ActD; 2 µg/mL) was added to inhibit mRNA expression and 300 nM of pretubulysin (PT), vincristine (VIN), colchicine (COL) or paclitaxel (PAC) was added under continuous TNF treatment for different durations (5 min, 15 min, 1 h, 4 h, 8 h, 12 h, 16 h and 24 h). Results were normalized on the respective GAPDH mRNA levels of the TNF control. The non-linear regression is based on the GraphPad Prism 'one-phase decay'. The corresponding R^2 values are shown in round brackets. (n=3)

Decay rate measurements of the VCAM-1 mRNA in the absence of MTA treatment revealed a half-life of $t_{1/2}$ = 3.6 h (Fig. 48). Addition of any of the destabilizing MTAs significantly increased the half-life of the VCAM-1 mRNA. Only the microtubule stabilizer PAC decreased the VCAM-1 mRNA transcript stability. These results show that the inhibitory effects of the depolymerizing MTAs on VCAM-1 are not due to an increased decay of the VCAM-1 mRNA.

3.5.3.4 ERK activity

The ERK MAPK is primarily involved in developmental processes, but is also known to partake in inflammatory activation by phosphorylation of cFos (1.3.2). Therefore, PT was tested for its influence on the activity of ERK (Fig. 49).

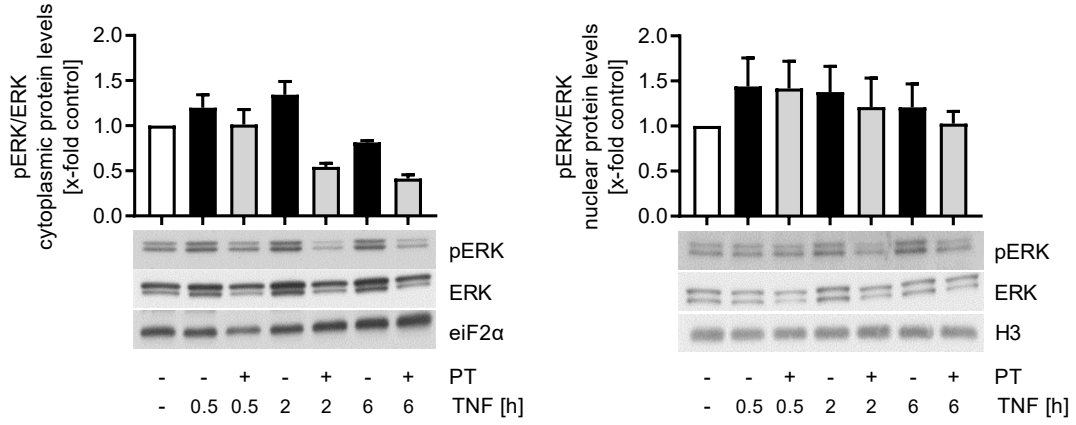

Figure 49. Pretubulysin reduces the ERK phosphorylation and slightly reduces total protein levels. Western blot analysis of the ERK phosphorylation ratio in the cytoplasmic fraction (left) and nuclear fraction (right). Confluent HUVECs were pre-treated with PT (300 nM) and activated with TNF for different durations (0.5, 2, 6 h). Results were normalized on the respective elongation initiation factor 2 α (eIF2α, cytoplasmic fraction) or histone 3 (H3, nuclear fraction). (n≥3)

Short treatment of HUVECs with PT for 0.5 h had no significant effect on the cytoplasmic or nuclear activity of ERK (Fig. 49). Extended treatment of 2 h and 6 h slightly reduced the ERK phosphorylation and protein levels in the cytoplasm and nucleus, suggesting an increased degradation of ERK upon treatment with PT. However, based on the intensity of the effects, it is evident that PT does not significantly influence ERK activity.

3.5.3.5 Summary of the PT-induced effects on MAPKs, AKT, as well as mRNA decay of VCAM-1 mRNA and mRNA and protein levels of IRF-1

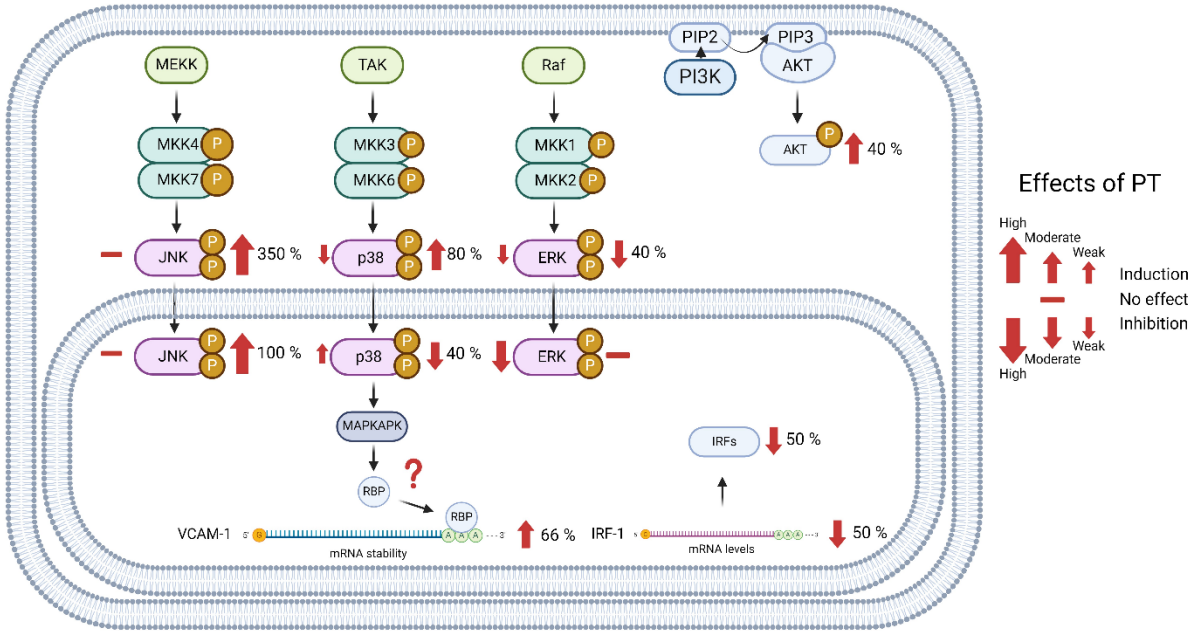

Figure 50. Graphical summary for the effects on the MAPKs JNK, p38 and ERK (left total protein, right activity) in the cytoplasm and in the nucleus, total AKT activity, VCAM-1 mRNA stability and mRNA and nuclear protein levels of IRF-1 after treatment with 300 nM of PT. Percentual representation of induction or inhibition due to PT. For time rows, the percentual increase or decrease represents the mean value over the treatment time.

Treatment with PT significantly induced the cytoplasmic and nuclear activity of JNK (Fig. 50). For p38, the cytoplasmic total protein levels were slightly reduced, while the phosphorylation levels appeared to be largely uninfluenced, leading to the presence of a cytoplasmic p38 fraction with increased activity. The nuclear total protein levels of p38 were increased after treatment with PT, but the phosphorylation was reduced. p38 also regulates the mRNA stability *via* MAPKAPKs and RNA-binding proteins (RBP). The stability of VCAM-1 mRNA was increased after treatment with PT. The cytoplasmic and nuclear ERK total protein and phosphorylation levels were also reduced. The activity of AKT, which is involved in the induction of GATA transcription factors, was induced. The levels of IRF-1 mRNA were reduced, leading to a decrease of the nuclear IRF-1 protein levels.

3.6 The influence of PT on the NFκB and AP-1 DNA-binding activity at the *icam-1*, *vcam-1* and *e-sele* promoters

PT had no negative influence on the signaling events that precede activation of the NFκB and AP-1 transcription factors, but significantly reduced the transcriptional activity of both factors. Based on this, PT was tested towards its influence on the DNA-binding activity of both transcription factors.

3.6.1. Impact of PT on NFκB enrichment in the promoters of *icam-1, vcam-1* and *e-sele*

The DNA-binding behavior of NFκB-p65 was tested by chromatin immunoprecipitation (ChIP), with primers encompassing the most promoter proximal NFκB-binding sites in the promoters of *icam-1*, *vcam-1* and *e-sele* (Fig. 51)

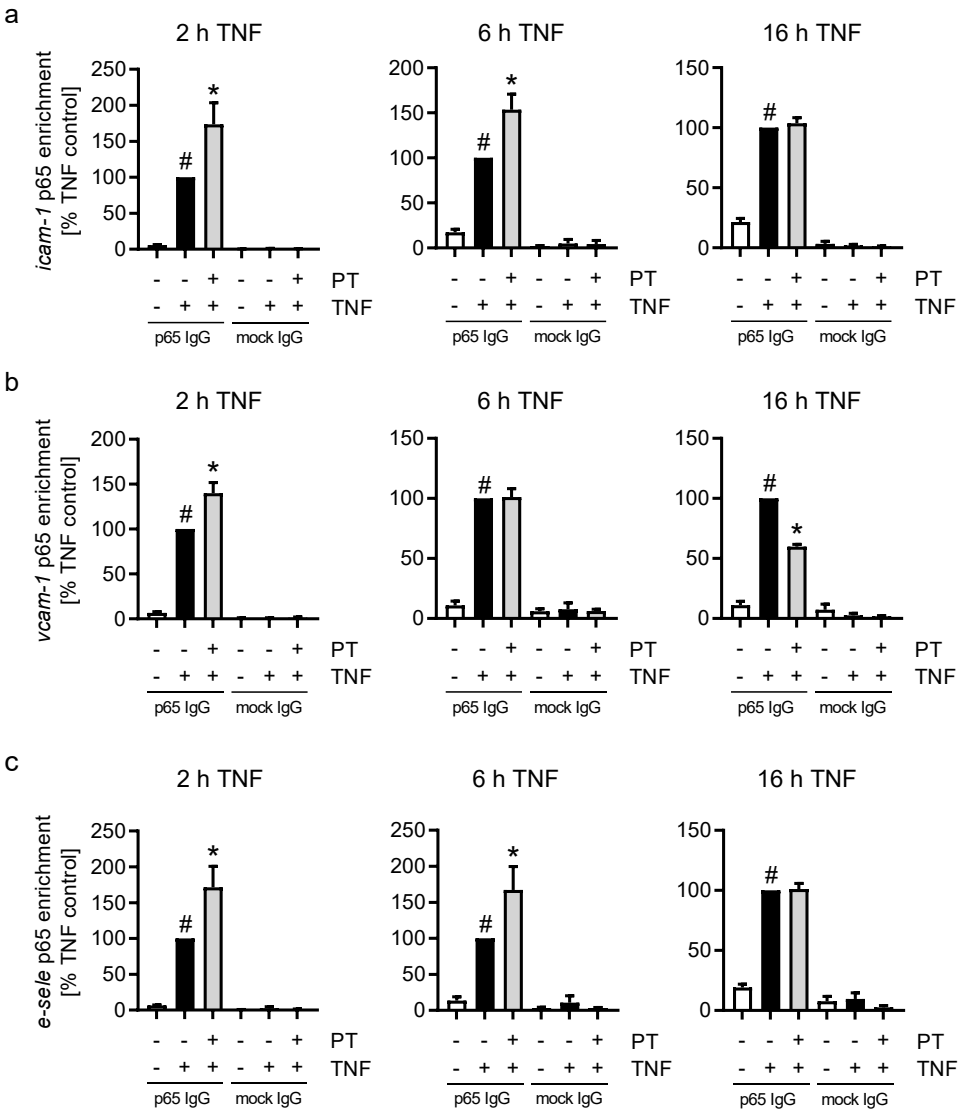

Figure 51. Pretubulysin increases the NFκB p65 promoter enrichment at short treatment times and leads to a time dependent decrease in p65 enrichment in the *icam-1* and *vcam-1* and *e-sele* promoters. Enrichment of NFκB-p65 in the *icam-1* (a) and *vcam-1* (b) and *e-sele* (c) promoters as shown by chromatin immunoprecipitation (ChIP). Confluent HUVECs were pre-treated with pretubulysin (PT; 300 nM) for 30 min and activated with TNF (10 ng/mL) for a duration of 2, 6, 16 h. ChIP was performed with a p65 binding antibody and the respective IgG mock antibody. Results were normalized on the background levels of a sequence of the *rpl13a* 3'-untranslated region. (n=3) Data are expressed as mean ± SEM. $^{\#}p \leq 0.05$ versus control, $^{*}p \leq 0.05$ versus TNF control.

Treatment with PT for 2 h significantly increased the p65 enrichment in the promoter of *icam-1* by approx. 75 %, *vcam-1* by approx. 40 % and *e-sele* by approx. 70 % (Fig. 51). For *icam-1* and *e-sele* enrichment remained high after 6 h of treatment. In contrast, the p65 enrichment in the *vcam-1* promoter

was reduced to the levels of the TNF control following 6 h of treatment. Extended treatment of 16 h reduced the p65 enrichment in the *icam-1* and *e-sele* promoters to the level of the TNF control, but significantly reduced the enrichment in the *vcam-1* promoter to approx. 50 % of the TNF control HUVECs.

3.6.2. Impact of PT on AP-1 enrichment in the promoters of *icam-1*, *vcam-1* and *e-sele*

In addition to NFκB, PT was also tested towards its influence on the enrichment of AP-1-cJun in the CAM promoters (Fig. 52).

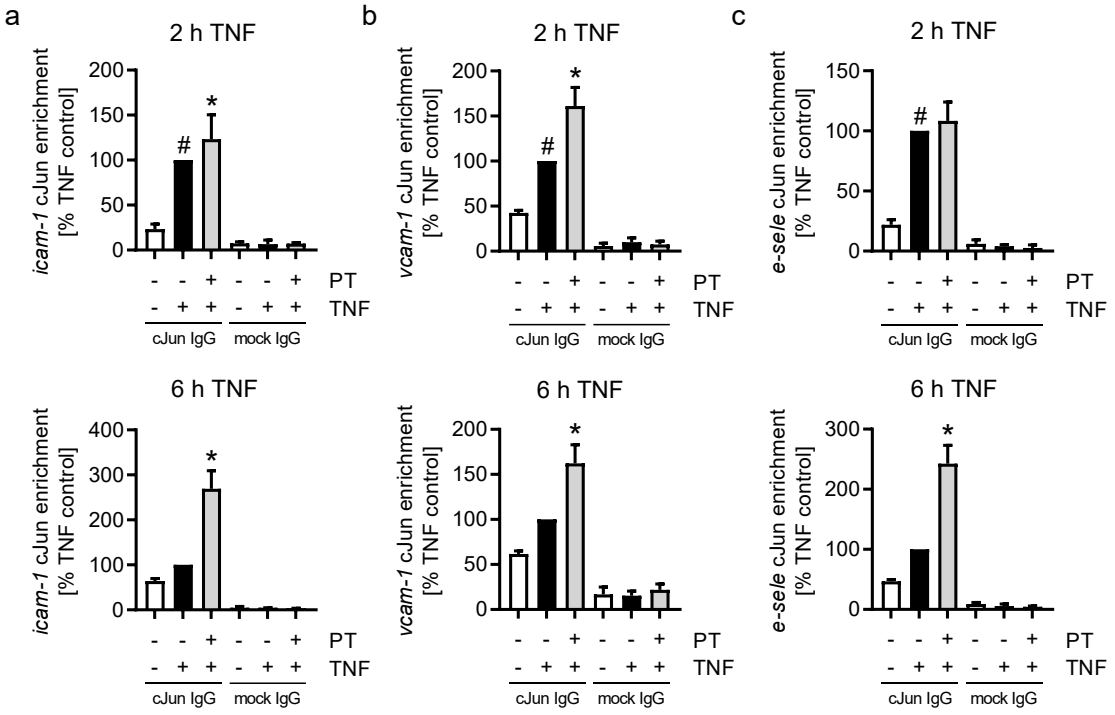

Figure 52. Pretubulysin increases the AP-1-cJun enrichment in the *icam-1* and *vcam-1* and *e-sele* promoters. Enrichment of AP-1-cJun in the *icam-1* (a), *vcam-1* (b) and *e-sele* (c) promoters as shown by chromatin immunoprecipitation (ChIP). Confluent HUVECs were pre-treated with pretubulysin (PT; 300 nM) for 30 min and activated with TNF (10 ng/mL) for a duration of 2 or 6 h. ChIP was performed with a cJun binding antibody and the respective IgG mock antibody. Results were normalized on the background levels of a sequence of the *rpl13a* 3'-untranslated region. (n=3) Data are expressed as mean ± SEM. $^{\#}p \leq 0.05$ versus control, $^{*}p \leq 0.05$ versus TNF control.

PT only marginally increased the enrichment of cJun in the *icam-1* and *e-sele* promoters following 2 h of treatment, but significantly increased the cJun enrichment in the *vcam-1* promoter (Fig. 52). In contrast, cJun was significantly enriched in the promoters of all CAMs following 6 h of treatment, when the overall cJun activity at the CAM promoters appeared to decrease, as seen by the lack of induction (control vs. TNF control).

3.7 Influence of PT on the recruitment of the RNA polymerase II to the CAM genes

3.7.1 Impact on RNA polymerase II enrichment at the CAM gene promoters

PT had no negative effect on the enrichment of NFκB and AP-1 at the CAM promoters and only reduced the NFκB-p65 levels in the *vcam-1* promoter after extended treatment. Based on the lack of negative regulation by PT, the compound was tested towards its effects on the recruitment of the RNA polymerase II (Pol II) to the CAM promoters (Fig. 53).

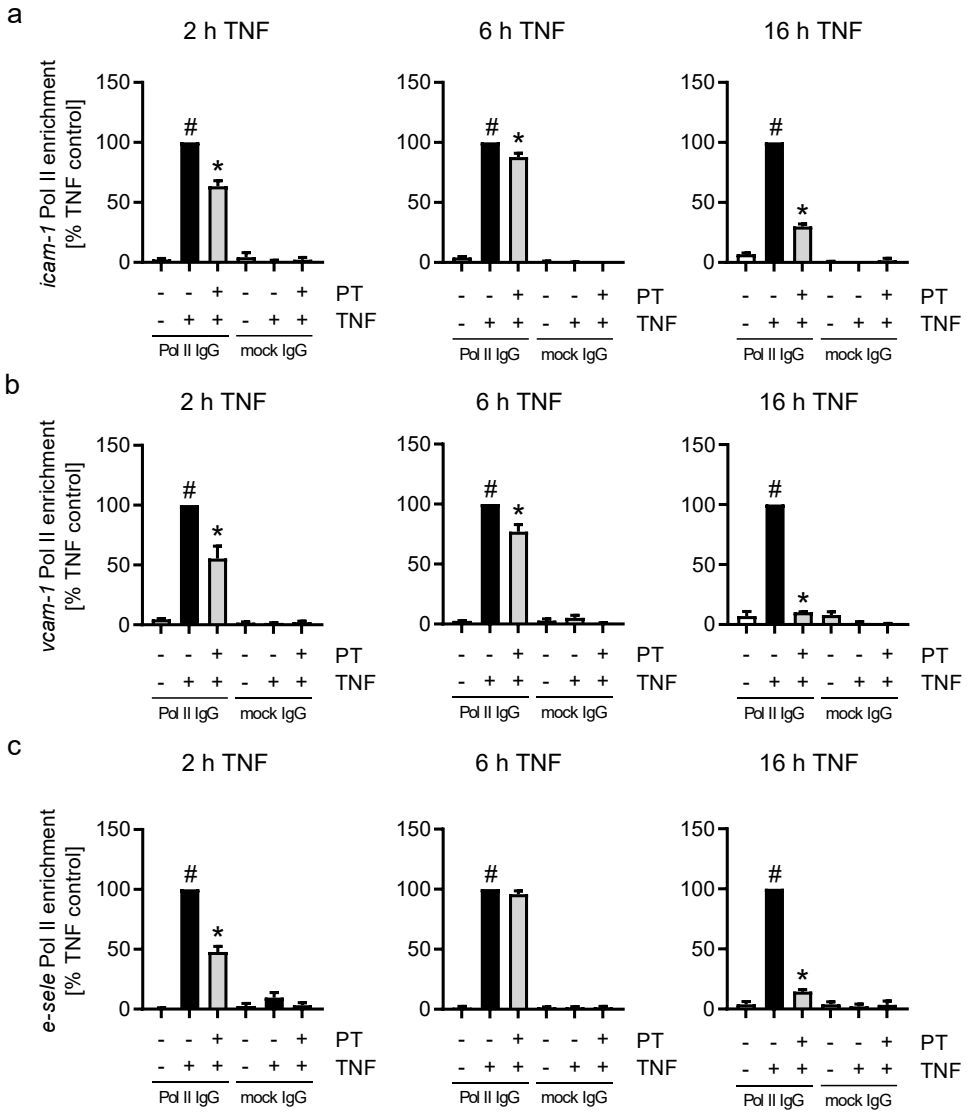

Figure 53. Pretubulysin decreases the RNA polymerase II enrichment at the *icam-1, vcam-1* and *e-sele* promoters in a time-dependent manner. Enrichment of the RNA polymerase II in the promoters of *icam-1* (a), *vcam*-1 (b) and *e-sele* (c) as shown by chromatin immunoprecipitation (ChIP). Confluent HUVECs were pre-treated with PT (300 nM) for 30 min and activated with TNF (10 ng/mL) for different durations (2, 6, 16 h). ChIP was performed with an RNA II polymerase antibody and the respective IgG mock antibody. Results were normalized on the background levels of a sequence of the *rpl13a* 3'-untranslated region. (n=3) Data are expressed as mean ± SEM. $^{\#}p \leq 0.05$ versus control, $^{*}p \leq 0.05$ versus TNF control.

PT moderately decreased the enrichment of Pol II upon 2 h of treatment in the promoters of all CAMs by approx. 50 % compared to the TNF control (Fig. 53). Interestingly, after 6 h of treatment the effects

decreased and were nearly fully lost in case of *e-sele*. Extended treatment of 16 h again reduced the enrichment of the Pol II at the CAM promoters. For *icam-1 and e-sele* Pol II enrichment was decreased by approx. 75 % and 80 %. In case of *vcam-1* enrichment was reduced to the level of the control cells, suggesting total inhibition of the VCAM-1 synthesis after 16 h of treatment.

3.7.2 Impact on RNA polymerase II enrichment at the CAM gene Pol II stalling sites

In addition to the CAM promoters, PT was also analyzed for effects on Pol II enrichment at the CAM gene Pol II stalling sites (Fig. 54).

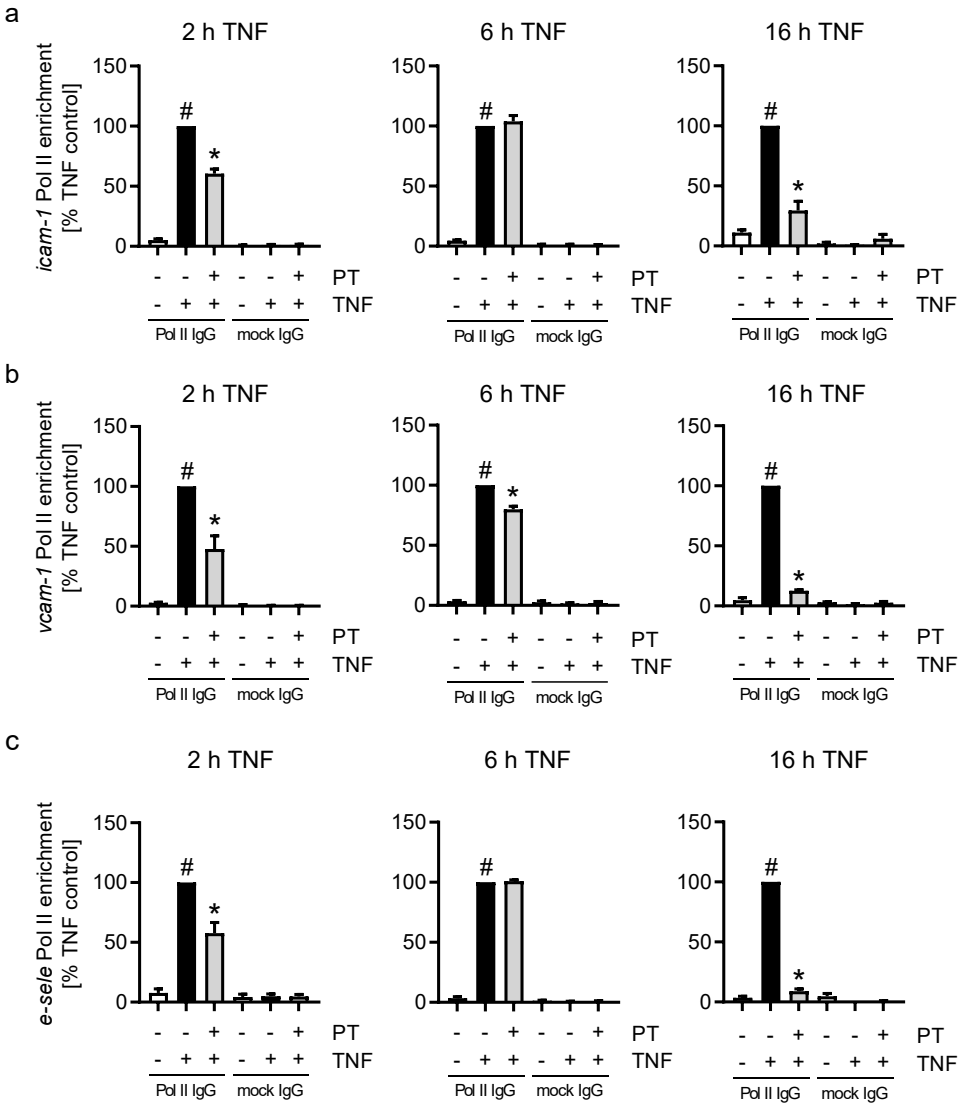

Figure 54. Pretubulysin decreases the RNA polymerase II enrichment at the *icam-1, vcam-1* and *e*-sele Pol II stalling sites in a time-dependent manner. Enrichment of the RNA polymerase II at the Pol II stalling sites of *icam-1* (a), *vcam*-1 (b) and *e-sele* (c) as shown by chromatin immunoprecipitation (ChIP). Confluent HUVECs were pre-treated with PT (300 nM) for 30 min and activated with TNF (10 ng/mL) for different durations (2, 6, 16 h). ChIP was performed with an RNA II polymerase antibody and the respective IgG mock antibody. Results were normalized on the background levels of a sequence of the *rpl13a* 3'-untranslated region. (n=3) Data are expressed as mean ± SEM. $^{\#}p \leq 0.05$ versus control, $^{*}p \leq 0.05$ versus TNF control.

The Pol II enrichment at the CAM gene stalling sites highly resembled that of the CAM promoters (Fig. 53), with a moderate decrease in Pol II enrichment after 2 h of treatment that is largely lost upon 6 h of treatment, but again strongly decreased after 16 h of treatment (Fig. 54).

3.7.3 Summary for the p65, cJun and Pol II enrichment at the *icam-1*, *vcam-1* and *e-sele* gene promoters

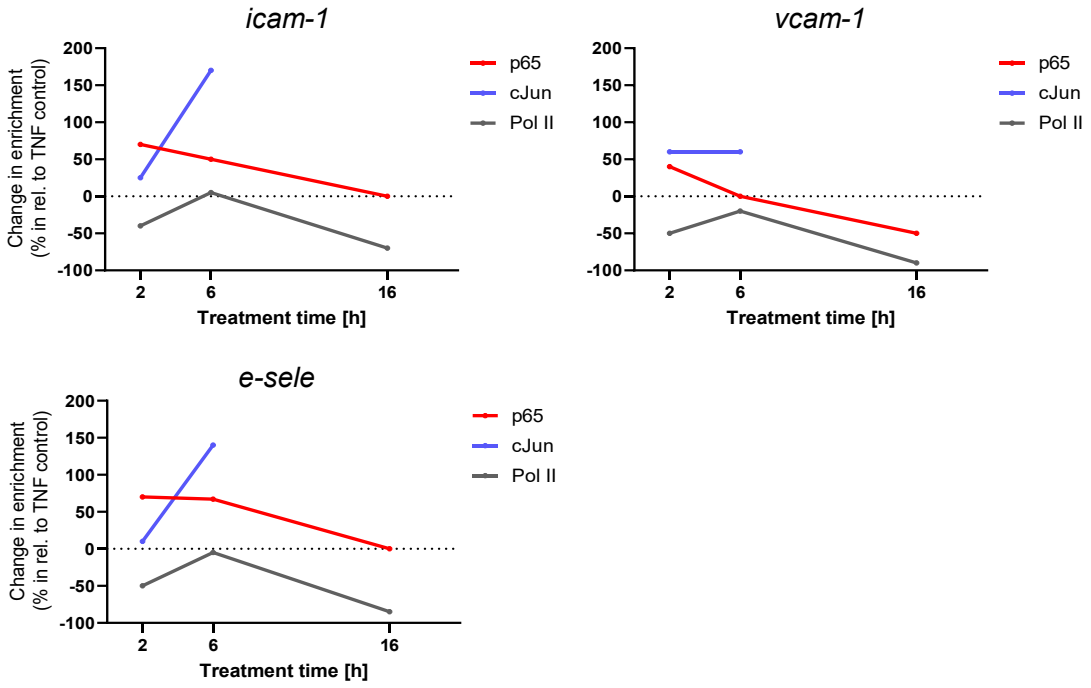

Figure 55. Percentual change in enrichment of p65, cJun and Pol II (stalling enrichment) at the promoters/genes *icam-1*, *vcam-1* and *e-sele,* in relation to the respective TNF control.

Comparison of the enrichment of p65 and cJun as well as the Pol II shows that the PT-induced changes in enrichment follow a similar behavior at the *icam-1* and *e-sele* promoters/genes (Fig. 55). For both genes, cJun levels were only slightly elevated after 2 h, but significantly increased after 6 h of treatment. In contrast, the induction of the cJun levels at the promoter of *vcam-1* was comparably stronger after 2 h of treatment, but did not increase further after 6 h of treatment. In addition, while the levels of p65 were similarly increased at the promoters of *icam-1* and *e-sele*, extended treatment did not induce a decrease in p65 enrichment below the value of the TNF control. In case of *vcam-1*, enrichment already approached TNF control levels after 6 h of treatment and decreased further to approx. 50 % of the corresponding TNF control after 16 h of treatment. The change in enrichment for Pol II was strikingly similar for all three genes tested. However, the magnitude of the change in enrichment of the Pol II was nearly identical for *icam-1* and *e-sele*. For *vcam-1,* the overall decrease of Pol II enrichment was slightly stronger with Pol II levels also being decreased after 6 h of treatment, when the Pol II levels were largely not influenced at the *icam-1* and *e-sele* gene.

3.7.4 Influence of different PT pre-treatment times on CAM transcript levels

PT induced a time-dependent pattern of Pol II enrichment at the CAM genes. To test how different pre-treatment times with PT influence the transcriptional activity at the CAM genes, the CAM mRNA levels were analyzed by qRT-PCR analysis after different pre-treatment times with PT (Fig. 56).

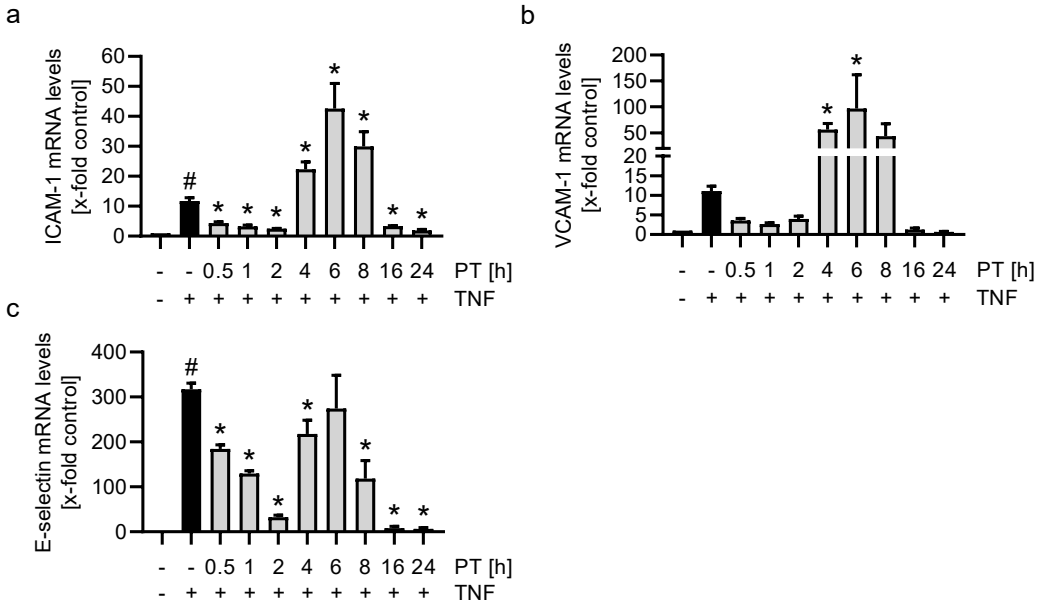

Figure 56. Pretubulysin increases CAM mRNA levels at mean pre-treatment times. qRT-PCR analysis of the mRNA levels of ICAM-1 (a), VCAM-1 (b) and E-selectin (c). Confluent HUVECs were pre-treated with PT (300 nM) for different durations (0.5, 1, 2, 4, 6, 8, 16, 24 h) and activated with TNF (10 ng/mL) for 1 h. Results were normalized on the respective GAPDH mRNA levels. (n=3) Data are expressed as mean ± SEM. $^{\#}p \leq 0.05$ versus control, $^{*}p \leq 0.05$ versus TNF control.

Stimulation with TNF for 1 h led to an approx. 10-fold increase in transcript levels for ICAM-1 and VCAM-1, but increased the E-selectin mRNA levels approx. 300-fold over the control cells (Fig. 56). Pre-treatment times with PT of 0.5 to 2 h decreased the mRNA levels of all CAMs in a time-dependent manner. Strikingly, the mRNA levels of all CAMs were increased again following pre-treatment times of 4 to 8 h and peaked at 6 h of pre-treatment with PT with an approx. 40-fold induction for the ICAM-1 mRNA, 100-fold induction for the VCAM-1 mRNA and 300-fold induction for the E-selectin mRNA. For ICAM-1 and VCAM-1 the mRNA levels following 6 h of pre-treatment were induced significantly over the TNF control, while the E-selectin mRNA levels approached the levels of the TNF control. Following 16 or 24 h of pre-treatment, the mRNA levels of all CAMs were reduced to the levels of the control cells.

3.7.5 Influence of different PT pre-treatment times on transcript levels of additional factors

PT was also analyzed for pre-treatment time-dependent induction of the transcript levels of the additional factors cJun, cFos, IRF-1 and IκBα (Fig. 57).

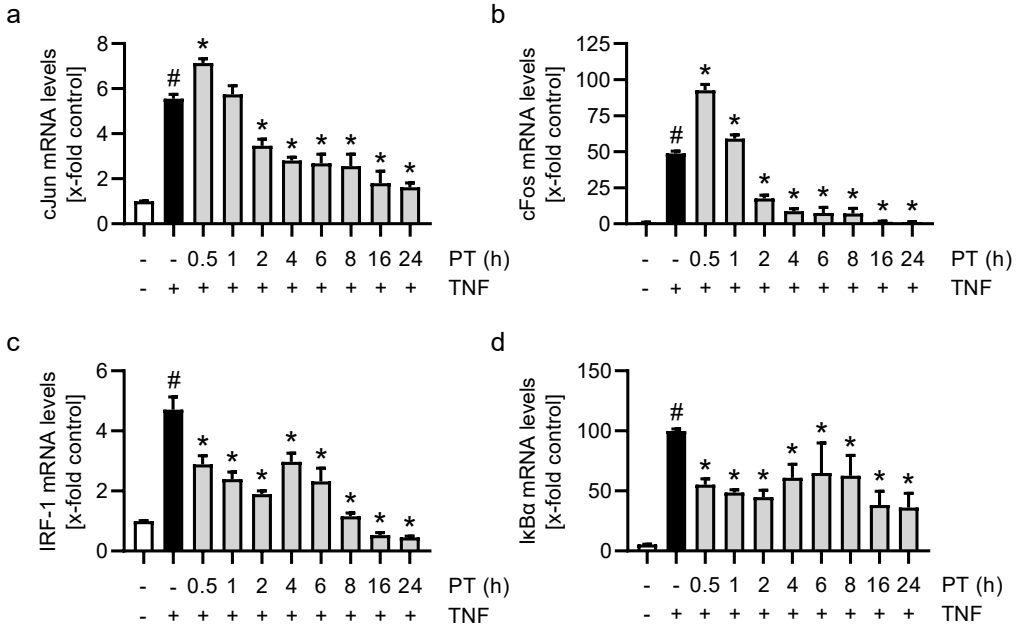

Figure 57. Different pre-treatment times with pretubulysin have a differential effect on the transcript levels of cJun, cFos, IRF-1 and IκBα. qRT-PCR analysis of the mRNA levels of cJun (a), cFos (b), IRF-1 (c) and IκBα (d). Confluent HUVECs were pre-treated with PT (300 nM) for different durations (0.5, 1, 2, 4, 6, 8, 16, 24 h) and activated with TNF (10 ng/mL) for 0.5 h. Results were normalized on the respective GAPDH mRNA levels. (n=3) Data are expressed as mean ± SEM. $^{\#}p \leq 0.05$ versus control, $^{*}p \leq 0.05$ versus TNF control.

Investigations of the influence of different pre-treatment times with PT revealed differential effects for different genes (Fig. 57). The transcript levels of the fast-response genes *cjun* and *cfos* were significantly increased upon short pre-treatment, but time-dependently reduced after longer pre-treatment times with PT (Fig. 57a/b). In contrast, the transcript levels of IRF-1 and IκBα were, similar to the CAMs, reduced after short pre-treatment with PT and increased at mean pre-treatment times, but again decreased after longer pre-treatment (Fig. 57c/d).

3.8 The influence of JNK activity on the PT-evoked effects on the CAMs synthesis

Based on the highly increased activity of the MAPK JNK after treatment with PT, the dependency of the PT-evoked effects on the activity of JNK was analyzed.

3.8.1 Influence of different PT treatment times on CAM transcript levels and sensitivity to JNK activity

PT exerted time-dependent effects on the recruitment of Pol II to the CAM genes and reduced the CAM mRNA levels at short and extended pre-treatment. Based on this, the dependency of the PT-evoked effects on the activity of JNK were determined by qRT-PCR analysis after short and extended treatment with PT (Fig. 58).

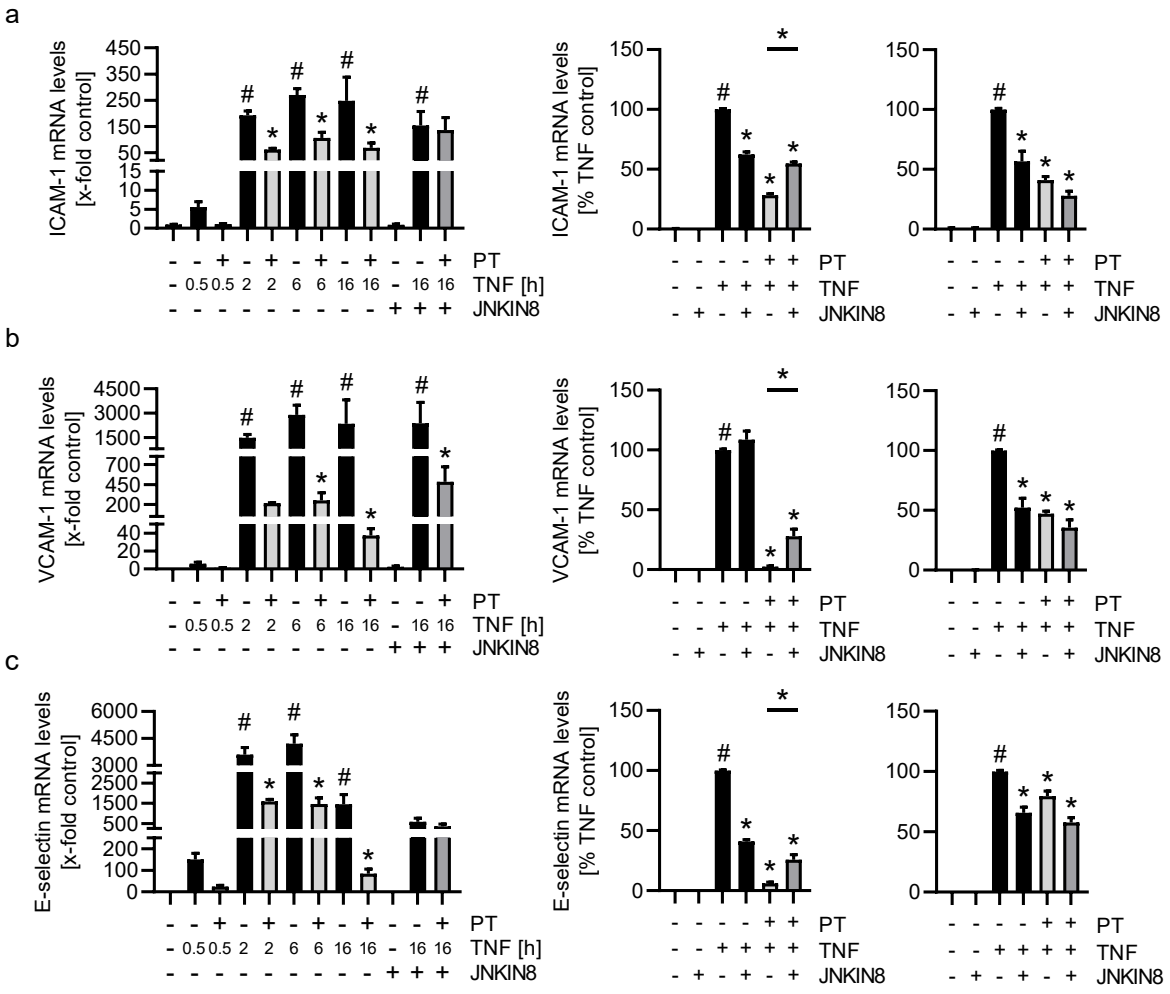

Figure 58. The pretubulysin-induced down-regulation of the ICAM-1 and VCAM-1 and E-selectin mRNAs and can be recovered by long-term inhibition of JNK activity. qRT-PCR analysis of the mRNA levels of ICAM-1 (a), VCAM-1 (b) and E-selectin (c) in dependency of different TNF induction and long-term JNKIN8 treatment time (left) and percentual representation of long-term TNF induction and JNK inhibition (middle) and short-term TNF induction and JNK inhibition (right). For inhibition of JNK activity HUVECs were pre-treated with JNKIN8 (5 μM) for 30 min, treated with PT (300 nM) for further 30 min and activated with TNF (10 ng/mL) for 16 h (a, b and c, left/middle; long-term JNK inhibition) or 1 h (a, b and c, right; short-term JNK inhibition). qRT-PCR analysis results were normalized on the respective GAPDH mRNA levels. (n≥3) Data are expressed as mean ± SEM. $^{\#}p \leq 0.05$ versus control, $^{*}p \leq 0.05$ versus TNF control. The bar with asterisk represents statistical significance over the corresponding data groups with $p \leq 0.05$.

TNF stimulation for 0.5 h only induced a 5-fold increase of ICAM-1 (Fig. 58a, left) and VCAM-1 (Fig. 58b, left) mRNA, but induced an approx. 150-fold increase in E-selectin mRNA (Fig. 58c, left). Following 2 h of stimulation, the mRNA levels of ICAM-1 and VCAM-1 were induced approx. 200-fold and 1500-fold, respectively, and did not decrease below these values after 6 h or 16 h of TNF stimulation. In case of E-selectin, transcript levels were increased above 3000-fold after 2 h and 6 h of stimulation, but declined to approx. 1500-fold after 16 h of stimulation. PT treatment strongly reduced the levels of all CAM mRNAs at all treatment times. Inhibition of JNK activity by the irreversible JNK inhibitor JNKIN8 and TNF stimulation for 16 h decreased the relative ICAM-1 mRNA levels to approx. 60 % and E-selectin mRNA levels to approx. 40 %, but did not affect the VCAM-1 mRNA levels. Inhibition of JNK in the PT-treated cells recovered the ICAM-1 and E-selectin mRNA levels from approx. 30 % to 55 % (Fig. 58a, left and mid) and from approx. 5 % to 25 %, respectively, suggesting a nearly full recovery of the PT-induced effects on relative ICAM-1 and E-selectin mRNA levels. In case of VCAM-1, inhibition of JNK recovered the mRNA levels for the PT-treated cells from approx. 2 % to 30 %. Inhibition of JNK and stimulation with TNF for 1 h decreased the relative mRNA levels of all CAMs by approx. 50 % (Fig. 58a/b/c, right). In contrast to the inhibition of the JNK activity after extended PT treatment, JNK inhibition in the short-term PT-treated HUVECs did not lead to recovery, but further decreased the relative mRNA levels.

3.8.2 Influence of JNK-inhibition on the induction of the fast-response gene *cfos*

cFos is known to be rapidly induced upon pro-inflammatory stimulation of cells (1.4.2). Since PT significantly increased the mRNA levels of cFos after short pre-stimulation, the increased cFos mRNA levels were tested towards sensitivity of JNK inhibition (Fig. 59).

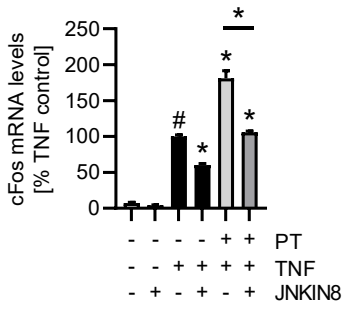

Figure 60. The pretubulysin-evoked induction of cFos mRNA is sensitive to JNK inhibition. qRT-PCR analysis of the mRNA levels of cFos in dependency of JNK inhibition. Confluent HUVECs were pre-treated with JNKIN8 (5 µM) for 30 min and treated with PT (300 nM) for 30 min and were activated with TNF (10 ng/mL) for 0.5 h. qRT-PCR analysis results were normalized on the respective GAPDH mRNA levels. (n=3) Data are expressed as mean ± SEM. $^{\#}p \leq 0.05$ versus control, $^{*}p \leq 0.05$ versus TNF control. The bar with asterisk represents statistical significance over the corresponding data groups with $p \leq 0.05$.

Inhibition of the JNK activity with JNKIN8 significantly reduced the PT-induced increase in cFos mRNA to the level of the TNF control cells, confirming the involvement of JNK activity in the PT-induced increase in cFos mRNA (Fig. 59).

3.8.3 Influence of JNK inhibition on the PT-induced down-regulation of the ICAM-1 and VCAM-1 cell surface levels

Inhibition of the activity of JNK after extended PT treatment notably recovered the mRNA levels of ICAM-1, VCAM-1 and E-selectin. In consequence, the effects of JNK inhibition on the PT-induced down-regulation of the ICAM-1 and VCAM-1 cell surface levels were investigated by flow cytometry (Fig. 60).

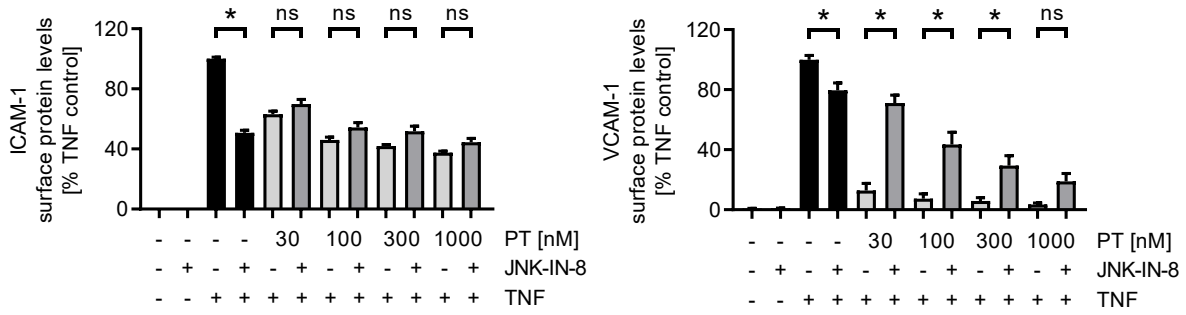

Figure 60. The pretubulysin-induced down-regulation the ICAM-1 and VCAM-1 cell surface protein levels can be recovered by long-term inhibition of JNK activity. Flow cytometric analysis of the effects of JNK inhibition on the PT-induced downregulation of ICAM-1 (left) and VCAM-1 (right) cell surface levels. Confluent HUVECs were pre-treated with JNKIN8 (5 µM) for 30 min and treated with different concentrations of PT (30, 100, 300, 1000 nM) and activated with TNF (10 ng/mL) for 24 h. ($n \geq 3$). The bar with asterisk represents statistical significance over the corresponding data groups with $p \leq 0.05$.

Inhibition of JNK reduced the cell surface levels of ICAM-1 by approx. 50 % and those of VCAM-1 by approx. 20 % following 24 h of TNF stimulation, indicating an increased sensitivity of the ICAM-1 promoter to JNK activity (Fig. 60). Inhibition of JNK in the PT-treated HUVECs recovered the cell surface levels of both CAMs at all concentrations tested. Recovery was significantly stronger for VCAM-1 with cell surface levels being recovered from 5 % to 30 % after treatment with 300 nM of PT and ICAM-1 levels being recovered from 40 % to 50 % of the TNF control.

3.9 Influence of PT on post-promoter transcriptional regulation

3.9.1 Influence of PT on the recruitment of the bromodomain-containing protein 4 at the *icam-1* and *vcam-1* genes

Short treatment with PT led to a reduction of the respective CAM mRNAs but increased mRNA levels for the fast-response genes like cJun and cFos. In contrast, transcript levels were significantly reduced after extended treatment with PT irrespective of the gene tested. In addition, the enrichment of the main transcription factors NFκB and AP-1 was strikingly increased after short treatment and only moderately reduced in case of the *vcam-1* gene after extended treatment. Based on this, PT was tested for its influence on the recruitment of the bromodomain-containing protein 4 (Brd4), responsible for recruiting pTEFb and enabling the release of the stalled Pol II from the stalling sites in the *icam-1* and *vcam-1* genes (Fig. 61).

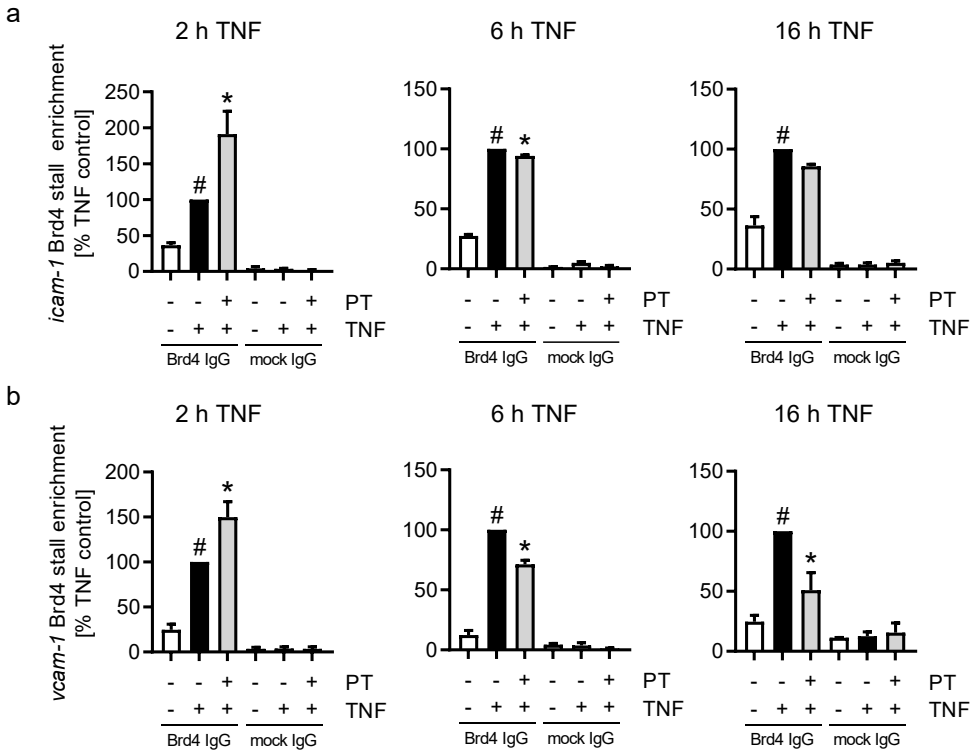

Figure 61. Pretubulysin increases Brd4 enrichment at short treatment times and leads to a time-dependent decrease in Brd4 enrichment at the *icam-1* and *vcam-1* RNA polymerase II stall site. Enrichment of Brd4 at the RNA polymerase stall sites in the *icam-1* (a) or *vcam-1* (b) after different treatment times with PT as shown by ChIP. Confluent HUVECs were pre-treated with PT (300 nM) and activated with TNF (10 ng/mL) for different durations (2, 6, 16 h). ChIP was performed with a Brd4 antibody and the respective IgG mock antibody. Results were derived based on 2 % of input DNA. (n=3) Data are expressed as mean ± SEM. $^{\#}p \leq 0.05$ versus control, $^{*}p \leq 0.05$ versus TNF control.

After 2 h of TNF stimulation, PT induced a significant increase in Brd4 enrichment in the Pol II stalling regions of *icam-1* and *vcam-1*. The Brd4 enrichment for *icam-1* was increased by approx. 90 % and for *vcam-1* by approx. 50 % compared to the TNF control cells (Fig. 61a/b). After 6 h of treatment time, the Brd4 enrichment was decreased to approx. 95 % in the *icam-1* stalling region and to 70 % in the *vcam-*

1 stalling region. Longer TNF stimulation and PT treatment of 16 h led only to a minor further decrease of Brd4 enrichment for *icam-1*, but further decreased the Brd4 enrichment in the *vcam-1* stalling region to approx. 50 % compared to the TNF control.

3.9.2 Summary for the p65, cJun, Pol II and Brd4 enrichment at the *icam-1* and *vcam-1* gene

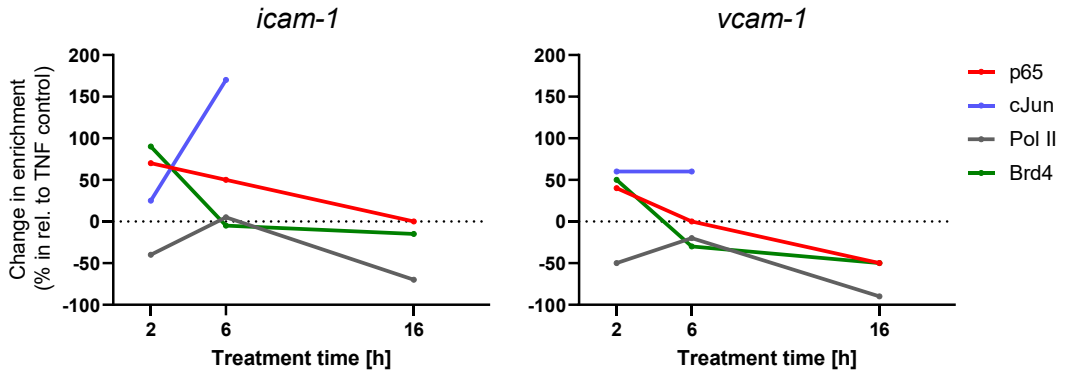

Figure 62. Percentual change in enrichment of p65, cJun, Pol II and Brd4 at the promoters/genes *icam-1* and *vcam-1* in relation to the respective TNF control.

Addition of the PT-induced change in enrichment for Brd4 at the *icam-1* and *vcam-1* genes revealed that for both genes, the Brd4 and Pol II enrichment followed an opposing pattern of enrichment (Fig. 62). The initial increase in Brd4 enrichment after 2 h of treatment was strikingly stronger in case of *icam-1*, compared to *vcam-1*. After 6 h of treatment, the change in Brd4 and Pol II enrichment for both genes was strikingly similar. Of note, pre-stimulation for 6 h led to a strong induction of the respective CAM mRNAs. Extended treatment of 16 h led only to a minor further decrease in Brd4 enrichment for both genes. However, it is evident that the change in enrichment for Brd4 closely resembles that of p65.

3.9.3 The dependency of the PT-evoked deregulation of Brd4 at the *icam-1* and *vcam-1* Pol II stalling sites on the activity of JNK

The PT-induced down-regulation of the CAMs is highly dependent on the activity of JNK. Due to that the influence of the JNK activity on the deregulation of Brd4 was tested by ChIP (Fig. 63).

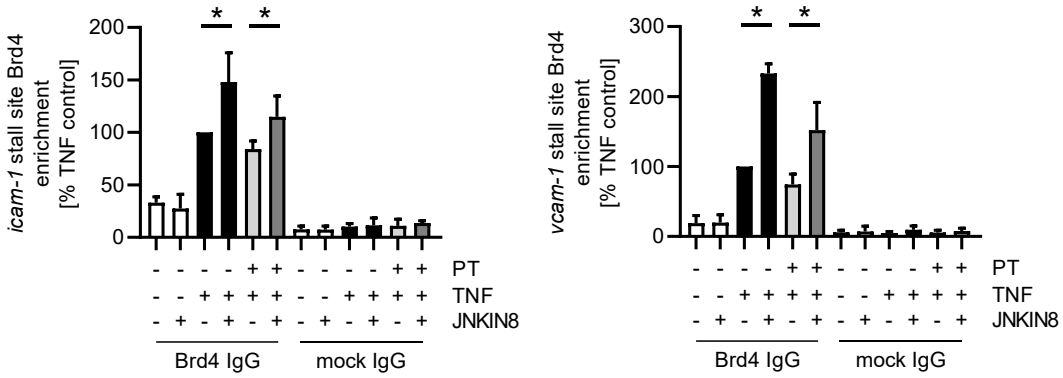

Figure 63. The pretubulysin-induced reduction of Brd4 enrichment in the *icam-1* and *vcam-1* RNA polymerase stalling sites can be reversed by inhibition of JNK. ChIP-based enrichment of Brd4 at the *icam-1* (left) and *vcam-1* (right) RNA polymerase stalling sites in dependency of JNK inhibition. Confluent HUVECs were pre-treated with JNKIN8 (5 µM) for 30 min, treated with PT (300 nM) for further 30 min and activated with TNF (10 ng/mL) for 6 h. ChIP was performed with an antibody against Brd4 or the respective mock antibody. Results were obtained based on 2 % of input. (n=3) The bar with asterisk represents statistical significance over the corresponding data groups with $p \leq 0.05$.

Inhibition of JNK increased the TNF-induced enrichment of Brd4 at the *icam-1* and *vcam-1* stalling site significantly, with Brd4 levels being increased to approx. 150 % for *icam-1* and 230 % for *vcam-1* (Fig. 63). Inhibiting the activity of JNK in the PT-treated HUVECs also significantly increased the enrichment of Brd4 for *icam-1* from approx. 85 % to 115 % and for *vcam-1* from approx. 75 % to 150 %.

3.9.4 The influence of the PT-induced JNK activity on Brd4 protein levels

Analysis of the dependency of the Brd4 enrichment on the activity of JNK clearly showed that the association of Brd4 with the *icam-1* and *vcam-1* genes is negatively regulated by JNK. To further understand how PT influences Brd4, the effects of PT on the total protein levels of Brd4 and the dependency of the Brd4 levels on the activity of JNK were tested by western blot analysis of the nuclear fraction (Brd4 could only be detected in the nucleus of HUVECs, Fig. 64).

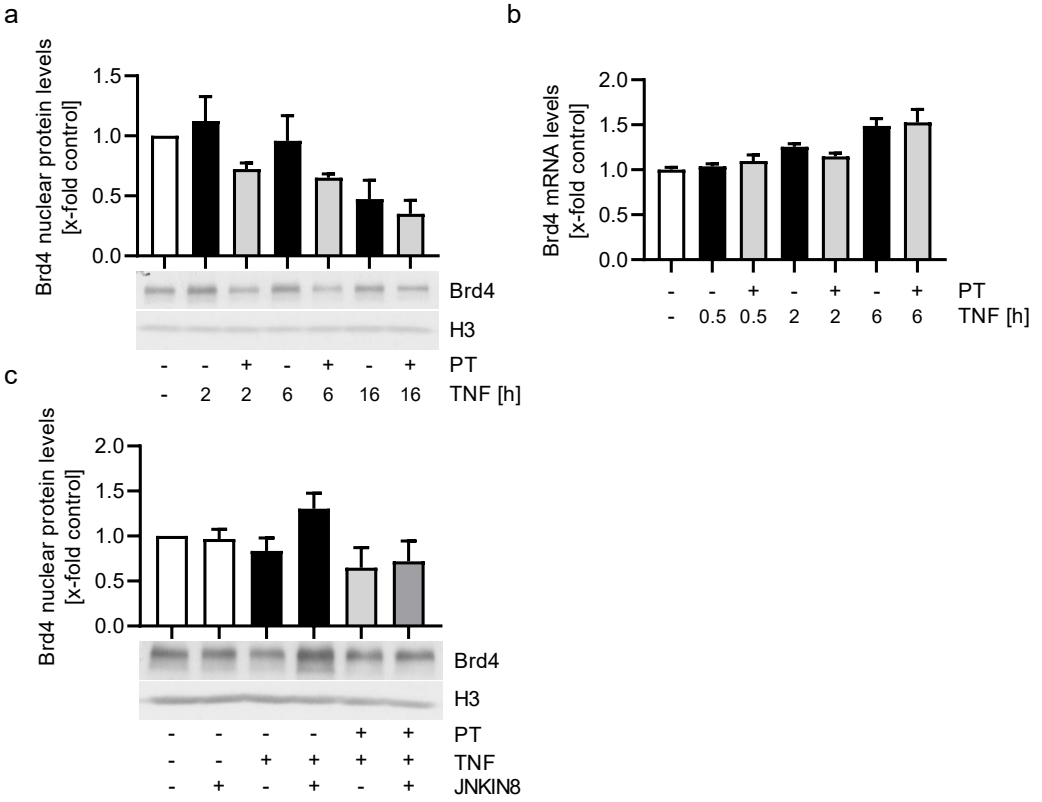

Figure 64. Pretubulysin treatment leads to a reduction of the Brd4 levels in the nuclear fraction, which can be reversed by inhibition of JNK. Western blot analysis of the Brd4 protein levels in the nuclear fraction (a), qRT-PCR analysis of the Brd4 mRNA levels (b) and nuclear Brd4 levels in dependency of JNK inhibition (c). Confluent HUVECs were pre-treated with PT (300 nM) for 30 min and activated with TNF (10 ng/mL) for durations of 2, 6 or 16 h (a) or 0.5, 2 and 6 h (b) or pre-treated with JNKIN8 (5 µM) for 30 min, treated with PT (300 nM) for further 30 min and activated with TNF (10 ng/mL) for 6 h (c). Western blot results were normalized on the respective histone 3 (H3) levels and qRT-PCR results were normalized on the respective GAPDH mRNA levels. (n=3)

Stimulation with TNF slightly increased the nuclear Brd4 protein levels after 2 h of stimulation, which decreased over the stimulation time to approx. 50 % of the control cells after 16 h of stimulation (Fig. 64a). Treatment with PT increased the apparent reduction of the Brd4 protein levels compared to the respective TNF controls, while not negatively affecting the Brd4 mRNA levels (Fig. 64b). Inhibition of JNK activity by JNKIN8 markedly reversed the reduction of the Brd4 protein levels after 6 h of TNF stimulation (Fig. 64c). This effect was also present in the PT-treated cells, albeit to a much lesser extent.

3.9.5 Influence of Brd4 knock-down on the cell surface levels of ICAM-1 and VCAM-1

PT induced an increased enrichment of Brd4 at the *icam-1* and *vcam-1* genes after short treatment, but decreased the enrichment after extended treatment times. While the Brd4 levels for *icam-1* were only slightly negatively influenced, Brd4 levels at the *vcam-1* gene were markedly decreased. Based on this differential enrichment at both genes, the effects of Brd4 knock-down on the cell surface levels of ICAM-1 and VCAM-1 were tested by flow cytometry (Fig. 65).

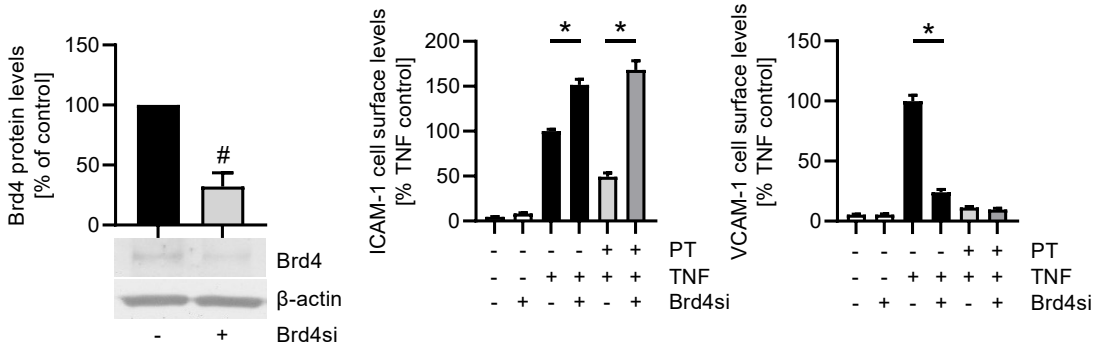

Figure 65. Knock-down of Brd4 leads to increased ICAM-1 cell surface levels, but reduced VCAM-1 levels. Western blot analysis of the total Brd4 protein levels (left) or flow-cytometric analysis of the ICAM-1 and VCAM-1 cell surface levels (middle and right) after Brd4 knock-down. Sub-confluent HUVECs were transfected with 100 nM of Brd4 siRNA or non-targeting siRNA and incubated for 48 h, pre-treated with PT (300 nM) for 30 min and activates with TNF (10 ng/mL) for 24 h and were used for flow-cytometry or western blot analysis. Western blot results were normalized on the respective β-actin levels (left). (n=3) Data are expressed as mean ± SEM. $^{\#}p \leq 0.05$ versus control. The bar with asterisk represents statistical significance over the corresponding data groups with $p \leq 0.05$.

Transfection of HUVECs with Brd4 siRNA (Brd4si) and incubation for 48 h reduced the Brd4 protein levels by approx. 50 % compared to the control cells transfected with non-targeting siRNA (Fig. 65, left). Knock-down of Brd4 significantly increased the TNF-induced cell surface levels of ICAM-1 by approx. 66 % (Fig. 65, mid), but reduced the VCAM-1 cell surface levels after 24 h of TNF stimulation by approx. 80 % (Fig. 65, right). Interestingly, addition of PT increased the ICAM-1 levels in the Brd4 knock-down cells further, but had no effect of the already significantly reduced VCAM-1 cell surface levels.

3.9.6 Influence of PT on repressional chromatin marks in the *icam-1* and *vcam-1* gene

PT deregulated Brd4 in both CAM genes. However, the knock-down of Brd4 revealed a different functionality of Brd4 at the genes of ICAM-1 and VCAM-1. To test how PT influences the overall transcriptional activity of the genes of ICAM-1 and VCAM-1, the *icam-1* and *vcam-1* genes were tested towards the presence of the repressional histone 3 lysine 9 tri-methylation marks (H3K9me3) after extended treatment with PT (Fig. 66).

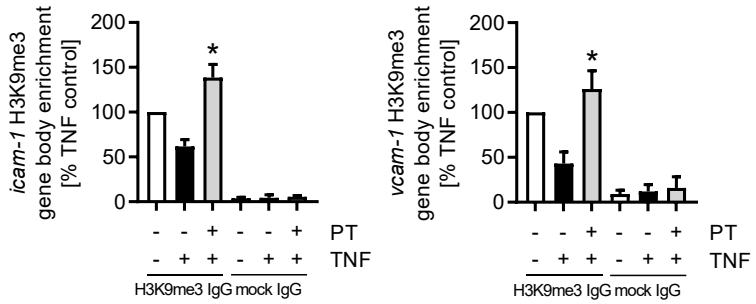

Figure 66. Pretubulysin increases H3K9me3 enrichment in the gene body of *icam-1* and *vcam-1* after extended treatment times. Enrichment of H3K9me3 in the gene body of *icam-1* (left) and *vcam-1* (right) as shown by ChIP. Confluent HUVECs were pre-treated with PT (300 nM) and activated with TNF (10 ng/mL) for 16 h. ChIP was performed with an H3K9me3 antibody and the respective IgG mock antibody. Results were derived based on 2 % of input DNA. (n=3) Data are expressed as mean ± SEM. *p ≤ 0.05 versus TNF control.

Compared to the control cells, TNF induction for 16 h decreased the levels of H3K9me3 in the *icam-1* gene to an approx. 50 % and in the *vcam-1* gene to approx. 40 % (Fig. 66). Surprisingly, treatment with PT increased the enrichment of H3K9me3 in both CAM genes to a similar extend. The H3K9me3 marks were increased by PT treatment to approx. 140 % for *icam-1* and 125 % for *vcam-1*.

4. Discussion

4.1 The destabilizing MTA PT reduces inflammation-associated processes in vascular endothelial cells

This project aimed at elucidating the anti-inflammatory potential of the destabilizing MTA PT and of MTAs already in clinical use with regard to the leukocyte adhesion cascade. By testing the anti-inflammatory effects of PT in a murine imiquimod-induced psoriasiform dermatitis (IMQPD) model, we clearly showed that PT reduces the cardinal signs of inflammation (redness, stiffness) *in vivo*. Testing of the effects of PT on the TNF-induced leukocyte adhesion in the murine cremaster muscle by intravital microscopy and in the *in vitro* setting under flow condition demonstrated that treatment with PT significantly reduces the adhesion of leukocytes to the vascular endothelial cells. The decreased firm adhesion of leukocytes is thereby based on the PT-induced and JNK activity-dependent inhibition of the synthesis of the CAMs ICAM-1 and VCAM-1, which is especially in case of VCAM-1, is connected to the deregulation of the recruitment of Brd4. The other destabilizing MTAs VIN and COL also inhibited the synthesis of ICAM-1 and VCAM-1. This is also represented by the fact that especially the depolymerizing MTAs reduced the promoter activity of AP-1 and NFκB to a different extent. Studies performed by Wang *et al.* (2018) [378] have already shown that treatment with the Brd-inhibitor JQ1 leads to a reduction of the generall promoter activity of NFκB. The observed differences in inhibition of the promoter activity of NFκB and AP-1 by the MTAs can be explained by the different potentials to depolymerize the microtubule skeleton. Over the course of this study, Filipčík *et al.* (2020) [379] have shown that the JNK upstream kinase MAPK kinase kinase 1 (MAP3K1, MEKK1) contains a cryptic tubulin-binding domain that binds to free tubulin and leads to kinase activation. Hence the strong increase in JNK activity upon treatment with depolymerizing MTAs and the resulting inhibition of the CAM synthesis are directly linked to the depolymerization of the microtubule cytoskeleton. Interestingly, testing the effects of the MTAs on the activity of JNK following 2 h of treatment revealed that especially PT and VIN induce a significant induction of JNK activity compared to the TNF-treated cells, while COL (and PAC) showed little effect on the phosphorylation of JNK. In addition, the effect of COL on the NFκB and AP-1 promoter activity after 6 h were slightly less pronounced compared to PT and VIN. This might be explained by a higher affinity of PT and VIN to depolymerize the microtubule skeleton. However, since COL also led to a reduction of the promoter affinity after 6 h of treatment, it is likely that the kinetics underlying the PT- and VIN-induced microtubule polymerization are faster compared to those for COL. This is also underlined by the fact that extended pre-treatment with any of the depolymerizing MTAs for 24 h induced the activity of JNK to a similar extent.

4.1.1 The microtubule-stabilizer PAC bears no anti-inflammatory potential

Interestingly, the microtubule stabilizer PAC also reduced the promoter activity of NFκB and AP-1, albeit to a lesser extent than the depolymerizing agents. This might be explained by the fact that PAC also led to an over-induction of JNK activity after extended treatment, which might also deregulate Brd4. It is known that many phosphatases, i.e. phosphatase 2α, associate with the microtubule cytoskeleton [380]. The increased stabilization of the microtubule skeleton by PAC might thereby reduce the overall activity of phosphatases that counteract the phosphorylation and hence activation of kinase targets. Hence, even though PAC might slightly deregulate Brd4, which leads to a decreased promoter activity, the overall outcome of the treatment with this stabilizing MTA concerning the leukocyte adhesion cascade is pro-inflammatory. This is also represented by the fact that PAC increased the cell surface levels of ICAM-1 and VCAM-1. In fact, several studies show a pro-inflammatory function of PAC. Son *et al.* (2019) [381] could show that treatment of bone marrow-derived macrophages with PAC induces TLR4-based activation of JNK and deactivation of IκB proteins, as well as increasing pro-inflammatory cytokine mRNA levels. In addition, they could show that PAC induced priming of the NLRP3 inflammasome, thereby facilitating the inflammatory response. Zhang *et al.* (2023) [382] examined the effects of PAC treatment in HUVECs and found that PAC increased the expression of pro-inflammatory factors, like TNF, IL-2 and IL-6, as well as the monocyte chemoattractant protein-1 (MCP-1) and CD137, which has been shown to induce CAMs in ECs [383, 384]. Additionally, they could show that treatment of mice with PAC significantly increased the expression of the CAMs E-selectin and VCAM-1 in mouse aortic ECs *in vivo* [382].

4.2 The effects of PT on the MAPKs p38 and ERK

While PT induced striking effects on the activity of JNK, the activities of p38 and ERK were only slightly influenced. The effects on JNK are directly connected to the depolymerization of the microtubule skeleton *via* induction of MAP3K1. Like JNK, the p38 kinase is also known to be activated by conditions that exert cellular stress [385–387]. Hence, the increased cytoplasmic activity and translocation of p38 into the nucleus of HUVECs after treatment with PT might correlate to the cell stress induced by microtubule depolymerization. In general, MAPKs are known to associate to the microtubules *via* JNK-interacting protein (JIPs) [388–391]. Direct binding or indirect binding of MAPKs via MAPK associated proteins to JIPs is thought to enable spatial localization of MAPKs for interaction with higher tier MAPKs or proteins of the dual-specificity phosphatase family (DUSPs) that deactivate the MAPKs [392–396]. The depolymerization of the microtubule cytoskeleton by MTAs might influence the activation of the p38 MAPK by impairing the spatial localization of the activating or deactivating MAPK signaling components. Treatment with PT induced the activity of p38 in the cytoplasm of the cells and while it increased the total protein levels of p38 in the nucleus of HUVECs, the activity of this nuclear p38 fraction was decreased compared to the TNF-stimulated control cells.

mRNA decay takes place in the cytoplasm of cells and is dependent on interaction of RBPs with AU-rich regions in the 3' non-translated regions of the mRNAs [397, 398]. The p38 kinase is known to be involved in activating proteins that stabilize or destabilize the mRNA via activation of nuclear MAPKAP2 [399, 400]. Upon activation by p38, the nuclear MAPKAP2 translocates to the cytoplasm of cells, were it regulates the activity of stabilizing or destabilizing RBPs. Hence, the decreased nuclear activity of p38 upon treatment with PT might also decrease the activation and nuclear export of MAPKAP2 and hence, omit the activation of the cytoplasmic RBPs. This could explain the increased half-life of the VCAM-1 mRNA after treatment with the depolymerizing MTAs.

Interestingly, PT reduced the total protein content of the MAPK ERK in the cytoplasm and the nucleus of HUVECs. This is of particular interest, because Lu *et al.* (2002) [401] have shown that the ERK kinase is regulated by ubiquitination through MAP3K1, which, next to its tubulin-binding domain, also contains a RING-domain with ubiquitin ligase activity. The increased MAP3K1 activity might thereby also deregulate ERK by inducing its degradation.

4.3 Depolymerizing MTAs induce pro-inflammatory NFκB and AP-1 signaling but disconnect promoter activity from constructive elongation

Based on the observed effects of PT on the pro-inflammatory NFκB and AP-1 signaling cascades it is evident that PT induces pro-inflammatory signaling. PT induced the activity of IKK and strongly induced the activity of JNK. Earlier studies have already demonstrated the pro-inflammatory behavior of the clinically used MTA COL *via* induction of the promoter activity of NFκB in the absence of pro-inflammatory stimuli [402]. Analyzing the effects of PT on the promoter enrichment of NFκB clearly showed an increased enrichment of this transcription factor after short treatment times and a general induction of AP-1-cJun as seen by ChIP and western blot analysis. The over-induction of JNK and the slightly increased nuclear GSK3β protein levels appeared to also increase the inhibitory phosphorylation in the phosphodegron motif of cJun. However, based on the intensity of the shifted cJun-phospho-S243 fractions compared to the total cJun fraction and the increased cJun enrichment in the CAM promoters, it is likely that the increased auto-induction of the *cjun* gene by cJun outweighs the inhibitory cJun phosphorylation by JNK or GSK3β. In case of NFκB, extended treatment led to a decrease in p65 enrichment in the promoter of *vcam-1* at a treatment time when the total p65 protein content was reduced by PT, while p65 enrichment in the *icam-1* promoter was not reduced below the levels of the TNF control. This might be explained by the reduced p65 protein levels and potential different affinities of NFκB to the NFκB-binding motifs in the CAM promoters. The NFκB-p50 protein levels were reduced already 6 h after treatment with PT. This fact also suggests a deregulation of the relative p65:p50 levels over time, which might further decrease the activity of NFκB at the promoters of target genes, because the p65:p50 NFκB heterodimer is known to have the highest DNA-binding affinity of the potential NFκB constituents [85]. The additional increase of IκBα protein levels after 10 h and 12 h of treatment

might also decrease the NFκB activity at these times and might be partially responsible for the decreased nuclear p65 levels at later treatment times. However, studies concerning the effects of the Brd-inhibitor JQ1 have shown that treatment with this inhibitor induces the ubiquitination and degradation of NFκB, suggesting a protective function of Brd4 on the activity of NFκB at target genes [403]. Thus, it might be possible that the JNK-induced eviction of Brd4 from the target genes also induces the degradation of NFκB, resulting in overall decreased p65 promoter activity. Based on the increased enrichment of NFκB after short treatment times and the general induction of AP-1-cJun, it is clear that PT rather induces pro-inflammatory signaling. However, these increased pro-inflammatory signaling events do not lead to increased expression of target genes, as seen by the reduced recruitment of Pol II at the same treatments times when the NFκB and AP-1 enrichment at the CAM promoters was significantly enriched. Comparison of the Pol II enrichment at the CAM promoters and the stalling regions suggests that exit of the Pol II from the promoter to the stalling site is not influenced by PT. However, the close proximity of both sites makes it difficult to distinguish the Pol II enrichment *via* ChIP. Nevertheless, especially with view on the deregulation of Brd4 after extended treatment with PT, it is clear that treatment with PT prevents the entry of the Pol II into constructive elongation.

4.4 PT induces different mechanisms of action based on the treatment time

PT significantly induced the enrichment of Brd4 at the genes of ICAM-1 and VCAM-1 following 2 h of treatment, which decreased over the treatment time and especially led to reduced Brd4 enrichment in the *vcam-1* gene. The initial increase in Brd4 at the CAM genes appeared to approximately follow the enrichment of NFκB-p65, which is in accordance with the fact that Brd4 binds directly to acetylated p65 (K310ac) [114]. However, following 6 h of treatment, the loss of Brd4 becomes more pronounced than the loss of p65 at the CAM genes, marking the beginning of the JNK-induced deregulation of Brd4 and the likely loss of pTEFb recruitment and activation by Brd4. Nishiyama *et al.* (2006) [404] have shown that Brd4 dissociates from chromosomes following treatment of cells with the microtubule-destabilizer nocodazole. In addition, they show that this mechanism is dependent on the activity of the JNK pathway and residues in the carboxy-terminal domain of Brd4. Based on this, we assume that the initial increase in Brd4 binding simply follows the enrichment of NFκB at the CAM genes. However, Song *et al.* (2020) [405] have shown that inhibition of the activity of JNK prior to 2 h of UV light exposure reduces the UV light damage-induced interaction of Brd4 with pTEFb. This indicates a positive regulation of the Brd4:pTEFb interaction due to the activity of JNK. Based on this, it might be possible that the activation of JNK initially stimulates the binding of Brd4 to acetylated p65 and association of Brd4 with pTEFb, but leads to reduced Brd4 binding over time. This behavior would fit well to the initial increase in expression for some target genes after treatment with PT, like the fast-response genes *cjun* and *cfos* and might reflect the functionality of Brd4 at different target genes. The fact that the initial increase in cFos mRNA was sensitive to JNK activity underlines this potential functionality. However, due to the fact

that both genes are sensitive to AP-1 induction, and in light of the strong activation of JNK by PT treatment, distinguishing both functionalities is difficult. With view on the CAMs, testing of the mRNA levels after different pre-treatment times revealed that PT inhibits the synthesis of CAM mRNAs after short pre-treatment times, induces the mRNA levels after mean pre-treatment times and (again) significantly reduces the mRNA levels after extended treatment periods. Comparison with the Brd4 and Pol II enrichment after 6 h of treatment, when the enrichment is largely not influenced by PT, and the general increased NFκB and AP-1 enrichment after short treatment, suggests that constructive transcription is not inhibited at these times. This is also demonstrated by the increased induction of the CAM mRNA after mean pre-treatment times with PT. However, under constant TNF stimulation, mRNA levels were also decreased at mean pre-treatment times, which suggests an involvement of additional mechanisms. Testing the effects of JNK inhibition upon extended treatment with PT clearly showed that JNK negatively regulates the DNA enrichment of Brd4 over time and increases the levels of the repressive H3K9me3 histone markers in the *icam-1* and *vcam-1* genes, inhibiting the expression of both genes. The increase in the repressive histone marks is likely based on the fact that Brd4 can no longer exert its function in recruiting and activating pTEFb and enable the release of the stalled Pol II as well as the initiation of the productive transcript elogantion (Fig. 67). Jackman *et al.* [344] argued that COL must enact its effects on the NFκB signaling cascade by disrupting the TNFR1 interaction with the intracellular NFκB signaling components due to microtubule depolymerization. However in this study, following 0.5 h or 2 h of treatment with PT, the nuclear NFκB-p65 protein levels were not negatively influenced and the NFκB-p65 levels in the CAM gene promoters were significantly increased and did not decrease below the levels of the TNF control after 6 h of treatment. Even following 16 h of

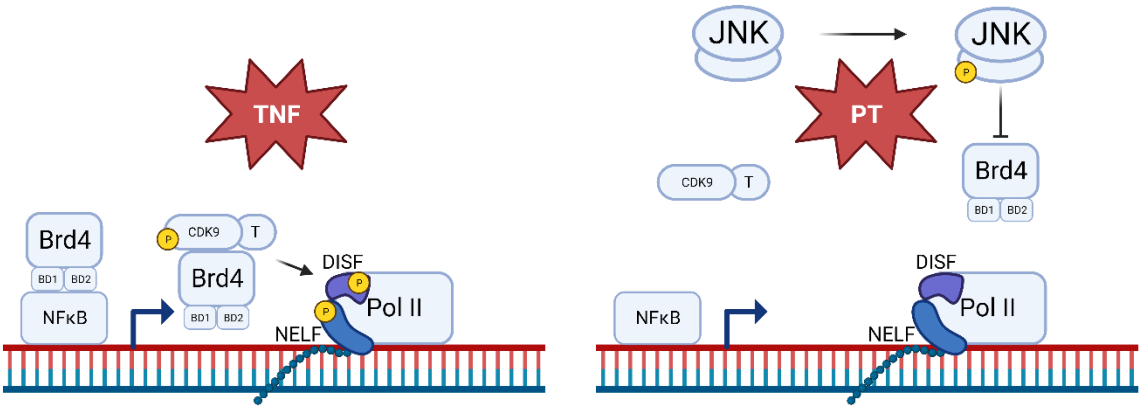

Figure 67. Mechanism for the effect of extended treatment with PT. Under normal conditions (left), TNF stimulation induces a correct functionality of Brd4, which binds to either NFκB and/or associates with the stalled Pol II in order to enable phosphorylation of NELF and DSIF, thus inducing constructive elongation. The strong activation of JNK after depolymerization of the microtubules due to PT (right) negatively regulates the association of Brd4 with acetylated NFκB or the stalling region. This prevents recruitment and activation of CDK9 and, hence, the exit of the stalled polymerase and also prevents the formation of an active chromatin environment for constructive transcription.

treatment with PT, the nuclear NFκB levels were only slightly reduced and the p65 levels at the promoters of *icam-1* and *e-sele* were not influenced. In addition, the PT-induced effects after extended

treatment are clearly reversible by JNK inhibition. Due to that, it is to argue that the increased JNK activity and the correlated eviction of Brd4 or related factors from the promoters/genes are the primary effects of the MDA-induced inhibition of NFκB-dependent pro-inflammatory target gene expression. While the inhibition of the CAM synthesis after extended treatment with PT is clearly the result of the elevated JNK activity, as seen by the sensitivity of the CAM mRNA levels to JNK inhibition, the mRNA levels could not be recovered upon inhibition of JNK and short treatment with PT. Due to that it is evident that the inhibition of the CAM synthesis after short treatment is based on a different mechanism. Under baseline conditions, the majority of the nuclear pTEFb is sequestered by association with HEXIM1 and a 7SK small nuclear RNA, thereby keeping it in an inactive state [192]. Upon the induction of cell stress, like present after depolymerization of the microtubule cytoskeleton, phosphatases enter the nucleus of cells, where they dephosphorylate CDK9 in the pTEFb:HEXIM1:7SK complex leading to the dissociation of the complex and the release of the sequestered pTEFb [406, 407]. However, Ouchida *et al.* (2003) [408] have shown that HEXIM1 itself can repress the transcriptional activity of NFκB by binding to the promoter bound NFκB, thereby inhibiting the association with transcriptional coactivators like p300. Thus, it might be possible that the initial and JNK-independent decrease in *icam-1* and *vcam-1* expression is due to a cell stress-induced repressional activity of the released HEXIM-1 (Fig. 68). Further studies are needed to clarify if HEXIM1 plays a role in the mechanism of repression of the CAMs after short treatment with depolymerizing MTAs.

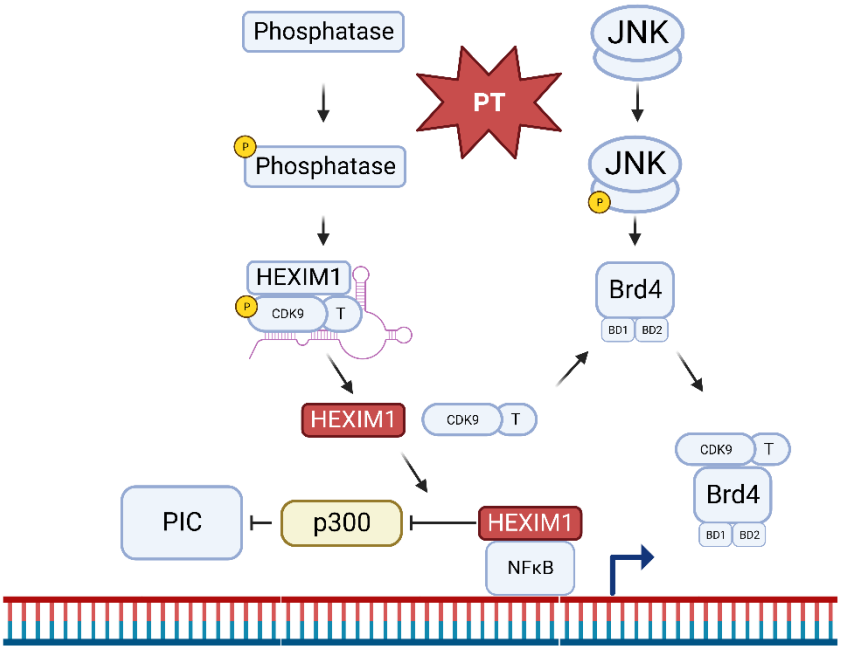

Figure 68. Potential mechanism for the effect of short time treatment with PT. Cell stress induced by microtubule depolymerization leads to the activation of phosphatases. Several phosphatases have been shown to dephosphorylate CDK9 in the pTEFb:HEXIM1:7SK RNA complex under conditions of cellular stress. Dephosphorylation of CDK9 induces the dissociation of the inhibitory complex and releases inactive CDK9 and HEXIM1, which might bind to NFκB and prevents association with transcriptional co-activators like p300, thus preventing proper formation of the PIC. PT treatment leads to activation of JNK, which might initially induce the interaction of Brd4 with CDK9 and enrichment at the stalling region. However, due to the improper formation of the PIC, transcription is reduced.

4.5 The effects of PT on the recruitment and activity of the Pol II at target genes

Treatment with PT interestingly led to a time-dependent and differential recruitment of Pol II to the promoters/genes of the CAMs. While the TNF-induced recruitment of Pol II was moderately reduced after short-treatment, it increased again after mean treatment times and approached the level of the TNF control. Extended treatment led to a significant reduction of Pol II at the CAM promoters and genes. This behavior might resemble the dual mechanism of PT after short and extended treatment. In case the effects observed after short treatment are induced by transcriptional repression of NFκB due to HEXIM1, it is likely that HEXIM1 reduces the transcriptional activity of NFκB by inhibiting association with transcriptional co-activators and hence impairs the formation of the PIC. This is also implied by the fact that the promoter exit of the Pol II appeared to not be inhibited by PT, since the enrichment of the Pol II at the promoters and the respective stalling sites was not differentially influenced. However, like already stated, the close proximity of both sites together with the given length of the chromatin fragments of up to 600 bp length makes analysis of stalling difficult. In addition, stalled polymerase has also been shown to back-track to the promoter region [409, 410]. The fact that the Pol II enrichment was only marginally influenced after mean treatment times with PT might correlate with the time-dependent loss of the activity of HEXIM1, which could increase the Pol II recruitment after these treatment times. After extended treatment, comparison of the Brd4 enrichment with the Pol II enrichment and the presence of the repressive H3K9me3 histone marks clearly shows that the loss of Brd4 omits the formation of an transcriptionally active histone environment, at least in case of the *vcam-1* gene. The fact that Brd4 recruits pTEFb and that pTEFb is responsible for the release of the stalled Pol II by phosphorylation of Pol II, NELF and DSIF makes it possible that stalling occurs. Proteomics approaches have also indicated a differential phosphorylation behavior concerning NELF subunits following treatment with nocodazole [411], but the physiological implications remains largely unclear. Studies concerning the stalling behavior of Pol II have shown that increased stalling reduces the recruitment of Pol II to the promoters of target genes and is also correlated with proteasome-based degradation of the stalled Pol II via ubiquitination of the Pol II Rbp1 subunit, which constitutes the catalytic center of Pol II [412–416]. Studies in yeast have correlated the E3 ubiquitin-ligase activity of elongin with poly-ubiquitination of the stalled Pol II [417]. In this study, knock-out of elongin inhibited the UV-light induced poly-ubiquitination and degradation of the Rbp1 subunit of Pol II. Based on this, it is also possible that PT increases stalling over time (represented by the again increased enrichment after 6 h of PT treatment) but leads to ubiquitination and degradation of the stalled Pol II, which is represented by the strongly decreased enrichment after extended treatment. Additional studies are needed to clarify if MTA treatment induces increased stalling of the Pol II or if different factors are involved in the time-dependent and differential recruitment of the Pol II.

4.6 Brd4 has a different functionality at the genes of ICAM-1 and VCAM-1

Analysis of the dependency of the association of Brd4 with the CAM genes on JNK activity clearly showed that Brd4 is negatively regulated by JNK. The increased JNK activity after PT treatment also induced the degradation of Brd4, which could be recovered by JNK inhibition. However, analysis of the time-dependent enrichment of Brd4 showed a much stronger decrease in case of *vcam-1* after extended PT treatment. In addition, the knock-down of Brd4 evoked increased ICAM-1 cell surface levels, but led to the expected reduction of the VCAM-1 levels in HUVECs. This clearly shows that Brd4 has a different functionality at both CAM genes. Earlier studies by Song *et al.* (2020) [405] have already demonstrated that Brd4 can either have an inductive or repressive function depending on the target gene. However, in this study, Song *et al.* have shown that for Brd4-repressed genes, knock-down of Brd4 still leads to a reduced recruitment of pTEFb to target genes, but does not influence the transcriptional activity of Pol II. This suggests the involvement of additional factors that confer transcriptional activation in Brd4-repressed genes. However, since the PT-induced inhibition of both CAMs after extended treatment with PT is sensitive to the activity of JNK, it is clear that these potential additional factors also react to increased JNK activity. This is also evident by the fact that for both genes, *icam-1* and *vcam-1*, extended PT treatment led to increased levels of the repressive H3K9me3 marks. Comparison of mRNA levels of the genes of cJun, cFos, IRF-1 and IκBα after different pre-stimulation times also demonstrated that different genes react differentially to PT treatment. While the fast-response genes *cjun* and *cfos* were highly induced after short treatment, the *irf-1* and *iκbα* genes were affected similar to the CAM genes, which in turn led to reduced nuclear levels of IRF-1 after short treatment, but likely also increased levels of IκBα after longer treatment times.

4.7 The effects of the PT-induced JNK activity on the functionality of Brd4

PT initially increased the association of Brd4 with target genes after short treatment with PT and led to a time dependent decrease in the association of Brd4 with the target genes. In addition, PT also slightly increased the degradation of Brd4, which could be reversed by JNK inhibition. By employing deletion studies, *Nishiyama et al.* (2006) [404] could show that the release of Brd4 from chromosomes after microtubule depolymerization is based on modification of residues in the C-terminal domain of Brd4, because mutants with deleted C-terminal domain were insensitive to microtubule depolymerization. The C-terminal domain of Brd4 is also implied in interaction with pTEFb and the RNA polymerase II [407, 418, 419]. Several studies, including this one, show that the initial JNK activation (by UV-light, Song *et al.* (2020) [405] or microtubule depolymerization, this study) likely induces the association of Brd4 with target genes. After extended treatment, the increased JNK activity appears to switch to a negative regulation of Brd4 and target gene association. This behavior is very similar to the mechanism underlying cJun activity, which is initially induced by JNK, but deactivated upon extended JNK activity, which also induces the degradation of cJun. The MAPKs, including JNK are proline-directed kinases, which target Ser/Thr residues that are followed by a proline [420]. JNK thereby binds the so called D-motif in its targets, i.e. in cJun, by binding this motif via its docking groove. The D-motifs are short and linear peptide sequences that are approx. 9 to 18 amino acids long and usually located on the N-terminus of the proteins [421]. However, the Brd4 sequence does not contain a motif similar to the D-motif of cJun. In addition, no direct interaction between JNK and Brd4 could be shown to this day. A general motif search concerning potential phosphorylation sites in the Brd4 sequence primarily results in potential phosphorylation sites for the casein kinase II and the protein kinase C, none of which are implied for being targeted by JNK. However, JNK has been shown to phosphorylate and activate the E3 ubiquitin ligase Itch, which is also implied in cJun turnover [422–425]. Itch has been shown to bind to proline-rich regions in target proteins that contain either of the proline-rich PPXY or PPLP consensus sequences in proteins via its WW (TrpTrp) domain and induce their ubiquitination and hence degradation [426–431]. In fact, Brd4 contains a proline-rich region in its C-terminal domain, which also harbors a PPLP motif (Fig. 69). The presence of the PPLP motif in the proline-rich region implies that Brd4 could be a target of the E3 ubiquitin ligase Itch. Hence, it is possible that the extended JNK activity upon PT treatment induces the activity of this ubiquitin ligase, which in turn ubiquitinates Brd4 to target it for proteasomal degradation. This explanation fits well to the fact that treatment with PT led to decreased protein levels of Brd4, which could be reversed by inhibition of JNK.

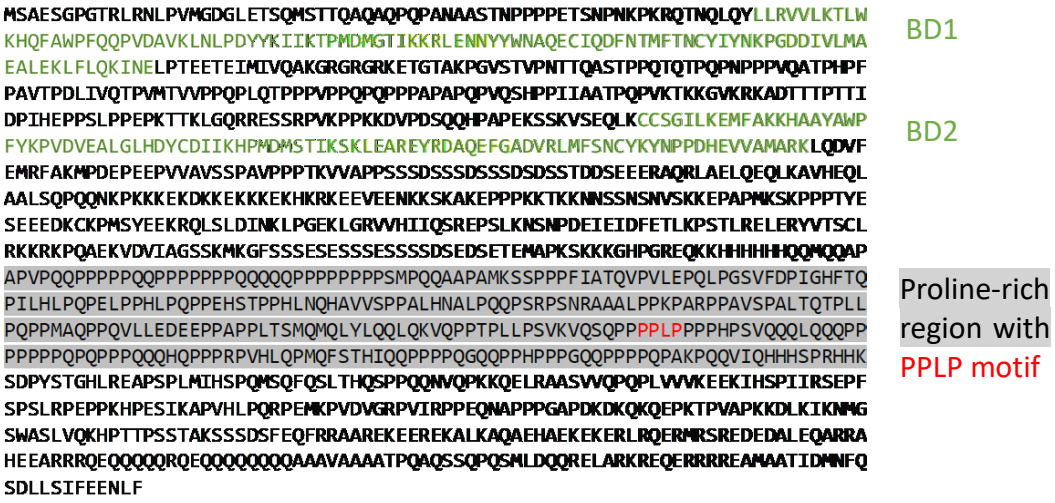

Figure 69. Brd4 contains a proline-rich region and a PPLP motif. The amino acid sequence of human Brd4 (O60885, BRD4_HUMAN) obtained from UniProt. The positions of the bromodomains (BD1 and BD2) in the N-terminal region of Brd4 (based on the Pfam search for known protein domains) and the proline-rich region in the C-terminus of the protein with the PPLP motif implied in binding of the E3 ubiquitin ligase Itch.

4.8 PT has differing effects concerning the CAM inhibition

Treatment with PT led to a clear reduction of the expression of the genes of E-selectin, ICAM-1 and VCAM-1. Based on the deregulation of Brd4 by the elevated JNK activity and the likely differing functionality of Brd4 at the CAM genes, it is difficult to analyze the influence of the differential transcription factor activity in regards to the actions of Brd4 and the resulting CAM expression. However, the fact that the PT-induced effects on the mRNA levels of the CAMs ICAM-1 and E-selectin could be reversed by inhibition of JNK to the levels of the JNKIN8-treated TNF controls, indicates that for these genes the JNK activity-induced eviction of Brd4 is likely the main reason for the PT-induced inhibition of ICAM-1 and E-selectin. In case of VCAM-1, the respective mRNA levels could only partially be reversed, indicating the influence of additional factors that contribute to the decreased VCAM-1 expression. Neish *et al.* (1995) [170] have demonstrated that IRF-1 has a crucial function in the expression of VCAM-1, with VCAM-1 reporter constructs being highly sensitive to the presence of IRF-1. In addition, IRF-1 has also been shown to directly interact with NFκB, which is also a prerequisite to enable full VCAM-1 expression [170, 432, 433]. Application of PT for durations that exceed the treatment times tested in this project will likely influence the expression of numerous transcription factors that are sensitive to the activity of NFκB and Brd4. However, in the scope of the treatment times tested in this project, treatment with PT induced a strong decrease in the TNF-induced IRF-1 mRNA and protein levels. It is likely that the decreased IRF-1 protein levels are partially responsible for the strong decrease in VCAM-1 expression due to PT.

4.9 The feasibility of the usage of PT in the treatment of inflammatory diseases

Based on their effects on the microtubule cytoskeleton, MTAs are largely known for their usage as chemotherapeutics. Application of MTAs in inflammatory diseases has been largely limited to COL. COL has been shown to be effective in the treatment of acute gout and acute calcium pyrophosphate crystal arthritis [434, 435], familial Mediterranean fever by inhibiting the inflammasome and reducing the frequency of fever attacks and the risk of amyloid renal failure [436–438] and Behçet's disease by significantly reducing the formation of different forms of aphthae or arthritis [353, 439, 440]. Additional studies have shown the effectiveness of COL in chronic cutaneous vasculitis, as well as initial and recurrent pericarditis [356, 441–446]. Newer clinical studies have also proven the effects of COL in treatment of stable coronary diseases by reducing cardiac arrest, acute coronary symptoms and myocardial infarction [447–449]. Just recently, COL has been shown to reduce the formation of plaques during atherosclerosis, which is connected to reduced leukocyte migration in cells of the aortic endothelium [330]. Testing of the concentration of COL in the plasma and in leukocytes have shown that colchicine is enriched in leukocytes [342]. It is likely, that the enrichment of COL in leukocytes significantly increases the effectiveness of COL on the migration and hence, infiltration of leukocyte during chronic inflammatory diseases. For PT, it is not known if leukocyte enrichment occurs. Based on this, it is not clear if PT has the same effects on the chemotactic migration of leukocytes over time. However, the comparison of the induction of JNK after short treatment with PT and COL showed that PT induces the activity of JNK much faster. This suggests the possibility that PT might be applicable at lower concentrations compared to COL while retaining the same efficacy, which might in turn reduce the adverse effects that are known to occur after treatment with MTAs. If PT does not lead to systemic inhibition of leukocyte migration, it might be applicable in a more targeted way to exclusively inhibit leukocyte adhesion during the leukocyte adhesion cascade, while not generally reducing the systemic activity of all leukocytes. However, more research into the effects of PT on systemic pro-inflammatory events is necessary to analyze how PT influences the immune system in a global manner and especially, how effective PT is in reducing systemic inflammation at concentration that are tolerable for *in vivo* application.

5. Conclusion and outlook

In conclusion, this study demonstrates that PT and other destabilizing MTAs clearly have an anti-inflammatory potential concerning the vascular endothelium by inhibiting the synthesis of the crucial pro-inflammatory adhesion cascade components ICAM-1 and VCAM-1. This, in turn, leads to reduced leukocyte adhesion to the endothelium. In addition, this study showed that the inhibition of CAM synthesis is the direct consequence of the microtubule depolymerization and the resulting activation of JNK and that this negatively regulates the association of Brd4 with target genes. Especially for the Brd4-induced *vcam-1* gene, the eviction of Brd4 leads to transcriptional repression. However, the JNK-dependent inhibition of the Brd4-repressed *icam-1* gene suggests the involvement of additional factors that confer transcriptional activation. Future studies should clarify the identity and role of these factors and how these factors react to the MTA-induced JNK activity, leading to inhibition of Brd4-repressed genes like *icam-1*. Several studies, including this one, show a dependency of the functionality of Brd4 on JNK activity. However, the molecular interactions leading to this dependency are unknown. Future studies should clarify if there is a direct interaction between JNK and Brd4, if this dependency is conveyed via additional factors downstream of JNK activity or if Brd4 is a target of the E3 ubiquitin ligase Itch and also, if this might have implications for the functionality of Brd4. In general, the time-dependent deregulation of the activity of Brd4 upon PT treatment suggests an influence on transcriptional events on a genome-wide scale. Future studies should analyze how depolymerizing MTAs influence the transcriptome of cells over time and in dependency of Brd4. Analysis of the mRNA transcriptome and comparison with Brd4 ChIP-coupled DNA-sequencing might reveal how MTAs influence the expression of Brd4-induced and -repressed target genes. In addition, further studies should tackle the pharmacokinetic properties of PT and other MTAs in comparison to COL, which is known to be enriched in leukocytes but appears to have a lower efficacy concerning the activation of JNK over time.

6. Summary

Chronic inflammatory diseases and the resulting morbidities belong to the leading causes of early death in humans. One of the main factors leading to the deterioration of health in patients with chronic inflammatory diseases is the pathological infiltration of leukocytes in healthy tissues, which leads to tissue damage and the propagation of sickness. The vascular endothelium, which lines the inside of the blood vessels, plays a crucial role in the inflammatory response, because it acts as an interface for interaction with leukocyte in order to enable leukocyte extravasation from the blood stream into the tissues. The adhesion of leukocytes to the cells of the endothelium during the leukocyte adhesion cascade are thereby mainly enabled *via* the cytokine-induced pro-inflammatory NFκB and AP-1 signaling cascades, which induce the upregulation of the main endothelial cell adhesion molecules ICAM-1, VCAM-1 and E-selectin. One of the most important pro-inflammatory cytokines is TNF, which induces the inflammatory state in cells by binding to the TNF receptor, leading to the activation of the before mentioned intracellular NFκB and AP-1 signaling cascades. A class of agents that are known for their anti-inflammatory properties and benefits in the treatment of chronic inflammatory diseases are the microtubule-targeting agents, which have been shown to also influence the inflammatory state in cells of the endothelium and the leukocyte adhesion cascade. Microtubule-targeting agents can be subdivided into microtubule destabilizers, which induce depolymerization of the microtubule cytoskeleton, and microtubule stabilizers, which impede the depolymerization of the microtubules. However, the underlying biomolecular events and effects exerted by microtubule-targeting agents on the cells of the vascular endothelium, and mechanisms how they affect the leukocyte adhesion cascade are largely unknown.

This study aimed at elucidating the effects of the novel microtubule-destabilizing agent pretubulysin, a precursor of the tubulysins inititally discovered in strains of the myxobacterium *Angiococcus disciformis* and the already clinically established microtubule-destabilizing agents colchicine, vincristine as well as the microtubule-stabilizer paclitaxel on the inflammatory processes that enable the leukocyte adhesion in TNF-activated human umbilical vein endothelial cells.

The anti-inflammatory potential of pretubulysin was first tested *in vivo* in an imiquimod-induced psoriasiform dermatitis mouse model. Compared to the control animals, treatment with pretubulysin significantly reduced the thickness as well as redness of the psoriasiform dermatitis lesions on the murine skin, showing that pretubulysin decreases the inflammatory state. To prove that this anti-inflammatory function is related to a decreased interaction of leukocytes with the endothelium, pretubulysin was tested *in vivo* by intravital microscopy of the TNF-activated mouse cremaster muscle. Treatment with pretubulysin led to a significantly decreased adhesion of leukocytes to the murine vascular endothelium, while slightly increasing the rolling flux of the leukocytes. In addition, treatment with pretubulysin significantly reduced the transmigration of the leukocytes through the endothelial cell layer and hence the leukocyte extravasation. The decreased leukocyte adhesion to endothelial cells due to pretubulysin was also confirmed in the *in vitro* setting by testing the adhesion of monocytic THP-1

cells under flow conditions. In this assay, treatment of TNF-activated human umbilical vein endothelial cell monolayers with pretubulysin led to a significant reduction of the THP-1 cell adhesion.

By utilizing flow cytometry, it could be shown that treatment of human umbilical vein endothelial cells with pretubulysin led to a concentration-dependent and significant inhibition of the TNF-induced cell surface levels of the main cell adhesion molecules ICAM-1 and VCAM-1, while the E-selectin levels remained largely unchanged. The effects of pretubulysin where comparable to those of the microtubule-destabilizers vincristine and colchicine and could also be confirmed in cells of the human dermal microvascular endothelial cell line 1. Treatment of human umbilical vein endothelial cells with the microtubule-stabilizer paclitaxel did not negatively influence the cell surface levels of ICAM-1 and VCAM-1. Instead, treatment with paclitaxel induced the cell surface levels to an even greater extent than TNF at the same concentrations that led to the aforementioned inhibition. This shows that paclitaxel has no anti-inflammatory potential in endothelial cells concerning the leukocyte adhesion cascade.

In addition, the influence of the microtubule-targeting agents on the total protein and mRNA levels of the cell adhesion molecules ICAM-1, VCAM-1 and E-selectin were tested by western blot and qRT-PCR analysis in human umbilical vein endothelial cells. Pretubulysin, vincristine and colchicine significantly reduced the total protein and mRNA levels of ICAM-1 and led to an almost full inhibition of the VCAM-1 total protein and mRNA levels. In contrast, treatment with paclitaxel had no discernible influence on the ICAM-1 and VCAM-1 total protein levels and only slightly reduced the respective mRNA levels. In case of E-selectin, all compounds reduced the total protein levels in an even manner, but only the microtubule-destabilizers led to a clear reduction of the mRNA levels, while paclitaxel again exhibited only a very slight reducing effect.

To exclude the possibility that any of these effects are based on cytotoxicity, the microtubule-targeting agents were also tested in cytotoxicity assays in human umbilical vein endothelial cells. Neither of the compounds had any significant negative effects on the metabolic activity, membrane integrity or cell viability. In addition, testing of the influence of pretubulysin and the other microtubule-targeting agents on the total *de novo* protein synthesis showed that the microtubule-destabilizers increased the total protein synthesis, while paclitaxel had no effect.

Testing of the influence of pretubulysin on the total TNF-receptor 1 levels by western blot analysis showed that the levels of this receptor remained stable after short and extended treatment periods with pretubulysin. Subsequent western blot analysis of the activity and protein levels of the TNF-induced NFκB-activating kinase IKK revealed that pretubulysin increases the phosphorylation and hence activity of this kinase at all tested treatment times, which also lead to increased IκBα degradation after short treatment times with pretubulysin. Further western blot analysis of cell fractions showed that the nuclear levels of NFκB-p65 were not influenced by pretubulysin after short and mean treatment times but led to a moderate reduction of the cytoplasmic and nuclear NFκB-p65 protein levels after extended treatment. The TNF-induced promoter activity of NFκB was tested by a reporter gene assay at times when the

NFκB-p65 levels were not influenced by pretubulysin. Treatment with pretubulysin decreased the promoter activity of NFκB significantly. Only treatment with vincristine led to results comparable to pretubulysin, with colchicine significantly reducing the promoter activity only at high concentration and paclitaxel having only a very slight negative influence. Wwestern blot analysis of the NFκB-p65 phosporylation levels at serine 468 and serine 536, which have been implied in decreasing the transactivatory potential and stability of NFκB-p65, showed that the respective phosphorylation levels remained largely unaffected.

Concerning the activity of the AP-1-inducing kinase JNK, western blot analysis revealed a strong increase in phosphorylation of this kinase after treatment with pretubulysin and also vincristine after short treatment, with colchicine having only very minor effects and paclitaxel having no influence on JNK phosphorylation. Only after prolonged treatment did colchicine induce the JNK activity comparable to pretubulysin and vincristine. However, extended treatment with paclitaxel also induced an increase in phosphorylation compared to the TNF control. Further western blot analysis of the AP-1-cJun protein levels showed that treatment with pretubulysin increased the protein levels of this transcription factor, which could also be traced back to increased mRNA levels of cJun, as shown by qRT-PCR analysis. Interestingly, treatment with pretubulysin induced an apparent and likely phosphorylation-dependent electromobility shift of cJun in the western blot analysis. Reporter gene analysis of the promoter activity of cJun showed that all microtubule-targeting agents decreased the promoter activity of AP-1, but treatment with the microtubule-destabilizers led to stronger effects compared to paclitaxel. Investigation of the inhibitory serine 243 phosphorylation of cJun by western blot analysis revealed that the phosphorylation levels were increased upon treatment with pretubulysin, which might in part also correlate to increased nuclear levels of GSK3β. While the cytoplasmic activity of the MAPK ERK was reduced upon treatment with pretubulysin, as shown by western blot analysis of cell fractions, the nuclear protein levels of this kinase were reduced, implying increased degradation. In addition, treatment with pretubulysin appeared to increase the translocation of the MAPK p38 into the nucleus of human umbilical vein endothelial cells but led to decreased activatory phosphorylation levels in the nuclear fraction, while increasing the phosphorylation levels in the cytoplasmic fraction. Due to the involvement of the p38 kinase in the regulation of the activity of RNA-binding protein, which regulate the stability of mRNAs, the VCAM-1 mRNA decay was tested upon treatment with the microtubule-targeting agents by qRT-PCR analysis. This revealed that treatment with the microtubule-destabilizers increased the half-life of the VCAM-1 mRNA, while treatment with paclitaxel led to a slight decrease.

Testing of the TNF-induced enrichment of NFκB-p65 in the promoters of *icam-1*, *vcam-1* and *e-sele* by chromatin-immunoprecipitation showed that pretubulysin induced the enrichment of this transcription factor at all three genes upon short treatment and only led to a significant reduction of the p65 levels at the promoter of *vcam-1* upon extended treatment. In comparison AP-1-cJun was enriched at the promoters of the cell adhesion molecules at all tested treatment times. Due to the fact that the enrichment

of NFκB-p65 and AP-1-cJun was largely not decreased by pretubulysin, the TNF-induced enrichment of the RNA polymerase II at the promoters of the cell adhesion molecules was also tested by chomatin-immunoprecipitation over time. This showed that pretubulysin moderately reduced the RNA polymerase II enrichment at all three cell adhesion molecule genes at short treatment times. These effects were largely lost at mean treatment times, but significantly increased after prolonged treatment periods with pretubulysin. Examination of the mRNA levels of the cell adhesion molecules in dependency of the pre-treatment time with pretubulysin by qRT-PCR analysis showed a comparable reduction of the respective mRNA levels after short pre-treatment, a significant induction of the mRNA levels at mean pre-treatment times, but a full repression of the mRNA levels after extended pre-treatment.

Due to the strong activation of JNK upon treatment with pretubulysin, the decreased cell adhesion molecule mRNA levels at short and extended treatment times were tested towards the sensitivity on the activity of JNK by utilizing a JNK inhibitor. Inhibition of JNK could partially reverse the effects on the cell adhesion molecule mRNA levels after extended treatment periods but had no effect concerning the decreased mRNA levels after short treatment with pretubulysin. In addition, flow cytometric analysis revealed that inhibition of JNK could also partially reverse the effects on the cell surface levels of ICAM-1 and VCAM-1.

Subsequent examination of the enrichment of the bromodomain-containing protein 4, responsible for recruiting the positive transcription elongation factor b that induces the release of stalled RNA polymerase II in genes, revealed that treatment with pretubulysin increased the enrichment of this factor around the RNA polymerase stalling site in the genes of ICAM-1 and VCAM-1 at short treatment times. However, extended treatment with pretubulysin induced a decrease of the enrichment of the bromodomain-containing protein 4, which was more pronounced in the case of the *vcam-1* gene. Investigation into the dependency of the *icam-1* and *vcam-1* gene enrichment of the bromodomain-containing protein 4 on the activity of JNK showed that inhibition of JNK significantly increased the enrichment of this factor, suggesting that the bromodomain-containing protein 4 is negatively regulated by JNK activity. In addition, western blot analysis revealed that treatment with pretubulysin led to decreased levels of the bromodomain-containing protein 4, which could also be reversed by JNK inhibition. This showed that treatment with pretubulysin induced increased and JNK-dependent degradation of this factor. Further examination into the dependency of the ICAM-1 and VCAM-1 cell surface levels on the bromodomain-containing protein 4 by knock-down experiments revealed that the *vcam-1* gene is positively regulated by this factor, while the *icam-1* gene was negatively regulated, as shown by decreased VCAM-1 and increased ICAM-1 cell surface levels upon knock-down. Nevertheless, chromatin-immunoprecipitation experiments showed that in case of both genes, extended treatment with pretubulysin increased the enrichment of repressive histone-3 lysine-9 trimethylation marks. This implies the presence of additional factors that confer the transcriptional repression of the *icam-1* genes upon treatment with pretubulysin, which are also negatively regulated by the increased JNK activity. Figure 70 summarizes the main results for the *in vitro* experiments performed in this study.

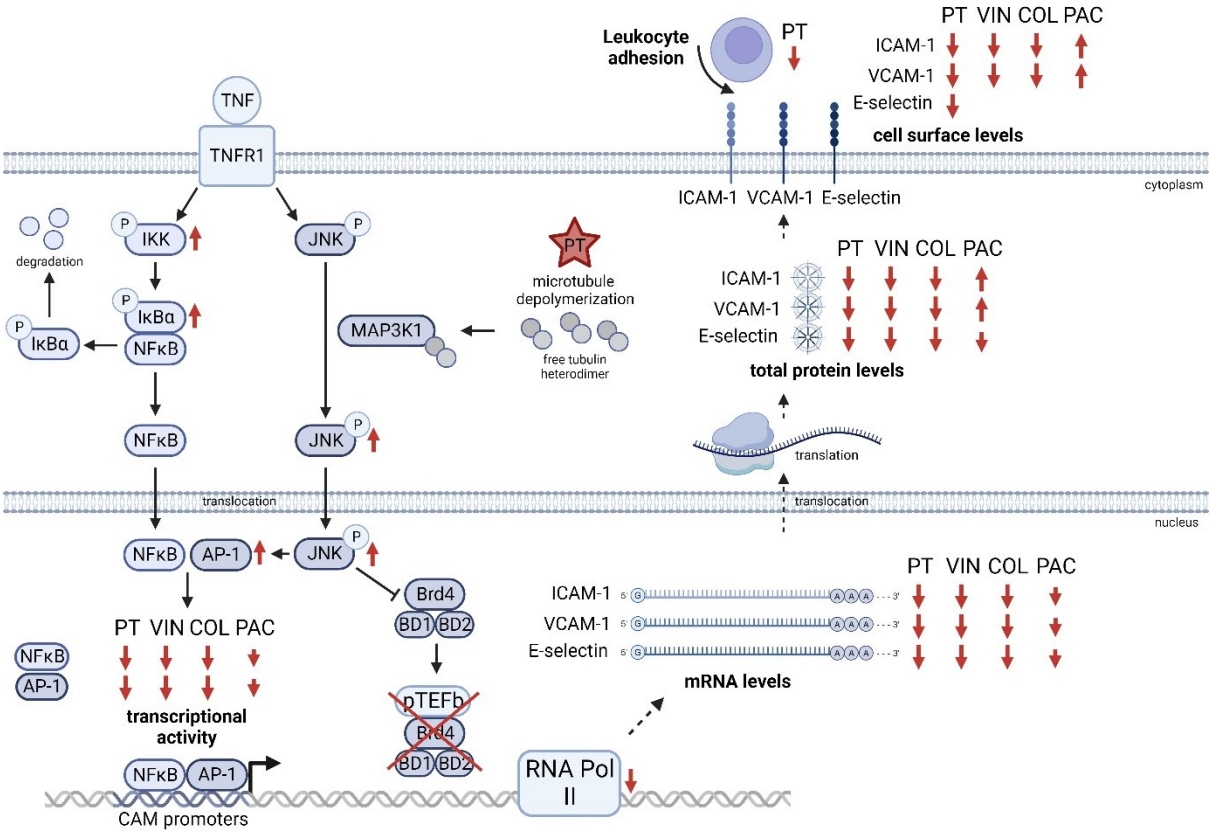

Figure 70. Graphical summary for the effects of pretubulysin (PT) (and vincristine, colchicine and paclitaxel) on inflammatory processes in endothelial cells (after treatment with 300 nM; decrease or increase in relation to the respective TNF control). Association of TNF with the TNF receptor leads to signal integration and intracellular activation of the IKK kinase in the NFκB pathway, as well as the c-Jun-N-terminal kinase (JNK) of the AP-1 activating pathway. Treatment with PT increased the phosphorylation and hence activation of IKK and the downstream degradation of IκBα, which sequesters NFκB in the cytosol, leading to the release of NFκB and subsequent translocation into the nucleus of the cells. PT-evoked microtubule depolymerization increases the concentration of soluble tubulin heterodimers. The increased cytosolic concentration of tubulin activates the tier 3 JNK upstream MAP kinase MAP3K, which has been shown to be activated upon binding of soluble tubulin. The increased MAP3K1 activity significantly induces the activity of JNK. The strongly activated JNK activates cJun in the AP-1 transcription factor, leading to the autoinduction of cJun transcription by activated cJun, increasing the cJun protein levels. NFκB and AP-1 both bind to the promoters of the cell adhesion molecules (CAMs), however the transcriptional activity of both factors is significantly reduced after treatment with the destabilizing microtubule-targeting agents (MTAs). TNF stimulation induces association of the bromodomain-containing protein 4 (Brd4,which contains two bromodomains, BD1 and BD2) with the positive transcription elongation factor b (pTEFb) in order to release the stalled RNA polymerase II in the non-translated regions downstream of the transcription start sites of the CAM promoters. The increased JNK activity upon PT was shown to negatively regulate the association of Brd4 with chromatin, likely preventing the proper formation of the pTEFb:Brd4 complex necessary for release of stalled RNA polymerase II. Additionally, treatment with PT also reduces the levels of the RNA polymerase in the promoters and stalling regions of the CAMs. The effects of the depolymerizing MTA resulted in decreased expression of CAM mRNA and total CAM protein levels as well as cell surface levels, which also led to reduce leukocyte adhesion to the endothelial cells.

7. Zusammenfassung

Chronische Entzündungen und die daraus resultierenden Morbiditäten gehören zu den häufigsten Ursachen für einen frühen Tod beim Menschen. Einer der Hauptfaktoren für die Verschlechterung des Gesundheitszustands bei Patienten mit chronischen-entzündlichen Erkrankungen ist die pathologische Infiltration von Leukozyten in gesundes Gewebe, die zu Gewebeschäden und dem Fortschreiten der Krankheit führt. Das vaskuläre Endothel, das die Innenseite der Blutgefäße auskleidet, spielt eine entscheidende Rolle bei der Entzündungsreaktion, da es als Schnittstelle für die Interaktion mit Leukozyten fungiert, um die Extravasation von Leukozyten aus dem Blutstrom in das Gewebe zu ermöglichen. Die Adhäsion von Leukozyten an die Zellen des Endothels während der Leukozyten-Adhäsionskaskade wird dabei hauptsächlich durch die Zytokin-induzierten pro-inflammatorischen NFκB- und AP-1-Signalkaskaden ermöglicht, die die Hochregulierung der wichtigsten endothelialen Adhäsionsmoleküle – ICAM-1, VCAM-1 und E-Selektin – bewirken. Eines der wichtigsten pro-inflammatorischen Zytokine ist TNF, das durch Bindung an den TNF-Rezeptor einen Entzündungszustand in den Zellen auslöst, der zur Aktivierung der zuvor erwähnten intrazellulären NFκB- und AP-1-Signalkaskaden führt. Eine Klasse von Wirkstoffen, die für ihre entzündungshemmenden Eigenschaften und ihren Nutzen bei der Behandlung chronischer Entzündungskrankheiten bekannt sind, sind die Mikrotubuli-bindenden Substanzen (microtubule-targeting agents, MTAs), die nachweislich auch den Entzündungszustand in Zellen des Endothels und die Leukozyten-Adhäsionskaskade beeinflussen können. MTAs lassen sich in Mikrotubuli-Destabilisatoren, die eine Depolymerisation des Mikrotubuli-Zytoskeletts bewirken, und Mikrotubuli-Stabilisatoren, die die Depolymerisation der Mikrotubuli verhindern, unterteilen. Die zugrundeliegenden biomolekularen Vorgänge und Wirkungen, die die MTAs auf die Zellen des Gefäßendothels haben, und wie MTAs die Adhäsionskaskade der Leukozyten beeinflussen, sind jedoch weitgehend unbekannt.

Ziel dieser Studie war es, die Auswirkungen des neuartigen Mikrotubuli-Destabilisators Prätubulysin, eines Vorläufers der Tubulysine, die ursprünglich in Stämmen des Myxobakteriums *Angiococcus disciformis* entdeckt wurden, auf die entzündlichen Prozesse zu untersuchen, die die Leukozyten-adhäsion in TNF-aktivierten primären Endothelzellen aus der menschlichen Nabelschnurvene (HUVECs) ermöglichen. Zusätzlich wurden auch die Auswirkungen der bereits klinisch etablierten Mikrotubuli-Destabilisatoren Colchicin und Vincristin sowie des Mikrotubuli-Stabilisators Paclitaxel untersucht.

Das entzündungshemmende Potenzial von Prätubulysin wurde zunächst *in vivo* in einem Imiquimod-induzierten psoriasiformen Dermatitis-Mausmodell getestet. Im Vergleich zu den Kontrolltieren verringerte die Behandlung mit Prätubulysin die Dicke sowie die Rötung der psoriasiformen Dermatitis-Läsionen auf der Mäusehaut signifikant. Dies zeigt, dass Prätubulysin den Entzündungszustand verringert. Um zu beweisen, dass der entzündungshemmende Effekt mit einer verringerten Interaktion von Leukozyten mit dem Endothel zusammenhängt, wurde die Wirkung von Prätubulysin *in vivo* mittels Intravitalmikroskopie des TNF-aktivierten Kremaster-Muskels der Maus untersucht: Die Behandlung

mit Prätubulysin führte zu einer signifikant verringerten Adhäsion von Leukozyten an das murine Gefäßendothel, während das sog. Rollen der Leukozyten leicht anstieg. Darüber hinaus verringerte die Behandlung mit Prätubulysin die Transmigration der Leukozyten durch die Endothelzellschicht und damit die Leukozytenextravasation erheblich. Die verringerte Adhäsion von Leukozyten an Endothelzellen durch Prätubulysin wurde auch *in vitro* bestätigt, indem die Adhäsion von monozytären THP-1-Zellen unter Flussbedingungen getestet wurde. In diesem Test führte die Behandlung einer TNF-aktivierten HUVEC-Schicht mit Prätubulysin zu einer signifikanten Verringerung der THP-1-Zelladhäsion.

Mittels Durchflusszytometrie konnte gezeigt werden, dass die Behandlung von HUVECs mit Prätubulysin zu einer konzentrationsabhängigen, signifikanten Hemmung der TNF-induzierten Zelloberflächenlevel der Zelladhäsionsmoleküle ICAM-1 und VCAM-1 führte, während die E-Selektin-Level weitgehend unbeeinflusst blieben. Die Wirkungen von Prätubulysin waren vergleichbar mit denen der Mikrotubuli-Destabilisatoren Vincristin und Colchicin und konnten auch in Zellen der humanen dermalen mikrovaskulären Endothelzelllinie HMEC-1 bestätigt werden. Die Behandlung von HUVECs mit dem Mikrotubuli-Stabilisator Paclitaxel hatte keinen negativen Einfluss auf die Zelloberflächenlevel von ICAM-1 und VCAM-1. Stattdessen induzierte die Behandlung mit Paclitaxel die Zelloberflächenlevel über die der TNF-Kontrolle hinaus bei denselben Konzentrationen, die zu der zuvor erwähnten Hemmung führten. Dies zeigt, dass Paclitaxel kein entzündungshemmendes Potenzial in Endothelzellen im Hinblick auf die Leukozyten-Adhäsionskaskade hat.

Darüber hinaus wurde der Einfluss der MTAs auf die Gesamtprotein- und mRNA-Levels der Zelladhäsionsmoleküle ICAM-1, VCAM-1 und E-Selektin mittels Western Blot und qRT-PCR-Analyse in HUVECs untersucht. Prätubulysin, Vincristin und Colchicin verringerten die Gesamtprotein- und mRNA-Level von ICAM-1 signifikant und führten zu einer nahezu vollständigen Hemmung der VCAM-1-Gesamtprotein und -mRNA-Level. Im Gegensatz dazu hatte die Behandlung mit Paclitaxel keinen erkennbaren Einfluss auf die ICAM-1- und VCAM-1-Gesamtproteinlevels und reduzierte die jeweiligen mRNA-Level nur geringfügig. Im Fall von E-Selektin verringerten alle MTAs die Gesamtproteinlevel gleichmäßig, aber nur die Mikrotubuli-Destabilisatoren führten zu einer deutlichen Verringerung der mRNA-Level, während Paclitaxel nur einen sehr geringen reduzierenden Effekt zeigte.

Um auszuschließen, dass diese Effekte durch Zytotoxizität beeinflusst werden, wurden die MTAs in Zytotoxizitätstests HUVECs getestet. Keiner der Wirkstoffe hatte signifikante, negative Auswirkungen auf die Stoffwechselaktivität, die Membranintegrität oder die Viabilität der Zellen. Die Prüfung des Einflusses von Prätubulysin und der anderen MTAs auf die gesamte De-novo-Proteinsynthese ergab, dass die Mikrotubuli-Destabilisatoren die Proteinsynthese erhöhten, während Paclitaxel keine Wirkung zeigte.

Die Prüfung des Einflusses von Prätubulysin auf die Gesamtproteinlevel des TNF-Rezeptors 1 mittels Western-Blot-Analyse ergab, dass die Proteinmenge dieses Rezeptors nach kurzer und längerer Behandlung mit Prätubulysin stabil blieb. Eine anschließende Western-Blot-Analyse der Aktivität und der Proteinlevel der TNF-induzierten NFκB-aktivierenden Kinase IKK ergab, dass Prätubulysin die Phosphorylierung und damit die Aktivität dieser Kinase bei allen getesteten Behandlungszeiten erhöhte, was auch zu einem erhöhten IκBα-Abbau nach kurzen Behandlungszeiten mit Prätubulysin führte. Weitere Western-Blot-Analysen von Zellfraktionen zeigten, dass die nukleären Proteinlevel von NFκB-p65 nach kurzen und mittleren Behandlungszeiten durch Prätubulysin nicht beeinflusst wurden, nach längerer Behandlung jedoch zu einer moderaten Verringerung der zytoplasmatischen und nukleären NFκB-p65-Proteinlevel führten. Die TNF-induzierte Promotoraktivität von NFκB wurde mit einem Reportergen-Assay zu Zeiten getestet, in denen die NFκB-p65 Levels nicht durch Prätubulysin beeinflusst wurden. Die Behandlung mit Prätubulysin verringerte die Promotoraktivität von NFκB signifikant. Nur die Behandlung mit Vincristin führte zu Ergebnissen, die mit denen von Prätubulysin vergleichbar waren, während Colchicin die Promotoraktivität nur bei hoher Konzentration signifikant verringerte und Paclitaxel nur einen sehr geringen negativen Einfluss hatte. Die Western-Blot-Analyse der NFκB-p65-Phosphorylierungs an Serin 468 und Serin 536, von denen man annimmt, dass sie das transaktivierende Potenzial und die Stabilität von NFκB-p65 verringern, ergab, dass beide Phosphorylierungsniveaus weitgehend unbeeinflusst blieben.

Was die Aktivität der AP-1-induzierenden Kinase JNK anbelangt, so ergab die Western-Blot-Analyse einen starken Anstieg der Phosphorylierung dieser Kinase nach einer kurzen Behandlung mit Prätubulysin und auch mit Vincristin, wobei Colchicin nur sehr geringe Auswirkungen hatte und Paclitaxel keinen Einfluss auf die JNK-Phosphorylierung zeigte. Erst nach längerer Behandlung induzierte Colchicin eine JNK-Aktivität, die mit der von Prätubulysin und Vincristin vergleichbar war. Eine verlängerte Behandlung mit Paclitaxel induzierte ebenfalls einen Anstieg der Phosphorylierung im Vergleich zur TNF-Kontrolle. Eine weitere Western-Blot-Analyse der AP-1-cJun-Proteinlevel zeigte, dass die Behandlung mit Prätubulysin die Proteinlevel dieses Transkriptionsfaktors erhöhte, was auch auf erhöhte mRNA-Level von cJun zurückgeführt werden konnte, wie eine qRT-PCR Analyse zeigte. Interessanterweise führte die Behandlung mit Prätubulysin zu einer offensichtlichen und wahrscheinlich phosphorylierungsabhängigen Verschiebung der Elektromobilität von cJun in der Western-Blot-Analyse. Die Reportergen-Analyse der Promotoraktivität von cJun zeigte, dass alle MTAs die Promotoraktivität von AP-1 verringerten; die Behandlung mit den Mikrotubuli-Destabilisatoren führte aber zu stärkeren Effekten im Vergleich zu Paclitaxel. Die Untersuchung der hemmenden Serin-243-Phosphorylierung von cJun durch Western-Blot-Analyse ergab, dass die Phosphorylierung nach Behandlung mit Prätubulysin verstärkt war, was zum Teil auch mit erhöhten nukleären Leveln der Kinase GSK3β korrelieren könnte. Während die zytoplasmatische Aktivität der MAPK ERK nach der Behandlung mit Prätubulysin reduziert war, wie die Western-Blot-Analyse von Zellfraktionen zeigte, waren die nukleären Proteinlevel dieser Kinase reduziert, was auf einen erhöhten Abbau schließen lässt.

Darüber hinaus schien die Behandlung mit Prätubulysin die Translokation der MAPK p38 in den Zellkern von HUVECs zu erhöhen, führte jedoch zu einem Rückgang der aktivierenden Phosphorylierung von p38 in der nukleären Fraktion, während das Phosphorylierungniveau in der Zytoplasmafraktion anstieg. Aufgrund der Beteiligung der p38-Kinase an der Regulierung der Aktivität von RNA-bindenden Proteinen, die die Stabilität von mRNAs regulieren, wurde der VCAM-1-mRNA-Zerfall nach Behandlung mit den MTAs durch qRT-PCR-Analyse getestet. Dabei zeigte sich, dass die Behandlung mit den Mikrotubuli-Destabilisatoren die Halbwertszeit der VCAM-1-mRNA erhöhte, während die Behandlung mit Paclitaxel zu einer leichten Abnahme führte.

Die Prüfung der TNF-induzierten Anreicherung von NFκB-p65 in den Promotoren von *icam-1*, *vcam-1* und *e-sele* durch Chromatin-Immunpräzipitation zeigte, dass Prätubulysin die Anreicherung dieses Transkriptionsfaktors an allen drei Genen bei kurzer Behandlung induzierte und nur bei längerer Behandlung zu einer signifikanten Verringerung der p65-Level am Promotor von *vcam-1* führte. Im Vergleich dazu war AP-1-cJun in den Promotoren der Zelladhäsionsmoleküle bei allen getesteten Behandlungszeiten angereichert. Da die Anreicherung von NFκB-p65 und AP-1-cJun durch Prätubulysin nicht wesentlich verringert wurde, wurde die TNF-induzierte Anreicherung der RNA-Polymerase II an den Promotoren der Zelladhäsionsmoleküle im Zeitverlauf getestet. Dabei zeigte sich, dass Prätubulysin die RNA-Polymerase-II-Anreicherung an allen drei Zelladhäsionsmolekül-Genen bei kurzen Behandlungszeiten mäßig reduzierte. Diese Effekte gingen bei mittlerer Behandlungsdauer weitgehend verloren, nahmen aber nach längerer Behandlung mit Prätubulysin deutlich zu. Die Untersuchung der mRNA-Level der Zelladhäsionsmoleküle in Abhängigkeit von der Vorbehandlungszeit mit Prätubulysin durch qRT-PCR Analyse zeigte eine vergleichbare Verringerung der jeweiligen mRNA-Level nach kurzer Vorbehandlung, eine signifikante Induktion der mRNA-Level bei mittleren Vorbehandlungszeiten, aber eine vollständige Inhibition der mRNA-Level nach längerer Vorbehandlung.

Aufgrund der starken Aktivierung von JNK nach der Behandlung mit Prätubulysin wurden die verringerten Zelladhäsionsmolekül-mRNA-Level nach kurzer und längerer Behandlung mit einem JNK-Inhibitor auf ihre Empfindlichkeit gegenüber der Aktivität von JNK getestet. Die Inhibition von JNK konnte die Auswirkungen auf die mRNA-Level der Zelladhäsionsmoleküle nach längerer Behandlung teilweise umkehren, hatte aber keine Auswirkungen auf die verringerten mRNA-Level nach kurzer Behandlung mit Prätubulysin. Darüber hinaus ergab eine durchflusszytometrische Analyse, dass die Inhibition von JNK auch die Hemmung der Zelloberflächenlevel von ICAM-1 und VCAM-1 teilweise umkehren konnte.

Eine anschließende Untersuchung der Anreicherung des Bromodomänen-enthaltenden Proteins 4, das für die Rekrutierung des positiven Transkriptions-Elongationsfaktors b verantwortlich ist der die Freisetzung der blockierten RNA-Polymerase II in Genen induziert ergab, dass die Behandlung mit Prätubulysin die Anreicherung dieses Faktors um die RNA-Polymerase-Stalling-Stelle an den Genen

von ICAM-1 und VCAM-1 bei kurzen Behandlungszeiten erhöhte. Eine längere Behandlung mit Prätubulysin führte jedoch zu einer Abnahme der Anreicherung des Bromodomänen-enthaltenden Proteins 4, die im Fall des *vcam-1*-Gens stärker ausgeprägt war. Die Untersuchung der Abhängigkeit der Anreicherung des Bromodomänen-enthaltenden Proteins 4 im *icam-1*- und *vcam-1*-Gen von der JNK-Aktivität ergab, dass die Inhibition von JNK die Anreicherung dieses Faktors signifikant erhöhte. Dies zeigt, dass das Bromodomänen-enthaltende Protein 4 durch die JNK-Aktivität negativ reguliert wird. Darüber hinaus ergab eine Western-Blot-Analyse, dass die Behandlung mit Prätubulysin zu einer Verringerung des Bromodomänen-enthaltenden Proteins 4 führte, die auch durch eine JNK-Inhibition rückgängig gemacht werden konnte. Dies zeigte, dass die Behandlung mit Prätubulysin einen verstärkten und JNK-abhängigen Abbau dieses Faktors auslöst. Weitere Untersuchungen zur Abhängigkeit der ICAM-1- und VCAM-1-Zelloberflächenlevel von der Aktivität des Bromodomänen-enthaltenden Proteins 4 durch Knock-down Experimente ergaben, dass das *vcam-1*-Gen durch diesen Faktor positiv reguliert wird, während das *icam-1*-Gen negativ reguliert wird, wie durch verringerte VCAM-1- und erhöhte ICAM-1-Zelloberflächenlevel nach Knock-down gezeigt wurde. Dennoch ergaben Chromatin-Immunpräzipitations-Experimente, dass bei beiden Genen eine verlängerte Behandlung mit Prätubulysin die Anreicherung von repressiven Histon-3-Lysin-9-Trimethylierungsmarkierungen erhöhte. Dies deutet auf das Vorhandensein zusätzlicher Faktoren hin, die die transkriptionale Repression des *icam-1*-Gens nach Behandlung mit Prätubulysin bewirken und die ebenfalls durch die erhöhte JNK-Aktivität negativ reguliert werden.

Abbildung 71 fasst die wichtigsten Ergebnisse der in dieser Studie durchgeführten In-vitro-Experimente zusammen.

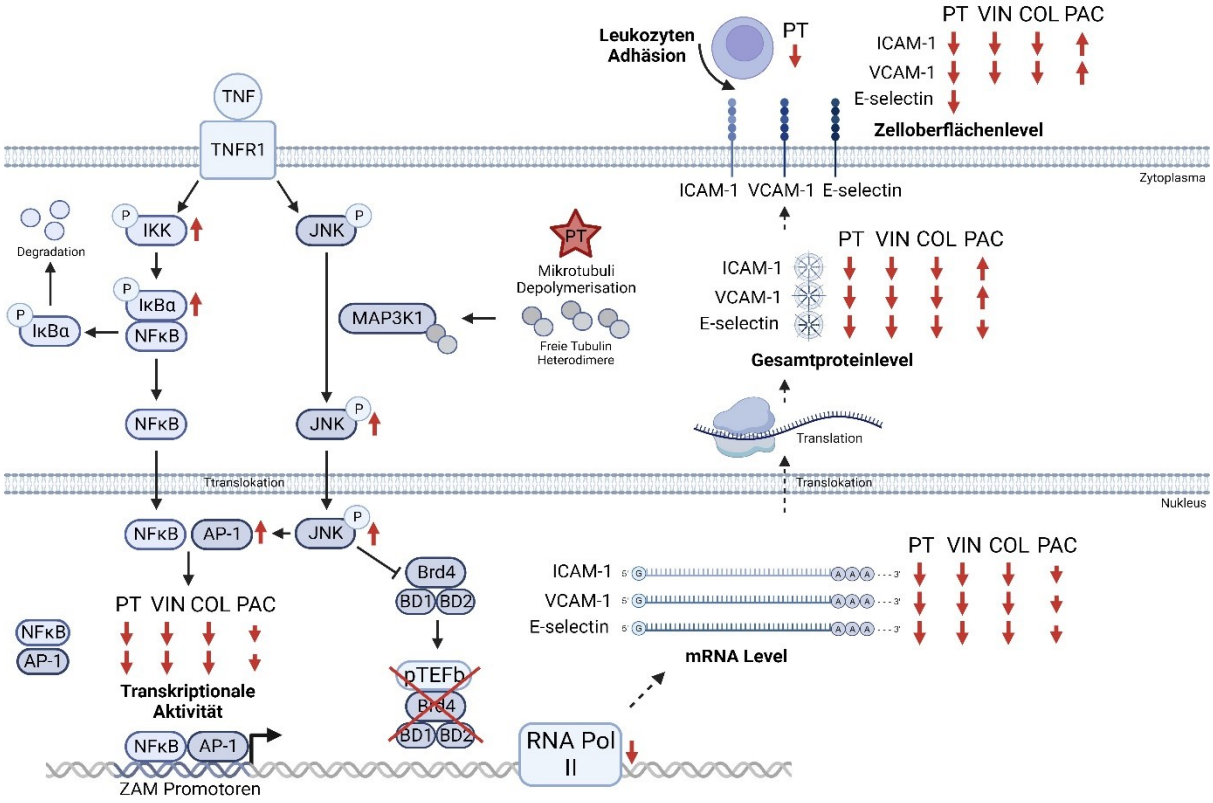

Abbildung 71. Grafische Zusammenfassung der Auswirkungen von Prätubulysin (PT) (und Vincristin, Colchicin und Paclitaxel) auf Entzündungsprozesse in Endothelzellen (nach Behandlung mit 300 nM; Abnahme oder Zunahme im Verhältnis zur jeweiligen TNF-Kontrolle). Die Assoziation von TNF mit dem TNF-Rezeptor führt zur Signalintegration und intrazellulären Aktivierung der IKK-Kinase im NFκB-Weg sowie der c-Jun-N-terminalen Kinase (JNK) des AP-1-Aktivierungsweges. Die Behandlung mit PT erhöhte die Phosphorylierung und damit die Aktivierung der IKK und den nachgeschalteten Abbau von IκBα, der NFκB im Zytosol sequestriert, was zur Freisetzung von NFκB und der anschließenden Translokation in den Zellkern führt. Die Mikrotubuli-Depolymerisation durch PT erhöht die Konzentration der löslichen Tubulin-Heterodimere. Die erhöhte zytosolische Tubulinkonzentration aktiviert die der JNK vorgeschaltete MAP-Kinase MAP3K der Stufe 3, die nachweislich durch die Bindung von löslichem Tubulin aktiviert wird. Die erhöhte MAP3K1-Aktivität induziert die Aktivität von JNK erheblich. Die stark aktivierte JNK aktiviert ihrerseits cJun im Transkriptionsfaktor AP-1, was zur Autoinduktion der cJun-Transkription durch aktiviertes cJun führt und die cJun-Proteinlevel erhöht. Sowohl NFκB als auch AP-1 binden an die Promotoren der Zelladhäsionsmoleküle (ZAMs), wobei die Transkriptionsaktivität beider Faktoren nach Behandlung mit den destabilisierenden Mikrotubuli-Targeting-Agents (MTAs) deutlich reduziert wird. Die TNF-Stimulation induziert die Assoziation des Bromodomänen-enthaltenden Proteins 4 (Brd4; enthält zwei Bromodomänen, BD1 und BD2) mit dem positiven Transkriptionselongationsfaktor b (pTEFb), um die blockierte RNA-Polymerase II in den nicht-translatierten Regionen stromabwärts der Transkriptionsstartstellen der ZAM-Promotoren freizusetzen. Es konnte gezeigt werden, dass die erhöhte JNK-Aktivität durch PT die Assoziation von Brd4 mit Chromatin negativ reguliert und wahrscheinlich die ordnungsgemäße Bildung des pTEFb:Brd4-Komplexes verhindert, der für die Freisetzung der blockierten RNA-Polymerase II erforderlich ist. Darüber hinaus verringert die Behandlung mit PT auch die Konzentration der RNA-Polymerase in den Promotoren und den abgewürgten Regionen der ZAMs. Die Wirkungen der depolymerisierenden MTAs führen zu einer verringerten Expression der ZAM-mRNA, der -Gesamtproteinlevel sowie der -Zelloberflächenlevel, was auch eine verringerte Leukozytenadhäsion an den Endothelzellen bedingt.

8. References

[1] 2017. A current view on inflammation. *Nature immunology* 18, 8, 825.

[2] Bennett, J. M., Reeves, G., Billman, G. E., and Sturmberg, J. P. 2018. Inflammation-Nature's Way to Efficiently Respond to All Types of Challenges: Implications for Understanding and Managing "the Epidemic" of Chronic Diseases. *Frontiers in medicine* 5, 316.

[3] Netea, M. G., Balkwill, F., Chonchol, M., Cominelli, F., Donath, M. Y., Giamarellos-Bourboulis, E. J., Golenbock, D., Gresnigt, M. S., Heneka, M. T., Hoffman, H. M., Hotchkiss, R., Joosten, L. A. B., Kastner, D. L., Korte, M., Latz, E., Libby, P., Mandrup-Poulsen, T., Mantovani, A., Mills, K. H. G., Nowak, K. L., O'Neill, L. A., Pickkers, P., van der Poll, T., Ridker, P. M., Schalkwijk, J., Schwartz, D. A., Siegmund, B., Steer, C. J., Tilg, H., van der Meer, J. W. M., van de Veerdonk, F. L., and Dinarello, C. A. 2017. A guiding map for inflammation. *Nature immunology* 18, 8, 826–831.

[4] 2018. Global, regional, and national age-sex-specific mortality for 282 causes of death in 195 countries and territories, 1980-2017: a systematic analysis for the Global Burden of Disease Study 2017. *Lancet (London, England)* 392, 10159, 1736–1788.

[5] Fullerton, J. N. and Gilroy, D. W. 2016. Resolution of inflammation: a new therapeutic frontier. *Nature reviews. Drug discovery* 15, 8, 551–567.

[6] Furman, D., Chang, J., Lartigue, L., Bolen, C. R., Haddad, F., Gaudilliere, B., Ganio, E. A., Fragiadakis, G. K., Spitzer, M. H., Douchet, I., Daburon, S., Moreau, J.-F., Nolan, G. P., Blanco, P., Déchanet-Merville, J., Dekker, C. L., Jojic, V., Kuo, C. J., Davis, M. M., and Faustin, B. 2017. Expression of specific inflammasome gene modules stratifies older individuals into two extreme clinical and immunological states. *Nature medicine* 23, 2, 174–184.

[7] Kotas, M. E. and Medzhitov, R. 2015. Homeostasis, inflammation, and disease susceptibility. *Cell* 160, 5, 816–827.

[8] Ferrucci, L. and Fabbri, E. 2018. Inflammageing: chronic inflammation in ageing, cardiovascular disease, and frailty. *Nature reviews. Cardiology* 15, 9, 505–522.

[9] Calder, P. C., Ahluwalia, N., Albers, R., Bosco, N., Bourdet-Sicard, R., Haller, D., Holgate, S. T., Jönsson, L. S., Latulippe, M. E., Marcos, A., Moreines, J., M'Rini, C., Müller, M., Pawelec, G., van Neerven, R. J. J., Watzl, B., and Zhao, J. 2013. A consideration of biomarkers to be used for evaluation of inflammation in human nutritional studies. *The British journal of nutrition* 109 Suppl 1, S1-34.

[10] Straub, R. H. 2017. The brain and immune system prompt energy shortage in chronic inflammation and ageing. *Nature reviews. Rheumatology* 13, 12, 743–751.

[11] Turvey, S. E. and Broide, D. H. 2010. Innate immunity. *The Journal of allergy and clinical immunology* 125, 2 Suppl 2, S24-32.

[12] Marshall, J. S., Warrington, R., Watson, W., and Kim, H. L. 2018. An introduction to immunology and immunopathology. *Allergy, asthma, and clinical immunology : official journal of the Canadian Society of Allergy and Clinical Immunology* 14, Suppl 2, 49.

[13] Li, D. and Wu, M. 2021. Pattern recognition receptors in health and diseases. *Signal transduction and targeted therapy* 6, 1, 291.

[14] Janeway, C. A. 2001. *Immunobiology 5. The immune system in health and disease / Charles A. Janeway ... [et al.]*. Garland; Edinburgh : Churchill Livingstone, New York.

[15] Gudkov, A. V. and Komarova, E. A. 2016. p53 and the Carcinogenicity of Chronic Inflammation. *Cold Spring Harbor perspectives in medicine* 6, 11.

[16] Ozinsky, A., Underhill, D. M., Fontenot, J. D., Hajjar, A. M., Smith, K. D., Wilson, C. B., Schroeder, L., and Aderem, A. 2000. The repertoire for pattern recognition of pathogens by the innate immune system is defined by cooperation between toll-like receptors. *Proceedings of the National Academy of Sciences of the United States of America* 97, 25, 13766–13771.

[17] Seong, S.-Y. and Matzinger, P. 2004. Hydrophobicity: an ancient damage-associated molecular pattern that initiates innate immune responses. *Nature reviews. Immunology* 4, 6, 469–478.

[18] Chen, L., Deng, H., Cui, H., Fang, J., Zuo, Z., Deng, J., Li, Y., Wang, X., and Zhao, L. 2018. Inflammatory responses and inflammation-associated diseases in organs. *Oncotarget* 9, 6, 7204–7218.

[19] Takeda, K. and Akira, S. 2005. Toll-like receptors in innate immunity. *International immunology* 17, 1, 1–14.

[20] Fitzgerald, K. A. and Kagan, J. C. 2020. Toll-like Receptors and the Control of Immunity. *Cell* 180, 6, 1044–1066.

[21] Chuenchor, W., Jin, T., Ravilious, G., and Xiao, T. S. 2014. Structures of pattern recognition receptors reveal molecular mechanisms of autoinhibition, ligand recognition and oligomerization. *Current opinion in immunology* 26, 14–20.

[22] Brennan, J. J. and Gilmore, T. D. 2018. Evolutionary Origins of Toll-like Receptor Signaling. *Molecular biology and evolution* 35, 7, 1576–1587.

[23] Kawasaki, T. and Kawai, T. 2014. Toll-like receptor signaling pathways. *Frontiers in immunology* 5, 461.

[24] Shimizu, T. 2017. Structural insights into ligand recognition and regulation of nucleic acid-sensing Toll-like receptors. *Current opinion in structural biology* 47, 52–59.

[25] Ghosh, S. and Karin, M. 2002. Missing pieces in the NF-kappaB puzzle. *Cell* 109 Suppl, S81-96.

[26] Hendrayani, S.-F., Al-Harbi, B., Al-Ansari, M. M., Silva, G., and Aboussekhra, A. 2016. The inflammatory/cancer-related IL-6/STAT3/NF-κB positive feedback loop includes AUF1 and maintains the active state of breast myofibroblasts. *Oncotarget* 7, 27, 41974–41985.

[27] Kyriakis, J. M. and Avruch, J. 2001. Mammalian mitogen-activated protein kinase signal transduction pathways activated by stress and inflammation. *Physiological reviews* 81, 2, 807–869.

[28] Lu, Y.-C., Yeh, W.-C., and Ohashi, P. S. 2008. LPS/TLR4 signal transduction pathway. *Cytokine* 42, 2, 145–151.

[29] Gohda, J., Matsumura, T., and Inoue, J. 2004. Cutting edge: TNFR-associated factor (TRAF) 6 is essential for MyD88-dependent pathway but not toll/IL-1 receptor domain-containing adaptor-inducing IFN-beta (TRIF)-dependent pathway in TLR signaling. *Journal of immunology (Baltimore, Md. : 1950)* 173, 5, 2913–2917.

[30] Kanayama, A., Seth, R. B., Sun, L., Ea, C.-K., Hong, M., Shaito, A., Chiu, Y.-H., Deng, L., and Chen, Z. J. 2004. TAB2 and TAB3 activate the NF-kappaB pathway through binding to polyubiquitin chains. *Molecular cell* 15, 4, 535–548.

[31] Sato, S., Sanjo, H., Takeda, K., Ninomiya-Tsuji, J., Yamamoto, M., Kawai, T., Matsumoto, K., Takeuchi, O., and Akira, S. 2005. Essential function for the kinase TAK1 in innate and adaptive immune responses. *Nature immunology* 6, 11, 1087–1095.

[32] Dostert, C., Grusdat, M., Letellier, E., and Brenner, D. 2019. The TNF Family of Ligands and Receptors: Communication Modules in the Immune System and Beyond. *Physiological reviews* 99, 1, 115–160.

[33] Brenner, D., Blaser, H., and Mak, T. W. 2015. Regulation of tumour necrosis factor signalling: live or let die. *Nature reviews. Immunology* 15, 6, 362–374.

[34] Yang, S., Xie, C., Chen, Y., Wang, J., Chen, X., Lu, Z., June, R. R., and Zheng, S. G. 2019. Differential roles of TNFα-TNFR1 and TNFα-TNFR2 in the differentiation and function of CD4+Foxp3+ induced Treg cells in vitro and in vivo periphery in autoimmune diseases. *Cell death & disease* 10, 1, 27.

[35] Su, Z., Dhusia, K., and Wu, Y. 2022. Understanding the functional role of membrane confinements in TNF-mediated signaling by multiscale simulations. *Communications biology* 5, 1, 228.

[36] Holtmann, M. H. and Neurath, M. F. 2004. Differential TNF-signaling in chronic inflammatory disorders. *Current molecular medicine* 4, 4, 439–444.

[37] Ruuls, S. R., Hoek, R. M., Ngo, V. N., McNeil, T., Lucian, L. A., Janatpour, M. J., Körner, H., Scheerens, H., Hessel, E. M., Cyster, J. G., McEvoy, L. M., and Sedgwick, J. D. 2001. Membrane-bound TNF supports secondary lymphoid organ structure but is subservient to secreted TNF in driving autoimmune inflammation. *Immunity* 15, 4, 533–543.

[38] Wajant, H., Pfizenmaier, K., and Scheurich, P. 2003. Tumor necrosis factor signaling. *Cell death and differentiation* 10, 1, 45–65.
[39] Hsu, H., Xiong, J., and Goeddel, D. V. 1995. The TNF receptor 1-associated protein TRADD signals cell death and NF-kappa B activation. *Cell* 81, 4, 495–504.
[40] Borghi, A., Verstrepen, L., and Beyaert, R. 2016. TRAF2 multitasking in TNF receptor-induced signaling to NF-κB, MAP kinases and cell death. *Biochemical pharmacology* 116, 1–10.
[41] Zhao, L., Fu, Q., Pan, L., Piai, A., and Chou, J. J. 2020. The Diversity and Similarity of Transmembrane Trimerization of TNF Receptors. *Frontiers in cell and developmental biology* 8, 569684.
[42] Hsu, H., Shu, H. B., Pan, M. G., and Goeddel, D. V. 1996. TRADD-TRAF2 and TRADD-FADD interactions define two distinct TNF receptor 1 signal transduction pathways. *Cell* 84, 2, 299–308.
[43] Hsu, H., Huang, J., Shu, H. B., Baichwal, V., and Goeddel, D. V. 1996. TNF-dependent recruitment of the protein kinase RIP to the TNF receptor-1 signaling complex. *Immunity* 4, 4, 387–396.
[44] Shu, H. B., Takeuchi, M., and Goeddel, D. V. 1996. The tumor necrosis factor receptor 2 signal transducers TRAF2 and c-IAP1 are components of the tumor necrosis factor receptor 1 signaling complex. *Proceedings of the National Academy of Sciences of the United States of America* 93, 24, 13973–13978.
[45] Vince, J. E., Pantaki, D., Feltham, R., Mace, P. D., Cordier, S. M., Schmukle, A. C., Davidson, A. J., Callus, B. A., Wong, W. W.-L., Gentle, I. E., Carter, H., Lee, E. F., Walczak, H., Day, C. L., Vaux, D. L., and Silke, J. 2009. TRAF2 must bind to cellular inhibitors of apoptosis for tumor necrosis factor (tnf) to efficiently activate nf-{kappa}b and to prevent tnf-induced apoptosis. *The Journal of biological chemistry* 284, 51, 35906–35915.
[46] Bertrand, M. J. M., Milutinovic, S., Dickson, K. M., Ho, W. C., Boudreault, A., Durkin, J., Gillard, J. W., Jaquith, J. B., Morris, S. J., and Barker, P. A. 2008. cIAP1 and cIAP2 facilitate cancer cell survival by functioning as E3 ligases that promote RIP1 ubiquitination. *Molecular cell* 30, 6, 689–700.
[47] Walczak, H. 2011. TNF and ubiquitin at the crossroads of gene activation, cell death, inflammation, and cancer. *Immunological reviews* 244, 1, 9–28.
[48] Ea, C.-K., Deng, L., Xia, Z.-P., Pineda, G., and Chen, Z. J. 2006. Activation of IKK by TNFalpha requires site-specific ubiquitination of RIP1 and polyubiquitin binding by NEMO. *Molecular cell* 22, 2, 245–257.
[49] Lo, Y.-C., Lin, S.-C., Rospigliosi, C. C., Conze, D. B., Wu, C.-J., Ashwell, J. D., Eliezer, D., and Wu, H. 2009. Structural basis for recognition of diubiquitins by NEMO. *Molecular cell* 33, 5, 602–615.
[50] Rahighi, S., Ikeda, F., Kawasaki, M., Akutsu, M., Suzuki, N., Kato, R., Kensche, T., Uejima, T., Bloor, S., Komander, D., Randow, F., Wakatsuki, S., and Dikic, I. 2009. Specific recognition of linear ubiquitin chains by NEMO is important for NF-kappaB activation. *Cell* 136, 6, 1098–1109.
[51] Grech, A. P., Gardam, S., Chan, T., Quinn, R., Gonzales, R., Basten, A., and Brink, R. 2005. Tumor necrosis factor receptor 2 (TNFR2) signaling is negatively regulated by a novel, carboxyl-terminal TNFR-associated factor 2 (TRAF2)-binding site. *The Journal of biological chemistry* 280, 36, 31572–31581.
[52] Mukai, Y., Nakamura, T., Yoshikawa, M., Yoshioka, Y., Tsunoda, S., Nakagawa, S., Yamagata, Y., and Tsutsumi, Y. 2010. Solution of the structure of the TNF-TNFR2 complex. *Science signaling* 3, 148, ra83.
[53] Park, Y. C., Ye, H., Hsia, C., Segal, D., Rich, R. L., Liou, H. C., Myszka, D. G., and Wu, H. 2000. A novel mechanism of TRAF signaling revealed by structural and functional analyses of the TRADD-TRAF2 interaction. *Cell* 101, 7, 777–787.
[54] Israël, A. 2010. The IKK complex, a central regulator of NF-kappaB activation. *Cold Spring Harbor perspectives in biology* 2, 3, a000158.
[55] Kalliolias, G. D. and Ivashkiv, L. B. 2016. TNF biology, pathogenic mechanisms and emerging therapeutic strategies. *Nature reviews. Rheumatology* 12, 1, 49–62.
[56] Sun, S.-C. 2011. Non-canonical NF-κB signaling pathway. *Cell research* 21, 1, 71–85.

[57] Shin, M., Franks, C. E., and Hsu, K.-L. 2018. Isoform-selective activity-based profiling of ERK signaling. *Chemical science* 9, 9, 2419–2431.
[58] Cuenda, A. and Rousseau, S. 2007. p38 MAP-kinases pathway regulation, function and role in human diseases. *Biochimica et biophysica acta* 1773, 8, 1358–1375.
[59] Bogoyevitch, M. A. 2006. The isoform-specific functions of the c-Jun N-terminal Kinases (JNKs): differences revealed by gene targeting. *BioEssays : news and reviews in molecular, cellular and developmental biology* 28, 9, 923–934.
[60] Widmann, C., Gibson, S., Jarpe, M. B., and Johnson, G. L. 1999. Mitogen-activated protein kinase: conservation of a three-kinase module from yeast to human. *Physiological reviews* 79, 1, 143–180.
[61] Zhang, W. and Liu, H. T. 2002. MAPK signal pathways in the regulation of cell proliferation in mammalian cells. *Cell research* 12, 1, 9–18.
[62] Stokoe, D., Macdonald, S. G., Cadwallader, K., Symons, M., and Hancock, J. F. 1994. Activation of Raf as a result of recruitment to the plasma membrane. *Science (New York, N.Y.)* 264, 5164, 1463–1467.
[63] Seger, R. and Krebs, E. G. 1995. The MAPK signaling cascade. *FASEB journal : official publication of the Federation of American Societies for Experimental Biology* 9, 9, 726–735.
[64] Ichijo, H. 1999. From receptors to stress-activated MAP kinases. *Oncogene* 18, 45, 6087–6093.
[65] Saha, R. N., Jana, M., and Pahan, K. 2007. MAPK p38 regulates transcriptional activity of NF-kappaB in primary human astrocytes via acetylation of p65. *Journal of immunology (Baltimore, Md. : 1950)* 179, 10, 7101–7109.
[66] Soni, S., Anand, P., and Padwad, Y. S. 2019. MAPKAPK2: the master regulator of RNA-binding proteins modulates transcript stability and tumor progression. *Journal of experimental & clinical cancer research : CR* 38, 1, 121.
[67] Lin, A. 2003. Activation of the JNK signaling pathway: breaking the brake on apoptosis. *BioEssays : news and reviews in molecular, cellular and developmental biology* 25, 1, 17–24.
[68] Lawler, S., Fleming, Y., Goedert, M., and Cohen, P. 1998. Synergistic activation of SAPK1/JNK1 by two MAP kinase kinases in vitro. *Current biology : CB* 8, 25, 1387–1390.
[69] Kumar, A., Singh, U. K., Kini, S. G., Garg, V., Agrawal, S., Tomar, P. K., Pathak, P., Chaudhary, A., Gupta, P., and Malik, A. 2015. JNK pathway signaling: a novel and smarter therapeutic targets for various biological diseases. *Future medicinal chemistry* 7, 15, 2065–2086.
[70] Gupta, S., Barrett, T., Whitmarsh, A. J., Cavanagh, J., Sluss, H. K., Dérijard, B., and Davis, R. J. 1996. Selective interaction of JNK protein kinase isoforms with transcription factors. *The EMBO Journal* 15, 11, 2760–2770.
[71] Ghoreschi, K., Laurence, A., and O'Shea, J. J. 2009. Janus kinases in immune cell signaling. *Immunological reviews* 228, 1, 273–287.
[72] Tsoyi, K., Jang, H. J., Nizamutdinova, I. T., Park, K., Kim, Y. M., Kim, H. J., Seo, H. G., Lee, J. H., and Chang, K. C. 2010. PTEN differentially regulates expressions of ICAM-1 and VCAM-1 through PI3K/Akt/GSK-3β/GATA-6 signaling pathways in TNF-α-activated human endothelial cells. *Atherosclerosis* 213, 1, 115–121.
[73] Fitzgerald, K. A., McWhirter, S. M., Faia, K. L., Rowe, D. C., Latz, E., Golenbock, D. T., Coyle, A. J., Liao, S.-M., and Maniatis, T. 2003. IKKepsilon and TBK1 are essential components of the IRF3 signaling pathway. *Nature immunology* 4, 5, 491–496.
[74] Aaronson, D. S. and Horvath, C. M. 2002. A road map for those who don't know JAK-STAT. *Science (New York, N.Y.)* 296, 5573, 1653–1655.
[75] Levy, D. E. and Darnell, J. E. 2002. Stats: transcriptional control and biological impact. *Nature reviews. Molecular cell biology* 3, 9, 651–662.
[76] Schindler, C. and Plumlee, C. 2008. Inteferons pen the JAK-STAT pathway. *Seminars in cell & developmental biology* 19, 4, 311–318.
[77] Osaki, M., Oshimura, M., and Ito, H. 2004. PI3K-Akt pathway: its functions and alterations in human cancer. *Apoptosis : an international journal on programmed cell death* 9, 6, 667–676.
[78] Ma, X. and Bai, Y. 2012. IGF-1 activates the P13K/AKT signaling pathway via upregulation of secretory clusterin. *Molecular medicine reports* 6, 6, 1433–1437.

[79] Yokota, J., Chosa, N., Sawada, S., Okubo, N., Takahashi, N., Hasegawa, T., Kondo, H., and Ishisaki, A. 2014. PDGF-induced PI3K-mediated signaling enhances the TGF-β-induced osteogenic differentiation of human mesenchymal stem cells in a TGF-β-activated MEK-dependent manner. *International journal of molecular medicine* 33, 3, 534–542.

[80] Fujita, T., Reis, L. F., Watanabe, N., Kimura, Y., Taniguchi, T., and Vilcek, J. 1989. Induction of the transcription factor IRF-1 and interferon-beta mRNAs by cytokines and activators of second-messenger pathways. *Proceedings of the National Academy of Sciences of the United States of America* 86, 24, 9936–9940.

[81] Yang, K., Shi, H.-X., Liu, X.-Y., Shan, Y.-F., Wei, B., Chen, S., and Wang, C. 2009. TRIM21 is essential to sustain IFN regulatory factor 3 activation during antiviral response. *Journal of immunology (Baltimore, Md. : 1950)* 182, 6, 3782–3792.

[82] Broad, A., Kirby, J. A., and Jones, D. E. J. 2007. Toll-like receptor interactions: tolerance of MyD88-dependent cytokines but enhancement of MyD88-independent interferon-beta production. *Immunology* 120, 1, 103–111.

[83] Yanai, H., Negishi, H., and Taniguchi, T. 2012. The IRF family of transcription factors: Inception, impact and implications in oncogenesis. *Oncoimmunology* 1, 8, 1376–1386.

[84] Harada, H., Takahashi, E., Itoh, S., Harada, K., Hori, T. A., and Taniguchi, T. 1994. Structure and regulation of the human interferon regulatory factor 1 (IRF-1) and IRF-2 genes: implications for a gene network in the interferon system. *Mol. Cell. Biol.* 14, 2, 1500–1509.

[85] Phelps, C. B., Sengchanthalangsy, L. L., Malek, S., and Ghosh, G. 2000. Mechanism of kappa B DNA binding by Rel/NF-kappa B dimers. *Journal of Biological Chemistry* 275, 32, 24392–24399.

[86] Ghosh, S., May, M. J., and Kopp, E. B. 1998. NF-kappa B and Rel proteins: evolutionarily conserved mediators of immune responses. *Annual review of immunology* 16, 225–260.

[87] Gilmore, T. D. 2006. Introduction to NF-kappaB: players, pathways, perspectives. *Oncogene* 25, 51, 6680–6684.

[88] Menetski, J. P. 2000. The structure of the nuclear factor-kappaB protein-DNA complex varies with DNA-binding site sequence. *Journal of Biological Chemistry* 275, 11, 7619–7625.

[89] Kunsch, C., Ruben, S. M., and Rosen, C. A. 1992. Selection of optimal kappa B/Rel DNA-binding motifs: interaction of both subunits of NF-kappa B with DNA is required for transcriptional activation. *Mol. Cell. Biol.* 12, 10, 4412–4421.

[90] Hoffmann, A., Natoli, G., and Ghosh, G. 2006. Transcriptional regulation via the NF-kappaB signaling module. *Oncogene* 25, 51, 6706–6716.

[91] Chen, Y. Q., Sengchanthalangsy, L. L., Hackett, A., and Ghosh, G. 2000. NF-kappaB p65 (RelA) homodimer uses distinct mechanisms to recognize DNA targets. *Structure (London, England : 1993)* 8, 4, 419–428.

[92] Guan, H., Hou, S., and Ricciardi, R. P. 2005. DNA binding of repressor nuclear factor-kappaB p50/p50 depends on phosphorylation of Ser337 by the protein kinase A catalytic subunit. *The Journal of biological chemistry* 280, 11, 9957–9962.

[93] Fan, C. M. and Maniatis, T. 1991. Generation of p50 subunit of NF-kappa B by processing of p105 through an ATP-dependent pathway. *Nature* 354, 6352, 395–398.

[94] Lin, L., DeMartino, G. N., and Greene, W. C. 1998. Cotranslational biogenesis of NF-kappaB p50 by the 26S proteasome. *Cell* 92, 6, 819–828.

[95] Orian, A., Gonen, H., Bercovich, B., Fajerman, I., Eytan, E., Israël, A., Mercurio, F., Iwai, K., Schwartz, A. L., and Ciechanover, A. 2000. SCF(beta)(-TrCP) ubiquitin ligase-mediated processing of NF-kappaB p105 requires phosphorylation of its C-terminus by IkappaB kinase. *The EMBO Journal* 19, 11, 2580–2591.

[96] Zarnegar, B. J., Wang, Y., Mahoney, D. J., Dempsey, P. W., Cheung, H. H., He, J., Shiba, T., Yang, X., Yeh, W.-C., Mak, T. W., Korneluk, R. G., and Cheng, G. 2008. Noncanonical NF-kappaB activation requires coordinated assembly of a regulatory complex of the adaptors cIAP1, cIAP2, TRAF2 and TRAF3 and the kinase NIK. *Nature immunology* 9, 12, 1371–1378.

[97] Liao, G., Zhang, M., Harhaj, E. W., and Sun, S.-C. 2004. Regulation of the NF-kappaB-inducing kinase by tumor necrosis factor receptor-associated factor 3-induced degradation. *The Journal of biological chemistry* 279, 25, 26243–26250.

[98] Ishinaga, H., Jono, H., Lim, J. H., Kweon, S.-M., Xu, H., Ha, U.-H., Xu, H., Koga, T., Yan, C., Feng, X.-H., Chen, L.-F., and Li, J.-D. 2007. TGF-beta induces p65 acetylation to enhance bacteria-induced NF-kappaB activation. *The EMBO Journal* 26, 4, 1150–1162.

[99] Zhong, H., SuYang, H., Erdjument-Bromage, H., Tempst, P., and Ghosh, S. 1997. The transcriptional activity of NF-kappaB is regulated by the IkappaB-associated PKAc subunit through a cyclic AMP-independent mechanism. *Cell* 89, 3, 413–424.

[100] Zhong, H., Voll, R. E., and Ghosh, S. 1998. Phosphorylation of NF-kappa B p65 by PKA stimulates transcriptional activity by promoting a novel bivalent interaction with the coactivator CBP/p300. *Molecular cell* 1, 5, 661–671.

[101] Buss, H., Dörrie, A., Schmitz, M. L., Frank, R., Livingstone, M., Resch, K., and Kracht, M. 2004. Phosphorylation of serine 468 by GSK-3beta negatively regulates basal p65 NF-kappaB activity. *The Journal of biological chemistry* 279, 48, 49571–49574.

[102] Schwabe, R. F. and Sakurai, H. 2005. IKKbeta phosphorylates p65 at S468 in transactivaton domain 2. *FASEB journal : official publication of the Federation of American Societies for Experimental Biology* 19, 12, 1758–1760.

[103] Mao, X., Gluck, N., Li, D., Maine, G. N., Li, H., Zaidi, I. W., Repaka, A., Mayo, M. W., and Burstein, E. 2009. GCN5 is a required cofactor for a ubiquitin ligase that targets NF-kappaB/RelA. *Genes & development* 23, 7, 849–861.

[104] Geng, H., Wittwer, T., Dittrich-Breiholz, O., Kracht, M., and Schmitz, M. L. 2009. Phosphorylation of NF-kappaB p65 at Ser468 controls its COMMD1-dependent ubiquitination and target gene-specific proteasomal elimination. *EMBO reports* 10, 4, 381–386.

[105] Mattioli, I., Geng, H., Sebald, A., Hodel, M., Bucher, C., Kracht, M., and Schmitz, M. L. 2006. Inducible phosphorylation of NF-kappa B p65 at serine 468 by T cell costimulation is mediated by IKK epsilon. *The Journal of biological chemistry* 281, 10, 6175–6183.

[106] Chen, L.-F., Williams, S. A., Mu, Y., Nakano, H., Duerr, J. M., Buckbinder, L., and Greene, W. C. 2005. NF-kappaB RelA phosphorylation regulates RelA acetylation. *Molecular and Cellular Biology* 25, 18, 7966–7975.

[107] Pradère, J.-P., Hernandez, C., Koppe, C., Friedman, R. A., Luedde, T., and Schwabe, R. F. 2016. Negative regulation of NF-κB p65 activity by serine 536 phosphorylation. *Sci. Signal.* 9, 442.

[108] Sizemore, N., Lerner, N., Dombrowski, N., Sakurai, H., and Stark, G. R. 2002. Distinct roles of the Ikappa B kinase alpha and beta subunits in liberating nuclear factor kappa B (NF-kappa B) from Ikappa B and in phosphorylating the p65 subunit of NF-kappa B. *The Journal of biological chemistry* 277, 6, 3863–3869.

[109] Sakurai, H., Chiba, H., Miyoshi, H., Sugita, T., and Toriumi, W. 1999. IkappaB kinases phosphorylate NF-kappaB p65 subunit on serine 536 in the transactivation domain. *The Journal of biological chemistry* 274, 43, 30353–30356.

[110] Lawrence, T., Bebien, M., Liu, G. Y., Nizet, V., and Karin, M. 2005. IKKalpha limits macrophage NF-kappaB activation and contributes to the resolution of inflammation. *Nature* 434, 7037, 1138–1143.

[111] Buss, H., Dörrie, A., Schmitz, M. L., Hoffmann, E., Resch, K., and Kracht, M. 2004. Constitutive and interleukin-1-inducible phosphorylation of p65 NF-{kappa}B at serine 536 is mediated by multiple protein kinases including I{kappa}B kinase (IKK)-{alpha}, IKK{beta}, IKK{epsilon}, TRAF family member-associated (TANK)-binding kinase 1 (TBK1), and an unknown kinase and couples p65 to TATA-binding protein-associated factor II31-mediated interleukin-8 transcription. *The Journal of biological chemistry* 279, 53, 55633–55643.

[112] Chen, L.-F. and Greene, W. C. 2004. Shaping the nuclear action of NF-kappaB. *Nature reviews. Molecular cell biology* 5, 5, 392–401.

[113] Quivy, V. and van Lint, C. 2004. Regulation at multiple levels of NF-kappaB-mediated transactivation by protein acetylation. *Biochemical pharmacology* 68, 6, 1221–1229.

[114] Huang, B., Yang, X.-D., Zhou, M.-M., Ozato, K., and Chen, L.-F. 2009. Brd4 coactivates transcriptional activation of NF-kappaB via specific binding to acetylated RelA. *Molecular and Cellular Biology* 29, 5, 1375–1387.

[115] Levy, D., Kuo, A. J., Chang, Y., Schaefer, U., Kitson, C., Cheung, P., Espejo, A., Zee, B. M., Liu, C. L., Tangsombatvisit, S., Tennen, R. I., Kuo, A. Y., Tanjing, S., Cheung, R., Chua, K. F., Utz, P. J., Shi, X., Prinjha, R. K., Lee, K., Garcia, B. A., Bedford, M. T., Tarakhovsky, A., Cheng, X., and Gozani, O. 2011. Lysine methylation of the NF-κB subunit RelA by SETD6 couples activity of the histone methyltransferase GLP at chromatin to tonic repression of NF-κB signaling. *Nature immunology* 12, 1, 29–36.

[116] Duran, A., Diaz-Meco, M. T., and Moscat, J. 2003. Essential role of RelA Ser311 phosphorylation by zetaPKC in NF-kappaB transcriptional activation. *The EMBO Journal* 22, 15, 3910–3918.

[117] Chen, L. 2002. Acetylation of RelA at discrete sites regulates distinct nuclear functions of NF-kappaB. *The EMBO Journal* 21, 23, 6539–6548.

[118] Kiernan, R., Brès, V., Ng, R. W. M., Coudart, M.-P., El Messaoudi, S., Sardet, C., Jin, D.-Y., Emiliani, S., and Benkirane, M. 2003. Post-activation turn-off of NF-kappa B-dependent transcription is regulated by acetylation of p65. *The Journal of biological chemistry* 278, 4, 2758–2766.

[119] O'Shea, E. K., Rutkowski, R., Stafford, W. F., and Kim, P. S. 1989. Preferential heterodimer formation by isolated leucine zippers from fos and jun. *Science (New York, N.Y.)* 245, 4918, 646–648.

[120] Halazonetis, T. D., Georgopoulos, K., Greenberg, M. E., and Leder, P. 1988. c-Jun dimerizes with itself and with c-Fos, forming complexes of different DNA binding affinities. *Cell* 55, 5, 917–924.

[121] Nakabeppu, Y., Ryder, K., and Nathans, D. 1988. DNA binding activities of three murine Jun proteins: stimulation by Fos. *Cell* 55, 5, 907–915.

[122] Kouzarides, T. and Ziff, E. 1988. The role of the leucine zipper in the fos-jun interaction. *Nature* 336, 6200, 646–651.

[123] Jaeschke, A., Karasarides, M., Ventura, J.-J., Ehrhardt, A., Zhang, C., Flavell, R. A., Shokat, K. M., and Davis, R. J. 2006. JNK2 is a positive regulator of the cJun transcription factor. *Molecular cell* 23, 6, 899–911.

[124] Aguilera, C., Nakagawa, K., Sancho, R., Chakraborty, A., Hendrich, B., and Behrens, A. 2011. c-Jun N-terminal phosphorylation antagonises recruitment of the Mbd3/NuRD repressor complex. *Nature* 469, 7329, 231–235.

[125] Arias, J., Alberts, A. S., Brindle, P., Claret, F. X., Smeal, T., Karin, M., Feramisco, J., and Montminy, M. 1994. Activation of cAMP and mitogen responsive genes relies on a common nuclear factor. *Nature* 370, 6486, 226–229.

[126] Nateri, A. S., Spencer-Dene, B., and Behrens, A. 2005. Interaction of phosphorylated c-Jun with TCF4 regulates intestinal cancer development. *Nature* 437, 7056, 281–285.

[127] Behrens, A., Sibilia, M., and Wagner, E. F. 1999. Amino-terminal phosphorylation of c-Jun regulates stress-induced apoptosis and cellular proliferation. *Nat Genet* 21, 3, 326–329.

[128] Wei, W., Jin, J., Schlisio, S., Harper, J. W., and Kaelin, W. G. 2005. The v-Jun point mutation allows c-Jun to escape GSK3-dependent recognition and destruction by the Fbw7 ubiquitin ligase. *Cancer Cell* 8, 1, 25–33.

[129] Sutherland, C. 2011. What Are the bona fide GSK3 Substrates? *International Journal of Alzheimer's Disease* 2011, 505607.

[130] ter Haar, E., Coll, J. T., Austen, D. A., Hsiao, H. M., Swenson, L., and Jain, J. 2001. Structure of GSK3beta reveals a primed phosphorylation mechanism. *Nature structural biology* 8, 7, 593–596.

[131] Abate, C., Luk, D., and Curran, T. 1991. Transcriptional regulation by Fos and Jun in vitro: interaction among multiple activator and regulatory domains. *Mol. Cell. Biol.* 11, 7, 3624–3632.

[132] Kovács, K. J. 1998. c-Fos as a transcription factor: a stressful (re)view from a functional map. *Neurochemistry international* 33, 4, 287–297.

[133] Bahrami, S. and Drabløs, F. 2016. Gene regulation in the immediate-early response process. *Advances in biological regulation* 62, 37–49.

[134] Angel, P., Hattori, K., Smeal, T., and Karin, M. 1988. The jun proto-oncogene is positively autoregulated by its product, Jun/AP-1. *Cell* 55, 5, 875–885.

[135] Tu, Y.-C., Huang, D.-Y., Shiah, S.-G., Wang, J.-S., and Lin, W.-W. 2013. Regulation of c-Fos gene expression by NF-κB: a p65 homodimer binding site in mouse embryonic fibroblasts but not human HEK293 cells. *PloS one* 8, 12, e84062.

[136] Monje, P., Hernández-Losa, J., Lyons, R. J., Castellone, M. D., and Gutkind, J. S. 2005. Regulation of the transcriptional activity of c-Fos by ERK. A novel role for the prolyl isomerase PIN1. *The Journal of biological chemistry* 280, 42, 35081–35084.

[137] Butcher, E. C. 1991. Leukocyte-endothelial cell recognition: three (or more) steps to specificity and diversity. *Cell* 67, 6, 1033–1036.

[138] Kansas, G. S. 1996. Selectins and their ligands: current concepts and controversies. *Blood* 88, 9, 3259–3287.

[139] McEver, R. P. and Cummings, R. D. 1997. Perspectives series: cell adhesion in vascular biology. Role of PSGL-1 binding to selectins in leukocyte recruitment. *J. Clin. Invest.* 100, 3, 485–491.

[140] Alon, R., Hammer, D. A., and Springer, T. A. 1995. Lifetime of the P-selectin-carbohydrate bond and its response to tensile force in hydrodynamic flow. *Nature* 374, 6522, 539–542.

[141] Lawrence, M. B., Kansas, G. S., Kunkel, E. J., and Ley, K. 1997. Threshold levels of fluid shear promote leukocyte adhesion through selectins (CD62L,P,E). *The Journal of Cell Biology* 136, 3, 717–727.

[142] Finger, E. B., Purl, K. D., Alon, R., Lawrence, M. B., Andrian, U. H. von, and Springer, T. A. 1996. Adhesion through L-selectin requires a threshold hydrodynamic shear. *Nature* 379, 6562, 266–269.

[143] Marshall, B. T., Long, M., Piper, J. W., Yago, T., McEver, R. P., and Zhu, C. 2003. Direct observation of catch bonds involving cell-adhesion molecules. *Nature* 423, 6936, 190–193.

[144] Berlin, C., Bargatze, R. F., Campbell, J. J., Andrian, U. H. von, Szabo, M. C., Hasslen, S. R., Nelson, R. D., Berg, E. L., Erlandsen, S. L., and Butcher, E. C. 1995. alpha 4 integrins mediate lymphocyte attachment and rolling under physiologic flow. *Cell* 80, 3, 413–422.

[145] CHESNUTT, B. C., SMITH, D. F., RAFFLER, N. A., SMITH, M. L., WHITE, E. J., and Ley, K. 2006. Induction of LFA-1-dependent neutrophil rolling on ICAM-1 by engagement of E-selectin. *Microcirculation (New York, N.Y. : 1994)* 13, 2, 99–109.

[146] Salas, A., Shimaoka, M., Kogan, A. N., Harwood, C., Andrian, U. H. von, and Springer, T. A. 2004. Rolling adhesion through an extended conformation of integrin alphaLbeta2 and relation to alpha I and beta I-like domain interaction. *Immunity* 20, 4, 393–406.

[147] Hundelshausen, P. von, Koenen, R. R., Sack, M., Mause, S. F., Adriaens, W., Proudfoot, A. E. I., Hackeng, T. M., and Weber, C. 2005. Heterophilic interactions of platelet factor 4 and RANTES promote monocyte arrest on endothelium. *Blood* 105, 3, 924–930.

[148] Campbell, J. J., Hedrick, J., Zlotnik, A., Siani, M. A., Thompson, D. A., and Butcher, E. C. 1998. Chemokines and the arrest of lymphocytes rolling under flow conditions. *Science (New York, N.Y.)* 279, 5349, 381–384.

[149] Chan, J. R., Hyduk, S. J., and Cybulsky, M. I. 2001. Chemoattractants induce a rapid and transient upregulation of monocyte alpha4 integrin affinity for vascular cell adhesion molecule 1 which mediates arrest: an early step in the process of emigration. *The Journal of Experimental Medicine* 193, 10, 1149–1158.

[150] Giagulli, C., Scarpini, E., Ottoboni, L., Narumiya, S., Butcher, E. C., Constantin, G., and Laudanna, C. 2004. RhoA and zeta PKC control distinct modalities of LFA-1 activation by chemokines: critical role of LFA-1 affinity triggering in lymphocyte in vivo homing. *Immunity* 20, 1, 25–35.

[151] Hyduk, S. J., Chan, J. R., Duffy, S. T., Chen, M., Peterson, M. D., Waddell, T. K., Digby, G. C., Szaszi, K., Kapus, A., and Cybulsky, M. I. 2007. Phospholipase C, calcium, and calmodulin are critical for alpha4beta1 integrin affinity up-regulation and monocyte arrest triggered by chemoattractants. *Blood* 109, 1, 176–184.

[152] Kim, M., Carman, C. V., and Springer, T. A. 2003. Bidirectional transmembrane signaling by cytoplasmic domain separation in integrins. *Science (New York, N.Y.)* 301, 5640, 1720–1725.

[153] Tadokoro, S., Shattil, S. J., Eto, K., Tai, V., Liddington, R. C., Pereda, J. M. de, Ginsberg, M. H., and Calderwood, D. A. 2003. Talin binding to integrin beta tails: a final common step in integrin activation. *Science (New York, N.Y.)* 302, 5642, 103–106.

[154] Phillipson, M., Heit, B., Colarusso, P., Liu, L., Ballantyne, C. M., and Kubes, P. 2006. Intraluminal crawling of neutrophils to emigration sites: a molecularly distinct process from adhesion in the recruitment cascade. *The Journal of Experimental Medicine* 203, 12, 2569–2575.

[155] Schenkel, A. R., Mamdouh, Z., and Muller, W. A. 2004. Locomotion of monocytes on endothelium is a critical step during extravasation. *Nature immunology* 5, 4, 393–400.

[156] Cinamon, G., Shinder, V., Shamri, R., and Alon, R. 2004. Chemoattractant signals and beta 2 integrin occupancy at apical endothelial contacts combine with shear stress signals to promote transendothelial neutrophil migration. *Journal of immunology (Baltimore, Md. : 1950)* 173, 12, 7282–7291.

[157] Muller, W. A. 2003. Leukocyte-endothelial-cell interactions in leukocyte transmigration and the inflammatory response. *Trends in Immunology* 24, 6, 327–334.

[158] Vestweber, D. 2002. Regulation of endothelial cell contacts during leukocyte extravasation. *Current Opinion in Cell Biology* 14, 5, 587–593.

[159] Shaw, S. K., Bamba, P. S., Perkins, B. N., and Luscinskas, F. W. 2001. Real-time imaging of vascular endothelial-cadherin during leukocyte transmigration across endothelium. *Journal of immunology (Baltimore, Md. : 1950)* 167, 4, 2323–2330.

[160] Carman, C. V. and Springer, T. A. 2004. A transmigratory cup in leukocyte diapedesis both through individual vascular endothelial cells and between them. *The Journal of Cell Biology* 167, 2, 377–388.

[161] Dvorak, A. M. and Feng, D. 2001. The vesiculo-vacuolar organelle (VVO). A new endothelial cell permeability organelle. *The journal of histochemistry and cytochemistry : official journal of the Histochemistry Society* 49, 4, 419–432.

[162] Millán, J., Hewlett, L., Glyn, M., Toomre, D., Clark, P., and Ridley, A. J. 2006. Lymphocyte transcellular migration occurs through recruitment of endothelial ICAM-1 to caveola- and F-actin-rich domains. *Nat Cell Biol* 8, 2, 113–123.

[163] Wang, S., Voisin, M.-B., Larbi, K. Y., Dangerfield, J., Scheiermann, C., Tran, M., Maxwell, P. H., Sorokin, L., and Nourshargh, S. 2006. Venular basement membranes contain specific matrix protein low expression regions that act as exit points for emigrating neutrophils. *The Journal of Experimental Medicine* 203, 6, 1519–1532.

[164] Roebuck, K. A. and Finnegan, A. 1999. Regulation of intercellular adhesion molecule-1 (CD54) gene expression. *Journal of leukocyte biology* 66, 6, 876–888.

[165] Iademarco, M. F., McQuillan, J. J., Rosen, G. D., and Dean, D. C. 1992. Characterization of the promoter for vascular cell adhesion molecule-1 (VCAM-1). *The Journal of biological chemistry* 267, 23, 16323–16329.

[166] Walton, T., Wang, J. L., Ribas, A., Barsky, S. H., Economou, J., and Nguyen, M. 1998. Endothelium-specific expression of an E-selectin promoter recombinant adenoviral vector. *Anticancer research* 18, 3A, 1357–1360.

[167] Whitley, M. Z., Thanos, D., Read, M. A., Maniatis, T., and Collins, T. 1994. A striking similarity in the organization of the E-selectin and beta interferon gene promoters. *Mol. Cell. Biol.* 14, 10, 6464–6475.

[168] Yockell-Lelièvre, J., Spriet, C., Cantin, P., Malenfant, P., Heliot, L., Launoit, Y. de, and Audette, M. 2009. Functional cooperation between Stat-1 and ets-1 to optimize icam-1 gene transcription. *Biochemistry and cell biology = Biochimie et biologie cellulaire* 87, 6, 905–918.

[169] Lechleitner, S., Gille, J., Johnson, D. R., and Petzelbauer, P. 1998. Interferon enhances tumor necrosis factor-induced vascular cell adhesion molecule 1 (CD106) expression in human endothelial cells by an interferon-related factor 1-dependent pathway. *The Journal of Experimental Medicine* 187, 12, 2023–2030.

[170] Neish, A. S., Read, M. A., Thanos, D., Pine, R., Maniatis, T., and Collins, T. 1995. Endothelial interferon regulatory factor 1 cooperates with NF-kappa B as a transcriptional activator of vascular cell adhesion molecule 1. *Mol. Cell. Biol.* 15, 5, 2558–2569.

[171] Umetani, M., Mataki, C., Minegishi, N., Yamamoto, M., Hamakubo, T., and Kodama, T. 2001. Function of GATA Transcription Factors in Induction of Endothelial Vascular Cell Adhesion Molecule-1 by Tumor Necrosis Factor-α. *ATVB* 21, 6, 917–922.

[172] Read, M. A., Neish, A. S., Luscinskas, F. W., Palombella, V. J., Maniatis, T., and Collins, T. 1995. The proteasome pathway is required for cytokine-induced endothelial-leukocyte adhesion molecule expression. *Immunity* 2, 5, 493–506.

[173] Schindler, U. and Baichwal, V. R. 1994. Three NF-kappa B binding sites in the human E-selectin gene required for maximal tumor necrosis factor alpha-induced expression. *Mol. Cell. Biol.* 14, 9, 5820–5831.

[174] Marui, N., Offermann, M. K., Swerlick, R., Kunsch, C., Rosen, C. A., Ahmad, M., Alexander, R. W., and Medford, R. M. 1993. Vascular cell adhesion molecule-1 (VCAM-1) gene transcription and expression are regulated through an antioxidant-sensitive mechanism in human vascular endothelial cells. *J. Clin. Invest.* 92, 4, 1866–1874.

[175] Neish, A. S., Williams, A. J., Palmer, H. J., Whitley, M. Z., and Collins, T. 1992. Functional analysis of the human vascular cell adhesion molecule 1 promoter. *The Journal of Experimental Medicine* 176, 6, 1583–1593.

[176] Ledebur, H. C. and Parks, T. P. 1995. Transcriptional regulation of the intercellular adhesion molecule-1 gene by inflammatory cytokines in human endothelial cells. Essential roles of a variant NF-kappa B site and p65 homodimers. *Journal of Biological Chemistry* 270, 2, 933–943.

[177] Ossipow, V., Fonjallaz, P., and Schibler, U. 1999. An RNA polymerase II complex containing all essential initiation factors binds to the activation domain of PAR leucine zipper transcription factor thyroid embryonic factor. *Mol. Cell. Biol.* 19, 2, 1242–1250.

[178] Lee, T. I. and Young, R. A. 2000. Transcription of eukaryotic protein-coding genes. *Annual review of genetics* 34, 77–137.

[179] Biddick, R. and Young, E. T. 2005. Yeast mediator and its role in transcriptional regulation. *Comptes Rendus Biologies* 328, 9, 773–782.

[180] Björklund, S. and Gustafsson, C. M. 2005. The yeast Mediator complex and its regulation. *Trends in Biochemical Sciences* 30, 5, 240–244.

[181] Ebmeier, C. C., Erickson, B., Allen, B. L., Allen, M. A., Kim, H., Fong, N., Jacobsen, J. R., Liang, K., Shilatifard, A., Dowell, R. D., Old, W. M., Bentley, D. L., and Taatjes, D. J. 2017. Human TFIIH Kinase CDK7 Regulates Transcription-Associated Chromatin Modifications. *Cell Reports* 20, 5, 1173–1186.

[182] Saunders, A., Core, L. J., and Lis, J. T. 2006. Breaking barriers to transcription elongation. *Nature reviews. Molecular cell biology* 7, 8, 557–567.

[183] Guenther, M. G., Levine, S. S., Boyer, L. A., Jaenisch, R., and Young, R. A. 2007. A chromatin landmark and transcription initiation at most promoters in human cells. *Cell* 130, 1, 77–88.

[184] Kim, T. H., Barrera, L. O., Zheng, M., Qu, C., Singer, M. A., Richmond, T. A., Wu, Y., Green, R. D., and Ren, B. 2005. A high-resolution map of active promoters in the human genome. *Nature* 436, 7052, 876–880.

[185] Muse, G. W., Gilchrist, D. A., Nechaev, S., Shah, R., Parker, J. S., Grissom, S. F., Zeitlinger, J., and Adelman, K. 2007. RNA polymerase is poised for activation across the genome. *Nature genetics* 39, 12, 1507–1511.

[186] Zeitlinger, J., Stark, A., Kellis, M., Hong, J.-W., Nechaev, S., Adelman, K., Levine, M., and Young, R. A. 2007. RNA polymerase stalling at developmental control genes in the Drosophila melanogaster embryo. *Nature genetics* 39, 12, 1512–1516.

[187] Rasmussen, E. B. and Lis, J. T. 1993. In vivo transcriptional pausing and cap formation on three Drosophila heat shock genes. *Proceedings of the National Academy of Sciences of the United States of America* 90, 17, 7923–7927.

[188] Wu, C.-H., Yamaguchi, Y., Benjamin, L. R., Horvat-Gordon, M., Washinsky, J., Enerly, E., Larsson, J., Lambertsson, A., Handa, H., and Gilmour, D. 2003. NELF and DSIF cause promoter proximal pausing on the hsp70 promoter in Drosophila. *Genes & development* 17, 11, 1402–1414.

[189] Yamaguchi, Y., Inukai, N., Narita, T., Wada, T., and Handa, H. 2002. Evidence that negative elongation factor represses transcription elongation through binding to a DRB sensitivity-inducing factor/RNA polymerase II complex and RNA. *Mol. Cell. Biol.* 22, 9, 2918–2927.

[190] Peterlin, B. M. and Price, D. H. 2006. Controlling the elongation phase of transcription with P-TEFb. *Molecular cell* 23, 3, 297–305.

[191] Zhou, Q., Li, T., and Price, D. H. 2012. RNA polymerase II elongation control. *Annual review of biochemistry* 81, 119–143.

[192] Michels, A. A., Fraldi, A., Li, Q., Adamson, T. E., Bonnet, F., van Nguyen, T., Sedore, S. C., Price, J. P., Price, D. H., Lania, L., and Bensaude, O. 2004. Binding of the 7SK snRNA turns the HEXIM1 protein into a P-TEFb (CDK9/cyclin T) inhibitor. *The EMBO Journal* 23, 13, 2608–2619.

[193] Smale, S. T. 2011. Hierarchies of NF-κB target-gene regulation. *Nature immunology* 12, 8, 689–694.

[194] Morinière, J., Rousseaux, S., Steuerwald, U., Soler-López, M., Curtet, S., Vitte, A.-L., Govin, J., Gaucher, J., Sadoul, K., Hart, D. J., Krijgsveld, J., Khochbin, S., Müller, C. W., and Petosa, C. 2009. Cooperative binding of two acetylation marks on a histone tail by a single bromodomain. *Nature* 461, 7264, 664–668.

[195] Dhalluin, C., Carlson, J. E., Zeng, L., He, C., Aggarwal, A. K., and Zhou, M. M. 1999. Structure and ligand of a histone acetyltransferase bromodomain. *Nature* 399, 6735, 491–496.

[196] Filippakopoulos, P. and Knapp, S. 2014. Targeting bromodomains: epigenetic readers of lysine acetylation. *Nature reviews. Drug discovery* 13, 5, 337–356.

[197] Devaiah, B. N., Lewis, B. A., Cherman, N., Hewitt, M. C., Albrecht, B. K., Robey, P. G., Ozato, K., Sims, R. J., and Singer, D. S. 2012. BRD4 is an atypical kinase that phosphorylates serine2 of the RNA polymerase II carboxy-terminal domain. *Proceedings of the National Academy of Sciences of the United States of America* 109, 18, 6927–6932.

[198] Devaiah, B. N., Case-Borden, C., Gegonne, A., Hsu, C. H., Chen, Q., Meerzaman, D., Dey, A., Ozato, K., and Singer, D. S. 2016. BRD4 is a histone acetyltransferase that evicts nucleosomes from chromatin. *Nature structural & molecular biology* 23, 6, 540–548.

[199] Korb, E., Herre, M., Zucker-Scharff, I., Darnell, R. B., and Allis, C. D. 2015. BET protein Brd4 activates transcription in neurons and BET inhibitor Jq1 blocks memory in mice. *Nature neuroscience* 18, 10, 1464–1473.

[200] Konuma, T., Di Yu, Zhao, C., Ju, Y., Sharma, R., Ren, C., Zhang, Q., Zhou, M.-M., and Zeng, L. 2017. Structural Mechanism of the Oxygenase JMJD6 Recognition by the Extraterminal (ET) Domain of BRD4. *Scientific reports* 7, 1, 16272.

[201] Rahman, S., Sowa, M. E., Ottinger, M., Smith, J. A., Shi, Y., Harper, J. W., and Howley, P. M. 2011. The Brd4 extraterminal domain confers transcription activation independent of pTEFb by recruiting multiple proteins, including NSD3. *Mol. Cell. Biol.* 31, 13, 2641–2652.

[202] Wu, T., Kamikawa, Y. F., and Donohoe, M. E. 2018. Brd4's Bromodomains Mediate Histone H3 Acetylation and Chromatin Remodeling in Pluripotent Cells through P300 and Brg1. *Cell Reports* 25, 7, 1756–1771.

[203] Taves, M. D., Gomez-Sanchez, C. E., and Soma, K. K. 2011. Extra-adrenal glucocorticoids and mineralocorticoids: evidence for local synthesis, regulation, and function. *American journal of physiology. Endocrinology and metabolism* 301, 1, E11-24.

[204] van Staa, T. P., Leufkens, H. G., Abenhaim, L., Begaud, B., Zhang, B., and Cooper, C. 2000. Use of oral corticosteroids in the United Kingdom. *QJM : monthly journal of the Association of Physicians* 93, 2, 105–111.

[205] Grad, I. and Picard, D. 2007. The glucocorticoid responses are shaped by molecular chaperones. *Molecular and cellular endocrinology* 275, 1-2, 2–12.

[206] Beato, M. 1989. Gene regulation by steroid hormones. *Cell* 56, 3, 335–344.

[207] Surjit, M., Ganti, K. P., Mukherji, A., Ye, T., Hua, G., Metzger, D., Li, M., and Chambon, P. 2011. Widespread negative response elements mediate direct repression by agonist-liganded glucocorticoid receptor. *Cell* 145, 2, 224–241.

[208] Rogatsky, I. and Ivashkiv, L. B. 2006. Glucocorticoid modulation of cytokine signaling. *Tissue antigens* 68, 1, 1–12.

[209] Nissen, R. M. and Yamamoto, K. R. 2000. The glucocorticoid receptor inhibits NFkappaB by interfering with serine-2 phosphorylation of the RNA polymerase II carboxy-terminal domain. *Genes Dev.* 14, 18, 2314–2329.

[210] Yang-Yen, H. F., Chambard, J. C., Sun, Y. L., Smeal, T., Schmidt, T. J., Drouin, J., and Karin, M. 1990. Transcriptional interference between c-Jun and the glucocorticoid receptor: mutual inhibition of DNA binding due to direct protein-protein interaction. *Cell* 62, 6, 1205–1215.

[211] McDonough, A. K., Curtis, J. R., and Saag, K. G. 2008. The epidemiology of glucocorticoid-associated adverse events. *Current opinion in rheumatology* 20, 2, 131–137.

[212] Cavaillon, J.-M. 2021. Once upon a time, inflammation. *The journal of venomous animals and toxins including tropical diseases* 27, e20200147.

[213] Jack, D. B. 1997. One hundred years of aspirin. *Lancet (London, England)* 350, 9075, 437–439.

[214] Desborough, M. J. R. and Keeling, D. M. 2017. The aspirin story - from willow to wonder drug. *British journal of haematology* 177, 5, 674–683.

[215] Sneader, W. 2000. The discovery of aspirin: a reappraisal. *BMJ (Clinical research ed.)* 321, 7276, 1591–1594.

[216] Vane, J. R. 1971. Inhibition of prostaglandin synthesis as a mechanism of action for aspirin-like drugs. *Nature: New biology* 231, 25, 232–235.

[217] Hawkey, C. J. 2005. COX-2 chronology. *Gut* 54, 11, 1509–1514.

[218] Mitchell, J. A., Akarasereenont, P., Thiemermann, C., Flower, R. J., and Vane, J. R. 1993. Selectivity of nonsteroidal antiinflammatory drugs as inhibitors of constitutive and inducible cyclooxygenase. *Proceedings of the National Academy of Sciences of the United States of America* 90, 24, 11693–11697.

[219] Funk, C. D. and FitzGerald, G. A. 2007. COX-2 inhibitors and cardiovascular risk. *Journal of cardiovascular pharmacology* 50, 5, 470–479.

[220] Das, U. N. 2005. Can COX-2 inhibitor-induced increase in cardiovascular disease risk be modified by essential fatty acids? *The Journal of the Association of Physicians of India* 53, 623–627.

[221] Sinniah, A., Yazid, S., and Flower, R. J. 2021. From NSAIDs to Glucocorticoids and Beyond. *Cells* 10, 12.

[222] Abdulla, A., Adams, N., Bone, M., Elliott, A. M., Gaffin, J., Jones, D., Knaggs, R., Martin, D., Sampson, L., and Schofield, P. 2013. Guidance on the management of pain in older people. *Age and ageing* 42 Suppl 1, i1-57.

[223] Onder, G., Pellicciotti, F., Gambassi, G., and Bernabei, R. 2004. NSAID-related psychiatric adverse events: who is at risk? *Drugs* 64, 23, 2619–2627.

[224] Sramek, M., Neradil, J., and Veselska, R. 2017. Much more than you expected: The non-DHFR-mediated effects of methotrexate. *Biochimica et biophysica acta. General subjects* 1861, 3, 499–503.

[225] Chan, E. S. L. and Cronstein, B. N. 2002. Molecular action of methotrexate in inflammatory diseases. *Arthritis research* 4, 4, 266–273.

[226] Belgi, G. and Friedmann, P. S. 2002. Traditional therapies: glucocorticoids, azathioprine, methotrexate, hydroxyurea. *Clinical and experimental dermatology* 27, 7, 546–554.

[227] Bangert, C. A. and Costner, M. I. 2007. Methotrexate in dermatology. *Dermatologic therapy* 20, 4, 216–228.

[228] Genestier, L., Paillot, R., Fournel, S., Ferraro, C., Miossec, P., and Revillard, J. P. 1998. Immunosuppressive properties of methotrexate: apoptosis and clonal deletion of activated peripheral T cells. *J. Clin. Invest.* 102, 2, 322–328.

[229] Silva, M. A., Klafke, J. Z., Rossato, M. F., Gewehr, C., Guerra, G. P., Rubin, M. A., and Ferreira, J. 2011. Role of peripheral polyamines in the development of inflammatory pain. *Biochemical pharmacology* 82, 3, 269–277.

[230] Flescher, E., Fossum, D., and Talal, N. 1991. Polyamine-dependent production of lymphocytotoxic levels of ammonia by human peripheral blood monocytes. *Immunology letters* 28, 1, 85–89.

[231] Rainsford, K. D., Parke, A. L., Clifford-Rashotte, M., and Kean, W. F. 2015. Therapy and pharmacological properties of hydroxychloroquine and chloroquine in treatment of systemic lupus erythematosus, rheumatoid arthritis and related diseases. *Inflammopharmacology* 23, 5, 231–269.

[232] Costedoat-Chalumeau, N., Dunogué, B., Morel, N., Le Guern, V., and Guettrot-Imbert, G. 2014. Hydroxychloroquine: a multifaceted treatment in lupus. *Presse medicale (Paris, France : 1983)* 43, 6 Pt 2, e167-80.

[233] Lee, S.-J., Silverman, E., and Bargman, J. M. 2011. The role of antimalarial agents in the treatment of SLE and lupus nephritis. *Nature reviews. Nephrology* 7, 12, 718–729.

[234] Padjen, I., Crnogaj, M. R., and Anić, B. 2020. Conventional disease-modifying agents in rheumatoid arthritis - a review of their current use and role in treatment algorithms. *Reumatologia* 58, 6, 390–400.

[235] Aletaha, D. and Smolen, J. S. 2018. Diagnosis and Management of Rheumatoid Arthritis: A Review. *JAMA* 320, 13, 1360–1372.

[236] Harrington, R., Al Nokhatha, S. A., and Conway, R. 2020. JAK Inhibitors in Rheumatoid Arthritis: An Evidence-Based Review on the Emerging Clinical Data. *Journal of inflammation research* 13, 519–531.

[237] Edwards, C. J., Blanco, F. J., Crowley, J., Birbara, C. A., Jaworski, J., Aelion, J., Stevens, R. M., Vessey, A., Zhan, X., and Bird, P. 2016. Apremilast, an oral phosphodiesterase 4 inhibitor, in patients with psoriatic arthritis and current skin involvement: a phase III, randomised, controlled trial (PALACE 3). *Annals of the rheumatic diseases* 75, 6, 1065–1073.

[238] Guagnozzi, D. and Caprilli, R. 2008. Natalizumab in the treatment of Crohn's disease. *Biologics : targets & therapy* 2, 2, 275–284.

[239] Caprilli, R. 2008. Natalizumab in the treatment of Crohn’s disease. *BTT*, 275.

[240] Blair, H. A. 2020. Crizanlizumab: First Approval. *Drugs* 80, 1, 79–84.

[241] McLean, L. P., Shea-Donohue, T., and Cross, R. K. 2012. Vedolizumab for the treatment of ulcerative colitis and Crohn's disease. *Immunotherapy* 4, 9, 883–898.

[242] Saltmarsh, M. and Goldberg, G. 2003. Miscellaneous Foods. In *Plants: Diet and Health*, G. Goldberg, Ed. Wiley, 210–225.

[243] Clardy, J., Fischbach, M. A., and Currie, C. R. 2009. The natural history of antibiotics. *Current biology : CB* 19, 11, R437-R441.

[244] Jung, H.-J., Kim, S.-G., Nam, J.-H., Park, K.-K., Chung, W.-Y., Kim, W.-B., Lee, K.-T., Won, J.-H., Choi, J.-W., and Park, H.-J. 2005. Isolation of Saponins with the Inhibitory Effect on Nitric Oxide, Prostaglandin E2 and Tumor Necrosis Factor-.ALPHA. Production from Pleurospermum kamtschaticum. *Biological & Pharmaceutical Bulletin* 28, 9, 1668–1671.

[245] Camacho-Barquero, L., Villegas, I., Sánchez-Calvo, J. M., Talero, E., Sánchez-Fidalgo, S., Motilva, V., and La Alarcón de Lastra, C. 2007. Curcumin, a Curcuma longa constituent, acts on MAPK p38 pathway modulating COX-2 and iNOS expression in chronic experimental colitis. *International immunopharmacology* 7, 3, 333–342.

[246] Kong, R., Kang, O.-H., Seo, Y.-S., Zhou, T., Kim, S.-A., Shin, D.-W., and Kwon, D.-Y. 2018. MAPKs and NF-κB pathway inhibitory effect of bisdemethoxycurcumin on phorbol-12-myristate-13-acetate and A23187-induced inflammation in human mast cells. *Molecular medicine reports* 17, 1, 630–635.

[247] Leclercq, I. A., Farrell, G. C., Sempoux, C., dela Peña, A., and Horsmans, Y. 2004. Curcumin inhibits NF-kappaB activation and reduces the severity of experimental steatohepatitis in mice. *Journal of hepatology* 41, 6, 926–934.

[248] Jiang, H., Deng, C.-S., Zhang, M., and Xia, J. 2006. Curcumin-attenuated trinitrobenzene sulphonic acid induces chronic colitis by inhibiting expression of cyclooxygenase-2. *World journal of gastroenterology* 12, 24, 3848–3853.

[249] Ammon, H. P., Safayhi, H., Mack, T., and Sabieraj, J. 1993. Mechanism of antiinflammatory actions of curcumine and boswellic acids. *Journal of ethnopharmacology* 38, 2-3, 113–119.

[250] Srivastava, K. C., Bordia, A., and Verma, S. K. 1995. Curcumin, a major component of food spice turmeric (Curcuma longa) inhibits aggregation and alters eicosanoid metabolism in human blood platelets. *Prostaglandins, leukotrienes, and essential fatty acids* 52, 4, 223–227.

[251] Kobayashi, T., Hashimoto, S., and Horie, T. 1997. Curcumin inhibition of Dermatophagoides farinea-induced interleukin-5 (IL-5) and granulocyte macrophage-colony stimulating factor (GM-CSF) production by lymphocytes from bronchial asthmatics. *Biochemical pharmacology* 54, 7, 819–824.

[252] Kang, B. Y., Chung, S. W., Chung, W., Im, S., Hwang, S. Y., and Kim, T. S. 1999. Inhibition of interleukin-12 production in lipopolysaccharide-activated macrophages by curcumin. *European journal of pharmacology* 384, 2-3, 191–195.

[253] Li-Weber, M., Giaisi, M., Treiber, M. K., and Krammer, P. H. 2002. The anti-inflammatory sesquiterpene lactone parthenolide suppresses IL-4 gene expression in peripheral blood T. *European journal of immunology* 32, 12, 3587–3597.

[254] Jain, N. K. and Kulkarni, S. K. 1999. Antinociceptive and anti-inflammatory effects of Tanacetum parthenium L. extract in mice and rats. *Journal of ethnopharmacology* 68, 1-3, 251–259.

[255] Tassorelli, C., Greco, R., Morazzoni, P., Riva, A., Sandrini, G., and Nappi, G. 2005. Parthenolide is the component of tanacetum parthenium that inhibits nitroglycerin-induced Fos activation: studies in an animal model of migraine. *Cephalalgia : an international journal of headache* 25, 8, 612–621.

[256] Smolinski, A. T. and Pestka, J. J. 2003. Modulation of lipopolysaccharide-induced proinflammatory cytokine production in vitro and in vivo by the herbal constituents apigenin (chamomile), ginsenoside Rb(1) (ginseng) and parthenolide (feverfew). *Food and chemical toxicology : an international journal published for the British Industrial Biological Research Association* 41, 10, 1381–1390.

[257] Johnson, S. 1986. *Feverfew. [a traditional herbal remedy for migraine and arthritis]*. Overcoming common problems. Sheldon Press, London.

[258] Fukuda, K., Hibiya, Y., Mutoh, M., Ohno, Y., Yamashita, K., Akao, S., and Fujiwara, H. 2000. Inhibition by parthenolide of phorbol ester-induced transcriptional activation of inducible nitric oxide synthase gene in a human monocyte cell line THP-1. *Biochemical pharmacology* 60, 4, 595–600.

[259] Piela-Smith, T. H. and Liu, X. 2001. Feverfew extracts and the sesquiterpene lactone parthenolide inhibit intercellular adhesion molecule-1 expression in human synovial fibroblasts. *Cellular immunology* 209, 2, 89–96.

[260] Kang, B. Y., Chung, S. W., and Kim, T. S. 2001. Inhibition of interleukin-12 production in lipopolysaccharide-activated mouse macrophages by parthenolide, a predominant sesquiterpene lactone in Tanacetum parthenium: involvement of nuclear factor-kappaB. *Immunology letters* 77, 3, 159–163.

[261] Hwang, D., Fischer, N. H., Jang, B. C., Tak, H., Kim, J. K., and Lee, W. 1996. Inhibition of the expression of inducible cyclooxygenase and proinflammatory cytokines by sesquiterpene lactones in macrophages correlates with the inhibition of MAP kinases. *Biochemical and biophysical research communications* 226, 3, 810–818.

[262] Mazor, R. L., Menendez, I. Y., Ryan, M. A., Fiedler, M. A., and Wong, H. R. 2000. Sesquiterpene lactones are potent inhibitors of interleukin 8 gene expression in cultured human respiratory epithelium. *Cytokine* 12, 3, 239–245.

[263] COOK, N. 1996. Flavonoids?Chemistry, metabolism, cardioprotective effects, and dietary sources. *Journal of the European Ceramic Society*, 66–76.

[264] Chekalina, N., Burmak, Y., Petrov, Y., Borisova, Z., Manusha, Y., Kazakov, Y., and Kaidashev, I. 2018. Quercetin reduces the transcriptional activity of NF-kB in stable coronary artery disease. *Indian heart journal* 70, 5, 593–597.

[265] Indra, M. R., Karyono, S., Ratnawati, R., and Malik, S. G. 2013. Quercetin suppresses inflammation by reducing ERK1/2 phosphorylation and NF kappa B activation in Leptin-induced Human Umbilical Vein Endothelial Cells (HUVECs). *BMC research notes* 6, 275.

[266] Tang, X.-L., Liu, J.-X., Dong, W., Li, P., Li, L., Zheng, Y.-Q., and Hou, J.-C. 2014. Intervention effect of quercetin on inflammatory secretion of cardiac fibroblasts. *Zhongguo Zhong yao za zhi = Zhongguo zhongyao zazhi = China journal of Chinese materia medica* 39, 12, 2314–2317.

[267] Maplestone, R. A., Stone, M. J., and Williams, D. H. 1992. The evolutionary role of secondary metabolites--a review. *Gene* 115, 1-2, 151–157.

[268] Goodson, H. V. and Jonasson, E. M. 2018. Microtubules and Microtubule-Associated Proteins. *Cold Spring Harbor perspectives in biology* 10, 6.

[269] Akhmanova, A. and Steinmetz, M. O. 2008. Tracking the ends: a dynamic protein network controls the fate of microtubule tips. *Nature reviews. Molecular cell biology* 9, 4, 309–322.

[270] Akhmanova, A. and Hoogenraad, C. C. 2015. Microtubule minus-end-targeting proteins. *Current biology : CB* 25, 4, R162-71.

[271] Delgehyr, N., Sillibourne, J., and Bornens, M. 2005. Microtubule nucleation and anchoring at the centrosome are independent processes linked by ninein function. *Journal of cell science* 118, Pt 8, 1565–1575.

[272] Mitchison, T. and Kirschner, M. 1984. Dynamic instability of microtubule growth. *Nature* 312, 5991, 237–242.

[273] Gudimchuk, N. B. and McIntosh, J. R. 2021. Regulation of microtubule dynamics, mechanics and function through the growing tip. *Nature reviews. Molecular cell biology* 22, 12, 777–795.

[274] Mandelkow, E. M., Mandelkow, E., and Milligan, R. A. 1991. Microtubule dynamics and microtubule caps: a time-resolved cryo-electron microscopy study. *The Journal of Cell Biology* 114, 5, 977–991.

[275] Aldaz, H., Rice, L. M., Stearns, T., and Agard, D. A. 2005. Insights into microtubule nucleation from the crystal structure of human gamma-tubulin. *Nature* 435, 7041, 523–527.

[276] Buey, R. M., Díaz, J. F., and Andreu, J. M. 2006. The nucleotide switch of tubulin and microtubule assembly: a polymerization-driven structural change. *Biochemistry* 45, 19, 5933–5938.

[277] Nawrotek, A., Knossow, M., and Gigant, B. 2011. The determinants that govern microtubule assembly from the atomic structure of GTP-tubulin. *Journal of molecular biology* 412, 1, 35–42.

[278] Pecqueur, L., Duellberg, C., Dreier, B., Jiang, Q., Wang, C., Plückthun, A., Surrey, T., Gigant, B., and Knossow, M. 2012. A designed ankyrin repeat protein selected to bind to tubulin caps the microtubule plus end. *Proceedings of the National Academy of Sciences of the United States of America* 109, 30, 12011–12016.

[279] Barlan, K. and Gelfand, V. I. 2017. Microtubule-Based Transport and the Distribution, Tethering, and Organization of Organelles. *Cold Spring Harbor perspectives in biology* 9, 5.

[280] Sweeney, H. L. and Holzbaur, E. L. F. 2018. Motor Proteins. *Cold Spring Harbor perspectives in biology* 10, 5.

[281] Barlan, K., Lu, W., and Gelfand, V. I. 2013. The microtubule-binding protein ensconsin is an essential cofactor of kinesin-1. *Current biology : CB* 23, 4, 317–322.

[282] Dixit, R., Ross, J. L., Goldman, Y. E., and Holzbaur, E. L. F. 2008. Differential regulation of dynein and kinesin motor proteins by tau. *Science (New York, N.Y.)* 319, 5866, 1086–1089.

[283] Nihalani, D., Wong, H. N., and Holzman, L. B. 2003. Recruitment of JNK to JIP1 and JNK-dependent JIP1 phosphorylation regulates JNK module dynamics and activation. *Journal of Biological Chemistry* 278, 31, 28694–28702.

[284] Zeke, A., Misheva, M., Reményi, A., and Bogoyevitch, M. A. 2016. JNK Signaling: Regulation and Functions Based on Complex Protein-Protein Partnerships. *Microbiology and molecular biology reviews : MMBR* 80, 3, 793–835.

[285] Whisenant, T. C., Ho, D. T., Benz, R. W., Rogers, J. S., Kaake, R. M., Gordon, E. A., Huang, L., Baldi, P., and Bardwell, L. 2010. Computational prediction and experimental verification of new MAP kinase docking sites and substrates including Gli transcription factors. *PLoS computational biology* 6, 8.

[286] Pérez-Peña, H., Abel, A.-C., Shevelev, M., Prota, A. E., Pieraccini, S., and Horvath, D. 2023. Computational Approaches to the Rational Design of Tubulin-Targeting Agents. *Biomolecules* 13, 2.

[287] Elie-Caille, C., Severin, F., Helenius, J., Howard, J., Muller, D. J., and Hyman, A. A. 2007. Straight GDP-tubulin protofilaments form in the presence of taxol. *Current biology : CB* 17, 20, 1765–1770.

[288] Alushin, G. M., Lander, G. C., Kellogg, E. H., Zhang, R., Baker, D., and Nogales, E. 2014. High-resolution microtubule structures reveal the structural transitions in αβ-tubulin upon GTP hydrolysis. *Cell* 157, 5, 1117–1129.

[289] Löwe, J., Li, H., Downing, K. H., and Nogales, E. 2001. Refined structure of alpha beta-tubulin at 3.5 A resolution. *Journal of molecular biology* 313, 5, 1045–1057.

[290] Prota, A. E., Bargsten, K., Zurwerra, D., Field, J. J., Díaz, J. F., Altmann, K.-H., and Steinmetz, M. O. 2013. Molecular mechanism of action of microtubule-stabilizing anticancer agents. *Science (New York, N.Y.)* 339, 6119, 587–590.

[291] Kellogg, E. H., Hejab, N. M. A., Howes, S., Northcote, P., Miller, J. H., Díaz, J. F., Downing, K. H., and Nogales, E. 2017. Insights into the Distinct Mechanisms of Action of Taxane and Non-Taxane Microtubule Stabilizers from Cryo-EM Structures. *Journal of molecular biology* 429, 5, 633–646.

[292] Prota, A. E., Bargsten, K., Northcote, P. T., Marsh, M., Altmann, K.-H., Miller, J. H., Díaz, J. F., and Steinmetz, M. O. 2014. Structural basis of microtubule stabilization by laulimalide and peloruside A. *Angewandte Chemie (International ed. in English)* 53, 6, 1621–1625.

[293] Dorléans, A., Gigant, B., Ravelli, R. B. G., Mailliet, P., Mikol, V., and Knossow, M. 2009. Variations in the colchicine-binding domain provide insight into the structural switch of tubulin. *Proceedings of the National Academy of Sciences of the United States of America* 106, 33, 13775–13779.

[294] Ravelli, R. B. G., Gigant, B., Curmi, P. A., Jourdain, I., Lachkar, S., Sobel, A., and Knossow, M. 2004. Insight into tubulin regulation from a complex with colchicine and a stathmin-like domain. *Nature* 428, 6979, 198–202.

[295] Gigant, B., Wang, C., Ravelli, R. B. G., Roussi, F., Steinmetz, M. O., Curmi, P. A., Sobel, A., and Knossow, M. 2005. Structural basis for the regulation of tubulin by vinblastine. *Nature* 435, 7041, 519–522.

[296] Cormier, A., Marchand, M., Ravelli, R. B. G., Knossow, M., and Gigant, B. 2008. Structural insight into the inhibition of tubulin by vinca domain peptide ligands. *EMBO Reports* 9, 11, 1101–1106.

[297] Maderna, A., Doroski, M., Subramanyam, C., Porte, A., Leverett, C. A., Vetelino, B. C., Chen, Z., Risley, H., Parris, K., Pandit, J., Varghese, A. H., Shanker, S., Song, C., Sukuru, S. C. K., Farley, K. A., Wagenaar, M. M., Shapiro, M. J., Musto, S., Lam, M.-H., Loganzo, F., and O'Donnell, C. J. 2014. Discovery of cytotoxic dolastatin 10 analogues with N-terminal modifications. *Journal of medicinal chemistry* 57, 24, 10527–10543.

[298] Prota, A. E., Bargsten, K., Diaz, J. F., Marsh, M., Cuevas, C., Liniger, M., Neuhaus, C., Andreu, J. M., Altmann, K.-H., and Steinmetz, M. O. 2014. A new tubulin-binding site and pharmacophore

for microtubule-destabilizing anticancer drugs. *Proceedings of the National Academy of Sciences of the United States of America* 111, 38, 13817–13821.

[299] Prota, A. E., Setter, J., Waight, A. B., Bargsten, K., Murga, J., Diaz, J. F., and Steinmetz, M. O. 2016. Pironetin Binds Covalently to αCys316 and Perturbs a Major Loop and Helix of α-Tubulin to Inhibit Microtubule Formation. *Journal of molecular biology* 428, 15, 2981–2988.

[300] Yang, J., Wang, Y., Wang, T., Jiang, J., Botting, C. H., Liu, H., Chen, Q., Yang, J., Naismith, J. H., Zhu, X., and Chen, L. 2016. Pironetin reacts covalently with cysteine-316 of α-tubulin to destabilize microtubule. *Nature communications* 7, 12103.

[301] Matthew, S., Chen, Q.-Y., Ratnayake, R., Fermaintt, C. S., Lucena-Agell, D., Bonato, F., Prota, A. E., Lim, S. T., Wang, X., Díaz, J. F., Risinger, A. L., Paul, V. J., Oliva, M. Á., and Luesch, H. 2021. Gatorbulin-1, a distinct cyclodepsipeptide chemotype, targets a seventh tubulin pharmacological site. *Proceedings of the National Academy of Sciences of the United States of America* 118, 9.

[302] Mühlethaler, T., Gioia, D., Prota, A. E., Sharpe, M. E., Cavalli, A., and Steinmetz, M. O. 2021. Comprehensive Analysis of Binding Sites in Tubulin. *Angewandte Chemie (International ed. in English)* 60, 24, 13331–13342.

[303] Mühlethaler, T., Milanos, L., Ortega, J. A., Blum, T. B., Gioia, D., Roy, B., Prota, A. E., Cavalli, A., and Steinmetz, M. O. 2022. Rational Design of a Novel Tubulin Inhibitor with a Unique Mechanism of Action. *Angewandte Chemie (International ed. in English)* 61, 25, e202204052.

[304] Kufe, D. W., Holland, J. F., and Frei, E. 2003. *Cancer medicine 6*. BC Decker, Hamilton Ont., Lewiston NY.

[305] Moudi, M., Go, R., Yien, C. Y. S., and Nazre, M. 2013. Vinca Alkaloids. *International Journal of Preventive Medicine* 4, 11, 1231–1235.

[306] Himes, R. H. 1991. Interactions of the catharanthus (Vinca) alkaloids with tubulin and microtubules. *Pharmacology & therapeutics* 51, 2, 257–267.

[307] Vacca, A., Iurlaro, M., Ribatti, D., Minischetti, M., Nico, B., Ria, R., Pellegrino, A., and Dammacco, F. 1999. Antiangiogenesis is produced by nontoxic doses of vinblastine. *Blood* 94, 12, 4143–4155.

[308] Hildebrand, J., Kenis, Y., Mubashir, B. A., and Bart, J. B. 1972. Vincristine neurotoxicity. *The New England journal of medicine* 287, 10, 517.

[309] Arnst, J. 2020. When Taxol met tubulin. *The Journal of biological chemistry* 295, 41, 13994–13995.

[310] Manfredi, J. J. and Horwitz, S. B. 1984. Taxol: an antimitotic agent with a new mechanism of action. *Pharmacology & therapeutics* 25, 1, 83–125.

[311] Bozkurt, M., Amlashi, F. G., and Blum Murphy, M. 2017. The role of chemotherapy in unresectable or metastatic adenocarcinoma of the stomach and gastroesophageal junction. *Minerva chirurgica* 72, 4, 317–333.

[312] McGuire, W. P., Hoskins, W. J., Brady, M. F., Kucera, P. R., Partridge, E. E., Look, K. Y., Clarke-Pearson, D. L., and Davidson, M. 1997. Comparison of combination therapy with paclitaxel and cisplatin versus cyclophosphamide and cisplatin in patients with suboptimal stage III and stage IV ovarian cancer: a Gynecologic Oncology Group study. *Seminars in oncology* 24, 1 Suppl 2, S2-13-S2-16.

[313] Loesch, D., Greco, F. A., Senzer, N. N., Burris, H. A., Hainsworth, J. D., Jones, S., Vukelja, S. J., Sandbach, J., Holmes, F., Sedlacek, S., Pippen, J., Lindquist, D., McIntyre, K., Blum, J. L., Modiano, M. R., Boehm, K. A., Zhan, F., Asmar, L., and Robert, N. 2010. Phase III multicenter trial of doxorubicin plus cyclophosphamide followed by paclitaxel compared with doxorubicin plus paclitaxel followed by weekly paclitaxel as adjuvant therapy for women with high-risk breast cancer. *Journal of clinical oncology : official journal of the American Society of Clinical Oncology* 28, 18, 2958–2965.

[314] Ohe, Y., Ohashi, Y., Kubota, K., Tamura, T., Nakagawa, K., Negoro, S., Nishiwaki, Y., Saijo, N., Ariyoshi, Y., and Fukuoka, M. 2007. Randomized phase III study of cisplatin plus irinotecan versus carboplatin plus paclitaxel, cisplatin plus gemcitabine, and cisplatin plus vinorelbine for

advanced non-small-cell lung cancer: Four-Arm Cooperative Study in Japan. *Annals of oncology : official journal of the European Society for Medical Oncology* 18, 2, 317–323.

[315] van Hagen, P., Hulshof, M. C. C. M., van Lanschot, J. J. B., Steyerberg, E. W., van Berge Henegouwen, M. I., Wijnhoven, B. P. L., Richel, D. J., Nieuwenhuijzen, G. A. P., Hospers, G. A. P., Bonenkamp, J. J., Cuesta, M. A., Blaisse, R. J. B., Busch, O. R. C., Kate, F. J. W. ten, Creemers, G.-J., Punt, C. J. A., Plukker, J. T. M., Verheul, H. M. W., Spillenaar Bilgen, E. J., van Dekken, H., van der Sangen, M. J. C., Rozema, T., Biermann, K., Beukema, J. C., Piet, A. H. M., van Rij, C. M., Reinders, J. G., Tilanus, H. W., and van der Gaast, A. 2012. Preoperative chemoradiotherapy for esophageal or junctional cancer. *The New England journal of medicine* 366, 22, 2074–2084.

[316] Csordás, G. and Hajnóczky, G. 2009. SR/ER-mitochondrial local communication: calcium and ROS. *Biochimica et biophysica acta* 1787, 11, 1352–1362.

[317] Ferlini, C., Cicchillitti, L., Raspaglio, G., Bartollino, S., Cimitan, S., Bertucci, C., Mozzetti, S., Gallo, D., Persico, M., Fattorusso, C., Campiani, G., and Scambia, G. 2009. Paclitaxel directly binds to Bcl-2 and functionally mimics activity of Nur77. *Cancer research* 69, 17, 6906–6914.

[318] Li, M., Yin, L., Wu, L., Zhu, Y., and Wang, X. 2020. Paclitaxel inhibits proliferation and promotes apoptosis through regulation ROS and endoplasmic reticulum stress in osteosarcoma cell. *Mol. Cell. Toxicol.* 16, 4, 377–384.

[319] Mikuła-Pietrasik, J., Witucka, A., Pakuła, M., Uruski, P., Begier-Krasińska, B., Niklas, A., Tykarski, A., and Książek, K. 2019. Comprehensive review on how platinum- and taxane-based chemotherapy of ovarian cancer affects biology of normal cells. *Cellular and molecular life sciences : CMLS* 76, 4, 681–697.

[320] Ren, X., Zhao, B., Chang, H., Xiao, M., Wu, Y., and Liu, Y. 2018. Paclitaxel suppresses proliferation and induces apoptosis through regulation of ROS and the AKT/MAPK signaling pathway in canine mammary gland tumor cells. *Molecular medicine reports* 17, 6, 8289–8299.

[321] Strobel, T., Swanson, L., Korsmeyer, S., and Cannistra, S. A. 1996. BAX enhances paclitaxel-induced apoptosis through a p53-independent pathway. *Proceedings of the National Academy of Sciences of the United States of America* 93, 24, 14094–14099.

[322] Dasgeb, B., Kornreich, D., McGuinn, K., Okon, L., Brownell, I., and Sackett, D. L. 2018. Colchicine: an ancient drug with novel applications. *The British journal of dermatology* 178, 2, 350–356.

[323] Kumar, A., Sharma, P. R., and Mondhe, D. M. 2017. Potential anticancer role of colchicine-based derivatives: an overview. *Anti-cancer drugs* 28, 3, 250–262.

[324] Leung, Y. Y., Yao Hui, L. L., and Kraus, V. B. 2015. Colchicine--Update on mechanisms of action and therapeutic uses. *Seminars in arthritis and rheumatism* 45, 3, 341–350.

[325] Robertson, S., Martínez, G. J., Payet, C. A., Barraclough, J. Y., Celermajer, D. S., Bursill, C., and Patel, S. 2016. Colchicine therapy in acute coronary syndrome patients acts on caspase-1 to suppress NLRP3 inflammasome monocyte activation. *Clinical science (London, England : 1979)* 130, 14, 1237–1246.

[326] Ben-Chetrit, E., Bergmann, S., and Sood, R. 2006. Mechanism of the anti-inflammatory effect of colchicine in rheumatic diseases: a possible new outlook through microarray analysis. *Rheumatology (Oxford, England)* 45, 3, 274–282.

[327] Phelps, P. 2008. Polymorphonuclear leukocyte motility in vitro: IV. Colchicine inhibition of chemotactic activity formation after phagocytosis of urate crystals. *Arthritis and rheumatism* 58, 2 Suppl, S25-33.

[328] Cronstein, B. N., Molad, Y., Reibman, J., Balakhane, E., Levin, R. I., and Weissmann, G. 1995. Colchicine alters the quantitative and qualitative display of selectins on endothelial cells and neutrophils. *The Journal of clinical investigation* 96, 2, 994–1002.

[329] Masson, W., Lobo, M., Molinero, G., Masson, G., and Lavalle-Cobo, A. 2020. Role of Colchicine in Stroke Prevention: An Updated Meta-Analysis. *Journal of stroke and cerebrovascular diseases : the official journal of National Stroke Association* 29, 5, 104756.

[330] Meyer-Lindemann, U., Mauersberger, C., Schmidt, A.-C., Moggio, A., Hinterdobler, J., Li, X., Khangholi, D., Hettwer, J., Gräßer, C., Dutsch, A., Schunkert, H., Kessler, T., and Sager, H. B.

2022. Colchicine Impacts Leukocyte Trafficking in Atherosclerosis and Reduces Vascular Inflammation. *Frontiers in immunology* 13, 898690.

[331] Dalbeth, N., Lauterio, T. J., and Wolfe, H. R. 2014. Mechanism of action of colchicine in the treatment of gout. *Clinical therapeutics* 36, 10, 1465–1479.

[332] Ng, G., Sharma, K., Ward, S. M., Desrosiers, M. D., Stephens, L. A., Schoel, W. M., Li, T., Lowell, C. A., Ling, C.-C., Amrein, M. W., and Shi, Y. 2008. Receptor-independent, direct membrane binding leads to cell-surface lipid sorting and Syk kinase activation in dendritic cells. *Immunity* 29, 5, 807–818.

[333] Zhou, R., Tardivel, A., Thorens, B., Choi, I., and Tschopp, J. 2010. Thioredoxin-interacting protein links oxidative stress to inflammasome activation. *Nature immunology* 11, 2, 136–140.

[334] Dostert, C., Pétrilli, V., van Bruggen, R., Steele, C., Mossman, B. T., and Tschopp, J. 2008. Innate immune activation through Nalp3 inflammasome sensing of asbestos and silica. *Science (New York, N.Y.)* 320, 5876, 674–677.

[335] Chen, C.-J., Shi, Y., Hearn, A., Fitzgerald, K., Golenbock, D., Reed, G., Akira, S., and Rock, K. L. 2006. MyD88-dependent IL-1 receptor signaling is essential for gouty inflammation stimulated by monosodium urate crystals. *J. Clin. Invest.* 116, 8, 2262–2271.

[336] Di Giovine, F. S., Malawista, S. E., Nuki, G., and Duff, G. W. 1987. Interleukin 1 (IL 1) as a mediator of crystal arthritis. Stimulation of T cell and synovial fibroblast mitogenesis by urate crystal-induced IL 1. *Journal of immunology (Baltimore, Md. : 1950)* 138, 10, 3213–3218.

[337] Shi, Y., Evans, J. E., and Rock, K. L. 2003. Molecular identification of a danger signal that alerts the immune system to dying cells. *Nature* 425, 6957, 516–521.

[338] Landis, R. C., Yagnik, D. R., Florey, O., Philippidis, P., Emons, V., Mason, J. C., and Haskard, D. O. 2002. Safe disposal of inflammatory monosodium urate monohydrate crystals by differentiated macrophages. *Arthritis and rheumatism* 46, 11, 3026–3033.

[339] Mariathasan, S., Newton, K., Monack, D. M., Vucic, D., French, D. M., Lee, W. P., Roose-Girma, M., Erickson, S., and Dixit, V. M. 2004. Differential activation of the inflammasome by caspase-1 adaptors ASC and Ipaf. *Nature* 430, 6996, 213–218.

[340] Martinon, F., Pétrilli, V., Mayor, A., Tardivel, A., and Tschopp, J. 2006. Gout-associated uric acid crystals activate the NALP3 inflammasome. *Nature* 440, 7081, 237–241.

[341] Tschopp, J., Martinon, F., and Burns, K. 2003. NALPs: a novel protein family involved in inflammation. *Nature reviews. Molecular cell biology* 4, 2, 95–104.

[342] Chappey, O. N., Niel, E., Wautier, J. L., Hung, P. P., Dervichian, M., Cattan, D., and Scherrmann, J. M. 1993. Colchicine disposition in human leukocytes after single and multiple oral administration. *Clinical pharmacology and therapeutics* 54, 4, 360–367.

[343] Ding, A. H., Porteu, F., Sanchez, E., and Nathan, C. F. 1990. Downregulation of tumor necrosis factor receptors on macrophages and endothelial cells by microtubule depolymerizing agents. *The Journal of Experimental Medicine* 171, 3, 715–727.

[344] Jackman, R. W., Rhoads, M. G., Cornwell, E., and Kandarian, S. C. 2009. Microtubule-mediated NF-kappaB activation in the TNF-alpha signaling pathway. *Experimental cell research* 315, 19, 3242–3249.

[345] Chia, E. W., Grainger, R., and Harper, J. L. 2008. Colchicine suppresses neutrophil superoxide production in a murine model of gouty arthritis: a rationale for use of low-dose colchicine. *British journal of pharmacology* 153, 6, 1288–1295.

[346] Roberge, C. J., Gaudry, M., Gilbert, C., Malawista, S. E., Médicis, R. de, Lussier, A., Poubelle, P. E., and Naccache, P. H. 1996. Paradoxical effects of colchicine on the activation of human neutrophilis by chemotactic factors and inflammatory microcrystal. *Journal of leukocyte biology* 59, 6, 864–871.

[347] 1997. A candidate gene for familial Mediterranean fever. *Nat Genet* 17, 1, 25–31.

[348] 1997. Ancient missense mutations in a new member of the RoRet gene family are likely to cause familial Mediterranean fever. The International FMF Consortium. *Cell* 90, 4, 797–807.

[349] Stoffels, M., Szperl, A., Simon, A., Netea, M. G., Plantinga, T. S., van Deuren, M., Kamphuis, S., Lachmann, H. J., Cuppen, E., Kloosterman, W. P., Frenkel, J., van Diemen, C. C., Wijmenga,

C., van Gijn, M., and van der Meer, J. W. M. 2014. MEFV mutations affecting pyrin amino acid 577 cause autosomal dominant autoinflammatory disease. *Annals of the rheumatic diseases* 73, 2, 455–461.

[350] Nair, J. R. and Moots, R. J. 2017. Behcet's disease. *Clinical medicine (London, England)* 17, 1, 71–77.

[351] Harper, R. M. and Allen, B. S. 1982. Use of colchicine in the treatment of Behçet's disease. *International journal of dermatology* 21, 9, 551–554.

[352] Wang, Z., Zu, X., Xiong, S., Mao, R., Qiu, Y., Chen, B., Zeng, Z., Chen, M., and He, Y. 2023. The Role of Colchicine in Different Clinical Phenotypes of Behcet Disease. *Clinical therapeutics* 45, 2, 162–176.

[353] Yurdakul, S., Mat, C., Tüzün, Y., Ozyazgan, Y., Hamuryudan, V., Uysal, O., Senocak, M., and Yazici, H. 2001. A double-blind trial of colchicine in Behçet's syndrome. *Arthritis and rheumatism* 44, 11, 2686–2692.

[354] Lazaros, G., Imazio, M., Brucato, A., Vlachopoulos, C., Lazarou, E., Vassilopoulos, D., and Tousoulis, D. 2018. The Role of Colchicine in Pericardial Syndromes. *Current pharmaceutical design* 24, 6, 702–709.

[355] Shah, S. R., Alweis, R., Shah, S. A., Arshad, M. H., Manji, A. A.-K., Arfeen, A. A., Javed, M., Shujauddin, S. M., Irfan, R., Shabbir, S., and Shaikh, S. 2016. Effects of colchicine on pericardial diseases: a review of the literature and current evidence. *Journal of community hospital internal medicine perspectives* 6, 3, 31957.

[356] Imazio, M., Bobbio, M., Cecchi, E., Demarie, D., Pomari, F., Moratti, M., Ghisio, A., Belli, R., and Trinchero, R. 2005. Colchicine as first-choice therapy for recurrent pericarditis: results of the CORE (COlchicine for REcurrent pericarditis) trial. *Archives of internal medicine* 165, 17, 1987–1991.

[357] Casula, M., Andreis, A., Avondo, S., Vaira, M. P., and Imazio, M. 2022. Colchicine for cardiovascular medicine: a systematic review and meta-analysis. *Future cardiology* 18, 8, 647–659.

[358] Weng, J.-H., Koch, P. D., Luan, H. H., Tu, H.-C., Shimada, K., Ngan, I., Ventura, R., Jiang, R., and Mitchison, T. J. 2021. Colchicine acts selectively in the liver to induce hepatokines that inhibit myeloid cell activation. *Nature metabolism* 3, 4, 513–522.

[359] Sandmann, A., Sasse, F., and Müller, R. 2004. Identification and analysis of the core biosynthetic machinery of tubulysin, a potent cytotoxin with potential anticancer activity. *Chemistry & biology* 11, 8, 1071–1079.

[360] Kretzschmann, V. K., Gellrich, D., Ullrich, A., Zahler, S., Vollmar, A. M., Kazmaier, U., and Fürst, R. 2014. Novel tubulin antagonist pretubulysin displays antivascular properties in vitro and in vivo. *ATVB* 34, 2, 294–303.

[361] Herrmann, J., Elnakady, Y. A., Wiedmann, R. M., Ullrich, A., Rohde, M., Kazmaier, U., Vollmar, A. M., and Müller, R. 2012. Pretubulysin: from hypothetical biosynthetic intermediate to potential lead in tumor therapy. *PloS one* 7, 5, e37416.

[362] Braig, S., Wiedmann, R. M., Liebl, J., Singer, M., Kubisch, R., Schreiner, L., Abhari, B. A., Wagner, E., Kazmaier, U., Fulda, S., and Vollmar, A. M. 2014. Pretubulysin: a new option for the treatment of metastatic cancer. *Cell death & disease* 5, 1, e1001.

[363] Schwenk, R., Stehning, T., Bischoff, I., Ullrich, A., Kazmaier, U., and Fürst, R. 2017. The pretubulysin-induced exposure of collagen is caused by endothelial cell retraction that results in an increased adhesion and decreased transmigration of tumor cells. *Oncotarget* 8, 44, 77622–77633.

[364] Rath, S., Liebl, J., Fürst, R., Ullrich, A., Burkhart, J. L., Kazmaier, U., Herrmann, J., Müller, R., Günther, M., Schreiner, L., Wagner, E., Vollmar, A. M., and Zahler, S. 2012. Anti-angiogenic effects of the tubulysin precursor pretubulysin and of simplified pretubulysin derivatives. *British journal of pharmacology* 167, 5, 1048–1061.

[365] Ullrich, A., Chai, Y., Pistorius, D., Elnakady, Y. A., Herrmann, J. E., Weissman, K. J., Kazmaier, U., and Müller, R. 2009. Pretubulysin, a potent and chemically accessible tubulysin

precursor from Angiococcus disciformis. *Angewandte Chemie (International ed. in English)* 48, 24, 4422–4425.

[366] Ades, E. W., Candal, F. J., Swerlick, R. A., George, V. G., Summers, S., Bosse, D. C., and Lawley, T. J. 1992. HMEC-1: establishment of an immortalized human microvascular endothelial cell line. *The Journal of investigative dermatology* 99, 6, 683–690.

[367] Tsuchiya, S., Yamabe, M., Yamaguchi, Y., Kobayashi, Y., Konno, T., and Tada, K. 1980. Establishment and characterization of a human acute monocytic leukemia cell line (THP-1). *International journal of cancer* 26, 2, 171–176.

[368] Jaffe, E. A., Nachman, R. L., Becker, C. G., and Minick, C. R. 1973. Culture of human endothelial cells derived from umbilical veins. Identification by morphologic and immunologic criteria. *The Journal of clinical investigation* 52, 11, 2745–2756.

[369] Nicoletti, I., Migliorati, G., Pagliacci, M. C., Grignani, F., and Riccardi, C. 1991. A rapid and simple method for measuring thymocyte apoptosis by propidium iodide staining and flow cytometry. *Journal of immunological methods* 139, 2, 271–279.

[370] van der Fits, L., Mourits, S., Voerman, J. S. A., Kant, M., Boon, L., Laman, J. D., Cornelissen, F., Mus, A.-M., Florencia, E., Prens, E. P., and Lubberts, E. 2009. Imiquimod-induced psoriasis-like skin inflammation in mice is mediated via the IL-23/IL-17 axis. *Journal of immunology (Baltimore, Md. : 1950)* 182, 9, 5836–5845.

[371] Gilliet, M., Conrad, C., Geiges, M., Cozzio, A., Thürlimann, W., Burg, G., Nestle, F. O., and Dummer, R. 2004. Psoriasis triggered by toll-like receptor 7 agonist imiquimod in the presence of dermal plasmacytoid dendritic cell precursors. *Archives of dermatology* 140, 12, 1490–1495.

[372] Miller, R. L., Gerster, J. F., Owens, M. L., Slade, H. B., and Tomai, M. A. 1999. Imiquimod applied topically: a novel immune response modifier and new class of drug. *International journal of immunopharmacology* 21, 1, 1–14.

[373] Baez, S. 1973. An open cremaster muscle preparation for the study of blood vessels by in vivo microscopy. *Microvascular research* 5, 3, 384–394.

[374] Mempel, T. R., Moser, C., Hutter, J., Kuebler, W. M., and Krombach, F. 2003. Visualization of leukocyte transendothelial and interstitial migration using reflected light oblique transillumination in intravital video microscopy. *Journal of vascular research* 40, 5, 435–441.

[375] Towbin, H., Staehelin, T., and Gordon, J. 1979. Electrophoretic transfer of proteins from polyacrylamide gels to nitrocellulose sheets: procedure and some applications. *Proceedings of the National Academy of Sciences of the United States of America* 76, 9, 4350–4354.

[376] Laemmli, U. K. 1970. Cleavage of structural proteins during the assembly of the head of bacteriophage T4. *Nature* 227, 5259, 680–685.

[377] Livak, K. J. and Schmittgen, T. D. 2001. Analysis of relative gene expression data using real-time quantitative PCR and the 2(-Delta Delta C(T)) Method. *Methods (San Diego, Calif.)* 25, 4, 402–408.

[378] Wang, H., Huang, W., Liang, M., Shi, Y., Zhang, C., Li, Q., Liu, M., Shou, Y., Yin, H., Zhu, X., Sun, X., Hu, Y., and Shen, Z. 2018. (+)-JQ1 attenuated LPS-induced microglial inflammation via MAPK/NFκB signaling. *Cell & bioscience* 8, 60.

[379] Filipčík, P., Latham, S. L., Cadell, A. L., Day, C. L., Croucher, D. R., and Mace, P. D. 2020. A cryptic tubulin-binding domain links MEKK1 to curved tubulin protomers. *Proceedings of the National Academy of Sciences of the United States of America* 117, 35, 21308–21318.

[380] Sontag, E., Nunbhakdi-Craig, V., Bloom, G. S., and Mumby, M. C. 1995. A novel pool of protein phosphatase 2A is associated with microtubules and is regulated during the cell cycle. *The Journal of Cell Biology* 128, 6, 1131–1144.

[381] Son, S., Shim, D.-W., Hwang, I., Park, J.-H., and Yu, J.-W. 2019. Chemotherapeutic Agent Paclitaxel Mediates Priming of NLRP3 Inflammasome Activation. *Frontiers in immunology* 10, 1108.

[382] Zhang, M., Lotfollahzadeh, S., Elzinad, N., Yang, X., Elsadawi, M., Gower, A., Belghasem, M., Shazly, T., Kolachalama, V. B., and Chitalia, V. 2023. Alleviating iatrogenic effects of paclitaxel via anti-inflammatory treatment. *Research square*.

[383] Olofsson, P. S., Söderström, L. A., Wågsäter, D., Sheikine, Y., Ocaya, P., Lang, F., Rabu, C., Chen, L., Rudling, M., Aukrust, P., Hedin, U., Paulsson-Berne, G., Sirsjö, A., and Hansson, G. K. 2008. CD137 is expressed in human atherosclerosis and promotes development of plaque inflammation in hypercholesterolemic mice. *Circulation* 117, 10, 1292–1301.

[384] Yuan, W., Xu, C., Li, B., Xia, H., Pan, Y., Zhong, W., Xu, L., Chen, R., and Wang, B. 2021. Contributions of Costimulatory Molecule CD137 in Endothelial Cells. *Journal of the American Heart Association* 10, 11, e020721.

[385] Faust, D., Schmitt, C., Oesch, F., Oesch-Bartlomowicz, B., Schreck, I., Weiss, C., and Dietrich, C. 2012. Differential p38-dependent signalling in response to cellular stress and mitogenic stimulation in fibroblasts. *Cell communication and signaling : CCS* 10, 6.

[386] Kyriakis, J. M., Banerjee, P., Nikolakaki, E., Dai, T., Rubie, E. A., Ahmad, M. F., Avruch, J., and Woodgett, J. R. 1994. The stress-activated protein kinase subfamily of c-Jun kinases. *Nature* 369, 6476, 156–160.

[387] Dérijard, B., Hibi, M., Wu, I. H., Barrett, T., Su, B., Deng, T., Karin, M., and Davis, R. J. 1994. JNK1: a protein kinase stimulated by UV light and Ha-Ras that binds and phosphorylates the c-Jun activation domain. *Cell* 76, 6, 1025–1037.

[388] Mooney, L. M. and Whitmarsh, A. J. 2004. Docking interactions in the c-Jun N-terminal kinase pathway. *The Journal of biological chemistry* 279, 12, 11843–11852.

[389] Kelkar, N., Standen, C. L., and Davis, R. J. 2005. Role of the JIP4 scaffold protein in the regulation of mitogen-activated protein kinase signaling pathways. *Molecular and Cellular Biology* 25, 7, 2733–2743.

[390] Buchsbaum, R. J., Connolly, B. A., and Feig, L. A. 2002. Interaction of Rac exchange factors Tiam1 and Ras-GRF1 with a scaffold for the p38 mitogen-activated protein kinase cascade. *Molecular and Cellular Biology* 22, 12, 4073–4085.

[391] Schoorlemmer, J. and Goldfarb, M. 2001. Fibroblast growth factor homologous factors are intracellular signaling proteins. *Current biology : CB* 11, 10, 793–797.

[392] Huang, C.-Y. and Tan, T.-H. 2012. DUSPs, to MAP kinases and beyond. *Cell & bioscience* 2, 1, 24.

[393] Kidger, A. M., Rushworth, L. K., Stellzig, J., Davidson, J., Bryant, C. J., Bayley, C., Caddye, E., Rogers, T., Keyse, S. M., and Caunt, C. J. 2017. Dual-specificity phosphatase 5 controls the localized inhibition, propagation, and transforming potential of ERK signaling. *Proceedings of the National Academy of Sciences of the United States of America* 114, 3, E317-E326.

[394] Kondoh, K. and Nishida, E. 2007. Regulation of MAP kinases by MAP kinase phosphatases. *Biochimica et biophysica acta* 1773, 8, 1227–1237.

[395] Kumar, G. S., Zettl, H., Page, R., and Peti, W. 2013. Structural basis for the regulation of the mitogen-activated protein (MAP) kinase p38α by the dual specificity phosphatase 16 MAP kinase binding domain in solution. *The Journal of biological chemistry* 288, 39, 28347–28356.

[396] Teng, C.-H., Huang, W.-N., and Meng, T.-C. 2007. Several dual specificity phosphatases coordinate to control the magnitude and duration of JNK activation in signaling response to oxidative stress. *The Journal of biological chemistry* 282, 39, 28395–28407.

[397] Coller, J. and Parker, R. 2004. Eukaryotic mRNA decapping. *Annual review of biochemistry* 73, 861–890.

[398] Goler-Baron, V., Selitrennik, M., Barkai, O., Haimovich, G., Lotan, R., and Choder, M. 2008. Transcription in the nucleus and mRNA decay in the cytoplasm are coupled processes. *Genes & development* 22, 15, 2022–2027.

[399] Winzen, R., Kracht, M., Ritter, B., Wilhelm, A., Chen, C. Y., Shyu, A. B., Müller, M., Gaestel, M., Resch, K., and Holtmann, H. 1999. The p38 MAP kinase pathway signals for cytokine-induced mRNA stabilization via MAP kinase-activated protein kinase 2 and an AU-rich region-targeted mechanism. *The EMBO Journal* 18, 18, 4969–4980.

[400] Dean, J. L. E., Sarsfield, S. J., Tsounakou, E., and Saklatvala, J. 2003. p38 Mitogen-activated protein kinase stabilizes mRNAs that contain cyclooxygenase-2 and tumor necrosis factor AU-rich elements by inhibiting deadenylation. *The Journal of biological chemistry* 278, 41, 39470–39476.

[401] Lu, Z., Xu, S., Joazeiro, C., Cobb, M. H., and Hunter, T. 2002. The PHD domain of MEKK1 acts as an E3 ubiquitin ligase and mediates ubiquitination and degradation of ERK1/2. *Molecular cell* 9, 5, 945–956.

[402] Rosette, C. and Karin, M. 1995. Cytoskeletal control of gene expression: depolymerization of microtubules activates NF-kappa B. *The Journal of Cell Biology* 128, 6, 1111–1119.

[403] Zou, Z., Huang, B., Wu, X., Zhang, H., Qi, J., Bradner, J., Nair, S., and Chen, L.-F. 2014. Brd4 maintains constitutively active NF-κB in cancer cells by binding to acetylated RelA. *Oncogene* 33, 18, 2395–2404.

[404] Nishiyama, A., Dey, A., Miyazaki, J.-I., and Ozato, K. 2006. Brd4 is required for recovery from antimicrotubule drug-induced mitotic arrest: preservation of acetylated chromatin. *Molecular biology of the cell* 17, 2, 814–823.

[405] Song, Y., Hu, G., Jia, J., Yao, M., Wang, X., Lu, W., Hutchins, A. P., Chen, J., Ozato, K., and Yao, H. 2020. DNA Damage Induces Dynamic Associations of BRD4/P-TEFb With Chromatin and Modulates Gene Transcription in a BRD4-Dependent and -Independent Manner. *Frontiers in molecular biosciences* 7, 618088.

[406] Chen, R., Liu, M., Li, H., Xue, Y., Ramey, W. N., He, N., Ai, N., Luo, H., Zhu, Y., Zhou, N., and Zhou, Q. 2008. PP2B and PP1alpha cooperatively disrupt 7SK snRNP to release P-TEFb for transcription in response to Ca2+ signaling. *Genes Dev.* 22, 10, 1356–1368.

[407] Yang, Z., Yik, J. H. N., Chen, R., He, N., Jang, M. K., Ozato, K., and Zhou, Q. 2005. Recruitment of P-TEFb for stimulation of transcriptional elongation by the bromodomain protein Brd4. *Molecular cell* 19, 4, 535–545.

[408] Ouchida, R., Kusuhara, M., Shimizu, N., Hisada, T., Makino, Y., Morimoto, C., Handa, H., Ohsuzu, F., and Tanaka, H. 2003. Suppression of NF-kappaB-dependent gene expression by a hexamethylene bisacetamide-inducible protein HEXIM1 in human vascular smooth muscle cells. *Genes to cells : devoted to molecular & cellular mechanisms* 8, 2, 95–107.

[409] Nudler, E. 2012. RNA polymerase backtracking in gene regulation and genome instability. *Cell* 149, 7, 1438–1445.

[410] Selth, L. A., Sigurdsson, S., and Svejstrup, J. Q. 2010. Transcript Elongation by RNA Polymerase II. *Annual review of biochemistry* 79, 271–293.

[411] Olsen, J. V., Vermeulen, M., Santamaria, A., Kumar, C., Miller, M. L., Jensen, L. J., Gnad, F., Cox, J., Jensen, T. S., Nigg, E. A., Brunak, S., and Mann, M. 2010. Quantitative phosphoproteomics reveals widespread full phosphorylation site occupancy during mitosis. *Science signaling* 3, 104, ra3.

[412] Mitsui, A. and Sharp, P. A. 1999. Ubiquitination of RNA polymerase II large subunit signaled by phosphorylation of carboxyl-terminal domain. *Proceedings of the National Academy of Sciences of the United States of America* 96, 11, 6054–6059.

[413] Auld, K. L., Brown, C. R., Casolari, J. M., Komili, S., and Silver, P. A. 2006. Genomic association of the proteasome demonstrates overlapping gene regulatory activity with transcription factor substrates. *Molecular cell* 21, 6, 861–871.

[414] Gillette, T. G., Gonzalez, F., Delahodde, A., Johnston, S. A., and Kodadek, T. 2004. Physical and functional association of RNA polymerase II and the proteasome. *Proceedings of the National Academy of Sciences of the United States of America* 101, 16, 5904–5909.

[415] Scharf, A., Grozdanov, P. N., Veith, R., Kubitscheck, U., Meier, U. T., and Mikecz, A. von. 2011. Distant positioning of proteasomal proteolysis relative to actively transcribed genes. *Nucleic acids research* 39, 11, 4612–4627.

[416] Verma, R., Oania, R., Fang, R., Smith, G. T., and Deshaies, R. J. 2011. Cdc48/p97 mediates UV-dependent turnover of RNA Pol II. *Molecular cell* 41, 1, 82–92.

[417] Ribar, B., Prakash, L., and Prakash, S. 2007. ELA1 and CUL3 are required along with ELC1 for RNA polymerase II polyubiquitylation and degradation in DNA-damaged yeast cells. *Molecular and Cellular Biology* 27, 8, 3211–3216.

[418] Jonkers, I. and Lis, J. T. 2015. Getting up to speed with transcription elongation by RNA polymerase II. *Nature reviews. Molecular cell biology* 16, 3, 167–177.

[419] Itzen, F., Greifenberg, A. K., Bösken, C. A., and Geyer, M. 2014. Brd4 activates P-TEFb for RNA polymerase II CTD phosphorylation. *Nucleic acids research* 42, 12, 7577–7590.

[420] Biondi, R. M. and Nebreda, A. R. 2003. Signalling specificity of Ser/Thr protein kinases through docking-site-mediated interactions. *The Biochemical journal* 372, Pt 1, 1–13.

[421] Garai, Á., Zeke, A., Gógl, G., Törő, I., Fördős, F., Blankenburg, H., Bárkai, T., Varga, J., Alexa, A., Emig, D., Albrecht, M., and Reményi, A. 2012. Specificity of linear motifs that bind to a common mitogen-activated protein kinase docking groove. *Sci. Signal.* 5, 245, ra74.

[422] Melino, G., Gallagher, E., Aqeilan, R. I., Knight, R., Peschiaroli, A., Rossi, M., Scialpi, F., Malatesta, M., Zocchi, L., Browne, G., Ciechanover, A., and Bernassola, F. 2008. Itch: a HECT-type E3 ligase regulating immunity, skin and cancer. *Cell death and differentiation* 15, 7, 1103–1112.

[423] Gao, M., Labuda, T., Xia, Y., Gallagher, E., Fang, D., Liu, Y.-C., and Karin, M. 2004. Jun turnover is controlled through JNK-dependent phosphorylation of the E3 ligase Itch. *Science (New York, N.Y.)* 306, 5694, 271–275.

[424] Anzi, S., Finkin, S., and Shaulian, E. 2008. Transcriptional repression of c-Jun's E3 ubiquitin ligases contributes to c-Jun induction by UV. *Cellular signalling* 20, 5, 862–871.

[425] Chang, L., Kamata, H., Solinas, G., Luo, J.-L., Maeda, S., Venuprasad, K., Liu, Y.-C., and Karin, M. 2006. The E3 ubiquitin ligase itch couples JNK activation to TNFalpha-induced cell death by inducing c-FLIP(L) turnover. *Cell* 124, 3, 601–613.

[426] Mund, T. and Pelham, H. R. B. 2009. Control of the activity of WW-HECT domain E3 ubiquitin ligases by NDFIP proteins. *EMBO reports* 10, 5, 501–507.

[427] Ingham, R. J., Gish, G., and Pawson, T. 2004. The Nedd4 family of E3 ubiquitin ligases: functional diversity within a common modular architecture. *Oncogene* 23, 11, 1972–1984.

[428] Lu, P. J., Zhou, X. Z., Shen, M., and Lu, K. P. 1999. Function of WW domains as phosphoserine- or phosphothreonine-binding modules. *Science (New York, N.Y.)* 283, 5406, 1325–1328.

[429] Qiu, L., Joazeiro, C., Fang, N., Wang, H. Y., Elly, C., Altman, Y., Fang, D., Hunter, T., and Liu, Y. C. 2000. Recognition and ubiquitination of Notch by Itch, a hect-type E3 ubiquitin ligase. *The Journal of biological chemistry* 275, 46, 35734–35737.

[430] Sudol, M. 1996. The WW module competes with the SH3 domain? *Trends in Biochemical Sciences* 21, 5, 161–163.

[431] Bernassola, F., Karin, M., Ciechanover, A., and Melino, G. 2008. The HECT family of E3 ubiquitin ligases: multiple players in cancer development. *Cancer Cell* 14, 1, 10–21.

[432] Drew, P. D., Franzoso, G., Becker, K. G., Bours, V., Carlson, L. M., Siebenlist, U., and Ozato, K. 1995. NF kappa B and interferon regulatory factor 1 physically interact and synergistically induce major histocompatibility class I gene expression. *Journal of interferon & cytokine research : the official journal of the International Society for Interferon and Cytokine Research* 15, 12, 1037–1045.

[433] Sgarbanti, M., Remoli, A. L., Marsili, G., Ridolfi, B., Borsetti, A., Perrotti, E., Orsatti, R., Ilari, R., Sernicola, L., Stellacci, E., Ensoli, B., and Battistini, A. 2008. IRF-1 is required for full NF-kappaB transcriptional activity at the human immunodeficiency virus type 1 long terminal repeat enhancer. *Journal of virology* 82, 7, 3632–3641.

[434] Terkeltaub, R. A., Furst, D. E., Bennett, K., Kook, K. A., Crockett, R. S., and Davis, M. W. 2010. High versus low dosing of oral colchicine for early acute gout flare: Twenty-four-hour outcome of the first multicenter, randomized, double-blind, placebo-controlled, parallel-group, dose-comparison colchicine study. *Arthritis and rheumatism* 62, 4, 1060–1068.

[435] Tabatabai, M. R. and Cummings, N. A. 1980. Intravenous colchicine in the treatment of acute pseudogout. *Arthritis and rheumatism* 23, 3, 370–374.

[436] Goldfinger, S. E. 1972. Colchicine for familial Mediterranean fever. *The New England journal of medicine* 287, 25, 1302.

[437] Dinarello, C. A., Wolff, S. M., Goldfinger, S. E., Dale, D. C., and Alling, D. W. 1974. Colchicine therapy for familial mediterranean fever. A double-blind trial. *The New England journal of medicine* 291, 18, 934–937.

[438] Zemer, D., Revach, M., Pras, M., Modan, B., Schor, S., Sohar, E., and Gafni, J. 1974. A controlled trial of colchicine in preventing attacks of familial mediterranean fever. *The New England journal of medicine* 291, 18, 932–934.

[439] Aktulga, E., Altaç, M., Müftüoglu, A., Ozyazgan, Y., Pazarli, H., Tüzün, Y., Yalçin, B., Yazici, H., and Yurdakul, S. 1980. A double blind study of colchicine in Behçet's disease. *Haematologica* 65, 3, 399–402.

[440] Davatchi, F., Sadeghi Abdollahi, B., Tehrani Banihashemi, A., Shahram, F., Nadji, A., Shams, H., and Chams-Davatchi, C. 2009. Colchicine versus placebo in Behçet's disease: randomized, double-blind, controlled crossover trial. *Modern rheumatology* 19, 5, 542–549.

[441] Callen, J. P. 1985. Colchicine is effective in controlling chronic cutaneous leukocytoclastic vasculitis. *Journal of the American Academy of Dermatology* 13, 2 Pt 1, 193–200.

[442] Imazio, M., Bobbio, M., Cecchi, E., Demarie, D., Demichelis, B., Pomari, F., Moratti, M., Gaschino, G., Giammaria, M., Ghisio, A., Belli, R., and Trinchero, R. 2005. Colchicine in addition to conventional therapy for acute pericarditis: results of the COlchicine for acute PEricarditis (COPE) trial. *Circulation* 112, 13, 2012–2016.

[443] Imazio, M., Brucato, A., Cemin, R., Ferrua, S., Belli, R., Maestroni, S., Trinchero, R., Spodick, D. H., and Adler, Y. 2011. Colchicine for recurrent pericarditis (CORP): a randomized trial. *Annals of internal medicine* 155, 7, 409–414.

[444] Imazio, M., Brucato, A., Cemin, R., Ferrua, S., Maggiolini, S., Beqaraj, F., Demarie, D., Forno, D., Ferro, S., Maestroni, S., Belli, R., Trinchero, R., Spodick, D. H., and Adler, Y. 2013. A randomized trial of colchicine for acute pericarditis. *The New England journal of medicine* 369, 16, 1522–1528.

[445] Maillard, H., Leclech, C., Peria, P., Avenel-Audran, M., and Verret, J. L. 1999. Colchicine for Sweet's syndrome. A study of 20 cases. *The British journal of dermatology* 140, 3, 565–566.

[446] Suehisa, S. and Tagami, H. 1981. Treatment of acute febrile neutrophilic dermatosis (Sweet's syndrome) with colchicine. *The British journal of dermatology* 105, 4, 483.

[447] Crittenden, D. B., Lehmann, R. A., Schneck, L., Keenan, R. T., Shah, B., Greenberg, J. D., Cronstein, B. N., Sedlis, S. P., and Pillinger, M. H. 2012. Colchicine use is associated with decreased prevalence of myocardial infarction in patients with gout. *The Journal of rheumatology* 39, 7, 1458–1464.

[448] Nidorf, M. and Thompson, P. L. 2007. Effect of colchicine (0.5 mg twice daily) on high-sensitivity C-reactive protein independent of aspirin and atorvastatin in patients with stable coronary artery disease. *The American journal of cardiology* 99, 6, 805–807.

[449] Nidorf, S. M., Eikelboom, J. W., Budgeon, C. A., and Thompson, P. L. 2013. Low-dose colchicine for secondary prevention of cardiovascular disease. *Journal of the American College of Cardiology* 61, 4, 404–410.

9. Appendix

9.1 Declaration

Hereby, I declare that the presented work, except where stated otherwise by reference or acknowledgment, was generated by myself under the supervision of my advisors during my doctoral studies. All contributions from colleagues are explicitly referenced in the thesis. The material listed below was obtained in the context of collaborative research:

Figure 21. Pretubulysin reduces inflammation in a murine psoriasiform dermatitis model, Mohammed A.F. Elewa, Igor Macinkovic, Andreas Weigert, Institute of Biochemistry I, Faculty of Medicine, Goethe University Frankfurt am Main, Germany, assay performance, data analysis and interpretation (their contribution); figure preparation (my contribution).

Figure 22. Pretubulysin reduces the interaction of leukocytes with the endothelium *in vivo,* Matthias Fabritius, Department of Otorhinolaryngology, Head and Neck Surgery, Walter Brendel Centre of Experimental Medicine, Clinical center at the University of Munich, Germany, assay performance and data analysis (his contribution), data interpretation, figure preparation (Rebecca Ingelfinger, my contribution).

Figure 27. Pretubulysin decreases the cell surface levels of CAMs, Rebecca Ingelfinger, Tobias Primke, Institute of Pharmaceutical Biology, Goethe University Frankfurt, Germany, assay performance and data analysis and interpretation (our contribution), figure preparation (my contribution).

Figure 29. The depolymerizing MTAs decrease the cell surface levels of ICAM-1 and VCAM-1 in a concentration-dependent manner, Rebecca Ingelfinger, Tobias Primke, Institute of Pharmaceutical Biology, Goethe University Frankfurt, Germany, assay performance and data analysis and interpretation (our contribution), figure preparation (my contribution).

Figure 31. The depolymerizing MTAs decrease the cell surface levels of ICAM-1 and VCAM-1 in a concentration-dependent manner in HMEC-1, Rebecca Ingelfinger, Tobias Primke, Institute of Pharmaceutical Biology, Goethe University Frankfurt, Germany, assay performance and data analysis and interpretation (our contribution), figure preparation (my contribution).

Whenever a figure, table or text is identical to a previous publication, it is stated explicitly in the thesis that copyright permission and/or co-author agreement has been obtained. The following parts of the thesis have been previously published:

Chapter 2.2.12 Map of pGL4.32[*luc2p*/NFκB-RE/Hygro] and pGL4.44[*luc2P*/AP1-RE/Hygro] vectors containing the *Photinus* luciferase gene *luc2P* under control of the NFκB or AP-1 response element (RE), respectively.

Chapter 3.1.2 Pretubulysin reduces the interaction of leukocytes with the endothelium *in vivo.* Published in the doctoral thesis of Rebecca Ingefinger (formerly Rebecca Schwenk).

9.2 Publications

9.2.1 Articles

Tobias F. Primke, Rebecca Ingelfinger , Mohammed A. F. Elewa, Igor Macinkovic, Andreas Weigert, Matthias P Fabritius , Christoph A Reichel, Angelika Ullrich, Uli Kazmaier, Luisa D. Burgers, Robert Fürst. *The Microtubule-Targeting Agent Pretubulysin Impairs the Inflammatory Response in Endothelial Cells by a JNK-Dependent Deregulation of the Histone Acetyltransferase Brd4.* Cells. 2023 Aug 21;12(16):2112.

Iris Bischoff-Kont, Tobias Primke, Lea S. Niebergall, Thomas Zech, Robert Fürst. *Ginger Constituent 6-Shogaol Inhibits Inflammation- and Angiogenesis-Related Cell Functions in Primary Human Endothelial Cells.* Front Pharmacol. 2022 Feb 25:13:844767.

9.2.2 Poster presentation

Tobias F. Primke, Rebecca Schwenk, Rebekka Schäfer, Matthias P. Fabritius, Christoph A. Reichel, Angelika Ullrich, Uli Kazmaier, Robert Fürst. The microtubule-targeting agent pretubulysin impairs inflammatory key features in endothelial cells *in vitro* and *in vivo*. DPhG annual meeting (2019).

Tobias F. Primke, Rebecca Schwenk, Matthias P. Fabritius, Christoph A. Reichel, Angelika Ullrich, Uli Kazmaier, Robert Fürst. The microtubule-targeting agent pretubulysin impairs inflammatory key features in endothelial cells *in vitro* and *in vivo*. DPhG annual meeting (2021).

Tobias F. Primke, Rebecca Schwenk, Matthias P. Fabritius, Christoph A. Reichel, Angelika Ullrich, Uli Kazmaier, Robert Fürst. The microtubule-targeting agent pretubulysin impairs inflammatory key features in endothelial cells *in vitro* and *in vivo*. DPhG annual meeting (2022).